An Investigation into the Optimal Operation of a Complex Heat Pump for the Complete Thermal Management of an Electric Vehicle in Cold Climates

by

James Jeffs

Thesis

Submitted to the University of Warwick

in partial fulfilment of the requirements

for degree of

Doctor of Philosophy in Engineering

University of Warwick, WMG

August 2019

Contents

List of Tables

List of Figures

Abbreviations

AAA	American Auto-mobile Association
AC	Alternating Current
ASHRAE	American Society of Heating and Air Conditioning Engineers
COP	Coefficient of Performance
DOD	Depth of Discharge
DP	Dynamic Programming
ECM	Equivilant Circuit Model
ECT	Electrochemical Thermal
EOL	End of Life
ES	Electrical Storage
ESS	Energy Storage System
EU	European Union
EV	Electric Vehicle
HETS	Hybrid Electrical/Thermal Storage
HEV	Hybrid Electric Vehicle
HPCU	Heat Pump Control Unit
HPTS	Heat Pump Thermal Storage
HPWH	Heat Pump Water Heater
HTC	High Temperature Circuit
HVAC	Heating Ventilation Air Conditioning
HWFET	Highway Fuel Economy Test
HX	Heat Excahnger
ICE	Internal Combustion Engine

JLR Jaguar Land Rover

MCU Motor Control Unit (not the Marvel Cinematic Universe)

MHEV Mild Hybrid Electric Vehicle

MPC Model Predictive Control

NEDC New European Drice Cycle

NN Neural Network

OCV Open Circuit Voltage

PCM Phase Change Material

PEEM Power Electronics and Electric Motor

PHEV Plug-in Hybrid Electric Vehicle

PID Proportional Integral Differential

POTS PTC only with Thermal Storage

PPC Peak Power Capability

PTC Positive Therma Coefficient

RC Resistor Capacitor

SAE Society of Automotive Engineers

SC03 Speed Correction Drive Cycle

SOC State of Charge

SSTOM Switching Schedule from Trajectory of Optimal Modes

SUV Sports Utility Vehicle

TMS Thermal Management Strategies

UDDS Urban Dynamometer Driving Schedule

W/OTB Without Thermal Storage

WEG Water/Ethylene Glycol

WLTP World harmonized Light duty Test Procedure

WMTC World Motorcycle Test Cycle

WTB With Thermal Storage

Nomenclature

$\bar{h}$	Average thermal conductance (W/K)
η	Efficiency (-)
μ	Viscosity (Pa s)
ν	Velocity (m/s)
ω	Rotational speed (rad/s)
ρ	Density (kg/m^3)
τ	Torque (Nm)
C	Capacity (Ah
C_l	Latent heat (kJ/kg)
C_p	Specific heat (kJ/kgK)
DOD	Depth of discharge (%)
E	Energy (J)
$E_{thermal}$	Thermal energy (J)
h	hermal conductance (W/K)
I	Current (A)
J	Cost
j_i	Components of cost (I = 1,2,3)
J_i^n	Cost at the i$^{\text{th}}$ time step using the nth operational mode.
k	Thermal conductivity (W/m^{2}K)

L	length (m)
n_i	Components of normalistion (i = 1,2,3)
N_{ts}	Total number of timesteps
P	Power (W)
P	Vector of static parameters (page 59)
Pr	Prandtl number (-)
Q	Heat flow (W)
Re	Reynolds number (-)
SOC	State of charge (Ah)
T	Temperature (degC/K)
t	Time
$T_{meltingzone}$	Temperature region in which materials melt (degC/K)
t_{start}	page 68
U_i^n	Control vector at the ith time step using the nth operational mode.
V	Voltage (V)
V_{drop}	Voltage drop (V)
V_{ocv}	Open circtuiy voltage
w_i	Components of weighting ($i = 1, 2, 3$)
X	Parameter vector
X_i^n	Vehicle state at the ith time step using the nth operational mode.
X_s	State variables

Acknowledgments

Firstly I would like to thank my supervisors, Dr. Dhammika Widanalage and Dr. Andrew McGordon for their continual and much appreciated advice, guidance and mentorship. I would also like to thank Dr. Simon Robinson and Jonathan Parsons from Jaguar Land Rover for their industrial supervision in this work. From Claytex, I would like to thank Alex Picarelli and Mike Dempsey for their support, guidance and patience in providing the technical support that was much required for this research.

I would also like to thank Yashraj Tripathy for providing the parameterisation and validation data which made my research possible. I want to express my gratitude to Sina Shojaei, for providing technical guidance which allowed me to achieve the outcomes of this thesis.

The work presented in this thesis was supported by Jaguar Land Rover in the form of an iCASE award and the Engineering and Physical Science Research Council.

I would like to extend my gratitude to Enrik Nako, Tim Jackson, Jess Watts, Hannah Burnage and everyone else involved in the Warwick archery club for providing a sometimes much needed break from the challenges of the past 4 years.

Thank you to my family; my mother Deborah Jeffs, father Adrian Jeffs and brother Oliver Jeffs, for support and encouragement. Finally, thank you to my wife Bethany Smith, for your limitless support, encouragement, patience and love; this adventure would have been impossible without you and has been all the more enjoyable with you.

Declarations

This thesis is submitted to the University of Warwick in support of my application for the degree of Doctor of Philosophy in Engineering. It has been composed by myself and has not been submitted in any previous application for any degree. The work presented was carried out by myself except where otherwise stated.

Signed: Date:

James Jeffs

Publications in support of application

Journal Publications:

Jeffs, James, et al. "Complex heat pump operational mode identification and comparison for use in electric vehicles." Energies 11.8, 2018 [27].

Conference Proceedings:

Jeffs, James, et al. "Use of a thermal battery with a heat pump for low temperature electric vehicle operation." 2017 IEEE Vehicle Power and Propulsion Conference (VPPC). IEEE, 2017 [28].

Jeffs, James, et al. "System level heat pump model for investigations into thermal management of electric vehicles at low temperatures." Proceedings of the 13th International Modelica Conference, 2019. No. 157. Linköping University Electronic Press, 2019 [1].

Abstract

Electric vehicles (EV) suffer two inconveniences at low temperatures; poor lithium ion battery performance and a cabin heating demand which must be satisfied by the battery and cannot be provided using waste heat from a internal combustion engine. Both of these issues combine to give a 40% to 70% reduction in range at -20°C. This leads to EV users having to potentially choose between range and comfort.

New technologies and strategies are being proposed to reduce the impact of cabin heating and battery performance reduction on range. Primarily, heat pumps are becoming the likely candidate for future thermal management in electric vehicles. A heat pump is agnostic to its heat source, leading to many potential heat recovery opportunities around the vehicle. Heat pumps have been criticised for poor response times, leading to the addition of thermal storage devices to reduce dependence on positive thermal coefficient (PTC) heaters. Researchers have explored some of the new possible architectures which a heat pump allows; however, with many architectures possible a systematic comparison of all possibilities needs to be made. A novel implementation of a cost function which can be varied in weighting to prioritise range or comfort, coupled with conventional optimisation techniques, is used to control the trade off between range and comfort. A simulation environment is used to identify the optimal sizing of the thermal battery, systematically identify and compare all possible vehicle architectures, and produce an optimal heating trajectory for the electric battery.

The results showed an average range extension of 22% compared to the baseline could be achieved by replacing the PTC heater with an optimised thermal battery, while simultaneously improving comfort by 28% over the temperature range of -15°C to 15°C. For the first time, a systematic and exhaustive comparison of potential combinations of thermal interactions on a heat pump system is performed. The result of this comparison showed that at -5°C, selecting the correct operational mode enabled the range to be tunable within a 10% window according to cost function priority, corresponding to a 18% variation in comfort. Finally, optimising the heating trajectory of the battery for different cost function priorities created a range window between 116.9km and 140.4km, with the comfort improving by 17% when reducing the range from 140.4km to 116.9km.

If an electric vehicle has multiple heat sources and sinks it is possible to select operational modes and control component interactions with the heat pump so that the trade off between range and comfort can be optimally controlled. This methodology may be repeated for different electric vehicles, using a different set of potential heat sources for the heat sink, and may also be repurposed to consider high temperature environments, thus contributing a systematic approach to addressing thermal management challenges in electric vehicles. The implementation of this methodology on a real vehicle would allow for the maximum thermal comfort to be delivered while ensuring there is enough range to meet the required duty cycle. This could potentially increase the uptake and acceptance of electric vehicles in regions where inhabitants experience cold winters.

Chapter 1

Introduction

1.1 The current political climate regarding the electrification of vehicles

The demand for electric vehicles is on the rise due to a gradual depletion of global oil reserves, growing concerns over carbon dioxide (CO_2) and other green house gases contributing towards climate change [29]. Increased understanding and concern over inner city air quality is also a driver for electrification in the transport sector [30]. Countries such as the UK (2040), France (2040), Germany (2050), China (2040) and others have announced plans to ban the sale of new petrol and diesel powered vehicles before the years given in parentheses.

1.2 A summary of current electrification options

On the path to zero emission vehicles, some mainstream automotive manufacturers are now offering a range of electrified vehicles. There are several accepted levels of electrification which include; electric vehicles (EVs), hybrid electric vehicles (HEVs) (which can be further split into micro, mild and full) and plug in hybrid electric vehicles (PHEVs). The accepted definition of a HEV from the Society of Automotive Engineers (SAE) terminology standards is "A vehicle with two or more energy storage systems, both of which must provide propulsion power; either together or independently" [31]. Examples of HEVs and PHEVs include; Toyota Prius (HEV and PHEV), Mitsubishi Outlander (PHEV), BMW i8 (PHEV) and Volkswagen Passat GTE (PHEV).

Current sales figures suggest that the market share of new electrified vehicles is dominated by HEVs, but this share is decreasing while the share held by PHEVs

and EVs is growing [32]. HEVs are characterised by their small batteries, less significant contribution to propulsion and reduced electric only range (if any) [33]. Meanwhile, PHEVs can have a considerable all electric range (e.g. 50km from the Mitsubishi Outlander PHEV [34]), and are characterised by larger batteries, larger contribution from the motor to total vehicle power and the ability to plug in to charge. Electric vehicles currently have a similar market share in the sale of new electrified vehicles to PHEVs, although it has been postulated that their public adoption has been limited by a phenomena known as range anxiety [35]. Range anxiety is the stress associated with the running out of electric energy before your destination or next charging opportunity. Methods for relieving range anxiety are available, for example the use of charger locating mobile applications such as ZapMap and Polar network [36, 37]. These applications allow users to check the location of charger stations, identify what type of chargers are available, whether the chargers are operational and sometimes whether a charger is occupied. This allows drivers to plan stops in advance of their journey hence reducing the stress associated with limited range.

1.3 Electrified vehicles operating in low temperatures

Range and therefore range anxiety can be made worse through operating in low temperatures, due to the impact of heating, ventilation and air conditioning (HVAC) on the energy consumption of vehicles, and the limited on-board energy storage of electric vehicles. Here low temperature is considered to be below 10°C, as this is the point at which electric battery performance begins to decline [9, 10, 12]. This problem can be particularly severe for electric vehicles at low temperatures, with range reductions of up to 70% at −20°C [21, 22]. Since HEVs rely heavily on their internal combustion engines, cabin heating can be accommodated through waste heat from the engine. In PHEVs it is desirable to minimise use of the internal combustion engine for emission reduction purposes, and therefore not as much waste heat is available for cabin heating. Research has been performed on the thermal management of PHEV vehicles in low temperature scenarios; Revereault *et al.* [38] found that at -18°C forced engine operation led to a 6% fuel saving when compared to normal operation with heat supplemented by positive thermal coefficient (PTC) heaters. PTC heaters use electrical energy stored in the battery to generate heat, and so it is preferential not to use them when maximising electric range. In another similar study by Shams-Zahraei *et al.* [39] it was found that forcing engine operation from the beginning of the journey led to a fuel saving of 34% when compared to

postponing engine operation until the battery is depleted. In both cases, using internal combustion waste heat reduced the use of PTC heaters.

1.4 The specific challenges of operating pure electric vehicles in cold climates

In order to sustain a cabin temperature of 10°C (when ambient is -20°C) a heat source of approximately 6.2kW is required for a mid sized light duty passenger vehicle [40]. This was based on work by Farrington *et al.* [41], who showed that the cabin heating requirement for a vehicle to sustain a temperature 30°C above ambient was linearly dependant on recirculation percentage. The required heat varied between 6.2kW and 1.2kW for 0% and 100% recirculation respectively. These estimations were based on a thermal loss of 50W/K through the car's surfaces. In another investigation Enthaler *et al.* [19] showed that an average of 7.6kW of heat would be needed to warm the cabin from −15°C during a 38 minute warm up period. Here the target temperature of the cabin was 20°C but the authors do not say when this is reached. These quantities of waste heat can be easily extracted from the engine in conventional vehicles. On the other hand, in pure electric vehicles the battery, power electronics and electric motor generate very little waste heat. For example, the motor and inverter operate at an efficiency of approximately 93% [42]. Assuming a vehicle efficiency of 225Wh/km this would lead to an average heat generation of 700W during the official world harmonised light duty test procedure. This is insufficient for keeping the cabin warm and so PTC heaters are required in EVs to provide sufficient cabin heating. PTC heaters have a maximum coefficient of performance of 1 [43] but typically perform at 0.95 [44], and so consume at least as much power as the heat that they supply. This extra load contributes to a significant range reduction for electric vehicles operating in low temperatures. To fully quantify and appreciate the range reduction, the effect of low temperature on the battery should also be considered.

Range anxiety is exacerbated when electric vehicles operate in cold climates by the addition of high HVAC loads compounded with the effects and consequences that cold weather has on electric battery performance. With regards to the battery's reduced performance, the primary concern for electric vehicles is the reduction in available capacity. Many studies have been performed to quantify the capacity loss as temperature reduces. A summary of some of the literature in this area can be seen in Figure 1.1. Here it can be seen that cells lose capacity as the temperature reduces, with a 15% to 50% loss being representative of what might be expected

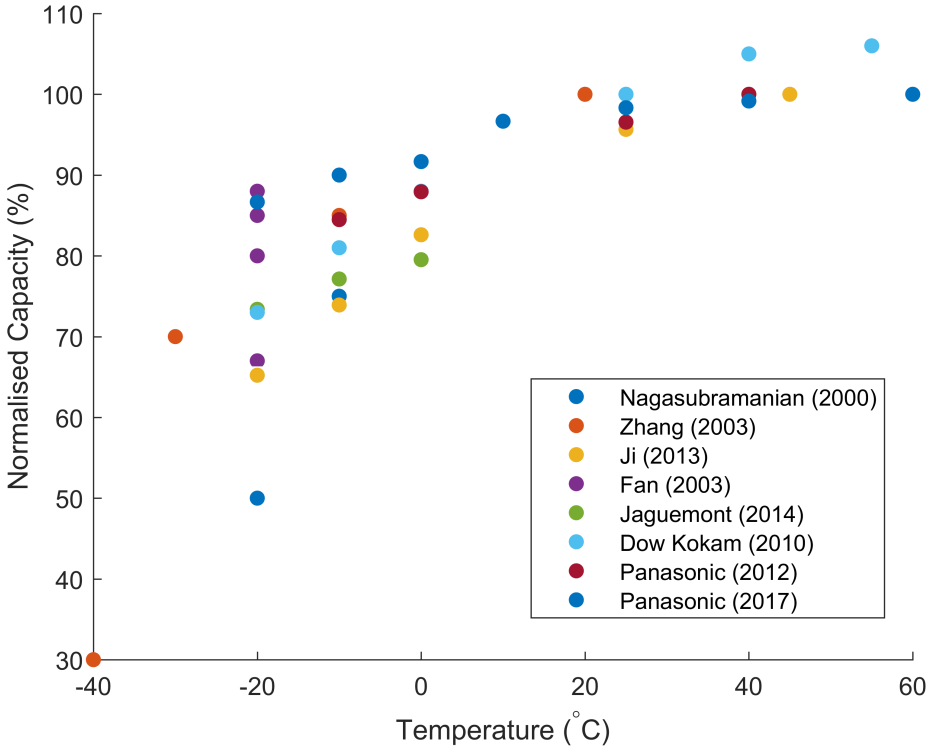

Figure 1.1: A summary of the capacity loss as a function of temperature as reported by the following sources; Nagasubramanian [7], Zhang [8], Ji [9], Jaguemont [10], Dow Kokam [11] (manufacturer) and Panasonic [12] [13] (manufacturer).

at −20°C. This will obviously have a significant effect on the range of an electric vehicle.

At low temperature the internal resistance of lithium ion cells increases [10] which leads to a reduction in the amount of power a cell is capable of providing [8,17]. Cold temperatures are also associated with an increase in ageing caused by lithium plating [45, 46]. The problem is particularly associated with charging and can cause battery end of life (80% capacity remaining) in as little as 100 charge cycles [47]. These low temperature effects are expanded upon in Chapter 2.

Research is being conducted into alternative chemistries to lithium ion; sodium ion batteries are a likely alternative due to the increased natural abundance of sodium and their intrinsic safety. However, they also have operating temperatures of 110°C to 130°C which changes the parameters of the problem [48]. If a cell chemistry were developed which had no low temperature performance issues then the low temperature range deficit would be reduced, but the need to develop more efficient cabin heating strategies would still exist.

1.4.1 Public perception of the problem

While it is important to quantitatively evaluate the problem using range and cell capacity metrics, it is also necessary to consider the public's perception of the issue. To do this a selection of internet articles has been curated to express the views of the public and the media. The titles and publication dates of these are given below.

1. Do Electric Vehicles Work in Cold Temperatures? March 2018 [49].
2. Electric car range is affected by extreme cold, but at least the cars can start. January 2018 [50].
3. An inconvenient truth: How much does cold weather reduce an electric car's range? February 2018 [51].
4. Electric Car vs. Winter. October 2017 [52].
5. Five electric cars tested in cold Norwegian winter: how did they do? March 2018 [53]
6. Driving electric cars in winter: tips from experienced owner. 2018 [54]
7. Motor Mouth: The inconvenient truth about EVs in cold weather. January 2018 [55]
8. Why do electric cars suck in cold weather? December 2018 [56]

From the titles presented, it is obvious that there is a negative association between electric vehicles and cold climates. Without giving details of each article, they give concise descriptions of the challenges faced by EVs in the winter, from both HVAC and battery perspective. They also offer tips on how to get the most range out of EVs in the winter; this commonly involves wearing more clothing to stay warm and turning the heating down or off. Some also talk about the inconvenience of not being able to rapid charge cold batteries. This was highlighted by a story dubbed "Rapidgate" from 2018, where the Nissan Leaf de-rated its rapid charging capabilities after repeated uses in a short time period [57]. Hence public acceptance of electric vehicles may be improved by a more efficient heating system which can maximise range and charging ability of the vehicle by keeping the battery warm and cheaply heating the vehicle's cabin to provide greater thermal satisfaction.

1.5 An overview of current research areas

Different heating strategies and mechanisms have been researched to tackle the problem of low temperature range deficit in electric vehicles. The aim here is to find the most energy efficient ways to produce heat to be used in the cabin and battery during low temperature operation. For battery specific research there are examples of testing being carried out as low as -40°C [58]. However, vehicle level research investigations often only go down to -20°C [21, 59, 60]. In terms of battery heating, lots of research has been conducted into heating cells efficiently, and the performance gain that can be achieved from doing so [58, 61, 62]. Preheating the battery and the cabin has also been explored as a solution for low temperature operation [59, 63]. Preheating is typically performed while the vehicle is plugged into the grid. If there is not a thermally efficient method to provide heat when the vehicle is unplugged, then the PTC heaters will continue to deplete the battery in order to maintain a comfortable cabin temperature. Heat pumps are one of the technologies that have been suggested as an efficient replacement or supplement to PTC heaters. A heat pump can be used to recover small amounts of heat and make it useful for heating [64]. Heat pumps have been used for around 30 years in residential and commercial buildings [65], but have undergone re-evaluation for automotive use within the past 6 years [24, 66]. It has also been seen that their efficiency increases when more waste heat is available [67]. Thermal energy storage is another solution that has been investigated to assist in cabin and battery heating. Thermal energy storage devices can store thermal energy received during a vehicle's charge, then release it into the cabin or battery during warm up, providing a good source of instant thermal power [38, 40]. In buildings, it has also been demonstrated that thermal batteries can increase the coefficient of performance (COP) of heat pumps by up to 50% by creating a hybrid thermal plant conceptually comparable to the drivetrain of a HEV [68].

Literature has highlighted a selection of potential heat sources which heat pumps can utilise, as well as the option to deliver heat to the battery. A systematic methodology is required which can identify and compare all possible operational modes which arise from these choices. The methodology should be used to identify which component to heat pump relationships are most important, allowing for further improvements to be gained through the control of these components. There are also no examples of an automotive orientated heat pump that makes use of a dedicated thermal battery. Examples exist of dual source heat pumps [24, 67], but neither consider waste heat from the transmission. Examples also exist of a dedi-

cated heat battery being used to supplement a heat pump [68], however not in an automotive context. The system model proposed in Chapter 5 is designed to explore the potential benefits of supplying a heat pump with thermal energy from a wide variety of thermal sources within a vehicle.

1.5.1 Cooperation with Jaguar Land Rover

This thesis and the work required to complete it was undertaken between September 2015 and August 2019, during which time Jaguar Land Rover finalised the design and began production of the Jaguar I-Pace, the brand's first full electric vehicle. This work was sponsored by Jaguar Land Rover as they had an interest in researching optimal thermal management solutions. This relationship granted access to a Dymola model built by Claytex for proving thermal management concepts, access to data tables to parameterise models, and access to Jaguar I-Pace vehicle specifications. As such, the model used for this research is based on the Jaguar I-Pace with thanks to the assistance from Jaguar Land Rover employees, data and models.

1.6 The research area

The challenge identified through the discussion in this chapter is to reduce the range deficit electric vehicles experience at low temperatures, which is caused by an increase in HVAC demand and a decrease in battery performance. While electric vehicles waste little heat, having multiple potential heat sources releases a plethora of thermal management opportunities to be explored. Hence, the objective of this research is to develop an optimisation framework which can manage the collection and distribution of thermal energy around the vehicle to maximise performance. The word performance is pivotal as this could be understood as range, which requires battery heating and so will inevitably reduce comfort. Conversely, performance could mean comfort, which would have the inverse effect of sacrificing range. Consequently some compromise between comfort and range must be struck; a theme that will continue throughout this thesis.

In completing this objective an investigation into the sizing of a thermal battery will be conducted, which will contribute new insight into how the inclusion of thermal storage affects electric vehicle performance. This will lead to the identification of all possible operational modes on a vehicle with multiple heat sources and sinks, which will be exhaustively compared in a manner not seen before in literature. Finally the dynamic heating of the electric battery will be optimised in a novel and promising application of dynamic programming.

1.7 The thesis structure

The remainder of the thesis is structured as follows; Chapter 2 explores the background to the problem in the area of interest, giving a comprehensive overview of the challenges faced at low temperatures due to both battery performance (capacity, power and ageing) and cabin heating requirements. This chapter is concluded with a summary of the challenge at the vehicle level. Chapter 3 explores the current state of research in the area of thermal management solutions for low temperature operation. At the end of this chapter the knowledge gap in thermal management solutions will be determined, which will influence the required capability of the model that will be used. This is concluded with the research question "In an electric vehicle with a heat pump, how can the combination of potential sources and sinks be systematically compared; hence identifying important components to be controlled to minimise energy consumption, maximise range and maximise comfort?", which is then broken down into three research objectives to be addressed individually in each of the results chapters.

Chapter 4 will cover the methodology used in the research. Here a selection of known optimisation techniques are combined with a cost function which can be varied according to whether battery performance or range is prioritised. This novel implementation is used to create thermal management strategies which can be tuned to either give the best range, the best comfort or compromise between the two. This is ultimately demonstrated in Chapter 8, where at $-7°C$ a 20% window in range can be controlled within a 20% window in comfort. This is achieved through the use of dynamically optimised heating trajectories prioritising either battery performance, comfort or a neutral mixture of the two.

Specific details of the model will be given in Chapter 5. Here the model is designed to replicate current commercially available state of the art, with the intention of producing solutions according to current possibilities. The research will not address the development of individual components within the heat pump itself, but is concerned with the operation of the system in relation to the heat pump.

The process created through Chapters 4 to 8 defines a methodology which can be used to evaluate and optimise thermal management architectures and control strategies on any electrified vehicle; hence contributing a systematic approach to optimising thermal management strategies according to whether comfort or range is prioritised.

1.8 Research contributions.

In Chapter 6 an optimisation of a thermal storage system will be performed. The scope of this search and analysis given goes beyond previous work in this area, which consisted of sizing a thermal battery to replace the PTC heater for one specific use case by LaClair *et al.* [69].

It will be shown that while researchers such as Leighton [24], Steiner *et al.* [70], Meyer *et al.* [71], Kim *et al.* [72], Lee *et al.* [66], Ahn *et al.* [67] and others have tested a range of different heat pump configurations between them and in isolation, this thesis provides a methodology for exhaustively testing and analysing all possible heat pump configurations given a list of potential heat sources and sinks. In Chapter 7 a method for identifying all heat pump configurations and comprehensively comparing them is presented, thereby contributing a complete and systematic approach to evaluating heat pump configurations.

In Chapter 8 the dynamic heating of the battery is optimised which will provide a balance between thermal comfort and range. This will extend upon the work of Shojaei *et al.* [73] by applying similar but adapted optimisation methodologies to a new temperature regime.

To accomplish these achievements a novel vehicle platform, discussed in Chapter 5, has been designed in the Dymola modelling environment [1]: the structure of which is unique in its reconfigurability, versatility and robustness to a range of operating conditions.

The structure and procedure of these achievements represents a new notional optimisation framework for the design of electric vehicles to be used in low temperature climates.

Chapter 2

Background to the Problem

To fully address the issue concerning low temperature range, a thorough understanding of the problem is needed. This chapter covers the known problems associated with low battery operating temperatures in Section 2.1 and electric vehicle operation in cold climates in Section 2.2. The combined effect of the issues presented is summarised in Section 2.3.

2.1 Battery

In this section the details relating to the challenges of operating batteries at low temperatures are discussed. lithium-ion batteries have an ideal operating range of 20°C to 40°C [74]. When the battery temperature is reduced to less than 10°C it starts to experience a reduction in performance in three main areas. Firstly, the energy storage capability of the battery starts to drop, at −20°C this can be a 15% to 50% reduction as shown in Section 1.4. Secondly, an increase in internal resistance reduces the battery's ability to provide peak power [75]. At −20°C the peak power capability drops to approximately 10% of its room temperature capability due to resistance increase [76]. The final concern when operating batteries at low temperatures is an increase in ageing causing the the battery to reach its end of life (EOL) quicker. The general consensus on the definition of EOL in the automotive industry is when the cell can no longer hold more than 80% of its original capacity [77]. Before details of the effects of low temperature on battery operation are discussed further, a brief description of how a lithium-ion cell operates will be given.

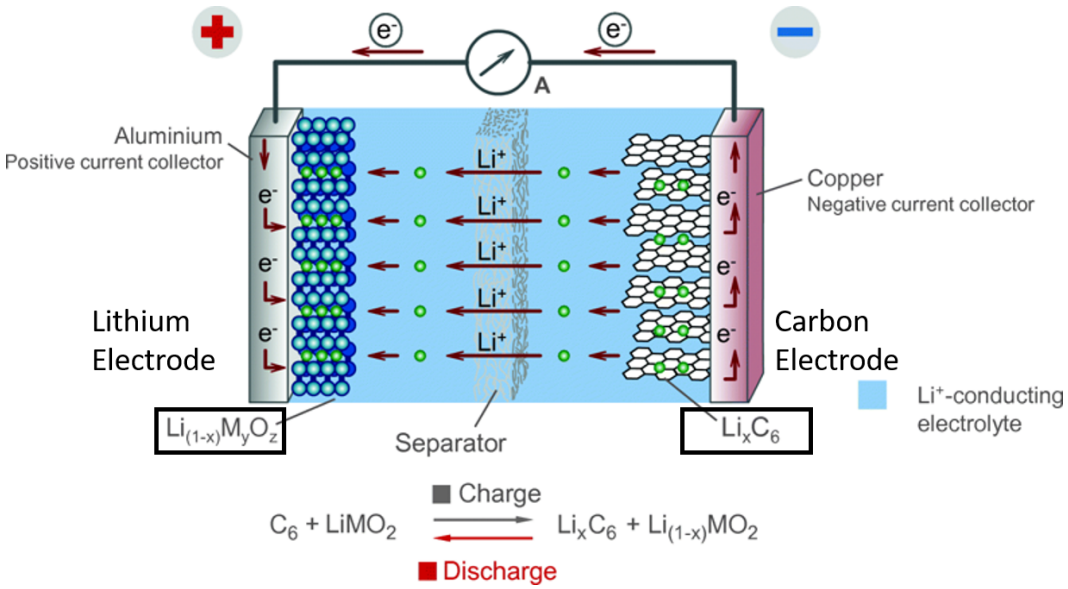

Figure 2.1: Schematic of lithium-ion cell operation, showing ion and electron movement [14].

2.1.1 lithium-ion Cell Operation

lithium-ion cells are charged and discharged through the movement of lithium-ions between two electrodes. These electrodes can be referred to as the anode or the cathode depending on whether the cell is being charged or discharged, so for simplicity they shall be referred to by their typical construct materials, hence the graphite electrode and the lithium electrode (e.g. $LiMO_2$). In a charged cell the carbon electrode is saturated with lithium atoms, forming LiC_6 particles. When a circuit is made an electron is freed from the graphite electrode releasing the lithium-ion into the electrolyte. The ion then travels through the separator and into the lithium electrode. The lithium and electron (from the circuit) meet in the lithium electrode, where they react with MO_2 to make $LiMO_2$. This process is described using Equation 2.1 [14].

$$C_6 + LiMO_2 \iff Li_xC_6 + Li(1-x)MO_2 \tag{2.1}$$

Here the left hand side denotes the discharged state of the cell and the right hand side denotes the charged state. Equation 2.1 corresponds to the process shown in Figure 2.1. Lithium has become the dominant technology in automotive application due to its high energy and power density in comparison to lead acid and nickel metal hydride alternatives. These previously played important roles in

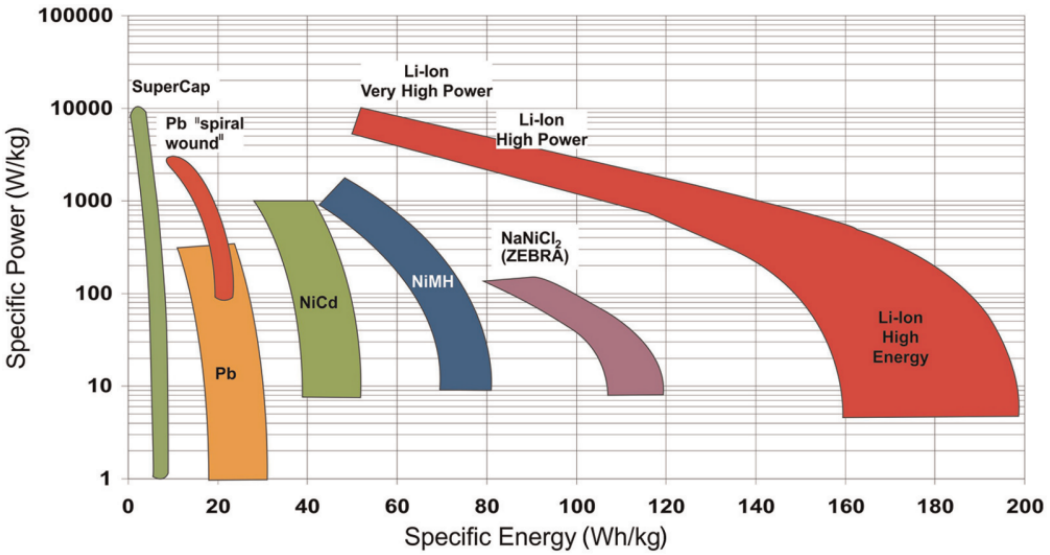

Figure 2.2: Ragone diagram showing energy and power density for a range of cell technologies is demonstrated [15].

early electrified vehicles such as the G-Wiz [78] (lead acid EV) and Toyota Prius [79] (NiMH HEV) but have since been superseded by lithium-ion. Super capacitors and hydrogen also play roles in modern energy storage. Super-capacitors offer high power density but low energy density, whilst hydrogen offers a more conventional refuelling experience at the cost of its production and storage being complex and expensive. These technologies (except hydrogen) are compared in the Ragone diagram shown in Figure 2.2. Hydrogen is excluded as its energy density is in the region of 40kWh/kg in liquid form, and so dwarfs the other technologies shown [80]. Although this is very high it suffers from being much less volumetrically dense and so it is very difficult to store large masses of hydrogen [80].

Research into new lithium based chemistries is ongoing with the objective of increasing energy and power densities. For example Li *et al.* [81] proposed $Li_2Ni_{1/3}Ru_{2/3}O_3$ which demonstrated cell level energy density in the region of 1000Wh/kg. While these technologies will undoubtedly increase the range of electric vehicles it is likely that some level of thermal management will always be required, and even if this is not the case, the vehicle range will always benefit from improved cabin heating efficiency. Improvements in battery technologies will not therefore change the general optimisation framework or methods presented in this thesis, however specific details within the methodology may need adjusting. For example in the case where a chemistry was unaffected by temperature then in Chapter 8 the battery would be removed as a heat sink and all effort would be concentrated

on optimising the heat delivery to the cabin.

Alternatively, trends may shift towards lithium-ion cells with solid state electrolyte. These offer improved stability and safety compared to liquid electrolyte, but typically only become operational at high temperatures. For example $LiBH_4$ requires heating to 120°C to become operational, at lower temperatures the electrolyte conductivity is too low to be useful. This will impact the thermal management of the vehicle as the battery temperature may need to be maintained. Alternatively it may be possible to extract some heat from the battery while its internal resistance ensures that it maintains a necessarily high temperature. Either option can be accounted for by small adjustments to the methodology. If the battery temperature can be maintained and does not need any management from the onboard HVAC, then the battery can be discounted from the thermal management system and efforts can be focussed on minimising cabin heating energy consumption or maximising comfort.

2.1.2 Capacity

In this section the effects of cold temperature on the battery's energy storage capability are discussed, including reviews of experiments investigating the problem. As ambient temperature drops, the internal resistance of cells increases, which causes a drop in terminal voltage when compared to operation at room temperature [77]. Since the energy capacity of a cell (in Wh) is given by the product of the nominal open circuit voltage (OCV) and Coulombic capacity, reducing terminal voltage leads to a reduction in the amount of energy the battery can actually supply. It also means more current has to be drawn for the same power requirement, depleting the battery faster. The Coulombic capacity of a cell is also reduced at low temperatures.

Jiang Fan [82] tested a selection of 18650 cells to investigate how capacity is dependent on ambient temperature. '18650' denotes cylindrical cells where the number refers to the size of the cell; 18mm in diameter and 65mm in length, with 0 denoting its circular shape. This is one of the first examples of investigations into the impact of low temperatures on a cell's capacity. The cells used were produced by 5 different manufacturers (the names of the manufacturers were not explicitly stated). The cells were discharged at a rate of 0.2C, where XC is the current required to fully deplete the battery in $1/X$ hours. During these discharge tests they found a range of capacity reductions depending on the cell manufacturer. At -20°C the reductions ranged from 12%-33%, and at -30°C and -40°C there were 30%-98% and 70%-100% reductions in capacity respectively. They concluded that the cells which showed very little capacity, or 0% capacity, did so due to their electrolyte freezing. This paper served as an introduction to capacity related problems caused

by operating cells at low temperatures.

More recently, in 2013 Ji *et al.* [9] developed an electrochemical thermal (ECT) model to be compatible with sub zero operation. In the paper they claim that despite such models already existing, they had not been validated below 0°C. To validate their model they tested a set of 18650 cells with a nominal capacity of 2.2Ah. During the capacity testing 1C discharges were performed at 45°C, 25°C, 0°C, −10°C and −20°C. Between the highest temperature and lowest temperature there was a 32% reduction in capacity. The results of their tests are presented in Figure 2.3. The model they used relied on knowing the battery temperature through the cycle, which was achieved using a thermal model of the battery. Specifically, the authors used a lumped thermal model, which uses a single heat capacitance for the cell and assumes convection is the only mode of heat loss, this is commonly used in literature. They found that the model as a whole was sensitive to h, which is the coefficient that describes convective heat flow to ambient, defined by,

$$h = \frac{Q}{T_{cell} - T_{ambient}}. \tag{2.2}$$

Here h is used to vary the cells thermal conductivity to ambient. Their results varied significantly with the choice of h, as can be seen in Figure 2.3b, but through validation data they found that $h = 28$W/K was the best fit, corresponding to a 38% loss in capacity. This highlights the importance of correctly parameterising the thermal interaction between cells and ambient when modelling cell capacity as a function of temperature.

In 2014 Jaguemont *et al.* [10] experimented with low temperature discharges of prismatic lithium-ion cells. They discharged the cells at a range of temperatures using a selection of discharge rates and recorded the cell's available energy capacity. The temperatures used were 25°C, 0°C, -10°C and -20°C, and discharge rates of 0.5C, 1C and 3C. The battery pack they were experimenting on was a 100Ah pack from a PosiPlus bucket truck. The pack is used to power the hydraulics for lifting the bucket, rather than using the engine and burning fuel. This paper is in a series where the authors are optimising thermal management for this pack and vehicle. The authors also suggest that this kind of research is currently limited to small applications and they believed this is the first example of expanding to pack size. In their investigations they found that, as expected, the available energy capacity fell with ambient temperature. While discharging at 0.5C, 40% of the energy capacity was lost moving from 25°C down to −20°C. At −20°C, 30% of the energy capacity was lost compared to room temperature when discharging at 1C, compared to 40% loss at 0.5C. This increase in available energy happened because

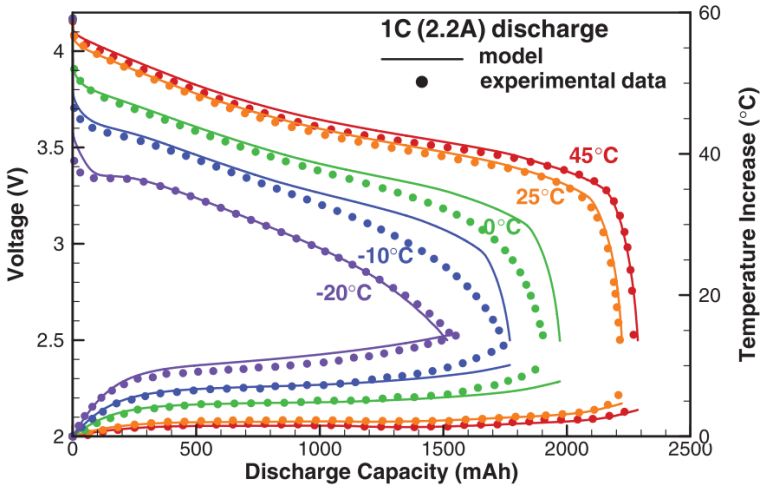

(a) Cell OCV through discharges at a range of temperatures.

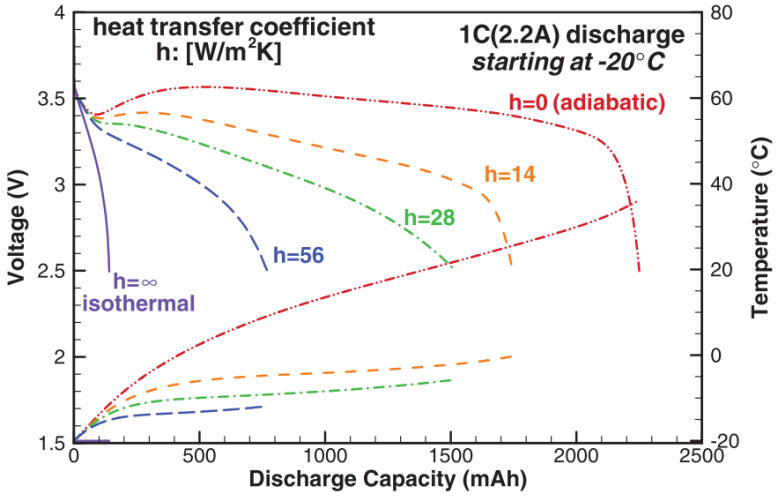

(b) Cell OCV through discharges at a range of temperatures.

Figure 2.3: Figure 2.3a shows the discharge capacity during a 1C discharge at various temperatures. Figure 2.3b. shows the effect that varying heat transfer coefficients to ambient have on the cells temperature, and therefore capacity during a discharge. Both are part of a report by Ji *et al.* [9]

the increased current caused sufficient internal ohmic heating that the battery was not as affected by the cold ambient conditions. However when the experiment was performed at 3C, the same benefit was not found. During the 3C, $-20°C$ test the battery quickly reached the minimum pack voltage and the test was terminated.

The problem of low temperature cell performance is something that is known to manufacturers. Some of them choose to present their own characterisation of low temperature performance on publicly available data sheets. Figure 2.4 shows information on cell capacity at different temperatures presented by two cell manufacturers, Dow Kokam (lithium polymer pouch cells) and Panasonic (lithium-ion 18650 cells). From these figures it can be seen that when reducing the temperature from $40°C$ to $-20°C$ the Dow Kokam cells lose approximately 30% of their high temperature capacity, whereas the Panasonics lose approximately 97% of their capacity. As discussed by Fan *et al.* [82], it is likely that the electrolyte froze during this experiment. A more recent version of Panasonic's cell shows better performance, this can be seen in Figure 2.5.

2.1.3 Peak Power Capability

To begin this section, appropriate pack sizing is discussed which gives context to the consequences of power reduction resulting from the low temperature operation of lithium-ion cells. In general the battery pack requirements vary between EVs, PHEVs and HEVs. For EVs the pack needs to have a high capacity to give it a usable range, while hybrid vehicles tend to use smaller packs, but require high power density. A summary of pack requirements can be found in Figure 2.6 [16]. Here the diagonal lines are C-rate; from inspection of Figure 2.6, electric vehicles are positioned across 2.5C to 6C. This indicates the C-rate while peak power is being drawn from the battery. Using this, 4C is chosen to exemplify the capability needed from a battery pack designed for an EV. The graph also shows that as electrification decreases, required C-rate increases. This means that the electrified part of mild HEVs (MHEVs) and HEVs may suffer more at low temperatures, although the vehicle performance may be less affected as it relies more heavily on the internal combustion engine. In some cases stop start vehicles rely on lithium-ion batteries for their starter motor; extremely low temperatures may prevent these vehicle from starting, in which case some thermal preconditioning may be needed. As for pure electric vehicles a reduction in usable C-rate may result in a loss of performance.

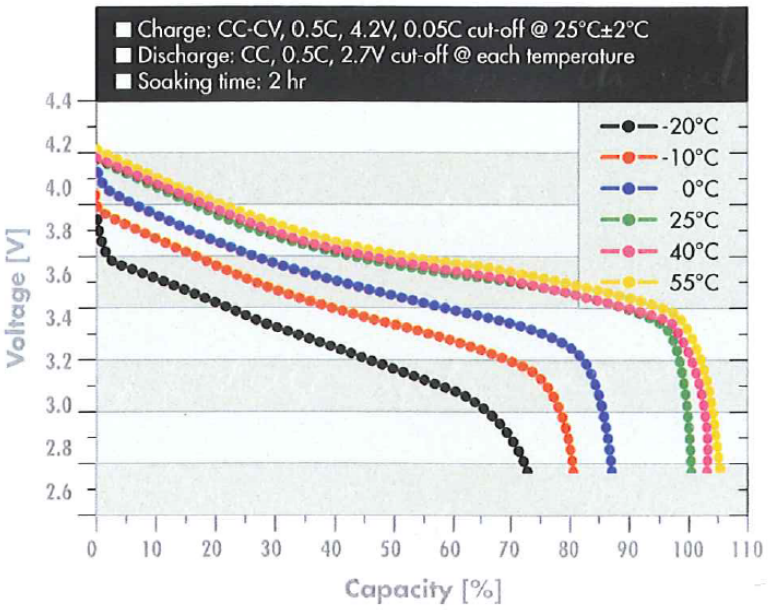

(a) Dow Kokam published battery performance.

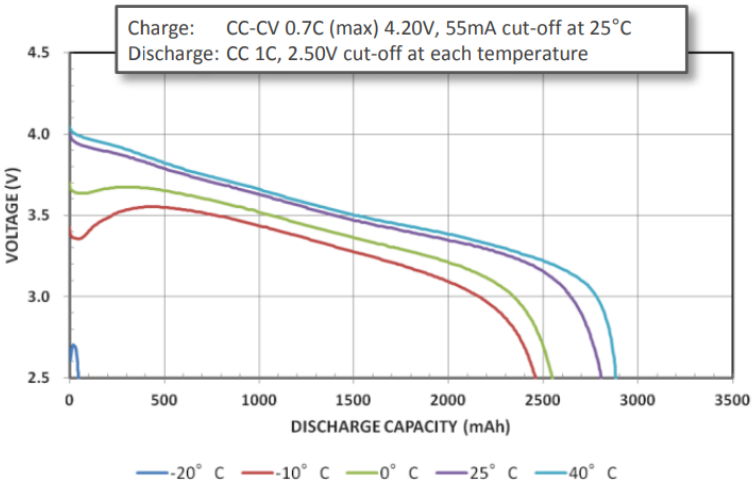

(b) Panasonic published battery performance.

Figure 2.4: Cell capacity as a function of temperature from two cell manufacturers, Dow Kokam (2.4a) and Panasonic (2.4b)

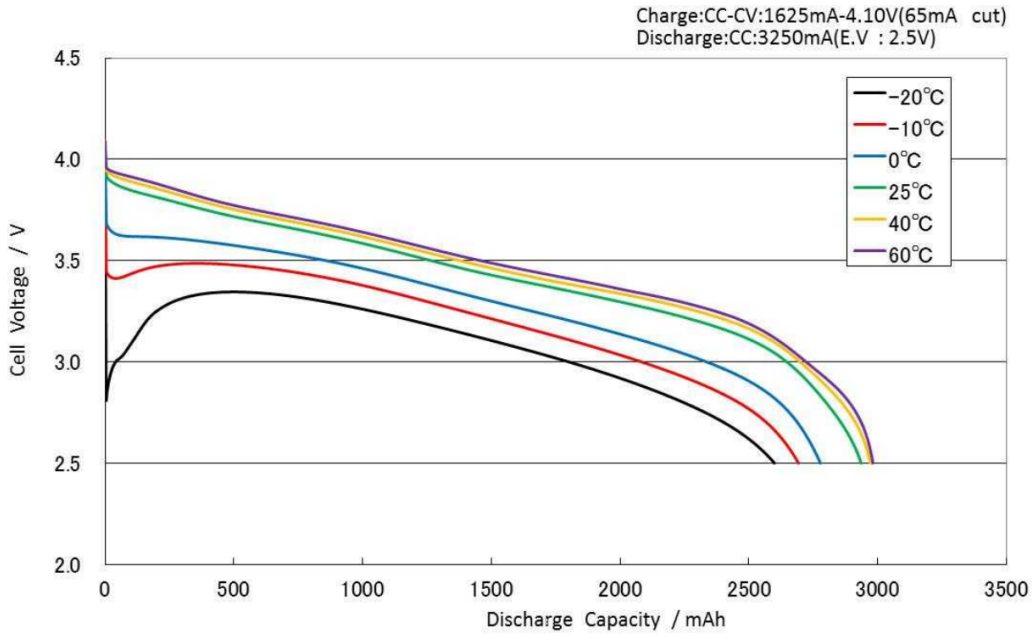

Figure 2.5: Cell discharge graph showing capacity as a function of temperature for Panasonic's NCR18650BF cell [13].

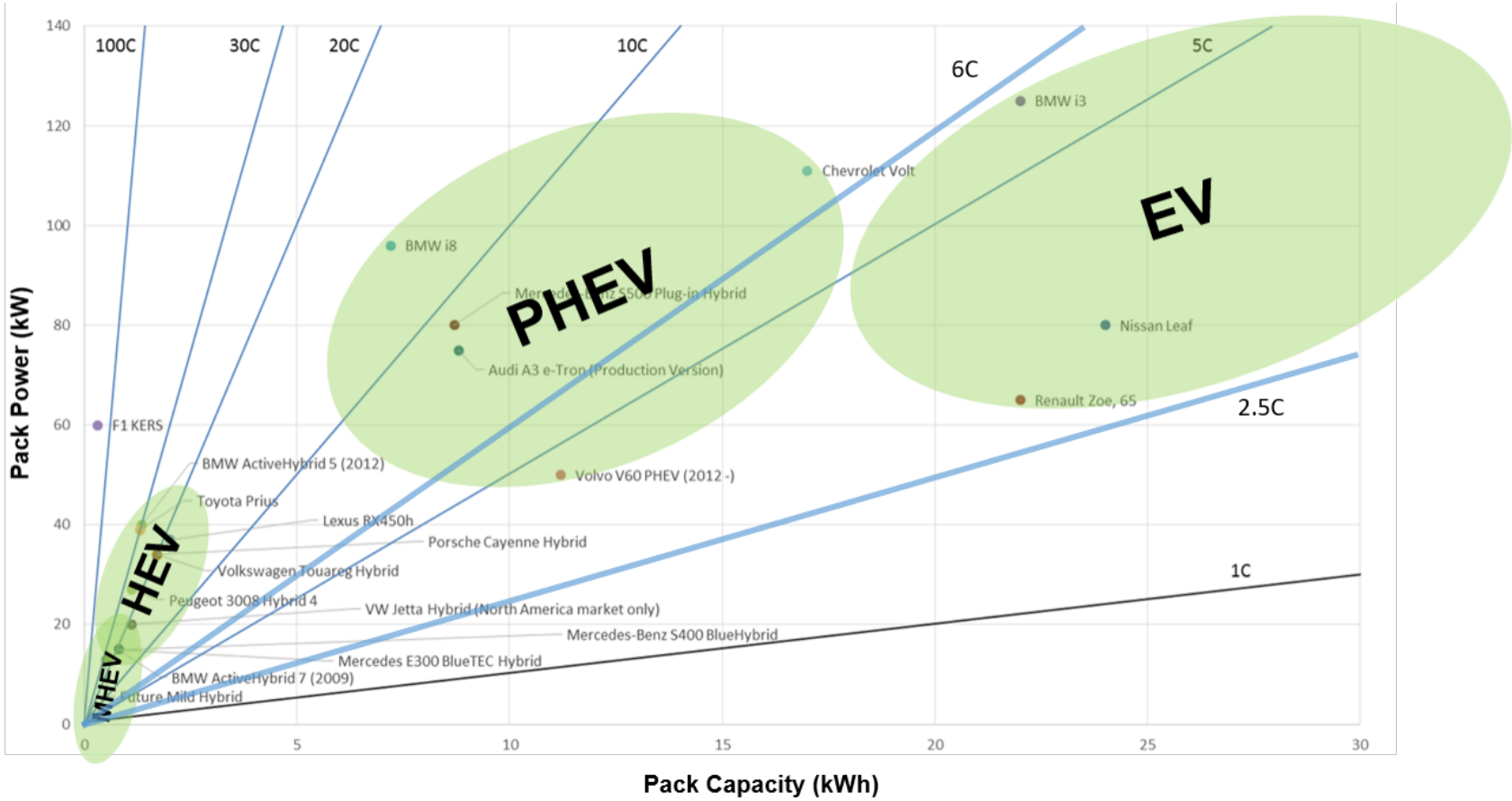

Figure 2.6: Here the different vehicle classifications are grouped in terms of pack size (kWh) and power (kW), where specific examples of available vehicles are given. C rate lines are given by the ratio of peak power to pack size [16]. The green areas represent the design region in which the classification is likely to exist.

In 2011 Zhang *et al.* [17] investigated a battery's peak power capability (PPC) using pulse tests. These were performed at 45°C, 25°C, 0°C and −10°C. When a fresh cell was tested at −10°C it experienced a 32% reduction in PPC when compared to cells held at 45°C. This can be seen in Figure 2.7. Here the cells being tested were prismatic $LiFePO_4$ cells designed for application in a hybrid vehicle. In 2012 Cho *et al.* performed an investigation into the effect that discharge rates at different temperatures have on a cell's power performance [75]. The cells they chose to investigate had a $LiCoO_2$ cathode and were designed for use in hybrids. 10 second pulses of between 0.2C and 21C were drawn from the cell at various temperatures. The cell was first tested at 25°C, where the cell was able to sustain a discharge rate of 21C for the full 10 seconds, however when the cell temperature was reduced to −5°C the cell could only sustain 5C without reaching minimum voltage, equating to a 76% reduction in power capability. While 5C would be perfectly adequate for EV operation, these cells are intended for HEV use and so this falls well below the 10C-100C operating window seen in Figure 2.6. In 2016 Zheng *et al.* [76] reported on results of an investigation into estimating power capability reduction of lithium-ion batteries at low temperatures. The cells used were $LiMn_2O_4$ cells with 8Ah capacity and 200A maximum discharge current. They used the hybrid pulse power characterisation test as proposed by the Idaho National Engineering and Environmental Laboratory [83]. Their research showed that at −20°C there is a minimum of 90% reduction in power capability compared to 50°C. Additionally the authors claim that at −20°C a maximum discharge rate of 3.5C could be achieved. While this is sufficient for EVs, it falls below the requirements of the intended use case of HEVs.

In the examples given the cell chemistries investigated have all been typical of power cells, opposed to energy cells, the difference being the focus on power density (kW/l and kW/kg) rather than energy density (kHh/l and kWh/kg). Power cells are typically used in HEVs where power delivery is the primary performance priority when specifying a battery, whereas EVs will typically use chemistries best for energy storage to maximise their range. For example the Dow Kokam cell from Figure 2.4a is an energy cell more applicable to EV use cases; it has a maximum discharge pulse current of 12C [11]. This is approximately half that of the cell used by Cho [75], and a fraction of the capability of the cells tested by Zheng [76]. To compare against another manufacturer, A123 claim their 18650 power cells can maintain a continuous discharge current of 20C [84]. During a search of the literature no examples of energy or EV application cell power capability tests were found. However by assuming that the power reduction in energy cells is equivalent to that

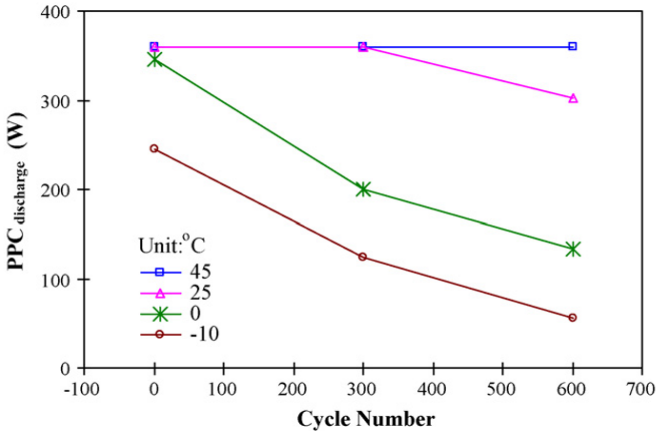

Figure 2.7: Pulse Power capability of cells held at different temperatures after 0, 300 and 600 pulse cycles (3C charge and discharge) [17].

of power cells, an estimation of the deficit can be made. A typical C-rate for a power cell is 20C, Zheng reported a C-rate of 3.5 could be achieved at $-20°C$, corresponding to an 82.5% reduction. If the Dow Kokam cell experienced an 82.5% reduction in maximum discharge rate, then it would be limited to approximately 2C. In the automotive world this limitation is likely to prevent maximum power use when compared to the typical maximum C-rate of 4C from Figure 2.6. For example, the maximum power generated by the Tesla Model S, which is known for being a very fast electric vehicle, requires a current of 4.8C [3]. This is used to deliver $0-60$mph times as little as 2.7s, and hence will only be used in extreme circumstances.

There is little evidence to suggest that users are concerned by the power capability of their vehicles at low temperatures. There is also no literature in which a vehicle has been tested using high C-rates at these temperatures. Typically if the ambient temperature is $-20°C$ then the roads may have ice on them and users will drive more carefully, therefore not reaching the cold temperature limitations of the vehicle. If the roads and tyres are cold, it is also unlikely that full power could be used without the tyres losing traction and compromising the vehicles stability. Additionally, in a report suggesting the revision of the definition of EOL, Saxena points out that for a typical EV a 70% reduction in power could be sustained with the vehicle still being able to complete representative drive cycles (UDDS, HWFET, US06) [35]. These reasons may explain why it is not common to hear concern of power reduction at low temperatures, especially when compared to the more pressing concern of range as covered in Section 1.4.1.

2.1.4 Ageing

One of the key motivations for battery thermal management is to prevent ageing, especially when charging [85, 86]. To prevent ageing at sub zero temperatures the current into the battery should be reduced [18, 85]. In battery electric vehicles this increases time taken to charge the battery, or could reduce utilisation of the regenerative braking system. Since EOL is defined at 80% [47] it is imperative that batteries are prevented from ageing since short battery life spans could cost manufacturers in warranty payouts.

There is a strong consensus in the literature that lithium plating as a result of sub zero charging is the leading loss mechanism of cycle-able lithium at low temperatures. This has been shown in studies such as one carried out by Waldmann *et al.* [45]. Here the authors recorded capacity loss of 18650 cells at $-20°C$ being subjected to a 1C charge then 1C discharge cycle. They showed that the cells aged 7.5 times quicker at $-20°C$ compared to $0°C$, then dismantled the cell. They claim to have visibly seen lithium deposition on the anode, causing the loss of cycle-able lithium and reducing capacity. Zinth *et al.* [46] were able to show through neutron diffraction that low temperature charging was causing a growth in diffraction peaks corresponding to carbon lattices containing lithium, which they correlated to capacity loss. From this they concluded that lithium plating in the cell was the dominant cause of low temperature capacity loss. In other literature Petzl *et al.* [47] also concluded that lithium plating was the cause of capacity loss. They came to this conclusion by analysing voltage profiles from the discharge of cells after various numbers of cycles, showing that the majority of capacity loss happens in the high voltage region attributed to lithium deposition on the anode. Here three different authors have used different methods to come to the same conclusion on the process of ageing as a result of sub zero charging.

To summarise the findings from literature concerning battery ageing, it seems apparent that researchers agree that lithium plating is the main concern for cell operation at low temperatures. Although lithium plating is a danger while charging, it appears that the consequences of discharging are either negligible or poorly understood, as reflected by the lack of literature found on discharging at low temperatures. It is clear that charging at low temperatures results in accelerated ageing, as proven by the 95% reduction in cycle-able life as found by Petzl *et al.* [47]. Avoiding ageing by charging can be done in two ways; increasing the battery temperature until ageing is not a concern (e.g. $10°C$) or reducing the charge rate to a safe level [18].

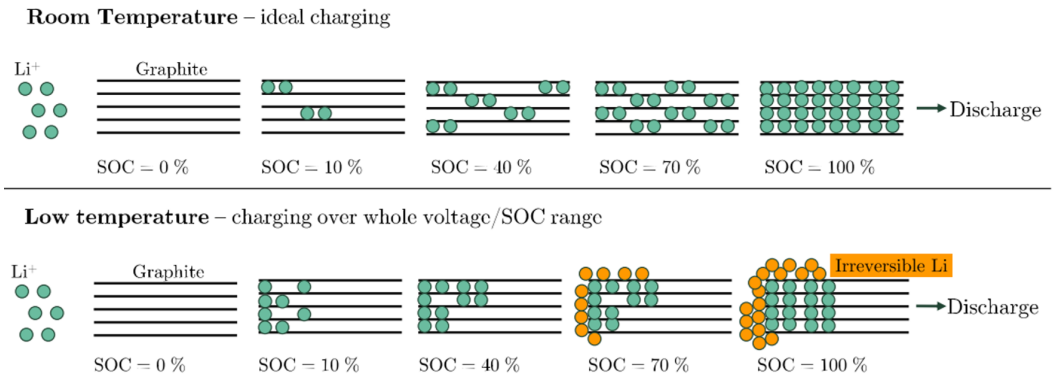

Figure 2.8: An illustration of the difference between ideal and low temperature charging [18].

2.1.5 The cause of poor performance at low temperatures

Many researchers have investigated the cause of poor performance of lithium-ion cells at low temperatures. One early example of this research is Huang et. al who, in 2000, investigated charging capacities of two different materials to be used as the graphite electrode [87]. They found two mechanisms which cause increased resistance and reduced Coulombic capacity at low temperatures; low Li-ion mobility reducing transport properties in the electrolyte interfaces and poor Li-ion diffusivity in the graphite electrode. While Li-ion mobility is important for resistance increase other authors have concluded that Li-ion diffusivity in the graphite electrode becomes the dominant cause of resistance increase at low temperatures. Here diffusivity refers to the ability of lithium-ions to diffuse within the carbon electrode, with poor diffusivity causing an increase in density of ions toward the surface of the electrode. The resistance attributed to this factor rises exponentially as temperature drops, and below $-10°C$ it dominates the total cell resistance [8, 88–90]. This exponential resistance increase is used to explain the poor power capability at low temperatures, poor diffusivity also explains poor Coulombic capacity and increased ageing since it hinders lithium extraction and injection into the graphite electrode. Poor extraction of lithium from the graphite electrode results in the cell reaching minimum operating voltage before all the lithium can be freed from the graphite. Poor injection prevents lithium dispersing into the graphite electrode, resulting in a high concentration of lithium on the graphite surface, this can lead to the formation of metallic lithium on the electrode surface (lithium plating). Poor diffusivity and lithium plating can be visualised in Figure 2.8.

2.1.6 Lithium-ion high temperature challenges

It should be noted that lithium-ion cells should also not be operated at excessively high temperatures, with the key concern being the impact that this has on battery ageing, and in extreme cases, catastrophic failure.

One of the benefits of increasing the temperature within the cell is a reduction in internal resistance [91]. This reduces voltage drop when current is drawn, and so reduces losses within the battery, increasing power availability and efficiency. However, an increase in temperature within the cell also leads to an increase in internal energy available for chemical reactions within the cell. These reactions can cause the formation and growth of the solid-electrolyte interface (SEI). This is a layer of residue which can form on either electrode and reduces lithium-ion injection and extraction from the electrodes, hence increasing resistance and reducing performance. Additionally, the SEI can be composed of compounds which themselves contain lithium. This represents a process of irreversible lithium loss and capacity reduction, causing the cell to prematurely reach its end of life [45].

In addition to increased cell ageing, high temperatures can also lead to the abrupt failure of a cell. Mechanisms for the cells failure include;

- dendrite growth leading to the puncturing of the separator and causing a short circuit,
- separator pores closing due to the separator melting, leading to extremely high internal resistance,
- gas generation through the evaporation of organic materials, leading to the cell bloating and potentially rupturing.
- separator melting and allowing electrode contact leading to a short circuit and potential thermal runaway,
- separator shrinkage leading to electrode contact at the edges, causing a short circuit and potential thermal runaway [92].

These process cause a complete failure of the cell and in some cases can lead to extreme safety risks such as fires and the release of hazardous chemicals [92].

Due to the effects of ageing and the potential for catastrophic battery failures many authors are conducting research into the thermal management of lithium-ion batteries at high temperatures [73, 93, 94]. While the focus of this thesis is on low temperature challenges related to lithium-ion operation, it is acknowledged that

there are still challenges at higher ambient temperatures. Hence, the methods contained within this thesis will be generic to thermal management and not specific to the low temperature regime exclusively. Where appropriate descriptions will be given of how the procedures used in this thesis can be adapted to address thermal management questions at higher ambient temperatures given the same vehicle architecture.

2.1.7 Concluding remarks regarding the operation of Lithium batteries at low temperatures

It is clear that operating a battery at low temperature impacts the performance that can be expected. The challenges faced include; the available capacity reducing by up to 50% at $-20°C$, the power capability being reduced by approximately 80% which could lead to vehicles not being able to produce their maximum power, and lithium plating potentially restricting charging rates increasing charge time by a factor of 10 [18]. It would also appear that these effects are symptoms of a common underlying cause; poor lithium diffusivity in the graphite electrode at low temperatures. Clearly research into improving low temperature diffusivity should be carried out as it seems the problem is well understood but solutions are not forthcoming. Despite this, the concern for this work is vehicle operation as a whole, including HVAC. Hence by finding an efficient way to heat the battery the symptoms of poor diffusivity will be mitigated, including, and paramount to this research, capacity reduction.

2.2 Cabin

Vehicles being used in cold climates must maintain a certain level of temperature and humidity in the cabin for two reasons. Primarily cabin temperature needs to be high and humidity low in order to prevent windows fogging. This is the safety perspective of climate control where the EU have regulations and targets on the ability of a vehicle to clear its screen of fog, mist and ice [95]. Secondly, the cabin should be held at a comfortable climate for the driver and passengers. Heating ventilation and air conditioning (HVAC) is the largest auxiliary load on electric vehicles. Typically the HVAC system consumes between 4.5kW and 7.8kW from the battery to heat the cabin [19, 40, 96]. This heat requirement could easily be met by the energy wasted by an internal combustion engine (ICE) used in conventional vehicles and HEVs. However the electronics in PHEVs and EVs do not waste as much heat. For example an electric motor is approximately 93% efficient [42], which means during a WLTP drive cycle, with a mean energy consumption of 17.5kWh/100km [97], the

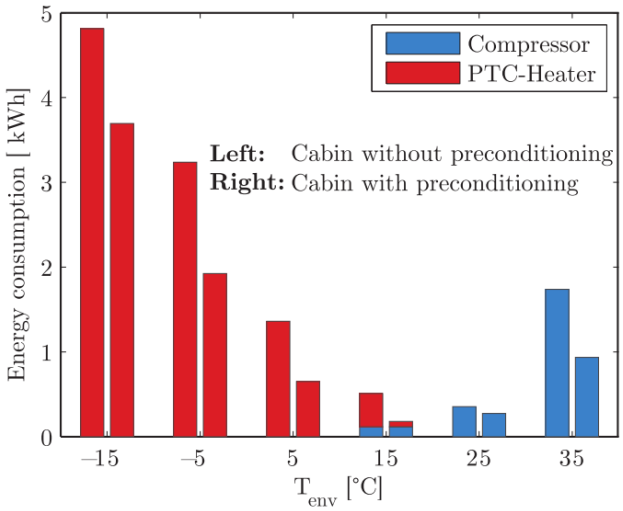

Figure 2.9: HVAC energy consumption over a range of temperatures as simulated by Enthaler *et. al* [19]

motor would waste an average of 500W.

Enthaler et al. used simulation to investigate the cabin heating load as a function of ambient temperature, which they used to improve a range prediction algorithm [19]. They assumed a small vehicle with a range of 150km and average energy consumption (for traction) of 15kWh/100km, which was simulated completing an unspecified highway drive cycle which took 38 minutes. The results of their simulations can be seen in Figure 2.9, where at $-15°C$ the HVAC energy consumption was approximately 4.8kWh corresponding to an average power consumption of 7.6kW.

The cabin has three modes of heat exchange; convection through panels to ambient, radiation and exhausted cabin air. Zheng et al. discuss how these can be approximated, leading to a method of calculating the required heating load for a cabin. In their work they focus on the cooling load under hotter conditions, however the majority of the work is transferable to heating under cool conditions as it is dominated by convection which is dependent on absolute temperature difference only. Their work showed that when cruising at 80km/h, the cabin requires 7.8kW of cooling, of which 2.4kW is exhausted from the cabin, and the remainder is lost due to convection and conduction through panels.

The research presented by Enthaler *et. al* and Zheng *et. al* shows the demand that cabin thermal management puts on the HVAC system [19,98]. Enthaler predicts a heating load of 7.6kW, which can be used as representative of cabin heating. To put this into perspective, the Jaguar I-pace uses approximately 225Wh/km [99]. So

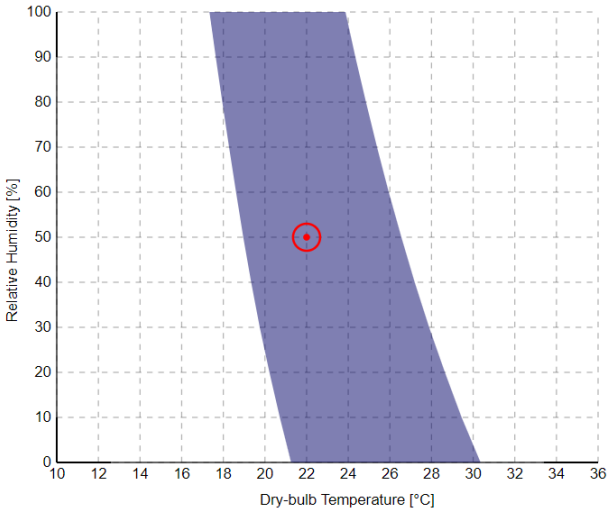

Figure 2.10: The shaded area shows the acceptable comfort zone in terms of relative humidity and air temperature, given by dry bulb temperature. It is assumed the occupant is wearing typical winter clothing. Graph has been created using CBE comfort tool from [20]

if the heating was to be run on full power (assume 7.6kW) for 15 minutes then that would be equivalent to 1900Wh, or approximately 8.4km of range lost. Furthermore, if it is assumed that the vehicle was averaging 80km/h in that time, then it would have covered just 30km using a total of 4500Wh for traction and 1900Wh for heating accounting for 30% of total energy consumption. This would lead to a 30% reduction in range before accounting for the additional effects of low temperature on the battery. The combination of these two affects are discussed in Section 2.3.

2.2.1 Cabin personal comfort

The American society of heating refrigeration and air-conditioning engineers (ASHRAE) have documents stating the acceptable temperatures for the cabin to be held. These are summarised here but can be seen in more detail in [100]. The standard is used to predict what conditions occupants will find comfortable in man-made environments. It is therefore applicable, but not limited to, cars, ships, planes, and buildings.

The comfortable region can be summarised by the graph in Figure 2.10, the shaded region of which shows where most people would find thermal comfort. As can be seen in the figure caption, the graph is representing the acceptable cabin conditions for an occupant wearing typical winter clothing and exerting little physical effort. A person should be able to stay idle in these conditions for an indefinite time

period, and remain comfortable. The red dot in Figure 2.10 represents conditions that an occupant will find neutral, not too cool or warm. Using this information a set point temperature of 22°C can be chosen, as the occupant will be comfortable regardless of humidity, allowing humidity to be removed from consideration.

Although cabin heating is a relatively simple problem to understand compared to the battery, it will still have a significant impact on range. It has been seen that the heating requirement to keep the cabin comfortable and safe is up to 7.6kW [19].

2.3 Complete range loss

The impact of cold climates on heating requirements and battery performance has been discussed. This section focusses on the combined impact and the effect on a vehicles range. As discussed by Reyes *et al.* [22], studies on vehicle level range reductions are limited. While some studies exist there is also a lot of discussion on the subject in the form of blogs, media and anecdotal evidence.

In a study by Meyer *et al.* [21] the impact of the operation of battery electric vehicles in cold climates was considered. Three consumer market EVs were tested over five different US standard drive cycles, ranging from steady state highway driving to heavy traffic city driving. The vehicles were tested on a rolling road in a climate chamber, but the specific vehicles used were not disclosed. Full range and abbreviated tests were carried out at 3 temperatures; 20°C (with heating off), −7°C (with heating on and off) and $-18/-20$°C (with heating on). The result of this study was a maximum range reduction of 60% at $-18/-20$°C with heating on compared to 20°C with heating off. Furthermore, at −7°C turning the heating on led to an additional 25% drop in range when compared to turning the heating off. These results can be seen in Figure 2.11. This paper shows the impact that heating has at low temperatures, but it is unfortunate that they were not able to test heating off at −20°C.

Reyes *et al.* [22] performed a similar study, but testing minimum range in the real world. They drove a 2012 Nissan Leaf and a Mitsubishi MiEV around the streets of Winnipeg, Canada. The vehicles were driven until the battery was depleted. The tests took place over a temperature range of 28°C down to −26°C. In both cars the heating was used, with the target temperature set to 21°C in the Nissan. The Mitsubishi did not have climate control, so the heating was on full for most of the time, and turned down to suit the driver. Hence the results from the Nissan Leaf are more robust. For the Nissan Leaf, the maximum ranges achieved

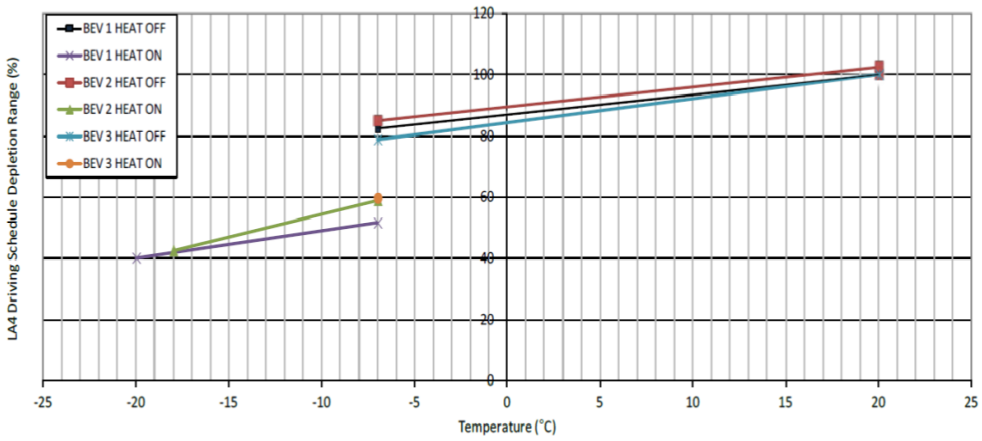

Figure 2.11: Here the range of EVs performing US drive cycle LA4 at various temperatures is presented as part of a study of the impact of low temperatures on EVs by Meyer *et al.* [21]. LA4 is a cycle which represents urban or city driving.

were $162-165$km at an ambient temperature of 28°C. At -26°C the range of the Leaf dropped to $43-45$km, a $65-70\%$ reduction in range due to the combined effect of reduced battery capacity and extra drain from the heating system. These results can be seen in Figure 2.12. They also found that at the lower and higher ends of their testing the range started to plateau. At the lower end this indicates that the heating system is dominant for range reduction. This can be concluded since below a certain temperature the heating needs to be on full power continuously, therefore any further range reduction is only caused by thermal effects on the battery.

In a report be Lindgren *et al.* [96] the authors set out to evaluate the impact of operating in sub zero climates. To do this they used driving data from Finland's traffic survey to simulate the operation of 212 different vehicles. To quantify the impact of the cold they measured vehicle efficiency in km/kWh. The authors use this set up to assess the benefits of preheating the cabin and battery, and the impact of improved charging infrastructure. Their initial findings were that the fleet would experience a reduction in vehicle efficiency of approximately 18% when operating at -10°C. However this does not correspond to an 18% reduction in range since they did not consider reduced battery capacity at low temperatures. They did however consider the need to heat the battery, it is therefore assumed that the battery stays warm enough to negate the effects of capacity reduction. In summary this report indicates that if the battery is kept warm, so that capacity reduction is not an issue, then range reduction will be 18%.

Both Reyes *et al.* and Meyer *et al.* used real cars under test conditions; by contrast Allen from Fleetcarma [101] published a report on the accumulated data

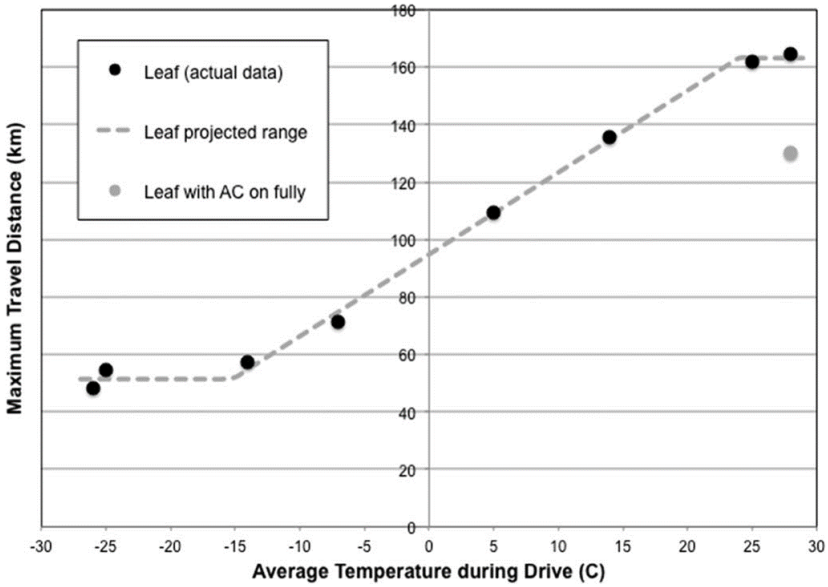

Figure 2.12: The range achieved at different temperatures by Reyes *et al.* [22] while operating a Nissan Leaf in the city of Winnipeg, Canada.

of more than 5400 Nissan Leaf journeys made in Canada over a 2 year period. In the data the ambient temperature ranged from 40°C to −26°C, with the maximum range of 105km (calculated from average vehicle efficiency) being achieved at approximately 30°C. At −26°C the range was reduced to 58km, 55% of its baseline range. This is a smaller reduction in range compared to the 60% and 70% reductions found by Meyer *et al.* and Reyes *et al.* respectively. One explanation for this could be that drivers are making a choice between range and heating [101], whereas both Meyer and Reyes prioritised heating in the search of minimum range. Another possible reason is that cars being used on a regular basis keep warmer due to thermal inertia, especially of the battery, and thus the effects of low temperatures are not as extreme as in the tests with higher controls. For example, both Meyer and Reyes left their vehicles to soak in the cold [21, 22]. Finally, Fleetcarma base their range estimation on efficiency rather than exhaustively running the vehicle until it is out of charge. Only considering efficiency does not capture the reduction in battery capacity, making low temperature conditions look less detrimental than they really are. Another example of discussion on the effects of low temperature on vehicle range is a news article on the American Auto-mobile Associations (AAA) website [102]. Here they report on a study performed at AAA's research facility in California. An electric vehicle was tested at 24°C and found to have an average range of 105 miles, then when the temperature was reduced to −18°C the range

reduced to 43 miles, a 57% reduction.

In both the AAA and Fleetcarma reports there is an emphasis on how drivers should be aware of the effects of reduced range, and various suggestions of how they can cope. This sentiment is reinforced by a blog on the MIT technology review website [103], where Bulis writes "There are some measures drivers can take to improve an EV's range. But with existing batteries and heaters, some loss of range is inevitable. Researchers are working on technological fixes that won't be ready for years." and "One way researchers might eventually improve cold weather performance....". These statements highlight that researchers are working to tackle the problem, but informs consumers that if they own an EV then they will have to adapt to different usage in cold climates for now. Bulis also acknowledges that the primary problem is the load that heating puts on the battery, as discussed by Reyes *et al.* and Meyer *et al.*. In summary, research has shown a range loss of $45 - 70\%$ when operating at $-18°\text{C}$ to $-26°\text{C}$, a loss which is dominated by the heating requirements of the vehicle.

When quantifying the effect of low temperature on electric vehicle operation the most important metric appears to be the reduction in range. This is reflected in studies such as Meyer [21] and Reyes [22]. It is also seen in the media and blogs, in such places as the American Auto-mobile Association news room [102] and MIT technology reviews [103]. The scholarly literature reports that the range reduction at low temperatures is up to 70% [22]. In the informal literature this translates to a perception that electric vehicles are bad in low temperatures [103], and that people should be aware and able to deal with it [102]. However this concern seems to be limited to range, there is very little mention of power capability and no mention of ageing in informal literature. Concerning the power capability, while it has been shown that on a cell level this could be a problem, as discussed in Section 2.1.3, it is probably rare that full power is demanded if ambient conditions are $-20°\text{C}$. As for ageing, it is likely that the reason the media have not covered ageing at low temperatures is because it has not yet become an issue. Hence the maximum range of the vehicle will be the most effective way to quantify the impact of low temperature operation.

It seems that when operating in cold temperatures there is a minimum range reduction of approximately 18% [96]. This corresponds to the case where the battery has sufficiently high thermal inertia to overcome capacity loss from low temperature, by not cooling down to the ambient temperature. However, in cases where the vehicle is left to soak, the range reduction can be up to 70% [22]. Currently the public perception of this is that electric cars have a poor range in the cold, and they

need to know how to deal with it. There also seems to be a consensus from Meyer *et al.* [21] and Reyes *et al.* [22] that the range loss at -20°C and below is dominated by the necessity to continually run high levels of heating. An efficient heating system would minimise heating load, while bringing the battery up to a reasonable operating temperature. This would improve the overall range and reduce the impact of sub zero temperatures on the battery's capacity, power capability and ageing.

2.4 Concluding points

- Lithium-ion cells suffer from a capacity loss of up to 50% at -20°C compared to 20°C [13].
- A typical heating load for the cabin at is up to 7.6kW [19].
- Using conventional PTC heating the combination of these factors is a range loss of between 40% and 70% when the temperature is reduced from 20°C to -20°C [21, 22].
- The direction of research should be in providing cabin heat at a lower energetic cost and providing heat to the battery for improved performance.

Chapter 3

Review of Current Thermal Management Solutions

In this chapter current research concerning heating systems is discussed. This includes heating systems and mechanisms which manage battery or cabin independently and combined systems to manage both battery and cabin together. Optimisation techniques within heating strategies are also discussed, covering the best way to manage available heat; this includes an overview of the advantages of key-off thermal management. The direction research has taken regarding thermal management has been identified, and literature has been assessed to explore opportunities for novelty and further progression.

3.1 Battery thermal management

One active area of research in the field of lithium-ion cell thermal management is the mechanism with which heat can be delivered to the battery. This includes consideration of heat pads in contact with the cell [104], internal heating through AC currents [58, 61, 105, 106], heat delivery through air ventilation [61, 104], liquid coolant circuits [107, 108] and heat pipe technologies [109].

The current standard amongst commercially available vehicles is to use liquid coolant to manage heat transfer to the battery. Vehicles which make use of this technology include Jaguar I-Pace, Tesla (various models) and Audi e-tron [110]. Liquid cooling represents the state of the art in thermal management, and will therefore be used as the standard for thermal management in this thesis.

3.1.1 Plugged in strategies

When the vehicle is plugged in there is the opportunity to administer thermal management while charging. Preconditioning the battery has been seen to be an effective thermal management strategy [59,63,96]. Adaptations to the standard constant current - constant voltage charging protocol have also been suggested with the intention of thermally managing the battery [18,85,111]. These techniques are not considered here as the motivation of the thesis is considering the thermal management of the vehicle during operation and attempting to improve the worst case scenario where the battery is cold at the start of the cycle. This scenario caused a 70% range reduction at $-26°C$, as seen in Chapter 1.

3.2 Cabin heating

In conventionally powered vehicles, the low efficiencies involved in burning fuels results in wasted heat; typically 60% to 70% of the energy contained in fuel is lost to heat [112]. In cold climates this can be used to heat the cabin for 'free', i.e. the waste heat has some value. A typical value for the heat power requirement of a cabin is approximately 5kW to 7kW; this is enough to maintain a cabin temperature of $20°C$ when the outside ambient temperature drops to $-10°C$ [40]. However in EVs, where there is very limited waste heat, supplying this heat in cold climates can be problematic.

Despite the reduction in available battery capacity, discussed in Section 2.1.2, when researchers experimented on vehicles in low temperatures, the conclusions indicated that cabin heating was the primary source of range loss. This conclusion was reached by both Meyer [21] and Reyes [22]. Reyes came to this conclusion after observing a plateau in capacity loss between $-15°C$ and $-26°C$. At these temperatures the heating needed to be kept on permanently. Therefore the increase in loss over this range was due to battery capacity loss rather than heating load which, over this range, was comparatively small. On the other hand, Meyer performed a direct comparison of heating on and heating off at $-7°C$. In this study he showed that having the heating on led to a 40% loss in range compared to a 15% loss in range with the heating off. For these reasons research is now being carried out to minimise the impact of heating on vehicle range.

While direct personal heating features exist, and personalised thermal management is an active research area [113–115], these technologies are not considered for two important reasons. Firstly they are supplementary to the cars HVAC system, and so the need for an efficient HVAC system still exists. Secondly, they do not

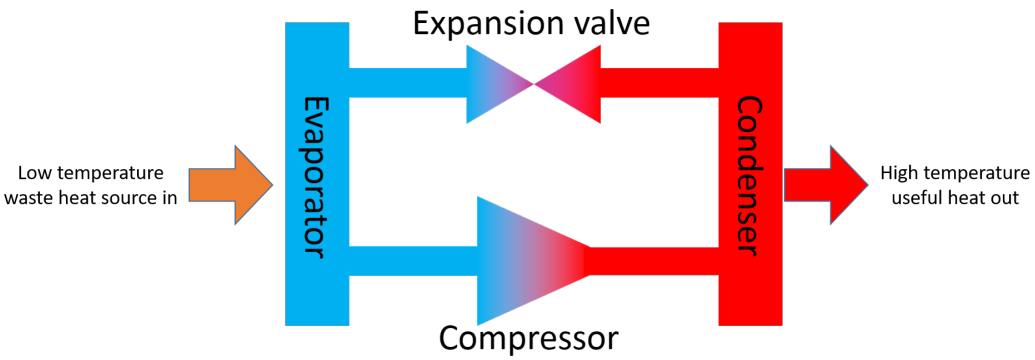

Figure 3.1: Schematic of the refrigeration loop which serves as a heat pump when heat is supplied to the evaporator and extracted from the condenser.

address the heating requirements of the battery. Instead the focus of this research is on a master thermal management system and strategy which addresses the complete vehicle needs.

3.3 Heat Pumps

Typically the heating power for cabins of EVs has been provided by PTC heaters, which have a power demand of around 5kW [116]. Since this power is not provided by waste, but directly from the drive battery in EVs and PHEVs, it has a significant effect on the electric only range and contributes to approximately 50% of the range reduction seen below $-7°C$ [21]. A heat pump can recover waste heat from sources around a vehicle using a coolant circuit, then use a refrigeration circuit to heat it further [64]. This can be achieved with four core components; a compressor, a condenser, an expansion valve and an evaporator [117]. A simple schematic of the heat pump core can be seen in Figure 3.1.

The process for extracting and rejecting heat using a refrigeration cycle is demonstrated in Figure 3.2, where the four core heat pump processes have been identified. Here the curved line indicates the regions in which the working fluid, in this case R134a, is a gas, a liquid, or a mixture. Thermal waste energy is transferred to the evaporator, through either an air to refrigerant heat exchanger (HX) or a coolant to refrigerant HX (referred to as the chiller). In Figure 3.2 this is shown at the bottom of the cycle in the evaporation phase; this increases the working fluids internal energy, known as enthalpy, but not its pressure. When enough heat has been dispensed into the refrigerant at the evaporator, a vapour is created, represented by the bottom right point in Figure 3.2. The vapour is then sucked into the compressor

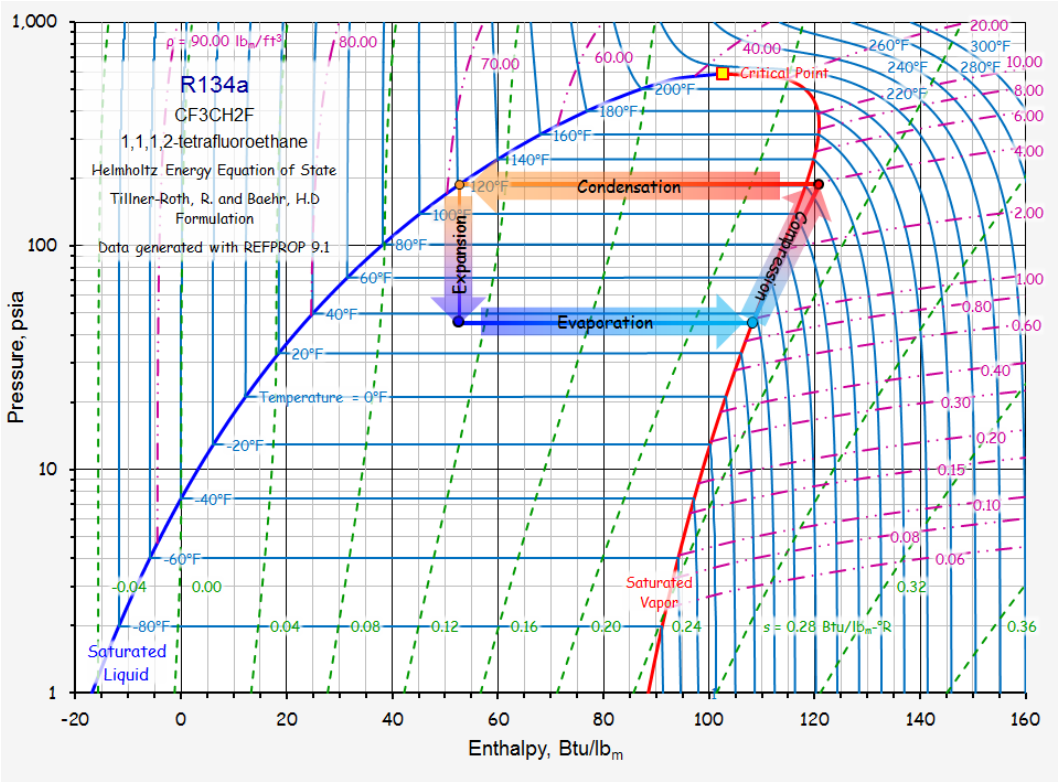

Figure 3.2: The four stages of the heat pump cycle are transposed onto a generic pressure enthalpy diagram. This is used to demonstrate how energy is collected, increased and released within the working fluid of the refrigeration cycle [118].

which increases both its internal energy and pressure. It can be seen in Figure 3.2 that at the end of the compression stage the working fluid is in a state to the right of the curved line, meaning it is entirely gaseous. The high internal energy is then extracted through the condenser; a low temperature medium removes heat from the refrigerant via a HX, causing the refrigerant to liquefy. This can be seen by the arrow at the top of the cycle in Figure 3.2. The liquid refrigerant then passes through an expansion valve which reduces the pressure and returns the liquid to the state (pressure and enthalpy) it was in at the start of the cycle. This part of the cycle is labelled expansion in Figure 3.2.

This is the basis of how a heat pump works. It is agnostic to the source of its heat input, allowing a variety of heat sources to be considered when it is implemented on a vehicle. The performance or efficiency of a heat pump is measured using COP (coefficient of performance), which is defined by

$$COP = \frac{Q_{out}}{P_{compressor}} \tag{3.1}$$

where Q_{out} is the heat extracted from the condenser and $P_{compressor}$ is the power consumed by the compressor. This is an important metric when evaluating heat pump performance and will be referred to throughout this chapter.

3.3.1 Examples of heat pumps outside of the electric vehicle domain

Heat pump technology has been used in water heating systems, or heat pump water heaters (HPWH), in domestic and commercial buildings since the 1950s [65]. The basis for these systems is to collect heat from ambient, or sometimes extract heat through a loop in the ground, then use a refrigeration cycle to intensify the heat. The heat produced can then be used to heat a water tank for example. Research into domestic heating applications is ongoing, with some countries considering large scale heat pumps for district heating of towns and cities [119]. However the application of heat pumps is now being extended to automotive heating [24, 66, 67].

Heat Pumps first appeared in the automotive context in the late 1990s and early 2000s. During this era diesel engines became more popular in small passenger vehicles and engine efficiencies improved. A consequence of this was a reduction in passenger thermal comfort as waste heat from the engine declined [120]. Examples of research into the area of heat pumps for supplementary heat in passenger vehicles includes a paper on the performance of a heat pump used to recycle engine waste heat by Antonijevic *et al.* [121] and the integration of an R 744 (Carbon Dioxide) heat pump into an Audi A4 by Hammer *et al.* [120] in cooperation with Audi and Daimler Chrysler. Despite this research, heat pumps did not become common in passenger vehicles. Diesels were criticised for their particulate output, which lead to exhaust gas recirculation, which reduced exhaust heat losses, restoring some heat for the cabin [122]. When combined with a small auxiliary PTC heater (which became common in ICE vehicles) this solved the cabin heating problem, and the heat pump was temporarily forgotten. However, engine development continued and thermal efficiencies have risen from approximately 33% in the early 2000s to nearly 40% today [123]. This reduction in thermal waste led to Hosoz *et al.* reconsidering automotive applications for heat pumps in 2015, when they published work on a supplementary heat pump to support a 1.9l diesel engine [124].

The system designed by Hosoz *et al.* [124] was capable of recovering heat from different engine components (not simultaneously) and using them as heat sources for the heat pump. The engine used in their test bench was a 1.9l diesel engine from a Fiat Doblo, with a maximum power of 77kW. The authors found that the best configuration of the heat pump used the engine coolant as the heat source.

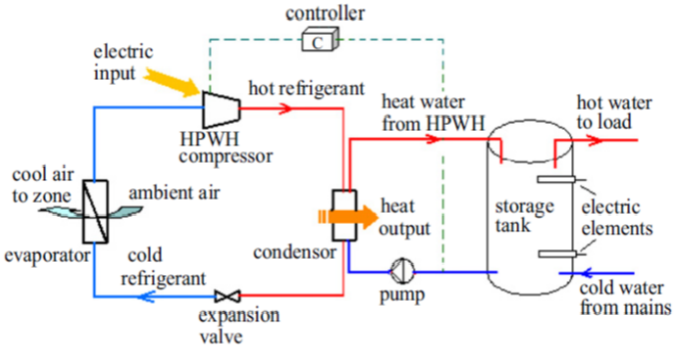

Figure 3.3: An example of a heat pump extracting heat from ambient to be used as a domestic water heater [23].

This arrangement achieved a maximum heating capacity of approximately 7kW and a COP of between 4 and 5 depending on compressor speed (slower compressor → less power → higher COP). This was an improvement over the baseline (no heat pump, conventional heater core), whereas when the exhaust or ambient were used as heat sources, the system failed to exceed baseline performance when the engine was above idle.

3.3.2 Heat pumps in the electric vehicle domain

The results of Hosoz *et al.* were published 5 years after the first sale of the Nissan Leaf, one of the first mainstream electric vehicles. The Nissan Leaf used PTC heaters in the earliest versions, which could considerably reduce range as described in Sections 2.3, to the point where some people would chose to not use the cabin heater and withstand the cold and "dress warmly" [125, 126]. Hence the demand for automotive heat pumps rose again and more work began on developing a heat pump suitable for use in an electric vehicle.

3.3.3 Potential thermal sources for heat pumps

Since heat pumps are agnostic to the heat source used, there is a wide range of components on an electric vehicle which could be considered as heat sources. De Gennaro *et al.* [127] showed that a typical electric vehicle has an average battery to wheel efficiency of 77.8% at −7°C across the NEDC, WLTC and WMTC drive cycles. This can be broken down into losses from the battery, motor and inverter, and the transmission. Williamson performed discharge tests on lithium-ion batteries and found them to be 97.61% efficient [42], although the author did not specify the temperature at which these efficiencies were found. Williamson also tested the

motor and inverter and found them to have a combined efficiency of approximately 93% [42] for motoring. The battery, inverter and motor therefore give a combined efficiency of 90.87%, which does not consider losses through the transmission. In a general study on electric vehicles Helms *et al.* assume a 95% and 90% efficiency for the battery and the motor and inverter respectively [128]. In studies on electric vehicles it is common to assume a transmission efficiency of 95% [128, 129]. The cabin also wastes heat; air is continuously cycled, allowing freshly heated air in and expelling old air. Extracting heat by chilling the cabin exhaust, then using that energy in the heat pump is another way in which heat may be harvested. This has been shown by BMW, who have demonstrated a 35% recovery in the heat from air exhausted from the cabin [130]. Within literature, authors have evaluated a range of these heat sources and have sometimes combined multiple sources. The following section describes a variety of research in this area.

3.3.4 Review of example heat pump architectures from literature

In some examples of the earlier research into heat pumps, only ambient air was considered as a heat source to supply the pump. In a study by Lee *et al.* [66] a heat pump designed for a large passenger vehicle (a bus) was characterised. They achieved a COP of approximately 2.4 while operating at an ambient temperature of 10°C, with a heating capacity of 23kW. This was sufficient to sustain the cabin at 27°C. Considering that the alternative to cabin heating is PTC heaters with a maximum COP of 1, this is a good indication that heat pumps can be an efficient way to heat the cabin. However this particular system could only collect heat from ambient if ambient was above 7°C, as this is the operational temperature of the chiller. As such it would not be suitable for ambient temperatures lower than 7°C.

In 2014 Ahn *et al.* characterised a heat pump system in which they used two sources of heat, ambient air and waste heat from the electric vehicle's motor. They mention that systems like this are rare and progress can be found by incorporating more waste heat. The design of their system is capable of collecting 2.3kW of heat from ambient (at 7°C) and 2.5kW of heat in the form of waste from the motor. By controlling the flow of coolant with a variable valve, they maintained the outdoor heat exchanger (used to collect heat from ambient) and the waste heat exchanger at 5°C. The waste heat used here was varied between 1kW and 2.5kW depending on the driving condition. The purpose of their research was to evaluate the benefit of incorporating the different heat pump source (waste heat only, ambient only and combined) into the HVAC system. All three conditions were tested with an ambient temperature of −10°C to 7°C. The success of their investigation was measured using

the COP and heating capacity of the system under the three operating conditions. Using the ambient and waste heat conditions separately, the authors were able to achieve maximum COPs of 3.1 and 3.2 respectively. These were achieved at 7°C ambient temperature with 2.5kW of heat wasted.

When the heating capacity of Ahn *et al.*'s [67] system was tested, it was discovered that the air only configuration is not viable at low ambient temperatures. This is because below the operational temperature of the evaporator (5°C), the heat pump is not able to collect thermal energy from ambient. In this circumstance the suction pressure of the compressor is reduced and the COP drops to approximately 1.6. At the higher ambient temperature (7°C) the system was capable of producing 2.5kW of heat. However, at the lower ambient temperature (−10°C) this fell to just 0.9kW. In the waste heat only condition the system produced between 1.3kW and 2.8kW, which was linearly proportional to the waste heat amount which was varied as described above. When the two heat sources were combined the maximum COP achieved was 3.4, which was produced while operating at 7°C. At −10°C the COP attained varied between 1.6 and 2.6. This was linearly proportional to the waste heat supplied to the pump, which was varied between 0 and 2.5kW. This demonstrates the impressive capability of a multi-source heat pump when operating in the extreme temperature regime. Given the linear relationship between waste heat supplied to the pump and COP, it should be concluded that the addition of more waste heat will further benefit the system.

In 2015 Leighton built a heat pump test rig that was intended for automotive use [24]. Figure 3.4 shows how the system would be used for both heating and cooling. This can be used to give an impression of how such a system could be integrated into the various thermal systems of the vehicle. In Figure 3.4, PEEM is the power electronics and electric motor, ESS is the energy storage system and WEG is the coolant. The system was tested on a test bench, rather than in a vehicle, which replicated a mid-sized battery electric vehicle, with a 24kWh storage capacity and 80kW electric motor. These are the same specifications as the Nissan Leaf, although it was not stated that this was the intended vehicle for the study. UDDS and HWFET drive cycles were used, where the system was tested down to an ambient temperature of −12°C. The results of this can be seen in Figure 3.5, where it can also be seen that at the lower temperatures there is a reduced benefit from using the heat pump. Reflecting on what is known from Ahn *et al.* [67] and Lee *et al.* [66], there are two explanations for this. Firstly, from Ahn's work, not enough waste heat was being collected from the motor and electronics to support the heat pump. Alternatively, the evaporator operational temperature was too high

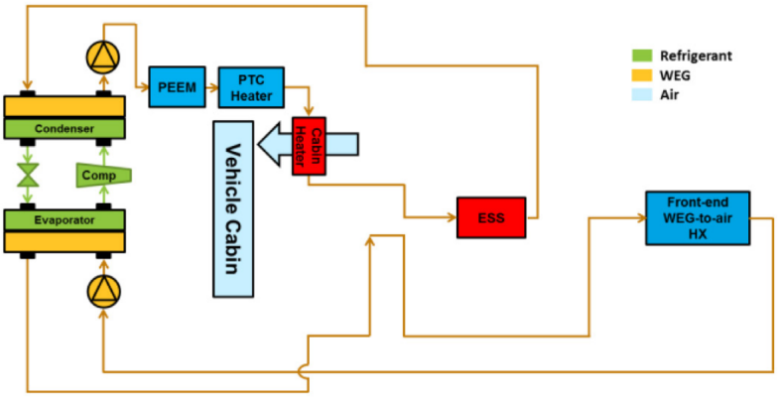

(a) Heat pump being used to heat the cabin and battery in cold atmospheric conditions.

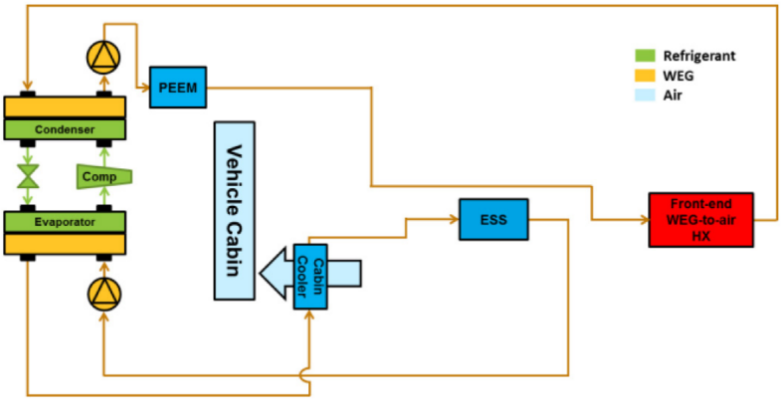

(b) Heat pump being used in air-conditioning mode to cool the cabin and battery in hot atmospheric conditions.

Figure 3.4: Schematics for heating and cooling modes used by Leighton *et al.* [24]

to make use of ambient at these temperatures. In the concluding remarks, Leighton *et al.* [24] stated that the decrease in performance of the heat pump, as ambient temperature dropped, was partially due to the reduction in suction pressure of the compressor with ambient temperature. They suggested that increasing the volumetric capacity of the compressor might be a way to improve the overall performance at low temperatures.

In 2018 the system described in Leighton *et al.* [24] was used in a hardware in loop test by Chowdhury *et al.* [131], in which the performance of the systems implementation on a Fiat 500e (EV) was evaluated. At 22°C the vehicle without HVAC consumed 196.4Wh/km (measured from the battery), then at −10°C, the vehicle using PTC heaters for both cabin and battery heating consumed 292.1Wh/km. Once the heat pump system was turned on this fell to 246.0Wh/km, representing a

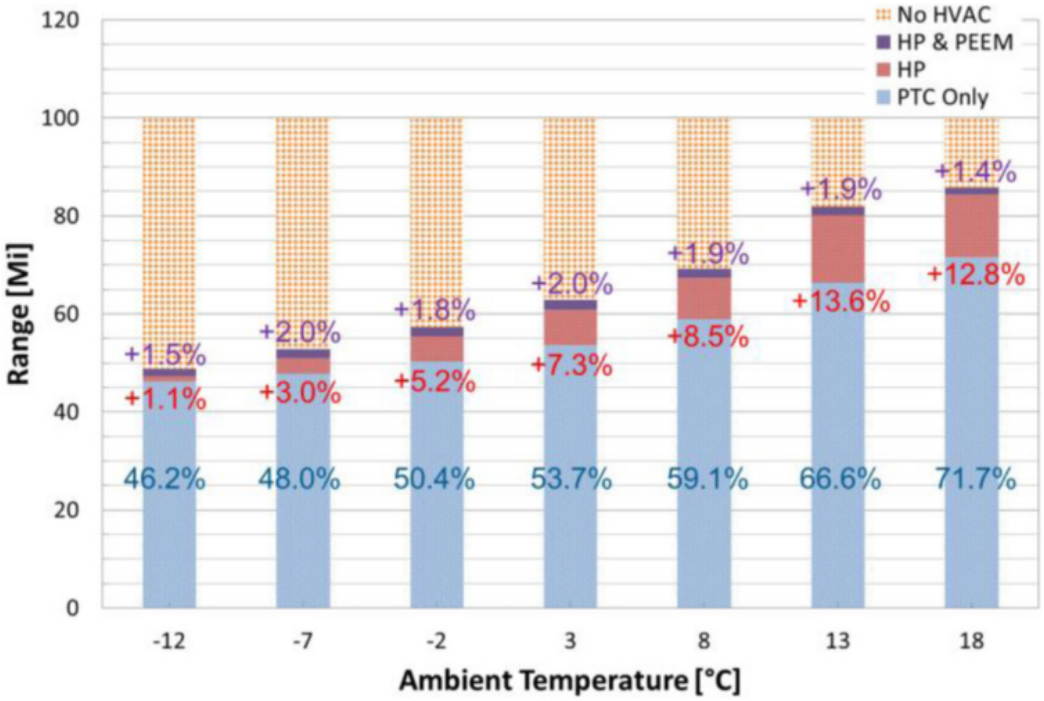

Figure 3.5: Improvement in range achieved by Leighton.

16% improvement in energy consumption.

In 2017 Steiner *et al.* [70] carried out simulations to assess the benefits of a heat pump which can extract heat from the motor, inverter, battery and ambient. In this example, the authors assume a battery mass of 175kg, and investigate two operational modes; one using the battery as a heat source and the other using ambient as a heat source. When using the battery as a heat source, this assumes that the battery is preconditioned and that the battery is not chilled to a point where it becomes inefficient, negating the efforts to reduce energy consumption. The preconditioned battery starts with a temperature of 35°C whereas the ambient temperature is −10°C. Using the authors' assumptions as to the thermal specifications of the battery, at least 1.5kWh of grid energy would be required to precondition the battery. This could be used to precondition the cabin instead, although if the battery is well insulated then it can be heated and then isolated, whereas the cabin would require continuous heat to maintain temperature. The scenarios were tested by simulating the warm up of a cabin from −10°C to 20°C. Both operational modes reached ≈ 19°C, where the target temperature was 20°C, in the 20 minute simulated run. Using the battery as a heat source the HVAC system used 0.66kWh, whereas with ambient as the only heat source 1.26kWh was used. The heat stored within the

battery reduces the work that the compressor needs to do, compared to extracting from ambient, which is how the energy saving is achieved. Additionally, while the motor and inverter where described as potential heat pump thermal sources during the introduction of their research, they were not mentioned as sources during the methodology or results.

Currently the use of heat pumps is hindered by their slow warm up times and the requirement of PTC heaters for fast thermal response. This was the conclusion of a paper written by Kim *et al.* [72] in 2012. In this work the authors investigated the heating performance of an ambient source heat pump supported by a 5kW PTC heater. The system was bench tested with a performance metric being the time taken to heat a volume of air from 0°C to 25°C. On its own, the heat pump reached this target in 40 minutes, while the PTC heater reached the target in approximately 13 minutes and the combined system took 8 minutes. The conclusion to this was that the heat pump still requires the assistance of a PTC heater to be used for cabin heating. This conclusion is further reinforced by the performance of heat pumps at very low temperatures as described in previous examples. However, as discussed in Section 3.3.5, a thermal storage device has the potential to replace the PTC heater for short warm up periods, hence the combination of a heat pump with a thermal storage device has the potential to completely negate the use of a PTC heater in electric vehicles.

In 2018 Meyer *et al.* investigated the use of thermal storage in addition to an automotive heat pump [71]. They based their research on the HVAC architecture of the Kia Soul EV, which utilises waste heat from the electric motor via a low temperature circuit. They evaluate two different heating architectures; a heat pump which could extract heat from thermal storage using the chiller (this operational mode shall be referred to as HPTS) and a PTC heating system with thermal storage (referred to as POTS). Here the motor was used as a thermal store and preheated during modes which made use of thermal storage. HPTS is also supported by a supplementary PTC during warm up if needed. In both operational modes, the thermal storage unit is preconditioned to 55°C and used to provide the majority of the heating demand, reducing the load on the heat pump or PTC heater. Testing was carried out on two Kia Soul EVs (heat pump and PTC variants) in a temperature controlled test chamber using the production vehicles heating control system, both modified to include the thermal storage unit. A cruising cycle at 50km/h at 5°C, −5°C and −18°C was used to evaluate the performance of the different systems. At −18°C the addition of the thermal storage system led to a 48% reduction in HVAC energy consumption for both HPTS and POTS, compared to their non thermal

storage counterparts (HP only and PTC only). This corresponds to a 19% and 22% increase in range at −18°C for HPTS and POTS compared to HP only and PTC only respectively. Although the HPTS system used the least energy under all scenarios, the authors pointed out that the POTS system used less energy than the HP only vehicle variant. They also identify areas of future research in this area which include:

1. Investigations into the most efficient ways to utilise waste heat on the vehicle.
2. Comparison of adding either a heat pump or thermal storage to a PTC only vehicle, i.e. HP + PTC vs POTS.

Returning to the context of buildings, thermal batteries have also been considered as a secondary heat source for heat pumps. In the following example the system proposed by Kaygusuz *et al.* [68] in 1995 uses solar energy to charge a thermal battery (a phase change material in this case) and then uses this in combination with ambient air to supply thermal energy to the heat pump. Here, thermal energy from the solar panels is stored in the thermal battery, then when needed this can supply the heat pump. The heat pump also uses ambient air and recycled house air as heat inputs. This system was simulated and experimentally tested in Turkey. Using this system they predicted an average COP of 4.0 over a 24 hour cycle (7^{th} March 1992, ambient temperature range of 7°C to 17°C), and when measured they recorded an average COP of 4.2. The logged data through the heating season (defined as November to May, inclusive) was presented and the average COP for each month was given. The lowest mean COP was 4.45, which was achieved in February, and the highest mean COP was 4.7, which was achieved in May. For comparison, a second heat pump architecture tested by Kaygusuz *et al.*, used in these conditions averaged a COP of 3.0. This second heat pump architecture could not store thermal energy so it was unable to utilise as much solar energy as the primary architecture. Using the thermal battery to manage the solar energy led to an approximate increase in COP of 50%. Given that current COP for automotive heat pumps is in the region of 2.4 to 3.2 [24, 66, 67], it is expected that the inclusion of a thermal battery could bring further benefits to the automotive system.

3.3.5 Thermal Energy Storage

In three of the examples from Section 3.3, thermal storage was used to assist the heat pump. In the two automotive contexts this was implemented using components on the vehicle, while in the domestic dwelling application a supplementary phase change

material based storage system was used. With thermal storage clearly playing a key role in state of the art heat pump architectures, it is important that this solution is considered. However this should not be an existing component. Steiner *et al.* [70], used the electric battery as thermal storage, but this research is concerned with the low temperature operation of the electric battery, hence this is not an option. Meyer *et al.* [71] used the motor as a thermal storage system, but Leighton *et al.* [24] and Ahn *et al* [67] demonstrated that the motor would be useful to the heat pump as a contributor of waste heat, which should be investigated separately from its potential as thermal storage. Instead a solution more aligned with the one seen in Kaygusuz *et al.* [68] is required, where a thermal storage system is added to the vehicle. In this section the use of thermal storage in the form of phase change materials is investigate for application in a heat pump system.

Phase change materials (PCMs) can be used to store up to 100Wh/kg of energy as a mixture of latent heat and internal thermal energy [132]. A thermal battery made from a PCM can be discharged until it reaches thermal equilibrium with the coldest part of the system, it can then no longer supply energy. It can be recharged either by waste heat or by a PTC heater during off board charging of the electrical battery. During charging, the material is heated to its melting point, where to further increase its temperature the heat source must supply enough energy to overcome the latent heat. This typically happens at around 52°C to 55°C for a paraffin based PCM [133], however other chemistries have been seen with higher melting points [132, 134].

In 2009 Sharma *et al.* [132] collated information on a selection of PCM materials which had promising characteristics making them suitable for use in thermal energy storage applications. In Table 3.1 examples of phase change materials are given, where some materials have been grouped under the following classes:

1. Paraffin wax, consisting of n-alkanes CH_3-$(CH_2)_n$-CH_3.
2. Non-paraffins, which behave in a similar way to paraffins, solidifying to a wax and releasing latent heat, that have a wide range of thermal properties.
3. Fatty acids, which are longer chain hydrocarbons, that tend to give higher latent heat releases compared to paraffins, and are less flammable, but are twice as expensive per unit mass.
4. Salt hydrates are super saturated salt water solutions which undergo a solid liquid transition as the salt hydrates or dehydrates at a given temperature.

The data in Table 3.1 has been collected from [2, 132, 135, 136].

Table 3.1: Example selection of phase change materials with a variety of suitable thermal properties. (∗) - the latent heat of ice/water would not be used since it is not favourable for the state transition to occur at such a low temperature, but is included as an example for reference.

Class	Material	Transition Temperature (°C)	Latent Heat kJ kg^{-1}	Specific heat Capacity kJ $kg^{-1}K^{-1}$
Non-transient	Water	-	2,257*	4.190
Paraffin	6499	68	190	2.130
	34 Carbons	75.9	269	2.130
Non-Paraffins	Beeswax	61.8	177	3.4
Fatty Acids	Acetamide	81	241	1.520
	Stearic Acid	69.4	199	1.200
Salt Hydrates	Ba(OH)_2.8H_2O	78	265	-
	Na_3PO_4.12H_2O	65	190	-

To be considered for thermal management it is desirable for these materials to have very high latent heat and specific heat capacities; for example the PCM used in [133] has a specific heat capacity of $\approx 2000 Jkg^{-1}K^{-1}$ and a latent heat of $181{,}000 Jkg^{-1}$. The paper showed that this thermal management method was able to prevent battery temperatures from rising over the melting point of the PCM in very light vehicles with good airflow (e.g. motorbikes). However, for light passenger vehicles, the necessity for high current and long usage times means that PCMs are not ideally suited for thermal management of the battery. This paper also only considers the case of high temperature thermal management of batteries, but still provides useful insight into typical parameters of PCMs, such as latent and specific heat capacities. Similarly, PCMs have also been considered for extending the time an engine can remain off in stop/start traffic by buffering the air conditioning system, here the materials chosen had melting points of 8°C and 11°C [137]. PCMs have also been investigated for use in PHEV type vehicles to provide rapid engine warm up times [38]. However, these examples are not as relevant to the specific problem of electric vehicle heating in low temperature climates.

In 2012 Shahidinejad *et al.* [40] proposed a thermal battery for use in a PHEV, which would charge during the vehicle's operation and be available to assist cabin heating on cold starts. In PHEVs this reduces the need to start the ICE, and in EVs it reduces load on the battery which would be spent on a PTC heater. Here

a 21kg paraffin based thermal battery was used to give a 21% energy saving in a PHEV cold start. The PCM melts at 56°C with a latent heat of $177,000 Jkg^{-1}$, hence giving a total thermal energy storage capacity of 1.08kWh. The system used here requires 5 litres of the PCM to be stored within each of the four seat cushions. One concern for this proposition is how the system would work in summer when heating is not required, as the hot seat cushions might become uncomfortable.

In 2016 LaClair *et al.* proposed the use of a 2.7kWh thermal battery weighing 33kg with a volume of 31l to cover the entire heating load for a 23 minute commute twice in a day (46 minutes total) [69]. The thermal battery had an operating temperature range of 60°C to 120°C, where 60°C was deemed the minimum temperature useful for cabin heating. LaClair *et al.* assumed an electrical battery with a capacity of 10kWh and average cabin heating requirement of 3.13kW, and thus concluded that adding the thermal battery increased the electrical energy available for traction by 38%.

In 2014 Taylor *et al.* designed a prototype thermal battery to be used to assist in low temperature starts [25]. They used erythritol as their PCM, a sugar alcohol commonly used as an artificial sweetener. The material was stored in an insulated steel container and a copper coil, which contained a coolant flow, was used as the heat exchanger in the material. They achieved an energy density of 100Wh/kg and a power density of 30W/kg (which could potentially be improved with a heat exchanger redesign). This was done at a cost of $\approx$ £177/kWh, making the overall package comparable to lithium-ion. However, unlike lithium-ion, a thermal battery is easy to manage and control, safer, and less prone to ageing.

The Ragone diagram shown in Figure 2.2 has been repeated in Figure 3.6 with the inclusion of the Sunamp [138] and Taylor *et al.* [25] examples mentioned above. Here it can be seen that the energy density of the product supplied by Sunamp is comparable to the energy and power densities of lithium-ion cells.

From the examples given above PCMs appear to be a promising technology in improving both the heating performance and range of electric vehicles. While most of the examples discussed have been centred on low temperature heating, it has also been shown that thermal storage can be applied to high temperature conditions and used to assist the air conditioning system [137]. Hence, were a system like this to be installed on a vehicle it could be swappable, having a high temperature pack in winter and a low temperature pack in the summer. In countries which experience large temperature differences between summer and winter it is common to change tyres according to the season, at the same time the thermal storage unit could be swapped. Considering the viability and applicability of thermal storage as a thermal

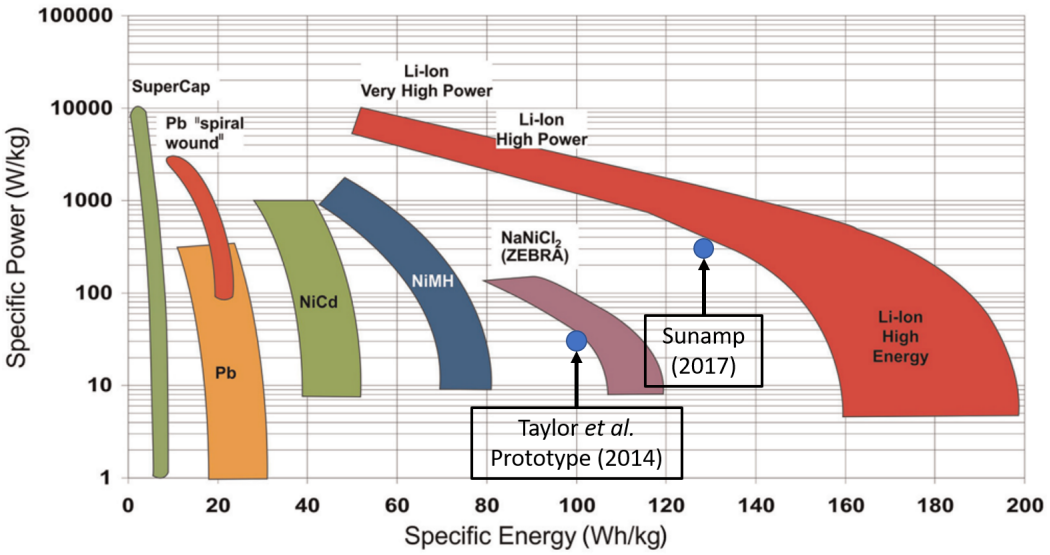

Figure 3.6: The Ragone diagram is repeated with the inclusion of examples of PCMs from Taylor *et al.* [25] and Sunamp [26].

management tool, it will be included in the options of different thermal management architectures explored.

3.3.6 Discussion of battery heating

Throughout the literature reviewed thus far there has been a variety of approaches towards battery thermal management. Chapter 2 demonstrated that at $-20°C$ a typical lithium-ion battery loses between 10% and 50% of its capacity, this was shown in Figure 1.1. This informed the motivation to seek out battery heating mechanisms, as summarised in Section 3.1. However, it can be seen in Section 3.3.2 that only Leighton *et al.* [24] considered battery heating as an operational mode for their heat pump. In contradiction to Leighton, Steiner *et al.* [70] considered the battery as a preheated heat source for the heat pump and cooled it to provide heat for the cabin. The advantage of heating the battery is that it provides more performance and can increase range, but this may come at a cost to energy consumption. To demonstrate this point a hypothetical example is given in Figure 3.7. Here two hypothetical battery thermal management strategies are visualised on data published by Dow Kokam. At $-20°C$ Dow Kokam report that their cell will retain 70% of its Coulombic capacity [11], if the battery remains at $-20°C$ its depth of discharge (DOD) will be 100% after Xkm, where X is 70% of the vehicles stated range. However, if the battery is heated cheaply during the same cycle, then the DOD will be closer to 70% after Xkm, but the total energy consumed will be similar. This can be visualised by

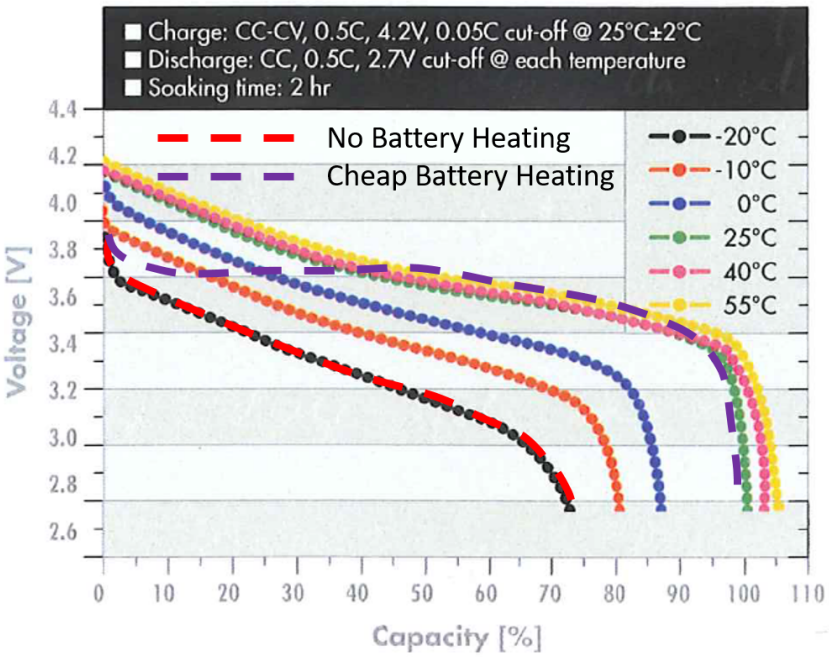

Figure 3.7: Cell capacity as a function of temperature from Dow Kokam with two hypothetical battery management strategies

Table 3.2: The total electrical energy consumption and DOD for two thermal management strategies [1].

Thermal Management Strategy	**Energy Consumed**	**DOD (from 100%)**
1	8.08 kWh	18.9 %
2	7.68 kWh	19.2 %

moving from the data gathered at $-20°C$ to the data representing $25°C$ in Figure 3.7.

The trade off between energy consumption and range improvement has been exemplified in a publication demonstrating the flexibility and capability of the model used in this research [1]. Figure 3.8 and table 3.2 show two thermal management strategies (TMS) relating to the battery during a drive cycle, here TMS 1 shows a heated battery, whereas TMS 2 shows a battery isolated from the heat pump. While TMS 1 uses additional energy to heat the battery, the higher average operating temperature results in a lower DOD compared to TMS 2 where energy is saved, but the battery uses a higher DOD due to lower average operating temperature.

These two examples serve two purposes. Firstly it is unclear whether there is an advantage in heating in the battery, as it may require additional energy, but

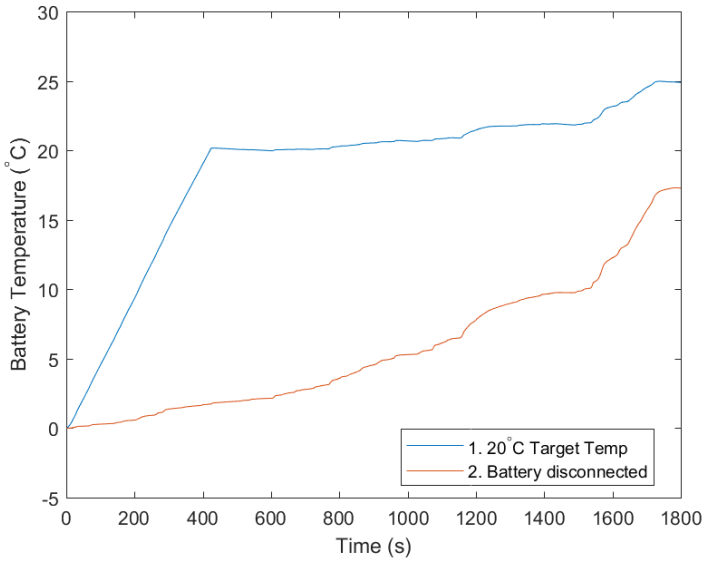

Figure 3.8: Battery temperature under two different thermal management strategies [1].

could also extend range. It is also noted that in the literature covered there is no example which compares heating the battery with not heating the battery in a vehicle with a heat pump. It is therefore not clear what impact battery heating will have on cabin heating, since the extra heating load may reduce the vehicles ability to maintain the same level of cabin heating. The second purpose of the examples is to show that there may be a trade off between energy consumption and range, with battery heating costing more, but releasing more battery capacity. Considering this, battery heating should be investigated in this research programme to understand how it controls energy consumption, range and comfort.

3.3.7 Summary of architectures

The baseline for automotive heating was previously the PTC heater with a COP of 1. It has been shown that during cold temperature operation the load of heating the cabin can reduce range by up to 70%. This deficit can be reduced by using a heat pump as shown by Leighton *et al.* [24]. It has also been shown that providing more heat to the heat pump and using a thermal battery to manage heat on a longer time scale brings increases to the heat pump's COP [67, 68, 70, 71]. However, further improvements to the automotive heat pump can be made in two ways; firstly including thermal storage, as shown by Steiner *et al.*, Meyer *et al.* and Kaygusuz *et al.* [68, 70, 71], to manage thermal load. Secondly, making use of other heat

sources on the vehicle, thus providing the heat pump with more waste heat, as shown by Ahn *et al.* and Leighton *et al.* [24, 67]. These innovations are expected to dramatically increase the COP of an automotive heat pump, hence reducing the energy consumed by heating, and increasing the available range of electric vehicles at low temperatures.

3.4 Discussion

It is known from Section 2.1.2 that battery capacity is reduced at low temperatures. This is why research has been conducted into efficiently heating the battery. From the research presented in Section 3.1 it was seen that the state of the art battery thermal management mechanism in commercially available vehicles is via liquid coolant. Hence this will be considered as the thermal management mechanism in this research.

Preconditioning is clearly beneficial to the system as a whole, and while scheduling of charging and preconditioning does provide a challenge to the grid, this area does not pose challenges for vehicle thermal management while driving. Those solutions are also only viable if you are able to plug in the vehicle between journeys, which is not always the case.

Cabin heating has been shown to be the dominant cause of electric vehicle range loss [21, 22]. Therefore addressing the energy consumption of cabin heating should be the dominant focus of the work. In Section 3.3 heat pumps were highlighted as a likely candidate to replace or supplement heat provided by PTC heaters. Many different heat sources and configurations were proposed by various researchers in Section 3.3, with a summary of the options identified in Table 3.3, which does not include the contributions of Hosoz *et al.* [124] and Kaygusuz [68], since these are not specific to electric vehicles.

3.5 Identification of knowledge gap

Primarily the gaps in knowledge identified in this area stem from one base concern; with the addition of a heat pump to an electric vehicle, what is the optimum way of managing thermal energy? With that in mind, literature has been studied and the gap in knowledge has been identified.

There now exists some examples of researchers considering thermal storage in addition to a heat pump [70, 71]. Steiner *et al.* used the existing electrical battery as a thermal storage device [70], while this is convenient it is not advisable to store

Table 3.3: Summary of current research in the area of vehicle thermal management through heat pumps.

	Heat Sources				
Author	**Ambient**	**Motor**	**Thermal Battery**	**Electric Battery**	**Notes**
Lee [66]	✓	-	-	-	-
Leighton [24]	✓	✓	-	*	* Provided heat to electric battery
Ahn [67]	✓	✓	-	-	-
Steiner [70]	✓	-	-	✓	-
Kim [72]	✓	-	-	-	-
Meyer [71]	✓	✓	✓	-	* Motor used as thermal storage
Suck [130]	✓	-	-	-	Extracted heat from cabin exhaust

Lithium batteries at a high temperature. Meyer *et al.* [71] used the motor and inverter as thermal storage devices coupled to a heat pump system. With thermal storage technology having similar costing and energy storage density to lithium-ion cells [25], it is possible that much larger and dedicated thermal storage solutions (possibly replacing some of the electrical storage) may be beneficial to the system. Hence the appropriate sizing of a thermal storage device should be investigated.

Table 3.3 represents the current state of the art in heat pump research and can be used to identify the next avenue of work. Many heat sources have been identified in current research; ambient, the motor, a thermal battery, the electric battery, the transmission and cabin exhaust (identified in Section 3.3.1). Some combinations of these sources have been considered in literature, but not all combinations have been explored. This can be seen in Table 3.3, where, for example, the combination of thermal battery and electric battery has not been explored. With additional components (transmission and cabin exhaust) even more potential combinations of heat sources become available. Furthermore, while a spread of combinations has been tested in literature, they have all been tested on different vehicles (simulated or real) and under different conditions. Considering this, it would be beneficial to test a vehicle using all possible combinations of potential heat pump sources, allowing a definitive comparison of possible operational modes and guiding future heat pump architectural design.

Using the information presented in Table 3.3 and the knowledge gained

through this chapter, the scope of this research can be set in a way which fills the knowledge gap. While multiple examples of heat pumps and heat pump configurations have been addressed, a list of potential heat sources and sinks can be made by considering all of the options presented in literature. These potential sources and sinks can then be combined exhaustively to explore all possible heat pump configurations.

The examples presented in Table 3.3 all use ambient as a heat source, hence ambient will be included as a non optional heat source on the vehicle. Likewise, since the heat pump is intended to provide better and energetically cheaper cabin heating, the cabin will also be included as a non optional heat sink for this research. Other components included in this research will be optional heat sources or sinks, and will define the vehicle's operational modes. Two examples in Table 3.3 use the heat pump to interact with the battery. In Leighton *et al.* [24] the battery is heated using a coolant loop in series with the cabin. In the other example of the heat pump interacting with the electric battery, Steiner *et al.* [70] pre heated the electric battery and used it as a thermal source for the heat pump. For this research the performance of lithium-ion batteries at low temperatures is a concern, and hence using the electric battery as a heat source would not appropriately address this concern. Instead it will be assumed that the electric battery starts in thermal equilibrium with ambient, and thus it should be treated as a heat sink. While Steiner et al. [70] uses the electric battery as thermal storage, Meyer uses the motor's thermal mass for thermal storage. Conversely, Leighton et al. [24] and Ahn et al. [67] use the motor directly for its waste heat. To address these discrepancies the motor is included as an optional heat source, reflecting the work of Leighton and Meyer, while thermal storage in the form of a PCM is added to the vehicle, as in LaClair et al. [69] and Shahidinejad et al. [40], both of whom included thermal storage on electrified vehicles without heat pumps. Table 3.3 also shows the cabin exhaust as a potential heat source which should be included. Finally, as identified in Section 3.3.3, the transmission should also be considered as a potential heat source as it has similar energy efficiency to the motor, which has been considered.

Table 3.4 has been created to summarise the options for heat sources collated through this chapter. Table 3.4 also shows a PTC heater as a fixed thermal source. This is included since examples from Table 3.3, such as Lee et al. [66], Leighton et al. [24], Meyer et al. [71] and Kim et al. [72] all make use of supplementary PTC heaters.

There has not been an exhaustive comparison of combinations of sources and sinks which considers the trade off between range and comfort. This is the

Table 3.4: List of thermal sources and sinks identified through reviewing literature.

Component	Source/Sink	Optional/Fixed
Cabin	Sink	Fixed
Electric Battery	Sink	Optional
Ambient	Source	Fixed
PTC heater	Source	Fixed
Motor	Source	Optional
Thermal Battery	Source	Optional
Transmission	Source	Optional
Cabin Exhaust	Source	Optional

knowledge gap addressed within this thesis.

Finally, since it has been established that the battery requires heating for maximum performance, but providing heat to the battery will jeopardise heating capacity available to the cabin. This will therefore reduce passenger comfort, creating a trade off between battery performance and cabin comfort. The binary approach take in the literature seen (battery thermal management either on or off) may not be sufficient to balance the needs of both the cabin and the battery. Hence the compromise between performance and cabin comfort should be considered and investigated.

3.6 Research question

From the identified gap in knowledge the following research question has been formulated: In an electric vehicle with a heat pump, how can the combination of potential sources and sinks be systematically compared; hence identifying important components to be controlled to minimise energy consumption, maximise range and maximise comfort?

3.7 Research objectives

The following research objectives have been reached to thoroughly address the research question posed in Section 3.6:

1. Chapter 6 addresses the objective; What is the optimal sizing of a thermal battery for application in an electric vehicle with a heat pump?

2. Chapter 7 addresses the objective; What opportunity is there in controlling

range and comfort through the systematic comparison and selection of a specific combination of heat sources and sinks?

3. Chapter 8 addresses the objective; What control can be gained over the balance of comfort and range through the dynamic control of battery heating during a drive cycle?

A simulation approach will be taken to perform this research, which is justified in Chapter 4. This will allow for fast evaluation and reconfiguration of different combinations of thermal sources and the optional electric battery sink, giving a broad spread of options to be tested. Chapter 5 provides an in-depth description of the model used to achieve these objectives, expanding on details most pertinent to the research and justifying each decision.

Chapter 4

Research methodology

This chapter describes the generic method which will be used when answering the research question. Each results chapter will contain its own specific methodology but will refer to details described in this chapter.

The chapter is structured as follows: A justification of the choice to use simulation is given, which includes an overview of Dymola, the simulation tool used. This is followed by an overview of optimisation options which will be required to maximise range and comfort. The testing scenarios, defined by drive cycle and temperature, are then described. Then the cost function is defined, which will then be used in all the optimisation work.

Chapters 1 and 2 introduced thermal management of electrified vehicles as a problem that is not limited to battery electric vehicles at low temperatures, but also concerns thermal management on (P)HEV vehicles and high ambient temperature concerns. At higher ambient temperature the concern of battery ageing and the amount of energy consumed by cabin and battery cooling motivates research [73, 93, 94, 109, 139]. While the research within this thesis targets the specific problem of battery electric vehicles at low ambient temperatures, the methodology used should be adaptable to suit the wider concerns of electrified vehicle thermal management over a range of ambient temperatures. Examples of where these changes can be made are provided throughout this chapter.

4.1 Simulation

In Section 3.5 a list of optional heat sources and the option to heat the battery were defined in Table 3.4. In Section 3.5 it was described that these sources and the sink had been tested in isolation, but had not been systematically and exhaustively

compared. To make that comparison a rig is needed which can dynamically switch between thermal sources, and dynamically heat the electric battery. Table 3.4 defines five dynamic connections to the heat pump. The physical creation of such a rig can be both complex and costly, while limiting the flexibility to make further investigations and architectural changes; hence simulation is used instead. A simulation environment provides the freedom to easily and cheaply create a model which can be flexibly changed to investigate all the necessary system architectures. Using simulation also removes the burden of negotiating, or funding time on a physical rig, and the assistance that would be needed to operate the rig.

In Section 3.3.6 it was suggested that the decision to heat the battery may lead to a trade off between energy consumption and range. With both being important factors in the design of an electric vehicle it is important that this trade off is investigated. Furthermore it was suggested in Section 3.3.6 that there may be a trade off between range and comfort. It was shown in Chapter 2 that both the cabin and battery require heating, the former for passenger comfort and the latter for performance. If this heat is to come from one source then heating both will reduce the ability to heat either individually, compromising comfort. However, if two heat sources are available then this potentially doubles the HVAC energy consumption, potentially reducing range. A cost function needs to be combined with optimisation techniques in order to control the balance of these three factors; energy consumption, range and comfort.

In order to complete the research objectives set in Section 3.7, there will be compromises between comfort and range. For example, Research Objective 1 states "What is the optimal sizing of a thermal battery for application in an electric vehicle with a heat pump"? Here adding thermal storage to the vehicle will improve comfort, but as seen in Steiner [70], there is still some energy cost associated with extracting the stored energy. There is therefore a trade off between the comfort gained and the additional energy required. This is further complicated by the increased ability of the vehicle to warm its electric battery if a thermal battery is added, hence potentially extending the range. The compromise between range and comfort extends to Research Objective 2, where in testing all possible combinations of the heat sources and sink available to the heat pump, some will provide lots of heat to the cabin at the expense of extra heat pump energy consumption; others will reduce energy expenditure, or improve battery performance at the expense of comfort. Here a method is needed which can balance the motivation to reduce energy consumption, and therefore extend range, while still providing thermal comfort. This extends to Research Objective 3, where the profile used to heat the battery will

indirectly define both comfort, since battery heating will reduce the vehicle's ability to heat the cabin, and battery performance and therefore range. Optimisation techniques will be coupled with a cost function which can be controlled to prioritise the cabin or the battery performance. This will allow for the vehicle's operation to be optimised according to different needs.

Due to the nature of optimisation algorithms, thousands of scenario evaluations need to be made, each altering the vehicle specification or control in some way. Whilst this is physically possible on a test bench, the practicality and cost of such an endeavour prevent bench testing from being a realistic option. For example, to optimally size the thermal battery, hundreds of potential designs need to be trialled. This can be done computationally with no significant cost, but physically may require the construction of many prototype designs at great material, labour and test facility costs. Due to the requirement of many evaluations, and complex changes in vehicle architecture, simulation is the only feasible option. In this area of research, simulation is a common approach. In 2010 Hofman *et al.* [129] used a numerical model to investigate a wide range of transmission and shifting control options on an electric vehicle.

In 2016 Shojaei *et al.* published an investigation into different cooling strategies for a PHEV in high temperature climates [139]. A 24 hour drive cycle was used to assess the impact on comfort, energy consumption and battery degradation when using different cooling strategies. These included cooling at different periods of the drive cycle, such as before or after the vehicle is used, and using different temperature set points. In total more than 10 evaluations of the test needed to be made. Using simulation rather than real world testing negated the need to use a rolling road and climate chamber for 10 days, which would have been prohibitively expensive. This represents a direct comparison to the work presented in this thesis, as multiple strategies are evaluated with the concern focussed on comfort and energy consumption, although in this research battery degradation is ignored as it has little impact at low temperatures (unless fast charging). Shojaei *et al.* used their model again in 2017, when they performed a dynamic optimisation on the cooling of the battery through a 24 hour cycle, again assessing the impact on comfort, energy consumption and battery degradation [73]. For their research, Shojaei *et al.* made many evaluations of their model for different vehicle states in order to find the optimum cooling strategy for the battery. The research of Shojaei *et al.* addresses a similar objective to the problem posed in research Objective 3 of Section 3.7, where the optimal heating of the battery through a drive cycle is considered.

Another example of simulation being used to address a control problem is

the work published by Jaguemont in 2015 [60]. Here dynamic optimisation was used to control the temperature set point for the battery of a hybrid vehicle left in cold conditions over night. Again, modelling was used as the dynamic programming algorithm needed information about many different possible operational states of the vehicle in order to produce the optimal control strategy.

The above examples show how authors and researchers have saved substantial hours of real world testing and the associated cost by using simulation in their investigations. Simulation allows for greater exploratory freedom as the user is less bound by financial and time constraints. The objectives posed in this thesis requires a great deal of exploration and the objectives share similarities with the examples described above, hence simulation has been chosen to maximise the acquisition of results and provide flexibility in potential systems which can be explored, as it bypasses the technical challenges associated with bench testing. The compromise associated with taking a simulation approach is the difficulty in ensuring the accuracy of the models used. To address this a validation strategy, described in Chapter 5, is used to establish trust within the models.

Having decided upon simulation there are a number of modelling environments researchers may choose from to construct their models. In the examples presented above Shojaei *et al.* use Dymola for their modelling, while Jaguemont *et al.* use MATLAB/SIMULINK for their modelling. Hofman *et al.* use a much simpler mathematical model for their work, with few equations which predict battery load, this could be implemented in EXCEL or MATLAB. Other options include Amesim, as used by Chalgren *et al.* [111] in their investigations into optimum coolant flow for engine warm up and comfort in an ICE vehicle. Other authors have used more specialised tools developed specifically for electric vehicle operation, such as BLAST-V (Battery Lifetime and Simulation Tool - Vehicles) [140], or have developed data-driven approximations [141, 142].

A simulation environment is required which is capable of physically modelling the heat pump system with the option of being reconfigurable to multiple system architectures. The tool must be proven within the industry in its ability to research similar problems. Libraries within the simulation tool must have some form of validation.

Here a data-driven approach, where a model is developed using the results of physical testing, is not possible, since there is not a rig in existence which can be used to acquire the data required to model a heat pump system with four optional heat sources and one optional sink. No dedicated tools for this problem existed, hence this was not an option either. While Simulink is a powerful and established tool within

the industry, it does not offer libraries dedicated to developing thermal management models. By comparison Amesim and Dymola both offer libraries dedicated to the simulation of thermal systems. Through this research's connections to Jaguar Land Rover, a tool was available at the start of this project which was made in Dymola (version 2019). It uses dedicated thermal management libraries and has been in a demonstrated as a tool for evaluating different operational modes on a heat pump vehicle [143]; making Dymola the best tool for this project.

Dymola has been used in vehicle level simulations similar to the research proposed here, examples of this include the investigations conducted by Shojaei *et al.* [139], Picarelli *et al.* [143] and Bellocchi *et al.* [144]. In 2016 Picarelli *et al.* developed a tool for Jaguar Land Rover for evaluating the benefit of different thermal management architectures on an electric vehicle with a heat pump, showing a state of the art and industrial application of the tool. Bellocchi *et al.* used Dymola to perform investigations into the benefit of an electric vehicle using a heat pump with a regenerative heat exchanger. In both [143] and [144] the authors use libraries within Dymola which are purpose built for flexible modelling. Dymola has the advantage of a wide choice of libraries containing specialised tools for automotive and thermal management applications. These dedicated libraries negate the reliance on component mapping and give the freedom to create diverse, original and physics based models.

With assistance and in cooperation with Jaguar Land Rover and Claytex, the model used by Picarelli *et al.* was used as a platform for this project. Along with the specialist thermal and vehicle libraries, VeSyMA-Powertrain and TLK-Thermal Systems, this provided an excellent starting point for the project. The libraries also provided powerful and flexible options when building new components. Libraries are also validated through annual Modelica conferences, where library providers have the opportunity to present and publish updates to their libraries, this validation provides an extra degree of confidence in the available tools [145–147].

The details of the model specifically are fully covered in chapter 5.

4.2 Optimisation

The optimisation procedures required to answer Research Objectives 1 and 3 of the Research Question are very different; the first requires a search algorithm and the third requires dynamic programming. Since the requirements for these two parts are different the choice of the specific algorithms used for each results chapter will be discussed independently in the relevant chapters. This section serves as an

introduction to optimisation.

Research Objective 1 requires the investigation of optimal thermal battery sizing when incorporating thermal storage into an electric vehicle. In a vehicle with a heat pump, thermal storage will have the positive impacts of providing heat for the cabin and battery. This will reduce the reliance on the PTC heater and heat pump, but at the cost of additional coolant pumping and compressor electrical consumption. There will therefore be a point where the increase in energy storage does not provide extra benefit to the cabin, but costs extra energy to the battery. In this research there are two proposed cases for the inclusion of the thermal battery which will be reported separately in Chapter 6. The first is the free addition of the thermal battery, with no consequences to the electric battery. In this case the optimisation will be looking to minimise the cost function defined in Section 4.5. The vehicle and therefore the cost function are going to be affected by the energy stored in the thermal battery and how much heat it can deliver. Therefore the optimisation should be looking to find the mass, charge temperature (the combination of mass and initial temperature define the thermal batteries stored energy) and heating capacity which minimise the cost function. Hence the mass, charge temperature and heat capacity define the control vector of the optimisation. If this method were to be re-applied at high temperatures the control vector would be the same, however, the temperature range would be much lower. The PCM would be charged to the minimum temperature of the chiller in order to help provide cooling to a vehicle in a high temperature climate. Additionally a secondary case will be considered where the total onboard storage is limited and the inclusion of thermal storage will be made at the detriment to electrical storage. Here there will be a turning point where the energy saved by including thermal storage does not outweigh the range reduction caused by reducing the battery's capacity. For this second case the charge temperature and heating capacity found when investigating the first case can be used, limiting the search to mass.

The control vector for thermal battery sizing optimisation requires constraints in order to perform an optimisation. However, the model's operation and control, as well as the specific thermal battery material details, need to be discussed in order to provide context to the constraint. Hence the details pertaining to the thermal battery model will be discussed in Section 5.6 and the optimisation constraints will be defined in Section 6.2.

4.2.1 Search algorithms

In this search a theoretical overview of search algorithms is provided. This will establish the options that are available to be used for the thermal battery sizing optimisation performed in Chapter 6. Here the algorithms are described in their pure theoretical forms, then in Chapter 6 the algorithm selected and details of its implementation are provided.

An optimisation algorithm is a process used to find a set of values which minimise a cost function, e.g. $f(x_n)$ where x_n represents a vector of variables. For example, when designing an engine, x_n could be a vector representing the number of cylinders, bore size, stroke length, etc. and $f(x_n)$ might return fuel consumption for a specific duty cycle.

Generally there are two varieties of optimisation algorithm referred to as direct and indirect search algorithms. Indirect searches, such as Newton's method, which uses in Equation 4.1 to update the search variables, require the cost function to be differentiable by the input variables. Due to the complexity of the model used for this investigation, deriving a differentiable equation to replace the model is not realistic. However, a direct search algorithm only requires the input variables and corresponding cost to search for the minimum. Typically they use an iterative approach to adjust the inputs until the cost can be reduced no further. These algorithms are unaffected by the complexity of the problem, but usually require considerably more iterations to locate the minimum.

$$x_{n+1} = x_n + \frac{f(x_n)}{f'(x_n)} \tag{4.1}$$

Table 4.1 makes comparisons between a range of direct search algorithms. The textbook explanation of how each algorithm works may be found in Appendix A. In Chapter 6 an initial investigation of the search space will be conducted, allowing for a suitable search algorithm to be chosen. The precise implementation and modifications made will then be discussed.

Table 4.1: The advantages and disadvantages of potential search algorithms, to be used in Chapter 6, are summarised.

Method	**Advantages**	**Disadvantages**
Random Methods	- Resistant to local minima. - Can be used when other methods fail due to sharply varying functions or shallow areas.	- Inefficient at finding precise global minima. - Difficult to set search termination criteria.
Grid search	- Guaranteed to find global minima to the required resolution.	- Requires a prohibitively large number of function evaluations.
Univarient	- Simple implementation - More efficient than Random and Grid searches for some problems*.	- Converges slowly if precise locations of global minima are required. - *Steep valleys can prevent the search from converging.
Pattern Search	- Improved version of Univarient. - Achieves rapid convergence.	- Can be susceptible to local minima
Powell's Method	- Extension of pattern search. - Converges quickly when problem can be well approximated as a quadratic.	- Can be susceptible to local minima - Less effective away from the minimum
Simplex (Nelder-Mead)	- Most efficient method computationally.	- Tendency to stagnate in shallow regions.
Genetic Algorithms	- Highly effective at finding global minima - If populations members can be evaluated in parallel it is highly efficient.	- If population members cannot be evaluated in parallel it can be very inefficient.

While these methods are introduced in the context of optimising a high temperature PCM, they can also be used in optimising the specification of a low temperature PCM. This modification would be used if a researcher or designer were interested in PCM implementation for operation in high temperature climates.

4.2.2 Operational modes

In Section 3.5 a knowledge gap was identified. While multiple potential heat pump configurations have been identified and examined in isolation, given that multiple potential thermal sources and sinks exist for a heat pump, a method should be created to exhaustively compare and contrast heat pump source and sink combinations. To address this a set of operational modes needs to be defined which encapsulate all possible combinations of the defined list of optional thermal sources and sinks. In this section the list of optional sources identified in Section 3.5 is restated, then their systematic combination into operational modes is explained.

In Chapter 3 an ensemble of heat pump configuration options, investigated by various authors was summarised in Table 3.3 and led to a list of optional heat pump sources and sinks given in Table 3.4. The list of optional sources and sinks from Table 3.4 were:

1. Motor (Source)
2. Thermal Battery (Source)
3. Electric Battery (Sink)
4. Transmission (Source)
5. Cabin Exhaust (Source)

As well as these optional sources and sinks, the list included; the cabin as a fixed sink, the PTC heat as a fixed source and ambient as a fixed source.

Two modes of operation can be defined for the components listed above, on and off (labelled 1 and 0), in reference to their connection to the heat pump. Here off is thermally isolated from the heat pump and on is thermally managed by the heat pump. Since each component has a binary control and there are 5 individual components, there are 2^5 unique combinations, which define the list of operational modes seen in Table 4.2. The operational modes are created by listing the numbers 0 to 31 as binary numbers (00000, 00001, ..., 11111) where each digit represents the state of the components given in the list above. This allows for all possible combinations of thermal contributors to be tested.

Table 4.2: List of heat sources, their operational mode options, and an example of how each operational mode is constructed.

	Heat Source				
Operational Mode	**Motor and Inverter**	**Thermal Battery**	**Electric Battery**	**Transmission**	**Cabin Exhausted**
1	0	0	0	0	0
2	0	0	0	0	1
3	0	0	0	1	0
4	0	0	0	1	1
5	0	0	1	0	0
6	0	0	1	0	1
7	0	0	1	1	0
8	0	0	1	1	1
9	0	1	0	0	0
10	0	1	0	0	1
11	0	1	0	1	0
12	0	1	0	1	1
13	0	1	1	0	0
14	0	1	1	0	1
15	0	1	1	1	0
16	0	1	1	1	1
17	1	0	0	0	0
18	1	0	0	0	1
19	1	0	0	1	0
20	1	0	0	1	1
21	1	0	1	0	0
22	1	0	1	0	1
23	1	0	1	1	0
24	1	0	1	1	1
25	1	1	0	0	0
26	1	1	0	0	1
27	1	1	0	1	0
28	1	1	0	1	1
29	1	1	1	0	0
30	1	1	1	0	1
31	1	1	1	1	0
32	1	1	1	1	1

The full exploration of these operational modes is performed in Chapter 7. Here the operational modes will be compared over the scenarios which will be defined in Section 4.3 using the cost function which will be defined in Section 4.5.

The process of identifying operational modes is not limited to the selection of potential sources and sinks identified here. If a different list were provided then a new set of operational modes could be defined. This could be expanded to include cabin heating in a situation where this is considered optional, or cabin cooling if high temperature ambient temperatures were considered. In this scenario battery cooling may be considered as an optional heat source or cooling sink.

4.2.3 Optimal control trajectories.

One of the key findings from Chapters 1 and 2 was that electric vehicle users must choose between comfort and range when using their vehicle in cold climates. Research Objective 3 addresses this by proposing the production of a set of control trajectories for battery heating which can used to either maximise comfort or range. This will allow the user to receive the most thermally comfortable experience while the vehicle is still able to meet the required range. In this section methods of producing optimal control trajectories are discussed. A method will be chosen based on the following criteria; it must be implementable given the nature of the problem and the use of simulation and it should produce the global minima.

The area of dynamic optimisation and control optimisation is broad, covering multiple academic fields [148]. The general formulation of an optimal control problem is to determine the control vector, $U(t)$, which creates a state path, $X(t)$, that minimises the cost function, J. This can be formally written as

$$J = F(X(t_0), t_0, X(t_{end}), t_{end}, P) + \int_{t_0}^{t_{end}} G(X(t), U(t), t, P)dt \tag{4.2}$$

where F and G are explicit functions of their variables and P is a vector of static parameters. The static parameters may be time dependant, such as vehicle velocity in a drive cycle, and will contribute to the cost, but are unaffected by the choice of control. For problems where J can be written explicitly as a function of X, U, t and P, these problems are solvable using a selection of mathematical approaches [148]. This is not applicable to this problem since the simulation environment cannot be reduced to a simple function of the state, control, time and static parameters. Instead an approach is needed where the cost, J, of Equation 4.2 can be found from inputs X, U, t and P, but the functions F and G are not known. In order to

identify an applicable methodology the field of automotive engineering is explored to identify solutions applied to analogous problems.

A comparable problem which has existed for some time now is optimising the power split between the ICE engine and electric motors in a HEV or PHEV vehicle. In this case, two power sources combine to drive the vehicle in a way which should minimise energy consumption. Parallels can be drawn to the problem set in Research Objective 3, where one heat source must be split across two sinks in a way which minimises the cost, the sinks here being the cabin and the battery. A variety of approaches have been found for the HEV problem and so it is here where a methodology applicable to Research Objective 3 will be found.

In a review by Cook *et al.* [149] three options for the control of power split in HEV problems are discussed. Firstly, heuristic control techniques in which a decision making machine is used to determine the power split between the two sources. These machines use methods such as rule based control, fuzzy logic and neural networks to decide how to split power. These approaches are usually reliant on the engineer's judgement and experience of what operating states should exist and how the machine should decide to transition between them. Optimisation mechanisms can then be applied to the controller, to improve state switching thresholds for instance, and improve the performance of the machine. However, this does not guarantee that the operation of the machine represents the global minimum that can be achieved. The second method discussed is based on static optimisation. Here the optimum power split is found in advance for points within a look up table which spans the state variables. An example of this approach can be seen in Johnson *et al.* [150] where a controller optimised the amount of torque (acceleration or regenerative) that the motor provided based on the current torque demand and operating speed of the vehicle. Here the controller decided the torque split based on steady state fuel and emission maps, given the engine's speed and the torque demand. This technique is only applicable when steady state approximations can be made about the system. The last approach discussed by Cook *et al* is the concept of dynamic optimisation. In a comparison between an optimised rule based controller and dynamic programming, it was shown that a strategy implemented based on the results of dynamic programming improved fuel consumption by 54% compared to a 31% improvement through a rule based controller [149].

The Equivalent Consumption Minimisation Strategy (ECMS) is another sub-optimal optimisation method which has become popular for use in the hybrid power split problem [151–153]. ECMS is a real-time implementable control strategy, which splits the instantaneous vehicle demand between the motor and ICE to minimise

total fuel cost. The optimisation of the power split can be performed instantaneously using a simplified energy consumption model which allows the controller to be implementable in real-time. The controller does not consider any future state of the vehicle when performing its optimisation and so its performance is sub-optimal compared to DP, which is used as a benchmark [151]. It is also designed for splitting the distribution of power according to a demand; however the problem addressed in this thesis is the decision to increase the demand on the HVAC system to provide heat to the battery, with the intention of benefiting from a more efficient battery later in the drive cycle. Since the ECMS is designed to address a specific problem and is sub-optimal by definition it is not suitable for use in this instance.

In the example given in Cook *et al.* [149] of the savings that can be found using dynamic optimisation the development of the dynamically optimised strategy used deterministic dynamic programming. Dynamic programming (DP) uses a dynamic model to evaluate the cost of an action as a function of the state parameters at multiple points in time during the dynamic model. This defines the cost matrix; known procedures can then be used to solve the control trajectory, giving the optimal control path. The resulting optimal path then represents the problem's global minimum solution. In practice the path created is specific to the drive cycle and initial conditions used in the problem, and so the found optimal path is not implementable on a vehicle. So in practice rules are extracted through the results of DP which are designed to imitate the results of the process. Given a sufficient variety of initial conditions and drive cycles this makes an effective control strategy, but is sub-optimal compared to the results of DP. The disadvantage of the DP method is the time required to produce a cost matrix for the problem. DP suffers from a problem known as the "curse of dimensionality" whereby the computational time required grows exponentially with the number of state variables and control variables. It is therefore only practical where the number of state and control variables is small, or evaluation time of the model is very small (millions per second).

DP is used in a range of literature concerned with the optimal control of electrified vehicles. For instance Perez *et al.* investigated the problem of splitting the power demand between the electric motor and internal combustion engine on a hybrid vehicle [154]. Here a dynamic programming approach was used to minimise the cost function over a drive cycle, resulting in an optimal trajectory describing how the demand should be split. In another example Wang *et al.* showed dynamic programming could reduce the fuel costs of a Toyota Prius by 30% [155]. This then translated into a 27% reduction when a rule based approach was extracted and implemented in a real time solution. Others describe how DP represents the

benchmark of what can be achieved in a dynamic problem [156, 157]. DP is also used in examples more closely comparable to the problem described in Research Objective 3. For example, Shojaei *et al.* use a similar approach to solve the problem of when the battery cooling system should be used over a 24 hour drive cycle in order to minimise energy consumption, maximise comfort and minimise battery degradation [73].

In summary, three control strategies have been identified as applicable to this problem, i.e. none require a cost which can be well defined as a function of the control and state variables. Rule based control offers ease of use, is optimisable (in respect to transition thresholds etc.) and would be implementable on a real vehicle. Static optimisation provides a compelling strategy for a system which can be well approximated as steady state. This is not the case for the methodology presented here, where the interest is coupled to the dynamics of the drive cycle and the variation in performance and comfort as the battery and cabin transition to target temperatures. Due to the interest in the transient nature of the problem, steady state assumptions should not be made when performing the optimisation. DP offers a technique which produces the global minima, and is seen as the benchmark against which other techniques are measured [156]. Its drawback is the computational time required compared to other techniques. Results from DP are specific to the initial conditions and drive cycle tested, preventing it from being an implementable control strategy on a vehicle, since its use requires precise knowledge of future events. Since the future cannot be accurately predicted for individual journeys (i.e. the strategy would be dependent on traffic which cannot be known in advance) the reality is that DP can only be used to guide the behaviour of implementable controllers.

For this research the requirements are that the global minima is found and that the solution is applicable to this problem. While rule based controllers offer ease of application to this problem, they do not in general yield an optimal solution. DP on the other hand is applicable, and does provide an optimal solution. Although it is not implementable on a real vehicle, the interest here is purely theoretical, so it is well suited as a tool to understand the maximum potential of optimal control in this system. Hence DP is selected as the optimal control tool to address Research Objective 3. The specific implementation of a DP tool is described in Chapter 8.

This methodology targets the dynamic heating of the electric battery, however in a high temperature climate the same methodology could be used to control the dynamic cooling of the battery. Here the trade off may be between energy costs of cooling, comfort and the prolonged operational life span of the battery, since reducing the operating temperature reduces ageing. Alternatively, if the battery

thermal management was not feasible on the vehicle, this methodology could be applied to cabin heating (or cooling) to control the trade off between cabin comfort and HVAC energy consumption. Hence this methodology is expandable to the wider electrified thermal management problem.

4.3 Testing scenarios

Here the ambient temperature range and selection of drive cycles is discussed. Drive cycles such as NEDC and WLTP (in Europe) are used as official measures of a car's performance, and it is therefore a manufacturer's obligation to minimise their cars' fuel consumption on these cycles. Manufacturers will also use there own custom drive cycles to establish whether the vehicle meets their expectations. For example a "Vmax" which manufacturers will use to establish that the vehicle can meet the desired maximum velocity. While official drive cycles are useful it should always be noted that real world driving is infinitely variable due to individual driving styles, routes and local geography, weather and other drivers. Therefore drive cycles are a best guess prediction of reality, but cannot guarantee the performance of the vehicle for the end user's specific and individual use case.

The variability in real world driving and use cases will have consequences that cannot be accounted for by official drive cycles. For example a gear ratio set for a driver who does short town journeys will be different than that of a driver who drives predominantly long motorway journeys. Neither of which can be accounted for with a single official drive cycle. To ensure that the vehicle performs optimally in a range of scenarios, a variation in drive cycles should be used, both in length and speed.

This research focuses around three drive cycles. The first, which will henceforth be referred to as the WarmUp cycle, is a simple cruising cycle which consisted of a 50km/h cruise for 30 minutes, followed by a 100km/h cruise for 30 minutes, then 30 minutes at rest, giving a total distance of 75km and total time of 1.5 hours. The WarmUp cycle is a test regularly used within Jaguar Land Rover to investigate HVAC performance, and hence its use is industrially relevant. The second and third cycles used are the New European Drive Cycle (NEDC) and the World Harmonised Light Vehicle Test Procedure (WLTP) respectively. A variation in cycles was used as it was deemed important to establish whether the dynamics of a drive cycle (the frequency and magnitude of acceleration and braking events) impacted the optimal thermal management. With regards to the cycles chosen, the WarmUp cycle is the least dynamic, while the WLTP is the most. This can be measured by the time

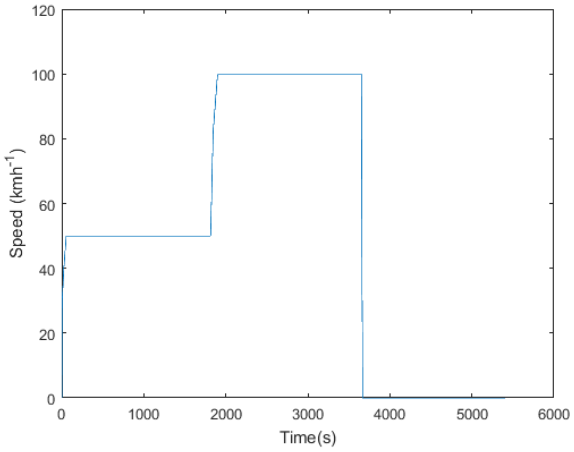

(a) WarmUp drive cycle

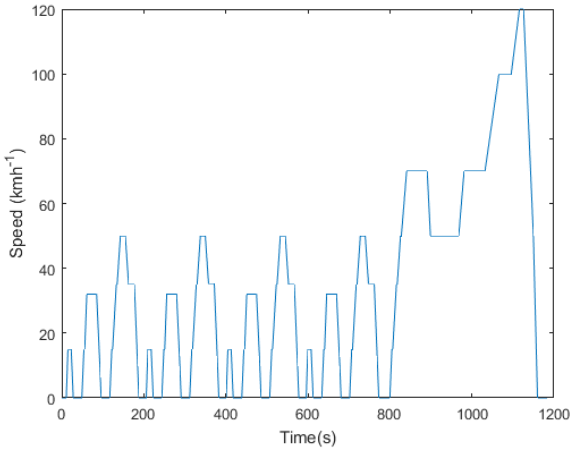

(b) NEDC drive cycle

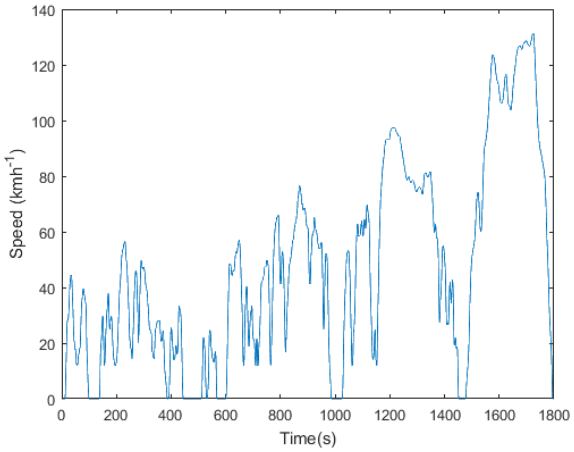

(c) WLTP drive cycle

Figure 4.1: The three drive cycles used during investigations.

spent accelerating; during the WarmUp cycle there are two acceleration events and one deceleration event, amounting to 2.5% of the drive cycle length. By contrast the vehicle is accelerating or braking for 36% of the NEDC cycle and 83.7% of the WLTP cycle [158]. This increase in cycle dynamics can be seen in Figure 4.1. NEDC and WLTP were specifically chosen because when this research commenced NEDC was the standard European testing procedure. However, by the end of the project it was superseded by the WLTP, making both cycles relevant for vehicle testing tools during this period. The variation in the dynamics of these cycles will be used to show that the optimisations performed are applicable in a range of operating conditions. This is important for establishing that the benefits found are repeatable regardless of operating conditions.

Other drive cycles that could have been used include; the Urban Dynamometer Driving Schedule (UDDS) [21], the Highway Fuel Economy Cycle Test (HWFET) [21], the Speed Correction Driving Schedule (SC03) [21], the NYCC Driving Cycle [21] and JC08 [159]. These are commonly used as test procedures in America, with the exception of JC08 which pertains to the Japanese market. This research however is designed to be relevant to European markets, which is also reflected in the choice of temperature range. It is therefore more appropriate that official European testing procedures are used to evaluate any potential benefits.

The temperature range used during investigation is from $-15°C$ to $15°C$, explored in $10°C$ increments. This range covers the range of temperatures expected during a European January. Kazan in Russia can expect to experience a minimum monthly average of $-16°C$, while Athens in Greece experiences a maximum monthly average of $14°C$ [160]. $14°C$ is also one of the prescribed temperatures for WLTP testing, the others being $23°C$ and $-7°C$. The combination of a drive cycle at a given ambient temperature will be referred to as a scenario.

4.4 Baseline

In this section the baseline configuration of the vehicle will be defined. This can be used as a reference, and unless stated otherwise will be the default configuration of all work. The configuration of the vehicle, with respect to the heat pump's abilities and thermal management architecture, has been set to reflect the state of the art available in modern electric vehicles. Hence improvements on this baseline represent potential improvements on state of the art.

The battery pack configuration for this vehicle is $108s3p$, which means 3 parallel strings of 108 cells in series. The selection of this configuration gives the

battery pack a nominal voltage of 400V, which is typical of many electric vehicle systems [161]. Other systems, such as the Porsche Taycan use 800V battery packs, which can be beneficial to power delivery and charging [162]. The change from 400V to 800V can be made by re-configuring the existing cells, and since the problems addressed by this thesis occur on a cell level, a change such as this would not impact the methodology or results. Alterations to the battery configuration can be made by increasing the number of strings in series, thereby not effecting the packs terminal voltage and ensuring compatibility with the motor and inverter.

The cells modelled have a capacity of $40Ah$ with a nominal voltage of $3.7V$, giving the pack a capacity of $48kWh$. The model used for this work is based on the Jaguar I-Pace, which has a pack configuration of $108s4p$ (using large capacity cells) and an advertised capacity of $90kWh$. The high thermal and energetic capacity of the $90kWh$ meant that the vehicle was easily able to complete all drive cycles and that energy savings were small in comparison to the pack size. For this reason the pack size was halved. The consequences of this were a much larger DOD and that the thermal management strategy had greater impact due to the lower thermal mass. A $48kWh$ capacity is also more representative of packs found in more affordable cars such as the Nissan Leaf and Renault Zoe, which are both available with $40kWh$ packs [163, 164]. Hence, for all of the work performed in this research a $48kWh$ battery pack is used.

While a change to battery pack sizing would change the results as it changes the thermal requirements, the methodology should not be changed for alternate pack sizing. A pack size change would likely have the most impact on the results presented in Chapter 7, which is concerned with what combination of components should be connected to the heat pump. A pack sizing change would likely alter the conditions under which electric battery heating is preferable, and therefore the conclusions on whether the battery should be heated. This would then expand into Chapter 8, where battery heating is dynamically controlled. Should a different pack size be used this may not be necessary, but in that case the same methodology could be used to control the next most important interaction between the heat pump and the vehicle.

For all testing, including baseline tests, it is assumed that the vehicle will start with a fully charged battery, 100% SOC, and in thermal equilibrium with the ambient atmosphere. This represents a use case where a vehicle has been left plugged in, but outside in the cold. This represents cases such as; charging at home on a drive over night, charging while the car is parked outside during a working day in extreme cold etc. Here the pack would be charged at the end of the drive cycle,

when the battery is warmest, therefore preventing damage through lithium plating. The battery would then cool down overnight and reach thermal equilibrium with ambient before the morning drive.

Research Objectives 2 requires the identification of which vehicle components should be connected to the heat pump to get the best performance from the vehicle. Several components can be chosen as potential heat sources, leading to many different possible configurations the heat pump may be operated in. There needs to be a baseline configuration which later improvements and alterations can be compared against. In this configuration the heat pump will extract heat from ambient and the motor, and deliver heat to the cabin and the battery. This reflects the capability of modern electric vehicles such as the Jaguar I-Pace [165]. Using the operational mode numbering convention defined in Section 4.2.2, this configuration aligns with operational mode number 20.

At the lowest testing temperatures the heat pump is less able to extract thermal energy from the ambient. In these circumstances a $4kW$ PTC heater is needed to support the heat pump. $4kW$ was chosen as the power of the PTC heater after consultation with Jaguar Land Rover as this, along with a $2.5kW$ compressor in the heat pump, reflects the HVAC power consumption of the I-Pace. $4kW$ is also representative of examples seen in literature with Kim *et al.* using a $5kW$ PTC to support their heat pump [72] and Shin *et al.* investigating new manufacturing techniques to produce a $4.85kW$ heater designed for electric vehicles. These examples are slightly higher than the $4kW$ heater used in this research, but neither of these studies used thermal storage to further supplement heating. In this research the combination of thermal storage, a PTC heater and a multiple source heat pump will ensure that the system's heating capacity will not be compromised. Unless otherwise stated the PTC heater will be used during all simulations and forms part of the baseline operational mode.

Unless otherwise stated the heating power requested by the cabin and battery will be 10kW each. This is the target heating power of the system, and in some conditions, i.e. very low temperatures, the system may not be able to achieve this (more detail on this is given in the model description in Chapter 5). Chapter 2 revealed that the cabin required up to 7.6kW to be sufficiently heated; 10kW was chosen as the target power so as to meet this requirement, while also giving the vehicle the capability to improve on comfort if possible. This also covers the extra capacity needed to heat the larger space of the SUV style Jaguar I-Pace cabin. The battery heating requirement was also set to 10kW, mirroring the cabin, with investigations to be conducted into how to optimally heat the battery through a

drive cycle carried out in Chapter 8.

Further descriptions of the operation of the vehicle model are found in Chapter 5. In Chapter 5 the model is fully explained, with component models justified and validated. A full vehicle validation is then performed and benchmarked against recorded electric vehicle behaviour from literature.

4.5 Cost function considering multiple objectives

The Research Question stated in Section 3.6 makes reference to the minimisation of energy consumption, maximisation of range and maximisation of comfort. The objectives chosen define optimality within the system. This section discusses, justifies and defines the objective function used to measure improvements. The objectives chosen reflect the concerns raised in Chapter 2. In Chapter 2 it was highlighted that the reason for the reduction in range at low temperatures could be broken down into two primary causes; increased HVAC consumption and reduced battery performance. To address these problems objectives should be chosen which directly reflect them. It might be sensible to minimise the HVAC consumption, however this may have unintended consequences. For example the HVAC energy consumption could be minimised by extracting heat from the gearbox and battery, but this might increase total energy consumption as it renders the battery and gearbox less efficient. To account for this, a metric should be used which captures the complete energy consumption of the vehicle, including all sources of losses.

The second stated objective is to maximise the vehicle's range. Typically optimisation implementations are structured to minimise a cost. Therefore DOD is used as the metric to be minimised in order to maximise range. This can be separated from reducing energy consumption since Chapter 2 showed that at low temperatures batteries have reduced capacity, hence increasing the temperature of the battery increases the remaining range, and reduces spent DOD. If the battery is heated early in the drive cycle it will be operating at a lower internal resistance and therefore a higher terminal voltage and will thus use less current for the same power. Examples of this were shown in Section 3.3.6. This will ultimately result in a higher final SOC, and hence DOD should be an objective to be minimised.

It may be argued that since DOD covers the requirement to maximise range then energy consumption should not be considered, or that it becomes redundant. However, energy consumption will directly affect the advertised vehicle efficiency and so the complete vehicle energy consumption should still be considered.

To avoid the system saving energy and maximising battery performance by

neglecting cabin heat, a comfort metric should be used. Without this it is likely the cabin comfort would be compromised in favour of the other metrics. These three objectives comprehensively and simply cover the concerns highlighted in Chapter 2, while avoiding adverse or inadvertent results. This section explains how these objectives are quantitatively measured and combined to give a single cost.

An ageing relating cost has not been considered as ageing is prevented by not utilising low temperature fast charging. However one may be implemented to extended the use of this cost function to cover high ambient operating temperatures. This would help to fulfil the requirement that the methodology is useable in the wider area of electrified vehicle thermal management.

4.5.1 Defining the objectives

As was highlighted in Chapter 2, one of the key concerns for uptake of electric vehicles is range anxiety. Electric vehicles can suffer from severe range loss in cold climates, with some researchers reporting up to 70% loss in range at $-20°C$ compared to $20°C$, with approximately half the loss being caused by the impact of heating on energy consumption, and the other half from poor battery performance.

The conclusions drawn from the literature review suggest the problem with electric vehicles at low temperatures is increased energy consumption or compromised cabin comfort. The first objective which can be extracted from this conclusion is energy consumption. Clearly to improve the range of an electric vehicle the energy consumption should be minimised. The energy consumed is measured from the open circuit voltage (OCV) component of the cell. This is chosen instead of the terminal voltage since terminal voltage will not take account of losses and inefficiencies inside the cell.

The energy consumption measured from the battery terminals can be calculated using Equation 4.3, where terminal voltage (V_T) and current (I) are measured at the terminal and ammeter seen in Figure 4.2. However, as can be seen in Figure 4.2 this only captures the energy consumed by the vehicle and neglects the losses inside the battery. Hence a complete energy consumption metric can be constructed by including the energy lost inside the cell. This could be calculated using the voltage drop, $V\_drop(T)$, across the RC network as seen in Figure 4.2 and defined in Equation 4.4. Here $V\_drop(T)$ is a function of temperature, as the temperature of the cell increases $V\_drop(T)$ reduces, corresponding to a more efficient cell. The total energy consumption can then be defined as in Equation 4.5

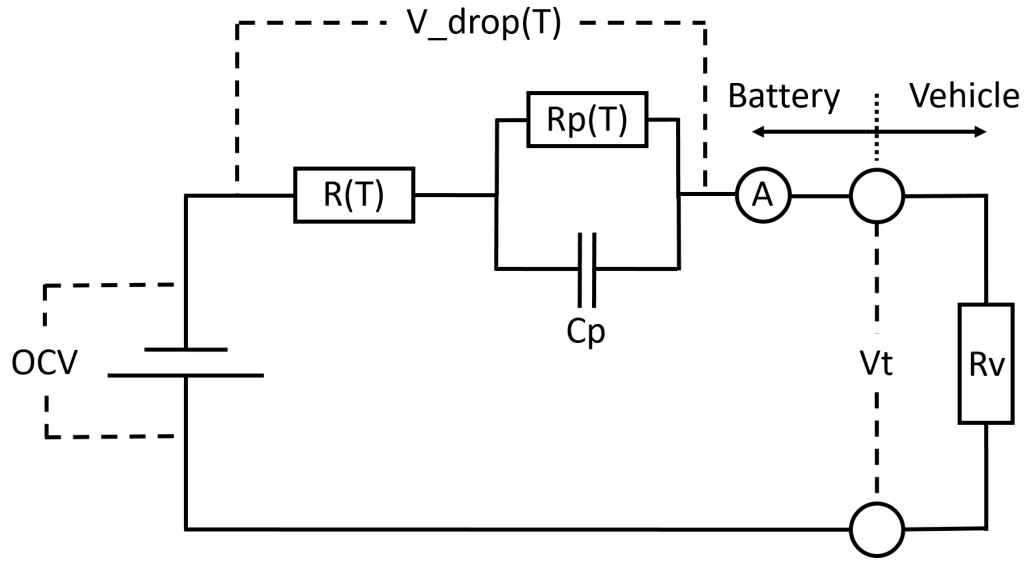

Figure 4.2: Schematic of battery model representing the measurements used and considered to produce metric $j1$.

$$E_t = \int_{t_0}^{t_{end}} I \times V_t dt \tag{4.3}$$

$$E_{loss}(T) = \int_{t_0}^{t_{end}} I \times V_{drop}(T) dt \tag{4.4}$$

$$E_{total} = E_t + E_{loss}(T) \tag{4.5}$$

E_{total} may be restated by combining the integrals from Equations 4.3 and 4.4, leading to Equation 4.6. Since the sum of voltage drops in the circuit must be equal to the voltage source, the OCV in this case, Equation 4.7 must be true. In which case the complete vehicle energy consumption, E_{total}, can be measured by the energy consumption through the OCV, as described by Equation 4.8.

$$E_t + E_{loss}(T) = \int_{t_0}^{t_{end}} I \times (V_{drop}(T) + V_t) dt \tag{4.6}$$

$$OCV = V_t + V_{drop}(T) \tag{4.7}$$

$$E_{total} = \int_{t_0}^{t_{end}} I \times OCV\, dt \tag{4.8}$$

The derivation performed in Equations 4.3 to 4.8 leads to the conclusion that the first cost metric, j_1, should be defined as

$$j_1 = \int_{t_0}^{t_{end}} V_{OCV} \times I dt. \tag{4.9}$$

Secondly, the DOD is used as an objective to be minimised. As discussed in Chapter 2, a battery's Coulombic capacity is dependent on its temperature, and therefore the effective DOD and conversely remaining range will also be dependent on the temperature of the battery. In the model used for this research this is accounted for by adjusting the effective capacity according to the temperature of the battery and current being drawn. A complete description of how this phenomena is captured is presented in Chapter 5. The battery DOD objective, j_2, is given in Equation 4.10.

$$j_2 = 100 - SOC(t_{end}) \tag{4.10}$$

Finally, the thermal comfort is considered. In Chapter 1 a list of eight articles and blogs was given concerning electric vehicles in cold weather; the dominant theme of which was that electric vehicles perform badly at cold temperatures and drivers would have to consciously choose between comfort and range. Considering this, a discomfort metric given in Equation 4.11 is introduced as the second objective to be minimised. Discomfort is chosen, rather than comfort, as the metric is intended to be minimised along with energy consumption and DOD.

$$j_3 = \int_{t_0}^{t_{end}} (T_{target} - T_{cabin}) dt \tag{4.11}$$

where T_{target} is 22°C (the cabin target temperature), which was the ideal temperature seen in Figure 2.10, and T_{cabin} is the actual cabin temperature. This metric describes the area bound by the actual cabin temperature and the target temperature. When this area is small the actual cabin temperature is on average closer to the target temperature compared to when this area is large. This method for measuring and improving comfort was used by Shojaei *et al.* in [73] with a slight alteration. In [73] the cabin temperature in their PHEV was compared against a conventional vehicle's cabin temperature, whereas here it is compared against the target temperature and so data from another vehicle is not required which simplifies the procedure and results. The weakness in this metric is that the cost would keep improving if the cabin temperature were to exceed the target (i.e. there is no penalty if the cabin were to become too hot). However, the control systems for the

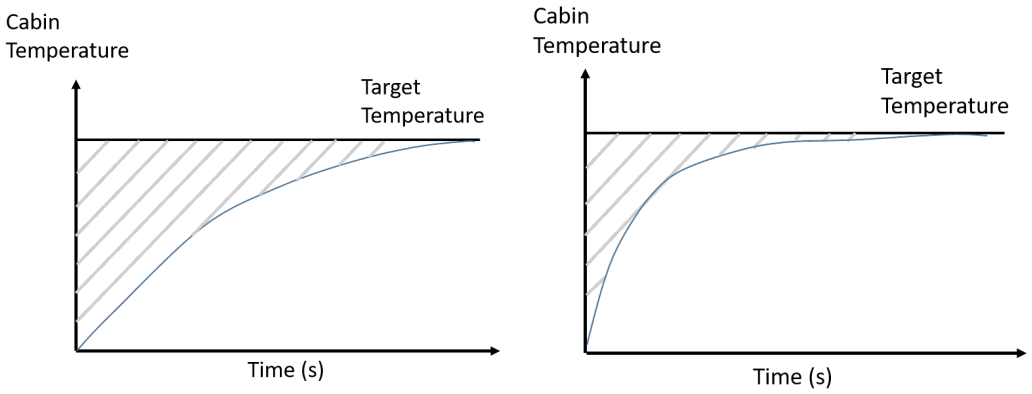

(a) Low thermal comfort, relating to a larger j_2 value.

(b) High thermal comfort, relating to a smaller j_2 value.

Figure 4.3: Examples used to depict j_2 which describes the shaded area between actual and target cabin temperatures.

HVAC prevent this from happening as is explained in Chapter 5.

j_1, j_2 and j_3 give the three objectives used in the multiple objective optimisation problem.

4.6 Combining the objectives

In order to combine them into one cost function to be minimised, J, normalisation and weighting factors have been used. These are seen as coefficients n_i and w_i respectively in Equation 4.12.

$$J = \sum_{i=1}^{i=3} n_i w_i j_i \tag{4.12}$$

Here n_i are the normalisation factors and w_i are the weighting factors. Normalisation factors are required since the metrics used occupy different magnitudes and comparing their raw result would bias the discomfort metric which is measured in the region of 10^5°Cs, hence improvements here would always dominate the cost metric. Normalisation allows for relative improvements to be measured and compared. n_i are generated by normalising each of the objective functions when the simulation is run on a given drive cycle at a given ambient temperature as in Equation 4.13. For this normalisation the vehicle is operated in a baseline configuration, which is set out in Section 4.4. A set of n_i will exist for all scenarios used, i.e. for all combinations of drive cycle and ambient temperature.

Table 4.3: The weighting factors used when optimisation priority is either neutral, battery weighted or cabin weighted.

Weighting Factor		Neutral	Battery	Cabin
Battery	w_1	1/4	1/3	1/6
	w_2	1/4	1/3	1/6
Cabin	w_3	1/2	1/3	2/3

$$n_i j_i^{baseline} = 1 \tag{4.13}$$

Here $j_i^{baseline}$ indicates that the metric is measured for the baseline case, hence when the system is re-evaluated using a new control strategy it will be compared in the cost function to the baseline case outlined in Section 4.4.

The weighting factors, w_i, are used to give priority to either the battery, the cabin or a compromise between the two, which will be referred to as neutral. The details of this can be seen in Table 4.3. Since j_1 and j_2 are both battery weighted objectives, they split the battery weighting between them, hence their weightings are 1/4 each for the neutral weighting, giving a total weighting of 1/2 to the battery objective. The bias weightings, i.e. battery or cabin weighted, give a 2/3 weighting to the preferred objectives. By definition, when operated in the baseline configuration, using any of the chosen weightings will result in $J = 1$. By default the neutral case is used, with the other weightings being explored when specified.

4.7 Concluding points

- A selection of optimisation search algorithms have been reviewed, and one will be selected to address Research Objective 1 in Chapter 6.
- All vehicle operational modes have been identified for exhaustive comparison to address Research Objective 2 in Chapter 7.
- Dynamic programming was identified as the method to be used to produce optimal battery heating trajectories in order to address Research Objective 3 in Chapter 8.
- Operational mode 20 was selected for a baseline against which improvements will be judged and 3 drive cycles were selected for testing.

- A cost function was defined which will guide optimisation searches and quantitatively compare vehicle performance.

Chapter 5

Model

5.1 Introduction

Chapter 1 stated that this research would use Dymola to develop a model for an electric vehicle which is based on, but expands upon, the current start of the art commercially available. Then in Chapter 3, a review into the state of the art thermal management research informed what the vehicle model should be capable of. In this chapter a model is developed which can utilise heat and redirect it via the heat pump to the cabin and the battery from the following thermal sources; the motor, transmission, thermal battery, cabin exhaust and ambient. Hence the primary requirement of the model is to utilise these thermal sources, while being able to optionally provide heat to the battery. This foundation requirement can be summarised by the capability of the model schematically demonstrated in Figure 5.1.

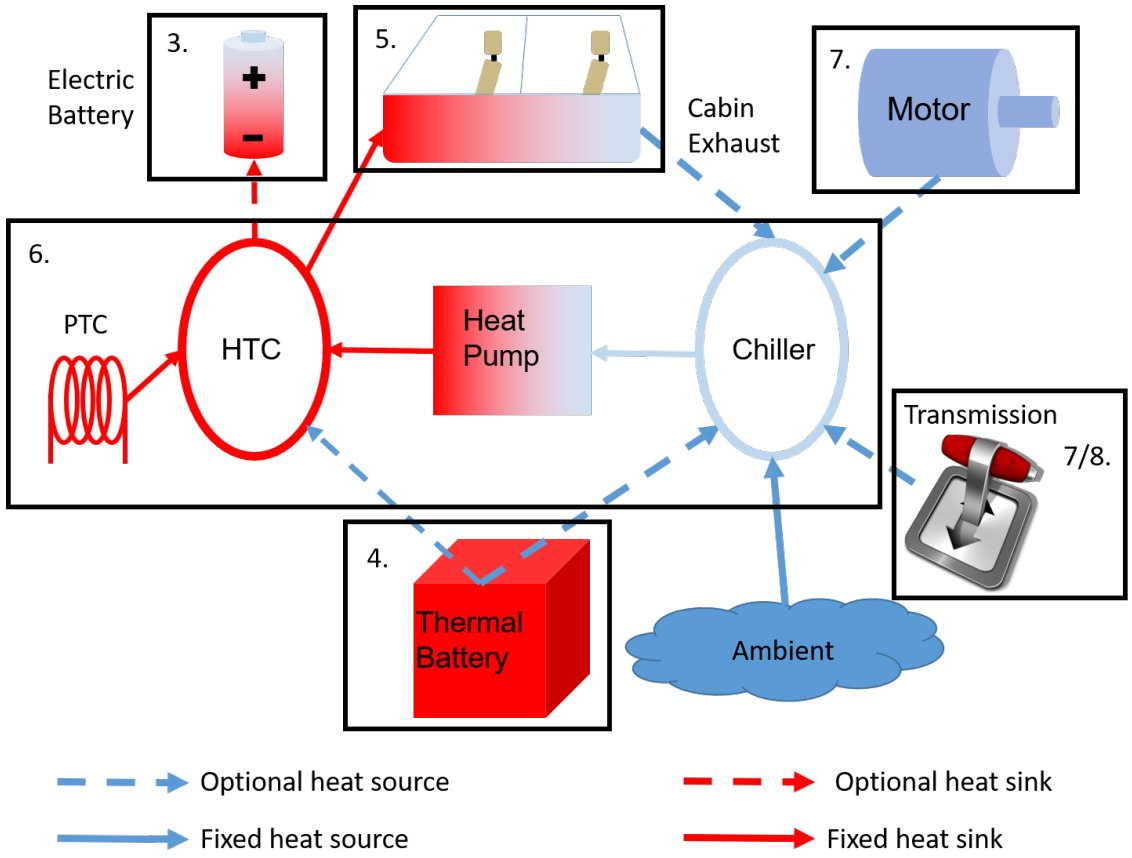

Figure 5.1: This schematic shows the thermal sources identified and how they should be able to exchange thermal energy. The numbering shown inside the black boxes corresponds to the sub-models labelled in Figure 5.2

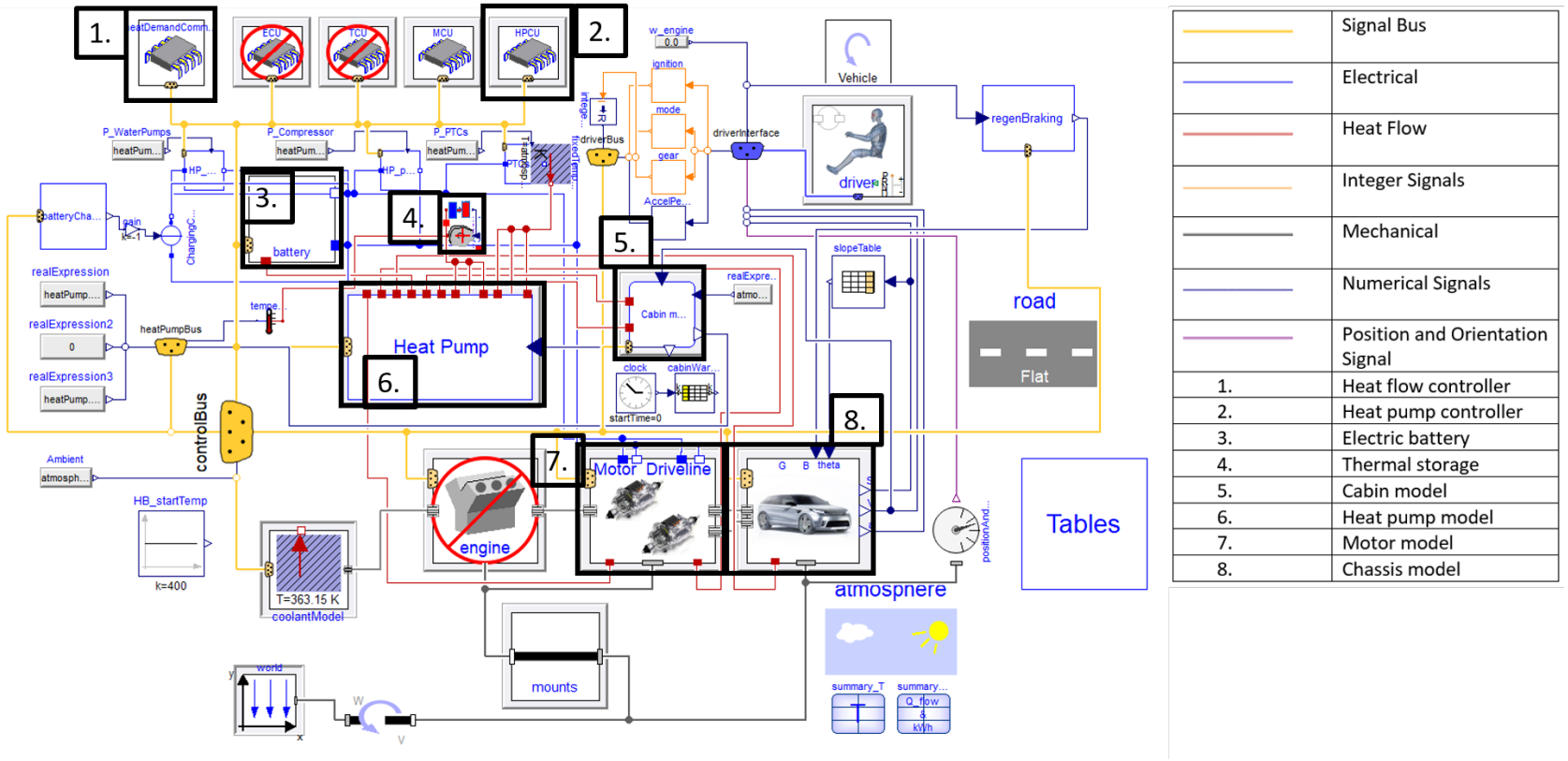

Figure 5.2: Here the top layer of the Dymola model is shown with most relevant sub-models labelled. Lines of different colours between sub-models indicate different types of physical connection which are identified in the legend.

Figure 5.2 shows how the system diagram shown in Figure 5.1 has been translated into a Dymola model. The numbers in each figure show where the major components of the system can be found within the Dymola model. Due to the size and complexity of the model it cannot be represented as a series of equations. Neither would it be practical to completely explain the modelling process, listing all Dymola components used and their configurations. Instead, this section will go through the key components of the system and explain how the models work from a schematic perspective. The full model is accessible through Claytex should one be inclined to explore the model completely.

Figure 5.1 shows thermal source options, the control of which will be used to answer the research objectives. Specifically, Research Objective 1, "What is the optimal sizing of a thermal battery for application in an electric vehicle with a heat pump", is addressed by optimally sizing the thermal battery component seen at the bottom of Figure 5.1. Research Objective 2, "What opportunity is there in controlling range and comfort through the systematic comparison and selection of a specific combination of heat sources and sinks" will be answered by exploring all possible combinations of optional thermal connections, seen in Figure 5.1, and comparing the performance of the resulting operational modes. Finally, by optimally controlling the thermal connection between the electric battery and the heat pump, seen in the top left of Figure 5.1, the third Research Objective, "What control can be gained over the balance of comfort and range through the dynamic control of battery heating during a drive cycle" will be addressed.

In addressing Research Objective 2, different combinations of heat sources will be explored. These different combinations of sources will represent different thermal management architectures, which will lead to a broad range of thermal demands on the vehicle. In response to this, the basic control of the model which will define rules as to when components are allowed to be connected to the heat pump and control the power demand for the heat pump will need to be constructed in a way which is robust to the different architectures. Here robust means that the model can be subjected to a wide variety of scenarios and thermal management architectures without encountering errors and failing. As an example, Dymola imposes temperature limits on different coolant fluids, which, if broken, cause the simulation to fail and stop. It will therefore be important that the model is controlled in a way which ensures these limits are not broken.

Chapter 4 also mentioned the need for this research to be translatable into other problems, such as high temperature thermal management. In this respect the model should be made in a way which would allow a user to reconfigure the vehicle

to test other thermal management scenarios.

This chapter describes how each of the components seen in Figure 5.1 are modelled and controlled to achieve the desired capability and robust operation. Each component will also have individual requirements in terms of fidelity, robustness or capability; these will be defined and discussed in the sections pertaining to each component. The vehicle and HVAC system modelled in this research are conceptual and hence not directly comparable in capability to any system on a vehicle. Additionally the battery used is not the same size or configuration as the battery on the Jaguar I-Pace, and so no pack level data exists for validation. Given this situation, a suitable validation strategy for the complete model and its sub-components needs to be used. Section 5.10 explains how the model and sub-components are compared to results found in literature pertaining to similar or comparable vehicles. For example it is known from Section 2 that electric vehicles should expect a range reduction of between 40% and 70% when the ambient temperature is reduced from 15°C to −15°C. Here the bounds for representative behaviour have been set and the model will be satisfactorily representative if the range reduction falls within these bounds while completing the same ambient temperature reduction.

It has been discussed in Chapter 4 that Dymola will be used as the modelling package for this work, with other researchers also supporting this choice [143, 166, 167]. The model used in this research is an adaptation of the model used by Picarelli *et al.* in [143]. The model used by Picarelli *et al.* was developed for JLR to demonstrate a vehicle that would be capable of using multiple thermal sources as well as having the battery as an optional heat sink. The model was originally based on a PHEV vehicle, and so had an engine. In Chapter 2 it was seen that in PHEV vehicles in cold climates the optimum thermal management strategy was to utilise the engine for heat, or if use of the ICE was prohibited then an electric vehicle thermal management solution was needed. Hence the problem was limited to battery electric vehicles. This project's connection to JLR lead to the availability of specifications and data pertaining to the Jaguar I-Pace, as well as an interest from JLR in using this platform. As such, the model was redeveloped to represent the Jaguar I-Pace. In the redevelopment of the model for this research the following system level changes were made;

- the internal combustion engine has been removed
- the battery size increased
- the motors duplicated to create a four wheel drive vehicle

- a thermal storage device with variable specific heat capacity was added.

The first three of these changes were necessary so that the model represented the Jaguar I-Pace, while the final was added to accommodate the inclusion of a thermal storage device based on a phase change material, as identified in Chapter 3. The ICE is replaced within the model, however it could be reintroduced should a user be interested in exploring HEV or PHEV thermal management strategies. Additionally there have been changes at a component level. These changes have been made to either increase fidelity in important components such as the battery, or improve robustness. Specific details of component changes will be provided in the relevant sections. The first of which will be the heat pump in Section 5.2.

Optimisation will be used in this research, requiring the model to undergo hundreds of evaluations, so a suitable simulation time limit should be set. Setting a limit of 10 minutes per evaluation allows for 144 simulation evaluations per day, or 1008 evaluations per week. This is fast enough to achieve the optimisations required within a reasonable time span.

5.2 Heat pump

The requirements for the heat pump model are that it is robust to varying thermal inputs and demands, and that it is capable of receiving heat from a variety of thermal sources, the combinations of which can be easily reconfigured.

The heat pump model has been redeveloped, varying from the one published in Picarelli *et al.* [143]. In Picarelli *et al.* the heat pump is modelled using a series of fixed thermal resistors which connect to thermally active components around the vehicle. A COP of 5 is then assumed for the heat pump refrigeration circuit and used to calculate the heat delivered and the compressor's power consumption. Since the heat pump is a pivotal component to this research a higher fidelity model was required. With no opportunity to map a physical heat pump, instead a physical heat pump model was created in Dymola. The model was then populated with specifications from Jaguar I-Pace where available and specifications from a Range Rover Sport when unavailable. The specifications of parts pertaining to the Range Rover Sport were found at [168].

Figure 5.3 shows the configuration of the heat pump's refrigeration cycle. R134a was used as the refrigerant, which is a common choice in literature concerning vehicle level heat pump research and is used on production vehicles [21, 67]. The use of a compressor, condenser, expansion valve and evaporator is the normal configuration for investigating vehicle level performance when using a heat

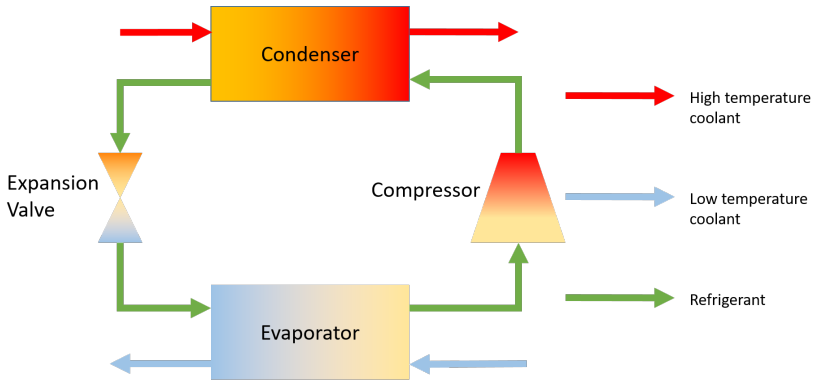

Figure 5.3: Here the heat pump's refrigeration is shown schematically. Heat is collected via coolant circuits and delivered to the evaporator, where it is upgraded through the compressor and extracted for heating using the condenser.

pump [24, 66, 67, 71]. Variations on this simple format exist, such as using a dual stage condenser; however research into these examples are limited to component testing [169, 170], rather than system integration, hence the simpler system is used.

In Figure 5.3 both the condenser and evaporator are modelled using refrigerant to liquid heat exchangers. This allows for heat to be collected and distributed using coolant circuits, these are the chiller and high temperature circuits respectively. The chiller circuit is used to extract heat from thermal sources, while the high temperature circuit is used to deliver heat to the battery and cabin, whilst receiving heat from the PTC heater and the thermal battery. This is in accordance with the schematic presented in Figure 5.1. The advantage of refrigerant to coolant exchangers, rather than a refrigerant to air heat exchanger, is that the coolant can be sent to different components around the vehicle and then be collected and sent to the heat exchanges, thereby collating the heat. This means that heat sources can easily be isolated from the heat pump by switching coolant valves to bypass the component; this process allows the heat pump system to meet the requirement that the system is capable of receiving heat from a variety of sources and that the combination of sources is easily reconfigurable. The details of how these bypass switches work and are controlled is give in Section 5.2.1.

The heat pump was required to be robust to different thermal configurations and a variety of heat supplies and demands. In the refrigerant circuit the primary risk which could cause the model to fail is that the refrigerant boils. This is prevented by using a proportional-integral-derivative controller (PID) which has the ability to override the compressor power demand received from the heat pump control unit (HPCU) to prevent the refrigerant pressure exceeding 3MPa [171]. The control for

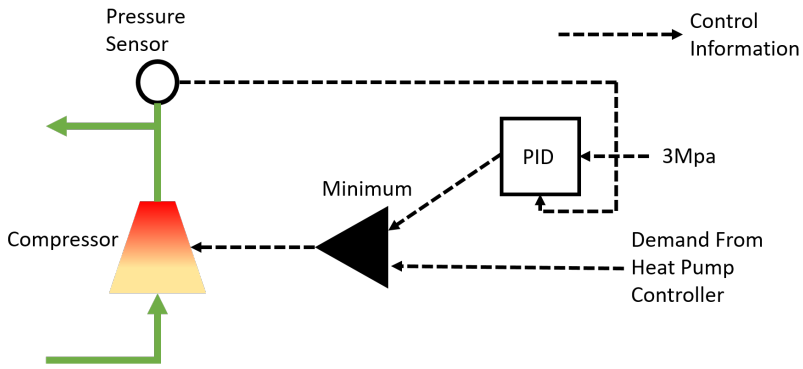

Figure 5.4: A pressure sensor and PID controller are used to prevent refrigerant pressure from exceeding operational limits and hence prevent the model from failing.

this can be seen in Figure 5.4. This measure prevents the refrigerant pressure from becoming too high, leading to the refrigerant boiling, hence ensuring the system is robust. Additionally the system needs to be robust to the high temperature and chiller circuits exceeding their operating conditions; measures to ensure this are detailed in Section 5.8.

Figure 5.5 provides an example of the operation of the heat pump using the baseline operating conditions, defined in Section 4.4. In this example the model is completing the WLTP drive cycle at 5°C. Figure 5.5 shows the pressure controller working as intended. At approximately 800s the pressure trajectory is expected to exceed 3MPa; however, the PID controller intervenes and reduces the compressor power. This intervention can be seen in the bottom graph of Figure 5.5 where the minimum value of compressor speed is used, as described by Figure 5.4. The pressure then recovers and drops again, creating a sawtooth shape until the system is able to stabilise.

Now that the refrigeration cycle has been demonstrated to meet the requirements set, Section 5.2.1 will explain how the coolant circuits interact with the thermally active components.

5.2.1 Heat pump coolant circuits

To answer Research Objective 2, defined in Section 3.7, the model needs to be capable of easily reconfiguring the heat pump's coolant architecture so that different combinations of components are connected in the thermal circuit of the heat pump. The requirement for the coolant circuits is therefore to create a coolant plumbing architecture which can easily connect and isolate components to and from the heat pump. Additionally, to meet the requirements of Research Objectives 1 and 3 there

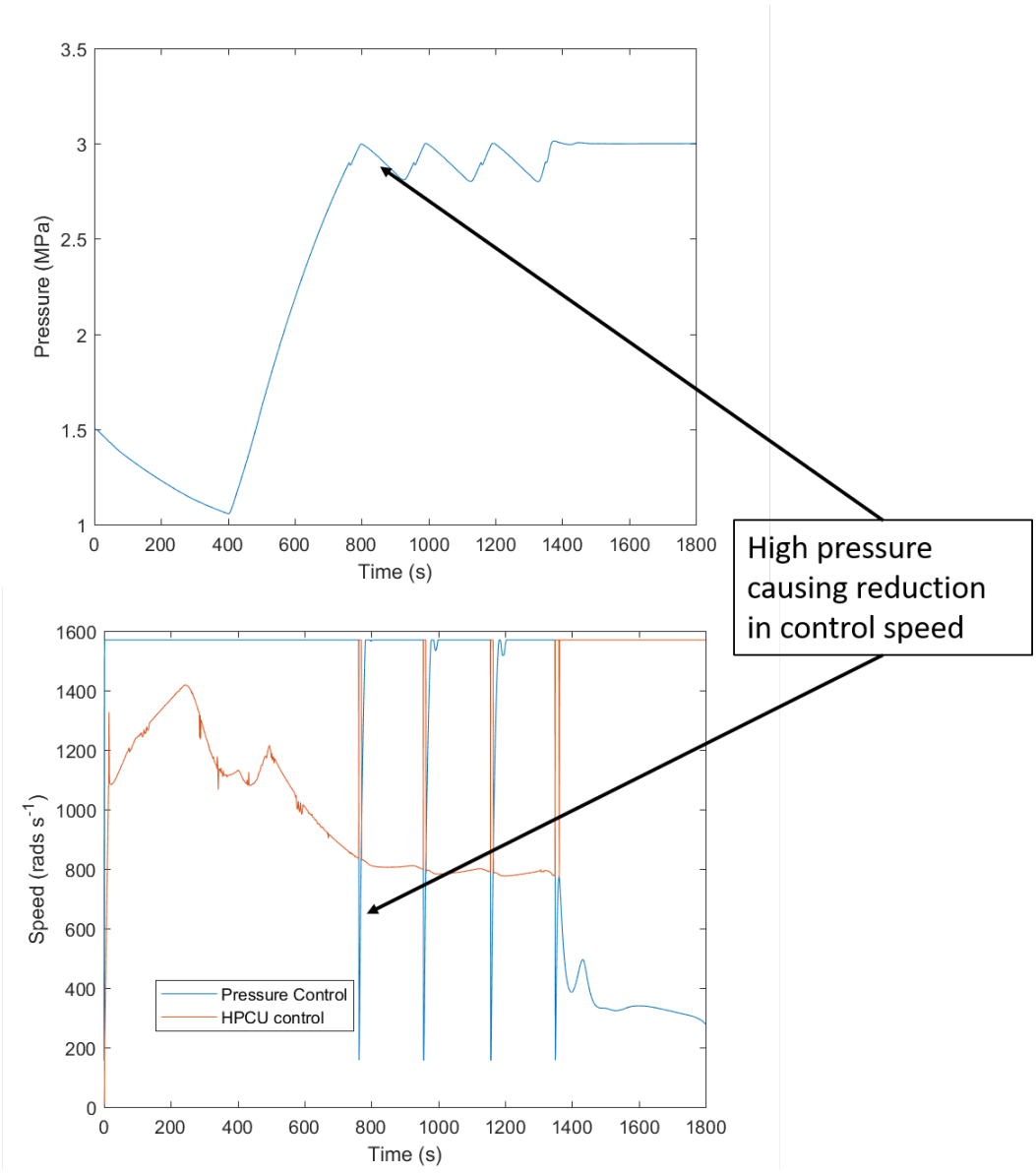

Figure 5.5: Compressor outlet pressure (top) and compressor control speed (bottom) as the vehicle is simulated in the baseline thermal configuration completing a WLTP drive cycle at 5°C. Here it can be seen that the pressure almost exceeds its limit of $3MPa$ in, but the pressure controller intervenes in Figure, preventing the model from failing due to boiled refrigerant.

will need to be some means to control heat flow. With regards to Research Objective 1, this allows for the thermal power of the thermal battery to be controlled and optimised, while Research Objective 3 requires different levels of heat delivery to be available for the electric battery. Hence there is a requirement that the coolant circuits needs to control or throttle the flow of heat between the coolant and the components.

The original model contained three coolant loops, one for the evaporator and two for a two stage condenser. This was designed with a PHEV architecture in mind. Changing to a EV negated the need for the mid temperature circuit, which was designed to be used with the ICE of the PHEV. The coolant circuits were linked to the thermally active components by versions of the "non-physical control" (which will be explained below), with fixed, rather than variable, thermal resistances. The "physical coolant switches" (explained below) have been created for this research. Coolant circuit target temperatures of $-10°C$ and $90°C$, for the chiller and high temperature circuit respectively, have been kept from the original model, along with the choice of a water/glycol mix for the coolant fluid.

To accommodate the requirements set, a model was constructed which is represented schematically in Figure 5.6. Here it can be seen that the model is split into two sub-systems. The first is the "physical coolant switch". This system uses heat exchangers parameterised using either Jaguar I-Pace or Range Rover Sport specifications, as mentioned previously. The physical switches have three purposes. Firstly they convert the thermal energy from vehicle components into heat in the coolant, which can then be collected and used by the refrigeration circuit, as described in Section 5.2. Secondly, since they are parameterised using existing components, they provide a physical limit to the amount of heat which can be exchanged between a component and the coolant. This ensurers the heat exchange between a component and the coolant has realistic limitations. Finally, the variable directional valve allows coolant to be diverted away from the component's heat exchanger, passing through a bypass pipe instead. This also reduces pumping costs since the bypass pipe has less impedance than the heat exchanger. The valve is altered depending on the value of the switch input. The flow is set to either 0.99, corresponding to 99% of the flow being directed through the heat exchange, or 10^{-8}, corresponding to 99.999999% of the flow being diverted through the bypass. 0% flow is not used as this caused the model to fail to initialise, so a very small flow was used instead. By setting the switch values in an external controller, discussed in Section 5.8, the model can be easily reconfigured to different combinations of thermal sources, thereby meeting the requirement set at the beginning of this section.

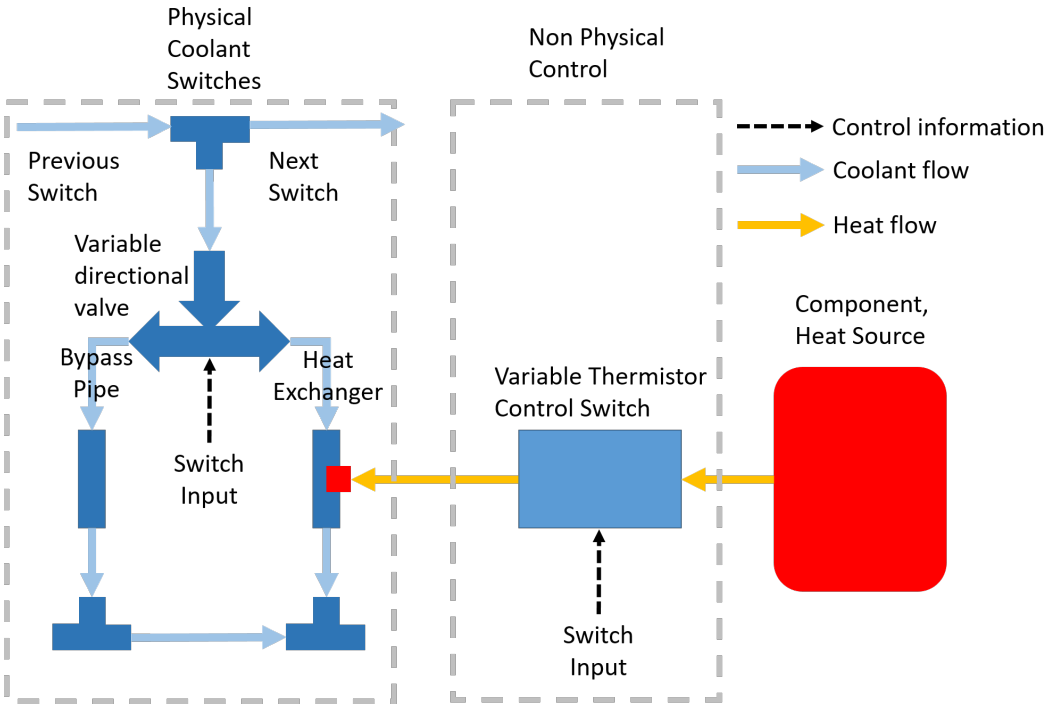

Figure 5.6: The coolant switching system is shown, which is used to connect and isolate components to and from the heat pump. In this example a heat source is given, if a heat sink where used the flow of heat between the component and the coolant would be reversed. The switch is broken into two sub-systems, the physical coolant flow and bypass, and a variable thermistor used to throttle and control the connection.

The second sub-system in Figure 5.6 is the "non-physical control". This system uses a PID controller to vary the thermal resistance between the heat source and the heat exchanger. This serves two purposes, firstly it can be used to isolate the component from the coolant. Although this is accounted for in the "physical coolant switch" it also needs to happen here. The isolation at this level prevents thermal exchange with the stationary coolant in the heat exchanger, which could lead to the coolant exceeding the model's temperature limitations inside the heat exchanger and cause a failure. Hence this precaution is made to increase the model's robustness. Secondly, the PID is used to throttle the component's thermal interaction, producing the desired heat exchange as per the requirements made at the start of this section.

The next step in producing the heat pump model is combining the switches for each component in the chiller and high temperature coolant loops. Figure 5.7 shows schematically how this is achieved. In Figure 5.7a it can be seen that all the sources are placed in parallel, while in Figure 5.7b this is not the case. In Figure 5.7b the battery, cabin and ambient act as heat sinks, while the thermal battery and PTC heater act as sources. Here it can be seen that the heat produced by the heat pump is split between the cabin and battery. If the heat pump is not able to meet the combined heating demand for both these components then one will receive less heat. Since the thermal contact to the battery is greater than the thermal contact to the cabin, if the battery is connected to the heat pump then the heat delivery to the cabin will be compromised. The consequence of this is shown in Section 5.7. In this case ambient is used as a heat sink in the case that the high temperature circuit becomes too hot and needs to reject some heat. This configuration also allows for an air-conditioning mode to be explored in the case where a user is interested in high ambient temperature thermal management. °C, the cabin cold thermal switch would also be opened in Figure 5.7a, providing cooling for the cabin. The thermal battery and PTC heater are placed in series before the heat sinks. This is designed so that maximum heat is available for the heat sinks. Furthermore, the thermal battery is placed before the PTC heater. This decision was made to minimise PTC heater consumption, with the thermal battery first the coolant is as close to operating temperature as possible before the PTC evaluates how much heat is needed, thereby minimising PTC consumption.

The PTC itself is controlled using a PID controller, with the target of getting the cabin to its target temperature of 22°C. However if the high temperature coolant circuit exceeds 85°C the PTC will turn off. This is to prevent the coolant circuit from exceeding its maximum operating temperature of 90°C.

In this section a set of requirements was given for the capability of the coolant

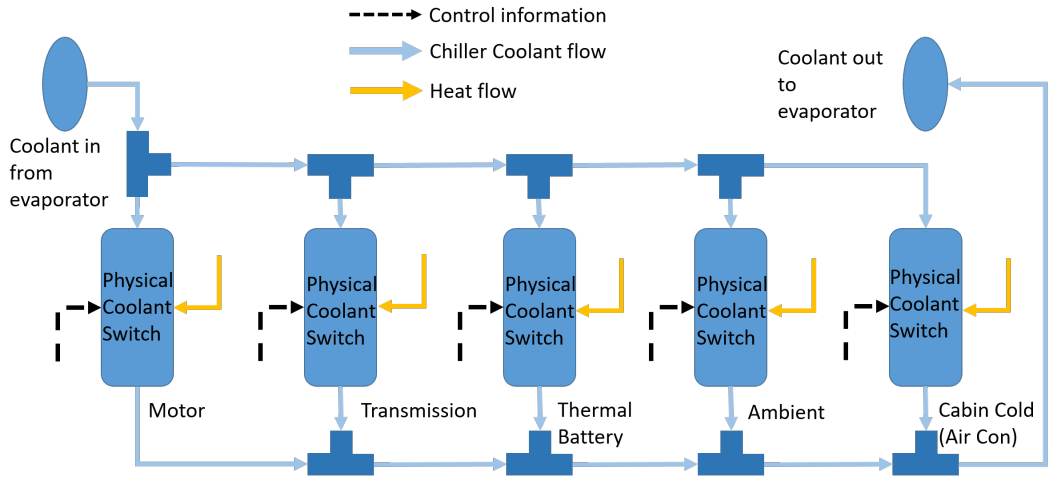

(a) Here the switches shown in Figure 5.6 are assembled in parallel, linking the stated components into the chiller coolant loop. Coolant will flow through this loop and into the evaporator shown in Figure 5.3 where the heat is extracted.

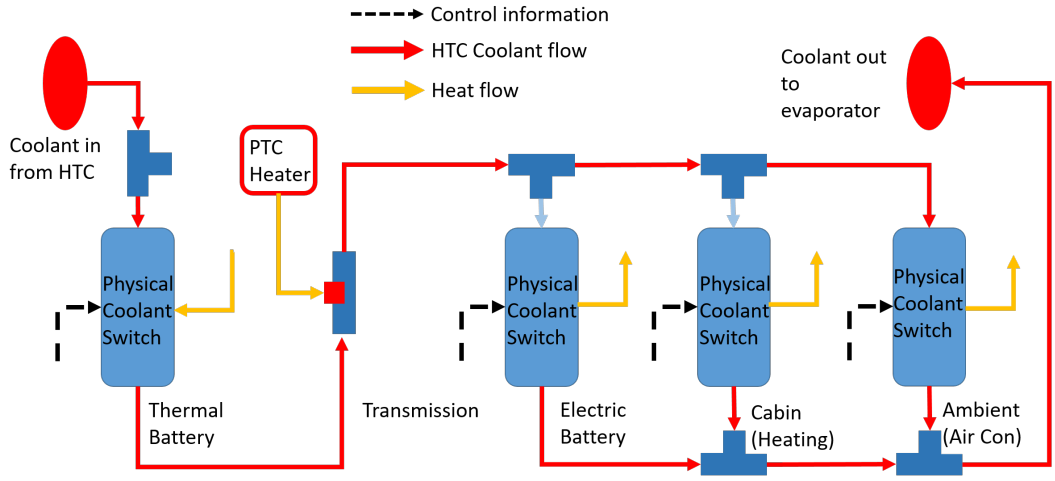

(b) Here the switches shown in Figure 5.6 are assembled to create the high temperature circuit.

Figure 5.7: Schematic representing the high temperature and chiller circuit coolant models

circuits and their interaction with thermally active vehicle components. Through the figures presented and explanations given it is seen that the models created are capable of meeting these requirements. Further proof of the models aptness will be provided in the remaining individual component sections, where the interaction of individual components with the heat pump will be demonstrated.

5.3 Battery

In order to address the Research Objectives the electric battery model needs to have some key capabilities. The focus of this work is on the balance of range and comfort, with battery heating needed to improve battery performance and therefore range, but at a cost to comfort. For this to be investigated a battery model is needed which captures the relationship seen between temperature and range. Furthermore, the model needs to accurately capture the heat required to warm the battery sufficiently to see improvements in performance. Hence, for the purpose of this research there are two aspects of battery modelling that are of interest: the electrical and thermal. The electric model needs to capture the battery dynamics discussed in the literature review, i.e. the capacity as a function of temperature needs to fit within the spectrum defined by Figure 1.1. In order to check this requirement has been met the battery model will be discharged over a temperature range of $-15°C$ to $15°C$ in $10°C$ increments and compared to the information presented in Figure 1.1. Should the found capacity reduction be in agreement with that from literature, the battery model will be deemed to have sufficiently captured low temperature battery dynamics.

The thermal model will be harder to validate. Firstly, as discussed in Section 4.4, the battery pack in this vehicle is effectively hypothetical, created to investigate a specific vehicle scenario. The pack is however based upon existing cells with data available for comparison, but the thermal data for these cells was collected in a thermal chamber and therefore will not be comparable to temperatures expected inside a thermally managed pack. To account for this the battery pack model will be reduced to a single cell in order to perform a validation against existing data. Since this is not representative of the thermal behaviour inside the pack setting, a numerical accuracy requirement will not carry any meaning. Hence the model will be qualitatively compared to available data to check that the modelled cell internal heat generation is representative of a real cell.

The battery's thermal connection to the heat pump will be demonstrated in the final part of this section. Here the battery model's interaction with the heat

pump will be shown to meet the requirements for component heat pump interaction set in Section 5.2.

The electrical model used for the research presented utilises a first order RC network equivalent circuit model, explained later in this section. By comparison the original model used just one resistor to capture the battery dynamics. Additionally the Coulombic counting method of SOC tracking has been updated with the addition of effective capacity adjustment, which is necessary to repeat the capacity versus temperature relationship seen in literature. Finally, the thermal model has been updated so that it exchanges heat with ambient, whereas the original model used a fully insulated thermal model for the battery. This increased fidelity in the thermal model prevents the method from underestimating the battery's heat requirements by enabling a realistic mode of heat loss.

Now that the model requirements for the electrical and thermal aspects of the battery have been set, and the state the model was received in explained, the model detail is discussed. Electric battery models in this area typically fall under 3 branches; electrochemical, empirical (based on data) and equivalent circuit models [172]. An equivalent circuit model (ECM) has been chosen to electrically represent the battery. The ECM is used in literature at vehicle level [173–175], it offers improved performance in terms of simulation time compared to electrochemical models, which typically require the simultaneous solution of a large number of partial differential equations [172]. This improvement in simulation time is such that real time operation and implementation of ECMs is possible, but would be impossible using an electrochemical model [172]. ECMs also offer improved accuracy over empirical models, which use data to infer relationships, but fail to capture battery dynamics under a dynamic load [172]. ECM refers to the treatment of the battery as if it were an electric circuit, where the battery dynamics are captured by a mix of resisters, capacitors and other electrical components. The advantage here is that each component is simple and can be modelled well and simulated quickly. The disadvantage is that it is a high level approximation to the internal workings of a cell and as such the accuracy of the model is lower than higher fidelity electrochemical models [172]. However, as discussed at the start of this section, the model will be deemed accurate enough if it can replicate the capacity/temperature relationships seen in literature. Since ECM just refers to the use of electronic components to represent the model, there are a number of valid circuits that can can be used. For this research a first order resistor capacitor (RC) circuit has been used, while a second order RC circuit was also considered. In comparison studies it has been shown that first order RC networks are one of the best performing ECMs [172, 176]. They have

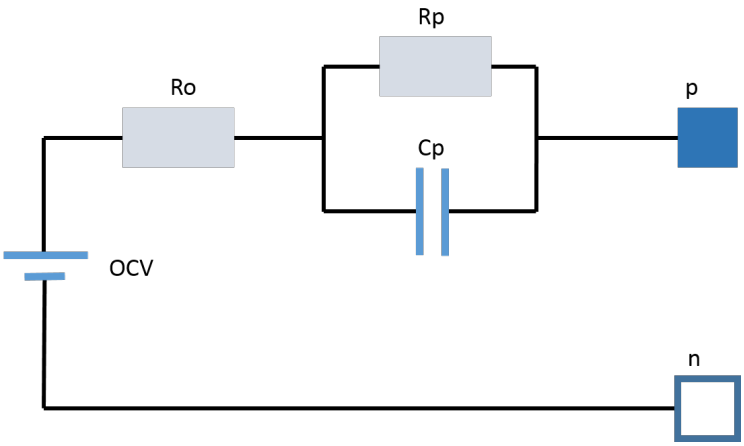

Figure 5.8: Diagram of 1^{st} order RC circuit. OCV is the open circuit voltage, Ro and Rp are resistors and Cp is a capacitor; P and N denote the positive and negative cell terminals respectively.

also been validated at $-20°$C with a mean voltage error of less than 3%, making them acceptably accurate for this work [177]. Second order RC networks usually offer better performance in terms of accuracy, but they are harder to parameterise and can become unreliable due to their lack of unique numerical solutions [178]. A diagram of a first order RC network can be seen in Figure 5.8.

Each of the resistors, capacitors and the open circuit voltage seen in Figure 5.8 need parameterising. As has been seen in the literature review, the terminal voltage of a cell is predominantly dependent on two variables, state of charge and cell temperature [76]. Each component then needs to be parameterised using a 2D lookup table dependent on these variables. For OCV only SOC was used as the dependent variable, making the approximation that it is independent of temperature. While a cell's OCV is dependent on temperature the variation in cell voltage is less than 1% over the temperature range of $0°$C to $40°$C, which is significant if the OCV is used for SOC estimation, but since that is not the case here it has not been accounted for [179]. Acquiring the necessary parameters across a range of temperatures, states of charge and currents is a formidable task and one that could not have feasibly been completed along with the other work needed for this project. I am indebted to my colleague Yashraj Tripathy [180], who had been conducting research on a cell suited to this type of vehicle. He was able to provide lookup tables for both first and second order RC circuits which could be integrated into the model [180]. The lookup tables for OCV, R_0 and R_p are scaled by the number of cells in series to create one string. These strings are then placed in parallel to create the pack. This defines the pack sizing and through changing the scaling of parameters and the

number of strings in parallel the pack size can be quickly and easily changed. This allows the user to quickly change to a different electric vehicle scenario.

Since the parameters of the ECM are dependent on both temperature and SOC, thermal and SOC models also needed to be developed to complete the battery model. An overview of the cell's thermal model can be seen in Figure 5.9. The thermal model uses loss information from the ECM and vehicle speed as inputs. The thermal model does not account for entropic heating, which becomes dominant at low C-rates (¡C/2) [181]. This decision was made since the vehicle is expected to be operated at more than C/2 for the majority of its use, as evidenced by Figure 2.6. The thermal loss from the ECM model is converted to a heat flow which is input to a heat capacitor, the heat capacitor then has two modes of thermal exchange. Firstly the battery may exchange heat with the thermal management system, i.e. high temperature loop from the heat pump. This mode of thermal exchange uses the thermal switch described in Section 5.2.1. Secondly, the battery loses heat to ambient through the underside of the vehicle. Battery packs are typically protected from damage by a metal casing, for example Tesla use a 6.25mm thick aluminium plate to protect the underside of their battery packs [182]. This added protection will produce a thermal capacitance which needs to be accounted for, as well as its heat loss to the ambient due to cold air flowing over the plate. The capacitor representing the metal plate has dimensions 2m×4m (approximate foot print of the I-Pace [165]) ×0.01m (rounded to nearest centimetre from Tesla's example), specific heat capacity of 0.902kJkg^{-1} and density of 2700kgm^{-3}, both of which correspond to aluminium [2]. The value of the conductance from the metal plate to ambient is calculated using Equation 5.1 [183].

$$\bar{h} = (0.037Re^{4/5} - 871)Pr^{1/3}\frac{k}{L} \tag{5.1}$$

where k, Re and Pr are the thermal conductivity, Reynolds number and Prandtl number of the convection fluid. The Reynolds number and Prandtl number are defined in Equations 5.2 and 5.3. L is the length of the surface over which the fluid is flowing.

$$Re = \frac{\rho v L}{\mu} \tag{5.2}$$

$$Pr = \frac{C_p \mu}{k} \tag{5.3}$$

where ρ, v, μ and C_p are density, velocity, dynamic viscosity and specific heat capacity of the convective fluid. The constants in these equations have been parameterised

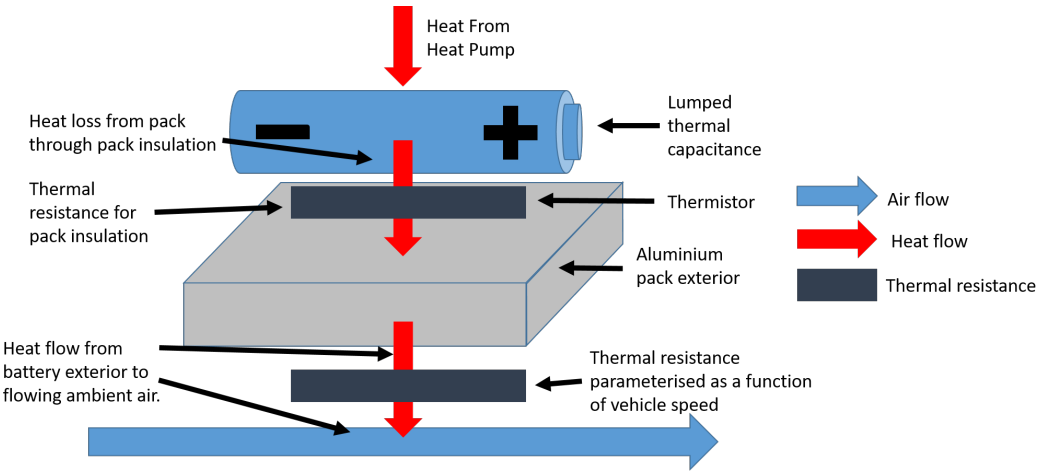

Figure 5.9: Thermal model for the battery.

using the values for air at $-23.15°C$, $1.85°C$ and $26.85°C$, which are given in Table 5.1. These values are interpolated for the given ambient temperature, then used in Equation 5.1.

Table 5.1: Air Constants used for flat plate in parallel flow convection block [2]

Parameter	**Value @ $-23.15°C$**	**Value @ $1.85°C$**	**Value @ $26.85°C$**	**Unit**
ρ	1.412	1.284	1.177	kg/m^3
μ	1.599×10^{-5}	1.725×10^{-5}	1.846×10^{-5}	$Pa.s$
k	2.227×10^{-5}	2.428×10^{-5}	2.624×10^{-5}	$kW/m.K$
Pr	0.720	0.713	0.707	N/A
C_p	1.0031	1.0038	1.0049	kJ/kgK

Equation 5.1 gives thermal conductivity for mixed boundary layer conditions, meaning there is a combination of laminar and turbulent flow over the plate. This assumption only holds while $5 \times 10^5 \leq Re \leq 10^8$. With an air temperature of $26.85°C$, the lower limit of $Re = 5 \times 10^5$ correlates to 5.4km/h or 1.5m/s. This speed is low enough that the approximation can be used without consideration of the laminar flow case, which would dominate in the 0m/s to 1.5m/s region [183]. It should also be mentioned that the convection block is operated with a minimum vehicle speed of 2m/s, which prevents the convection value from becoming negative and maintains some ambient heat exchange when the vehicle is stationary.

The SOC has two important roles in the battery model, firstly it dictates the value of parameters in the ECM. Secondly, as seen in Chapter 2 the Coulombic capacity of a cell is dependent on ambient temperature, which should be reflected in the SOC model, i.e. at lower temperatures the SOC drains more quickly than it

would at high temperatures due to the reduction in Coulombic capacity. To achieve this the coulomb counting technique has been used with a slight alteration. Coulomb counting is a common technique for tracking a cell's SOC, it integrates current as seen in Equation 5.4 [184].

$$\Delta SOC = \int_0^{t_{end}} \frac{100}{C \times 3600} \times I(t)dt \tag{5.4}$$

where C is capacity in Ah, t is time in seconds, t_{end} refers to the duration of the duty cycle and $I(t)$ is the time dependent current. However, this does not capture the loss in Coulombic capacity at low temperatures. To remedy this an additional factor is brought in which uses the temperature dependent effective capacity. The Coulomb counting equation then becomes,

$$SOC(t) = SOC_{init} - \frac{1}{C_{eff}} \int_{t_0}^{t} I(t)dt \tag{5.5}$$

Here an additional lookup table which contains information about the percentage of capacity available as a function of temperature is implemented. This is then used to scale the Coulomb counting equation by the factor C_{eff}, seen in Equation 5.5. Examples of this adjustment to Coulomb counting can be seen in literature [180] and [185].

The battery model's interaction with the heat pump, when using the baseline operational mode defined in Section 4.4, is presented in Figure 5.10. In Figure 5.10a it can be seen that as the battery is heated the temperature rises quickly at the beginning of the cycle. When the battery gets to its target temperature it is disconnected from the heat pump, this can be seen from the gradient change in battery temperature in Figure 5.10a just before 400s. This is also seen in Figure 5.10b, which shows the amount of heat sent to the battery from the heat pump. Here it can be seen that although 10kW of heat is requested for the battery, as described in Section 4.4, the heat pump is not able to meet this demand. However, the extra capacity required to meet the requested heat will be provided by the addition of thermal storage to the system. This will be demonstrated in Section 5.6.

In summary, this section has made a set of requirements, then by considering battery modelling options from literature a model has been constructed. This model expands upon the original model, adding fidelity to both the electric and thermal models with the intention of capturing battery effects seen in literature and producing a thermal model which does not under estimate the thermal requirements for battery heating. By comparing the model's capacity predictions during a 0.1C discharge to recorded data in literature, the battery model was shown to

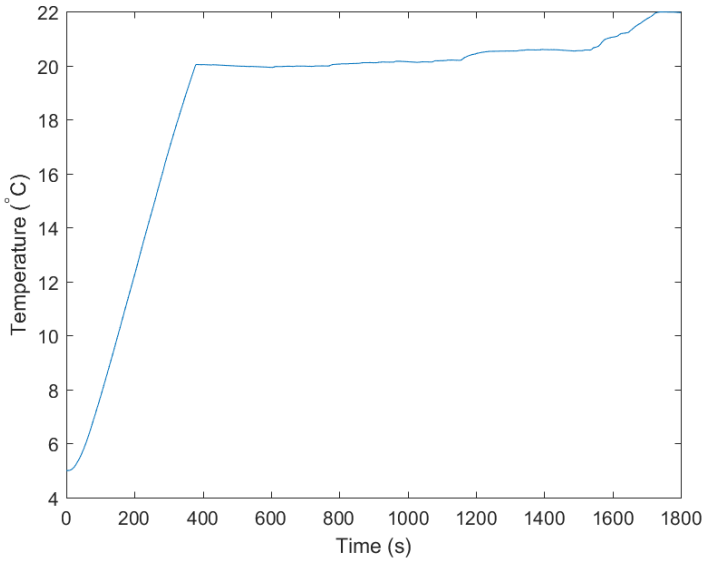

(a) Battery temperature response.

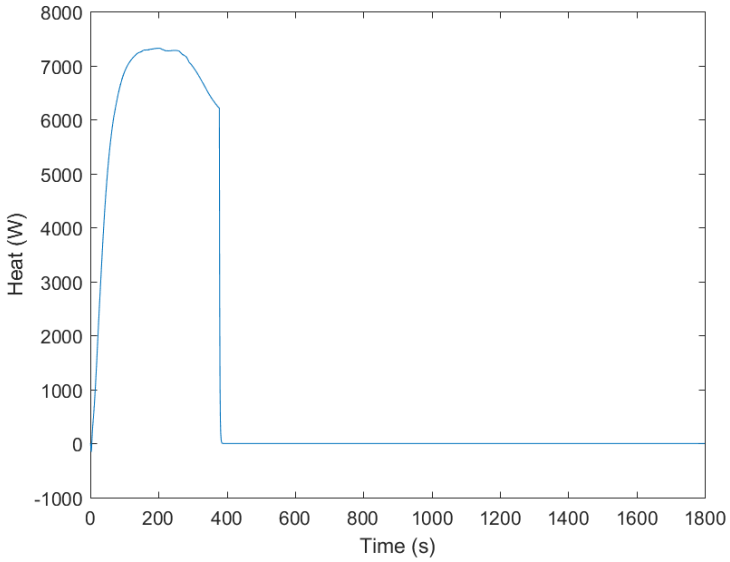

(b) Heat delivered to the battery.

Figure 5.10: Here the interaction between the heat pump and battery is demonstrated.

successfully meet the criteria that it is representative of known low temperature behaviour. Additionally the thermal model was shown to produce representative internal heating. Although increased accuracy in this area may be desirable it is not wholly necessary. The model is designed so that it may be reconfigured to represent other vehicle needs, while the method is designed to be applicable to any electric vehicle. Finally the model was shown to produce the desired interaction with the heat pump. Here it was seen that the heat pump in the baseline operational mode was unable to produce the requested battery heat, but in Section 5.6 the addition of thermal storage will be demonstrated to bridge this deficit.

5.3.1 Regenerative braking

The vehicle also supports the ability to make use of regenerative braking, which is a feature that was not present in the original model. This feature was added to further incentivise battery thermal management. The regenerative braking is limited by battery temperature, with charge acceptance maps being provided by JLR. Hence if the battery is warmed then it can make more use of regenerative braking and therefore will be more energy efficient, this will lower the cost associated with j_1 defined in Section 4.5. The vehicle's braking control is set up to operate in series, meaning that the mechanical brakes are only engaged when the braking demand exceeds the regenerative braking capacity. This capacity is defined by the charge acceptance, which protects the battery from ageing and damage, and the motors' torque limitations. The motors are capable of producing 350Nm of torque each. A braking split of 70% front and 30% rear is assumed for vehicle stability. Hence 350Nm is 70% of the total regenerative braking force which can be applied, this means the rear motor should be limited to three sevenths of its maximum capability, giving 150Nm of braking torque availability. The system therefore has a combined braking torque of 500Nm at the motors. Using a final drive ratio of 4.5:1, this translates to a maximum torque of 2250Nm at the wheels. Should the torque demand exceed this, or a reduced value due to reduced charge acceptance, then the mechanical brakes will become engaged to provide the remaining request.

Figure 5.11 has been included to provide an example of the regenerative braking during the WLTP cycle at 5°C. Figure 5.11a demonstrates the battery charge acceptance limit reducing the amount of regenerative braking which can be utilised when the battery is cold. By the end of the cycle, in Figure 5.11b, the battery has warmed and regenerative braking can dominate the braking request.

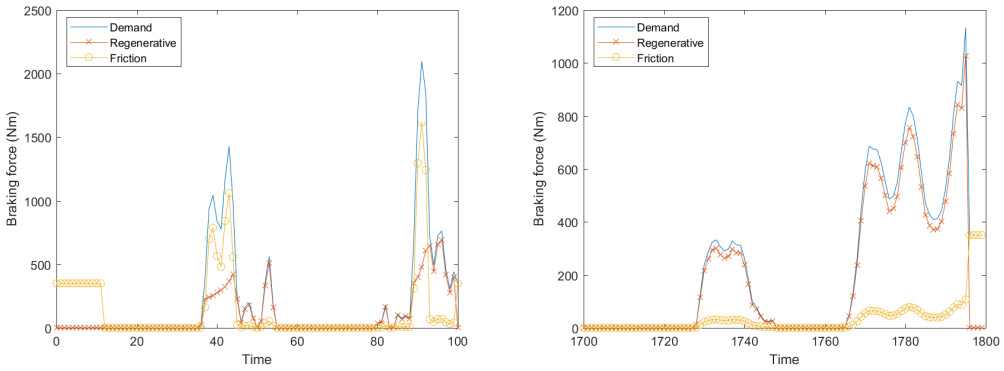

(a) Braking split at the beginning of WLTP drive cycle.

(b) Braking split at the end of WLTP drive cycle.

Figure 5.11: Here the capability of the regenerative braking system is demonstrated. In Figure 5.11a the battery is cold and therefore friction braking is dominant. At the end of the drive cycle the battery is fully warmed up and regenerative braking dominates, this is seen in Figure 5.11b.

5.4 Motor

In Chapter 3 the motor was identified as one of the potential heat sources for the heat pump. As such it requires a thermal model. Here the thermal model has been designed conservatively, ensuring heat is lost to ambient and within the motor core. Hence the requirement for the motor's thermal model is that it interacts correctly with the heat pump, as described in Section 5.2 and that a significant proportion (more than 25% for example) of its heat is lost to sinks other than the heat pump. This choice was made so that the motor waste heat available is not over estimated, therefore increasing the challenge of waste heat utilisation within the research. The original model contained a single heat capacitance, which could only make thermal exchange with the heat pump.

The motors are duplicated, representing the Jaguar I-Pace's four wheel drive system, but otherwise the mechanical model of the motor is unchanged from the original model. It was received with efficiency maps, from JLR, for the motor's (including inverter) efficiency as a function of speed, torque and voltage. Since this data has come from a trusted source it has remained in the model un-altered. The efficiency maps are used to calculate how much waste heat is generated, which is used in the thermal model. The remainder of this section describes the motor's thermal model and demonstrates its interaction with the heat pump.

There are two modes of energy loss through the motor; ohmic heating through

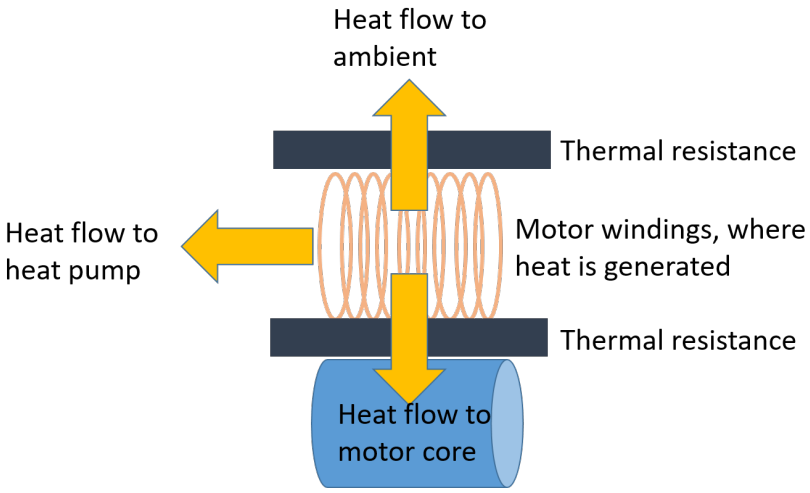

Figure 5.12: A schematic interpretation of the motor thermal model is shown. Here it can be seen that the motor's heat is generated in the windings; where it flows to either the core, the ambient or the heat pump.

resistance in the windings and friction of moving parts in the motor. For simplicity it has been assumed that the heat generated through friction is negligible and all heat is generated within the motor windings [186]. The thermal model for the motor can be seen in Figure 5.12, where there are thermal masses for both the core and the windings. The ohmic losses are generated in the windings, which are connected to the thermal management system and also dissipate heat to ambient. Here the heat pump is set to request 1000W of heat from the motors (500W each). This value was chosen as it is 10% of the average tractive effort required for the three drive cycles used. Hence if a lower efficiency limit of 90% is assumed for the motor then this request will be met. The heat flow is described by,

$$Q_{motor} = Q_{windings} + Q_{core} + Q_{TM}^{motor} + Q_{ambient} \tag{5.6}$$

where

$$Q_{windings} = (1 - \eta)\tau\omega. \tag{5.7}$$

Here η, τ and ω are the motor's efficiency, torque and speed respectively. For each simulated time step, η is found using an efficiency map with inputs; voltage, torque and speed. Q_{TM}^{motor} is the heat flow due to thermal management of the motor. This is the heat extracted by the chiller loop of the heat pump. Q_{core} is the heat flow between the windings and the motor core. This is given by,

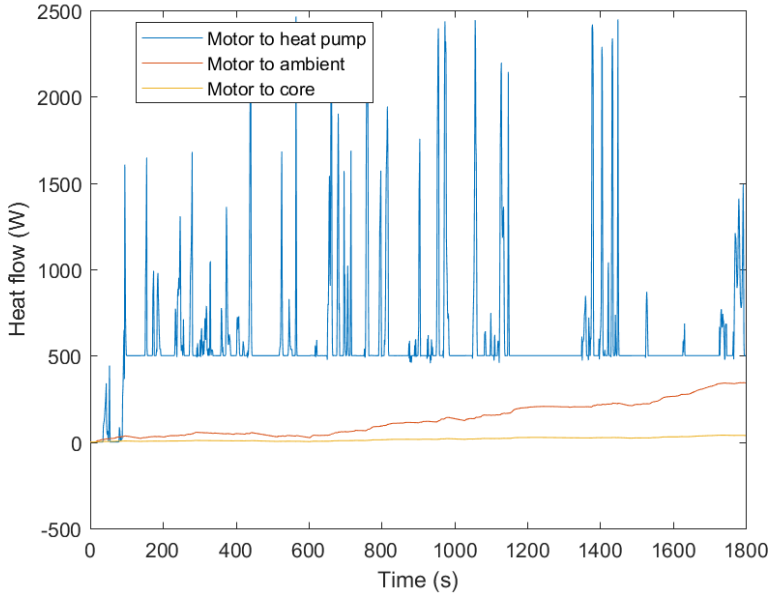

Figure 5.13: The motor model's thermal exchanges, corresponding to the baseline heat pump operational mode at 5°C on WLTP, are presented. The motor loses the majority of its heat to the heat pump. Here the request of 500W of extraction has been set and was met. Ambient also contributes to a significant amount of heat loss, accounting for 39% of the motors thermal loss at the end of the cycle.

$$Q_{core} = h_{motor}(T_{core} - T_{windings}). \tag{5.8}$$

Finally $Q^{motor}_{ambient}$ is defined in equation 5.9.

$$Q^{motor}_{ambient} = h_{windings}(T_{windings} - T_{ambient}) \tag{5.9}$$

More complex thermal models which make use of computational fluid dynamics to predict, in detail, heat flow within the motor are available, but are computationally heavy and are intended for defect and fault prediction [187]. For this research a simple model of this nature is sufficient [188].

The motor's heat flows are presented in Figure 5.13, corresponding to the baseline heat pump operational mode at 5°C on WLTP. This is used to check that the motor thermal model has met the requirements set. The motors are configured to supply 1000W of waste heat to the heat pump, equating to 500W per motor, Figure 5.13 shows that this demand is met and controlled. Here it can be seen that the motor loses the majority of heat to the heat pump. A significant proportion of heat is lost to ambient, accounting for 39% of the motor's heat exchange by the end of

the cycle. Another detail that may be noticed is the spikes in heat exchange. These will be caused by spikes in motor power, for instance accelerating or regeneratively braking. Since the exchange to the heat pump is controlled by a PID the spikes occur when the PID fails to throttle the additional heat and then recovers.

The motor has been shown to correctly interact with the heat pump and lose heat to ambient in a way which satisfies the requirements set.

5.5 Transmission

The transmission is unchanged from the original model, with the exception of it's duplication to correspond to a four wheel drive vehicle. The transmission uses an efficiency look up table, provide by JLR, which accounts for variations in temperature and torque. The heat losses corresponding to the transmission's inefficiency are used to heat a lumped capacitance with thermal exchanges to the heat pump and ambient. This model was parameterised by Claytex and JLR, and in the absence of updated efficiency tables, the ones provided were left untouched. A thermal exchange of 1500W was set, to be split across the front and rear transmissions, i.e. 750W each. This is a slight increase over the motor to account for the transmission including the gearbox and differentials. Figure 5.14 shows that this demand is not fully met, implying that either the transmission does not heat up sufficiently to meet the demand, or it is physically limited by the heat exchangers.

Figure 5.15 shows the temperature of the transmission compared to the chiller which is used to extract the heat. It is seen that the temperature difference reaches 25°C at the end of the cycle. Since transmissions usually have an operating temperature of above 80°C [189] it seems likely that the transmission is not sufficiently warm to exchange the requested 1500W.

5.6 Thermal Storage

In Chapter 3, one of the thermal management solutions identified was the inclusion of thermal storage. In the original model thermal storage was provided by the thermal mass of the ICE; however since this research is focussed on electric vehicles this is not an option. Instead the literature reviewed indicated that a phase change material would be an ideal material to provide thermal storage. One of the key features of the phase change material is the energy stored in the latent heat. This energy and the material's transition should be captured in the model. This will be achieved using a specific heat capacity which is a function of temperature, thereby

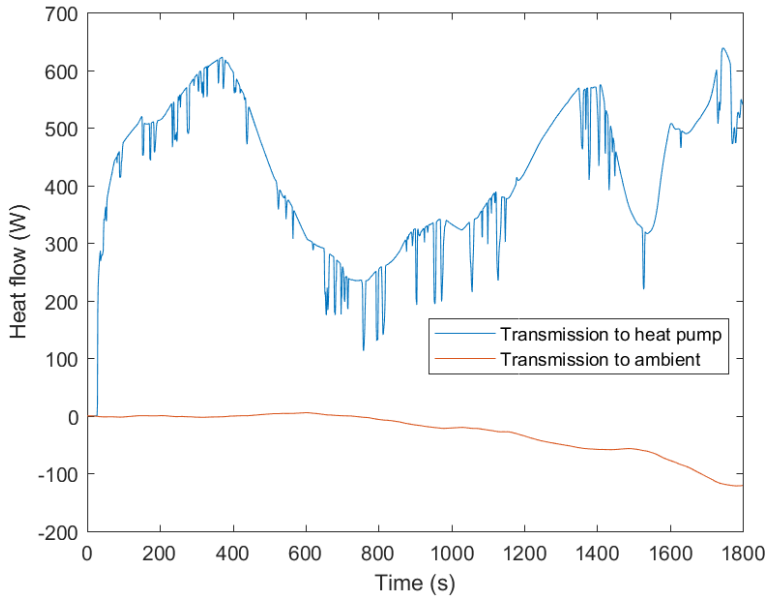

Figure 5.14: Here the transmission's thermal exchange with the heat pump is demonstrated. For this the WLTP cycle was used at an ambient temperature of 5°C.

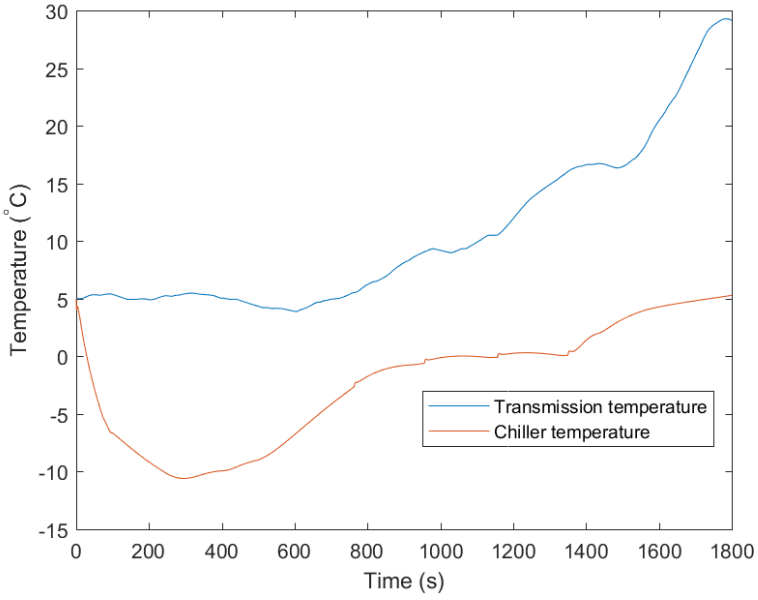

Figure 5.15: Here the transmissions temperature and chiller temperature are shown, these define the amount of heat that can be exchanged between the transmission and chiller circuit. For this the WLTP cycle was used at an ambient temperature of 5°C.

enabling the user to create a specific heat profile according to their chosen material.

There is a wide choice of material properties to choose from within the review of materials carried out by Sharma [132]. For this application a material should be chosen which has high latent heat and specific heat values in comparison to alternatives; these are important as they define the energy storage per kilogram. The material should also have a melting point close to operational temperature of the high temperature circuit (90°C). This maximises the opportunity to heat the high temperature circuit since it ensures the latent heat could be discharged into the high temperature circuit, providing the most heat to the system without engaging additional compressor power to discharge the thermal battery through the chiller. The melting point should not be higher than 100°C as this could lead to the high temperature circuit boiling and causing the model to fail. The material should also be cheap compared to alternatives, making its inclusion and adoption more likely. Sharma *et al.* presented the latent heat and melting points for hundreds of materials, so the details of each will not be covered; however generalities can be made about each class of material. Sharma *et al.* did not present specific heat capacities, so when potential materials were identified other sources were used to compare specific heat.

From the review by Sharma *et al.* [132], Paraffins had melting points mostly above 50°C, and up to 76°C, and latent heats ranging from 170kJ/kg to 268kJ/kg. Non-paraffins, organic materials such as alcohols and fatty acids with paraffin like properties, generally had a melting point range of 8°C to 127°C. The non-paraffin materials in the temperature range of 75°C to 100°C (close to the operating temperature of the high temperature circuit) all had low latent heat values, ranging from 102kJ/kg to 174kJ/kg. Non-paraffins are typically twice as expensive as paraffins. Another class of materials considered was fatty acids, which had melting points between 16.7°C and 102°C. Acetamide was one potential candidate which came from this group. It had a melting point of 81°C and a latent heat of 241kJ/kg. However upon further investigation its specific heat capacity was lower than alternatives, with a value of 1.1kJ/kgK , compared to paraffin's typical specific heat of 2.1kJ/kgK [2]. Salt hydrates had some promising characteristics but were overlooked due to the complexity of their implementation, requiring containment in a continuously rotating vessel. Finally metallics and eutectics were considered. Metallics had low latent heat values, all below 90kJ/kg while eutectics had better latent heat values up to 218kJ/kg; these occurred at melting point points below 65°C.

Paraffin was chosen as a material class after considering the options presented by Sharma et al.; paraffin showed the best specific and latent heat values in

Table 5.2: Thermal properties of paraffin 70-75 are given.

Property	**Value**
Melting Point ($T_{melting}$)	75°C
Specific Heat (Solid)	$2.06kJkg^{-1}K^{-1}$
Specific Heat (Liquid)	$2.34kJkg^{-1}K^{-1}$
Specific Heat (Average, C_p)	$2.2kJkg^{-1}K^{-1}$
Latent Heat (C_l)	$169kJkg^{-1}$
Mass density (solid)	$917kgm^{-3}$
Mass density (Liquid)	$822kgm^{-3}$
Conductivity	$0.21Wm^{-1}K^{-1}$

the temperature range close to the operating temperature of the high temperature circuit. It was also half the cost of non paraffins. Paraffin is also a choice supported in literature, with Shahidinejad *et al.* [40] and LaClaire *et al.* [69] both choosing paraffin in their research.

The review by Sharma *et al* did not present specific heat values of the PCMs reviewed, hence another source was required to attain all necessary details to model a paraffin PCM. Ukrainczyk *et. al* [134] performed characterisation work on a material called paraffin 70-75 , the details of which have been used to parameterise the PCM in this research. The properties pertaining to paraffin 70-75 are given in Table 5.2. For simplicity in this work the average specific heat value is used regardless of phase. This corresponds to a negligible energy storage increase of 0.8% compared to if the phase specific heat values were preserved.

A maximum operating temperature of the thermal battery is needed in order to constrain the optimisation control vector [mass, charge temperature, thermal power] discussed in Section 4.2.1. This can be set using the known degradation point of the chosen PCM. One piece of information which was missing from the characterisation of Ukrainczyk *et. al* [134] was the maximum temperature of the material. However, Song *et al.* [190] performed an investigation into characterising flame retardant phase change materials, during which they showed that the thermal breakdown of paraffin began between 150°C and 200°C, measured by mass loss. Considering this result an upper temperature limit of 140°C is imposed on the thermal battery to ensure a safety margin.

The heat flow from the thermal battery to the heat pump is described by,

$$Q_{HB} = Q_{TM}^{HB}. \tag{5.10}$$

where Q_{HB} is the heat flow out of the thermal battery, and Q_{TM}^{HB} is the heat flow

from the thermal battery to the thermal management system. The thermal battery is assumed to be well insulated and does not lose heat to ambient. It gives all of its heat to the thermal management system via the HTC and then the Chiller. The specific heat capacity however needs to be treated differently to other components, as it will experience a phase change where a large amount of energy is released. As such the specific heat capacity is modelled using a lookup table were there is a spike to incorporate the material's latent heat. This can be seen in Figure 5.16. Although in the work of Ukrainczyk *et al.* [134] it was shown that the latent heat is released over a temperature range, for simplicity it has been assumed that the latent heat is released over a 1°C phase change window, the same assumption was made in the thermal battery sizing work of Taylor *et al.* [25]. By using this assumption, and therefore neglecting the exact specific heat profile of the material, there will be some consequences on the temperature profile of the thermal battery while discharging. When discharging, this model will hold a steady temperature while releasing latent heat, this results in a low temperature differential during the melting phase, as seen in Figure 5.17b. By comparison, using a known and smoother specific heat profile with a wider melting window would result in a faster discharge over a larger temperature region while melting. Hence, the consequences of using the 1°C melting approximation are that the heat delivery to the heat pump and the temperature at which the thermal battery switches from the high temperature circuit to the low temperature circuit will be different. These factors will lead to changes in heat delivery to the cabin and battery and changes in heat pump energy consumption. Song *et al.* showed that the phase change window for paraffin is approximately 10°C, which is 6.7% of the 150°C operating window of the thermal storage unit, defined between the thermal battery's maximum operating temperature and chiller operating temperature [190]. It is not expected that this approximation will have an impact on the results.

The thermal storage is charged to a high temperature and first used to bring the high temperature circuit close to operating temperature. When it can no longer exchange heat with the high temperature circuit it is disconnected and reconnected to the chiller circuit. Finally, when it can no longer supply heat to the chiller circuit it is disconnected and isolated from the heat pump. Figure 5.17 demonstrates this process using the example of the WarmUp cycle at −15°C using the baseline operational mode with the addition of the heat pump. The events described can be seen in Figure 5.17 where the temperature of the thermal battery is presented, along with the differential of thermal battery temperature, which more clearly shows switching events in the cycle.

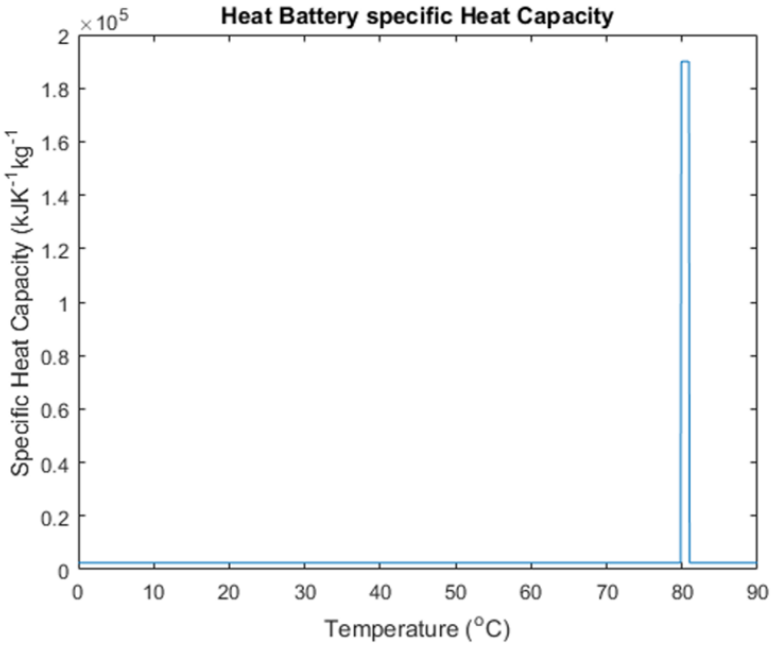

Figure 5.16: Specific heat capacity profile as a function of temperature for the thermal battery including spike at materials melting point.

From Figure 5.17b the abrupt changes in temperature differential act as markers for key events in the discharge of the thermal battery. The first happens at approximately 180s where the thermal battery enters the temperature range where phase change occurs, here the temperature drops very slowly as the latent heat is released. The second marker occurs at 570s, here the PCM has melted and normal discharge is resumed. As the thermal battery discharges the differential temperature decreases until it can no longer supply heat to the high temperature circuit, at which point it switches to the low temperature circuit, seen at 720s. This phase continues until the thermal battery can no longer supply heat to the chiller circuit, at this point the thermal battery is disconnected from the heat pump, seen at 2100s. This means that between 720s and 2100s (23 minutes) the heat pump is working at full load. After 2100s the chiller loop temperature decreases as the heat pump works. When the chiller loop is sufficiently cold it can be reconnected to the thermal battery, until they have once again reached the same temperature. This process repeats, creating the pulsing seen in Figure 5.17b, until the thermal battery reaches the minimum operating temperature of the chiller ($-10°$C). This process shows how the thermal battery interacts with the heat pump. The additional heat supplied by the thermal battery is also enough to increase the system's heating capacity so that the full 10kW of battery heating can be supplied. This can be seen in Figure 5.18.

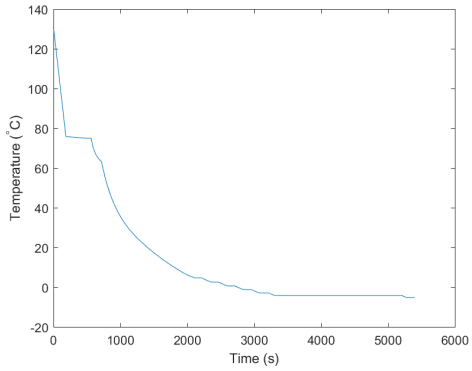

(a) Temperature profile of thermal battery.

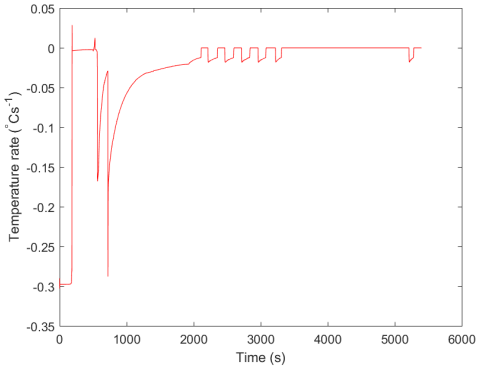

(b) Differential of thermal battery temperature.

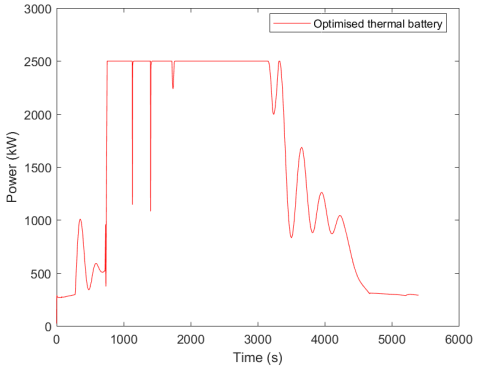

(c) Compressor power consumption.

Figure 5.17: Analysis into thermal battery temperature at $-15°C$ completing the WarmUp drive cycle.

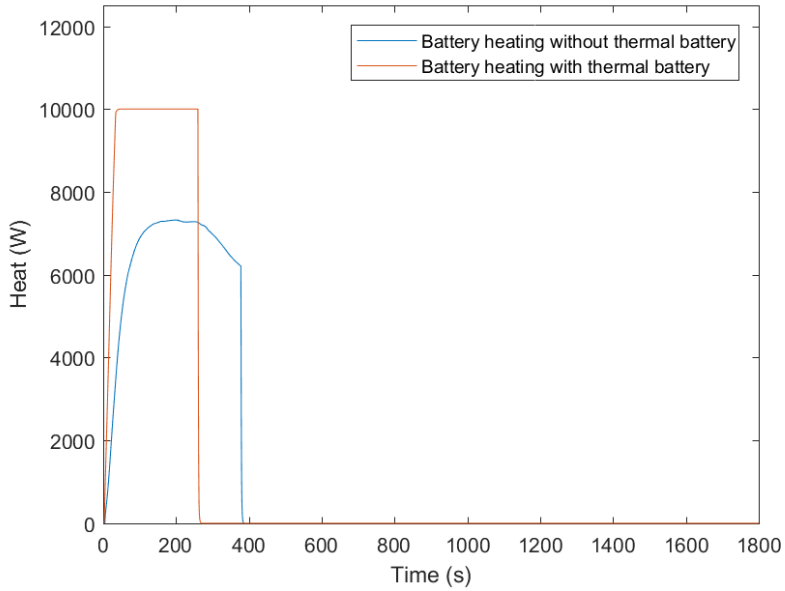

Figure 5.18: The additional heat supplied from the thermal battery is enough that the battery heating can be maintained at $10kW$ until the battery reaches target temperature.

In this section the requirements for a specific material were set with paraffin selected from a review of materials; a specific example was then found and used to parameterise the model. The discharge procedure governing the thermal batteries interaction with the heat pump was explained and demonstrated using Figure 5.17.

5.7 Cabin

The cabin model is one of the higher priority components as an accurate heating demand is required to assess and optimise the operation of the heat pump. Here the heating demand required in the model will be compared to those seen in literature to establish that the model is accurate enough to produce reliable heating demands. Using this criteria the cabin should require between 4.5kW to 7.8kW at $-15°$C as seen in Section 2.2 [19, 40, 96].

The model for the cabin was inherited from JLR and Claytex and utilises a dual zone air model. The first zone dominates the cabin volume and is used to measure cabin temperature for comfort. The second zone is much smaller and represents the air around the cabin exhaust. This second, smaller zone is used by the heat pump to extract heat from the cabin exhaust. The model measures the

specific enthalpy of the air exhausted from the cabin and produces a prescribed thermal extraction equivalent to 30% of the heat exhausted, this is in accordance with claims made by BMW [130].

In addition to the original model, two more thermal capacitances have been added, one for the hard furnishings (dashboard, door panels, glass etc.) and one for the soft furnishings (such as the seats). These thermal capacitances are connected to the air volume using thermal resistances parameterised through sizing and convection estimations since the exact specifications were unknown.

5.8 Controllers

This section contains an overview of the control system for the vehicle. These controllers are used to ensure that the drive cycle is completed and that the cabin and battery are sufficiently heated without exceeding the temperature limits of the coolant circuit. To achieve this the controllers can be split into two categories; mechanical and thermal.

5.8.1 Mechanical Controllers

The mechanical controllers are made up of the driver component and the motor controller unit. The driver component contains the drive cycle information which is used to generate an acceleration demand between 0% and 100% throttle. This throttle demand is sent to the motor controller unit (MCU), which converts the normalised throttle demand to a torque request between 0Nm and 350Nm per motor. The MCU then passes this torque request to the motors, which is dealt with as described in Section 5.4. This component was mostly unchanged since the original model, the only difference being the inclusion of a negative torque demand input for regenerative braking, explained in Section 5.3.1.

5.8.2 Thermal Controllers

5.8.2.1 Mass Flow

The thermal control, at the top level, is split into three components contained in the HPCU. These three sub controllers are the switch controllers, loop controllers and the mass flow controllers. The latter of these is the most simple of the controllers, it consists of three ramps which are used to set the desired mass flow of the fluid in the heat pump coolant loops. This controller and the parameters therein are unaltered from the original model.

5.8.2.2 Switches

The switches controller is divided into sub-controllers for each component. The most simple of these controllers are the motor switch and the transmission switch, in these cases the switches can be set to on or off, with a control to disconnect the component if temperature targets or limits are reached. This control measures the temperature difference between the component and chiller and only allows a connect to be made if the component is more than 0.5°C above that of the chiller. This test ensure that heat flows from the component to the chiller and not vice versa. This logic exists for all thermal sources, while the reverse logic is imposed for the battery, i.e. the battery may only be connected to the HTC when the circuit temperature exceeds the electric battery's temperature.

The controllers for the thermal battery and the electric battery are slightly more complex. Unlike the previously mentioned components, the battery will need to disconnect from the HTC when it reaches operating temperature, while the thermal battery first discharges into the HTC, then switches to the chiller. In the case of the electric battery, the switch initially connects the electric battery to the HTC, in order to warm up the electric battery. When the electric battery reaches target temperature (20°C) the electric battery is disconnected from the heat pump, however, if its temperature then falls below 15°C it will be reconnected to the HTC. This ensures that the controller attempts to keep the electric battery above 15°C, which is the recommended minimum operating temperature for a lithium ion cell [191]. In the case of the thermal battery, it is initially connected to the HTC in order to bring the circuit up to temperature quickly and aid cabin and electric battery heating while the heat pump is warming up. When the thermal battery can no longer provide heat to the HTC, it is disconnected from the HTC and connected to the chiller circuit. This is then used to extract the remaining heat stored in the thermal battery until it can no longer provide heat, at which point the thermal battery is disconnected from the vehicle's thermal management system, the details of this discharge process were given in Section 5.6.

The capabilities of these controllers have been seen in examples presented in Figures 5.10,5.13,5.14 and 5.18.

5.8.2.3 Compressor controller

The compressor controller sets the power demand for the compressor. This demand is set according to the following requirements; achieve cabin target temperature, achieve battery target temperature, do not exceed maximum operating temperature

of the HTC and do not exceed the minimum operating temperature of the chiller circuit. The first two of these requests ensures the cabin and battery are supplied with enough heat, while the latter two prevent the model from failing due to exceeded temperature limits. This is an important requirement for making the model robust. The original model set the compressor demand only according to the chiller temperature. This approach led to coolants exceeding maximum temperatures and too much heat production for the cabin and battery.

The compressor controller is split into two sub-controllers, the chiller controller and the HTC controller. The high temperature loop controller controls the connection between the HTC and ambient. This is used when the heat pump is in air conditioning mode and the HTC is required to exhaust heat to ambient.

The chiller controller is used to set the compressor power demand for the heat pump, which is then executed by a PID controller attached to the compressor as described in Section 5.2. PID controllers are used to create compressor power demands according to the current and target temperatures of the cabin, battery, HTC and chiller circuit. The demand chosen is the minimum of the HTC demand, chiller circuit and maximum demand of either the cabin or battery. Here the maximum of the cabin and battery demands is passed to the minimum stage, a logical step which maximises the heat generated for cabin and battery heating, while preventing the high temperature and chiller circuits from going beyond their target temperatures. A simplification of this logic and control strategy can be seen in Figure 5.19. This system may be criticised as overcomplicated, however, since the heat pump uses refrigerant to coolant heat exchangers, both of which are subject to temperature and pressure restrictions, it is necessary for ensuring the model is robust. Without these controls in place the system becomes vulnerable to the following list of issues:

- Freezing the coolant.
- Boiling the coolant.
- Boiling the refrigerant.
- Over-heating or under-heating the battery.
- Over-heating or under-heating the cabin.

These issues either lead to the model encountering errors, or failing to correctly thermally manage the battery or cabin.

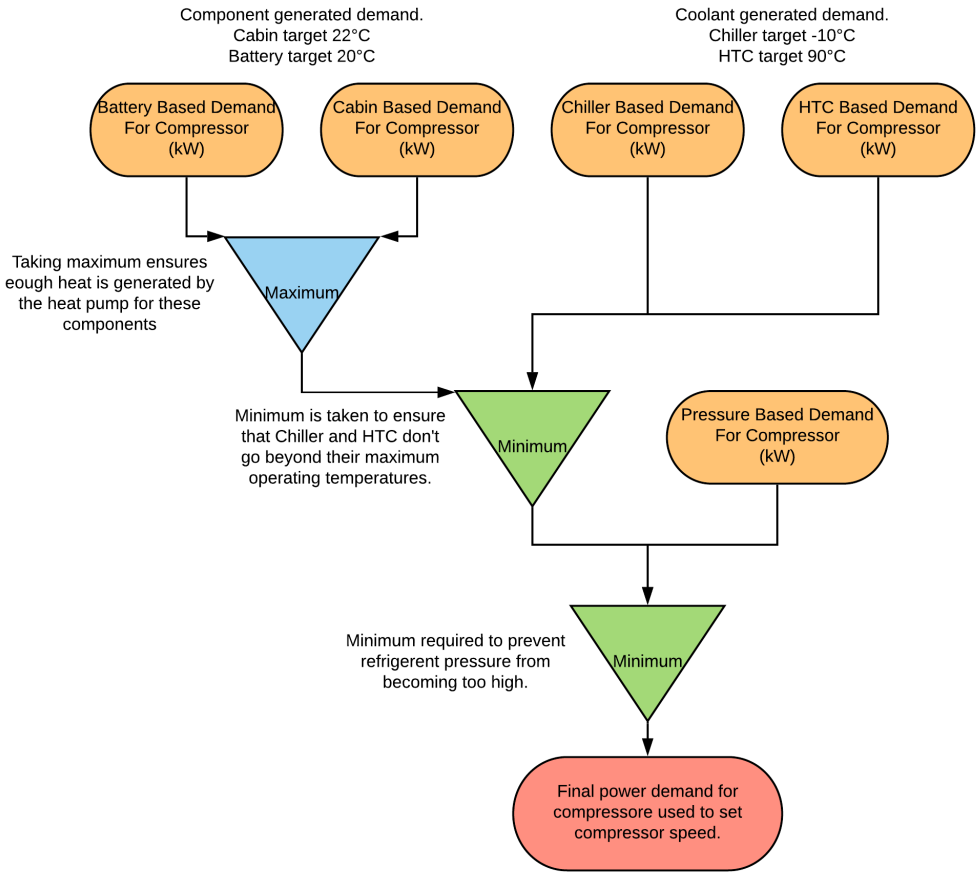

Figure 5.19: A simplification of the control strategy which controls and manages compressor speed through individual system demands. Orange boxes show demands created by PID controllers according to component needs. The red box shows the final compressor power demand which is used to control compressor speed.

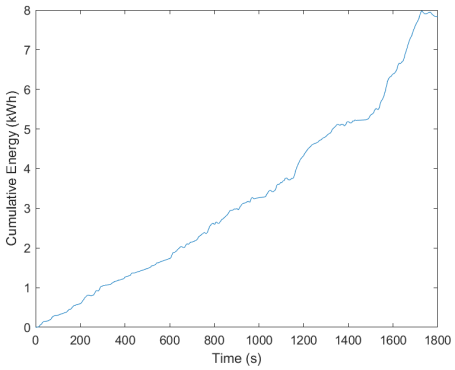

(a) Cumulative energy consumption

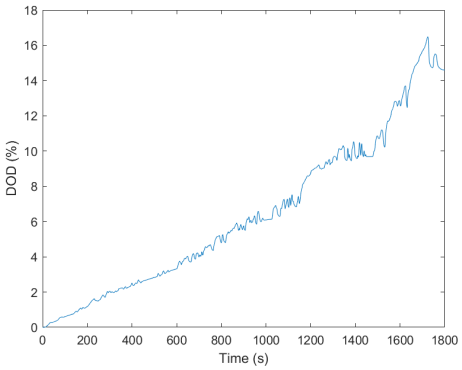

(b) Depth of discharge

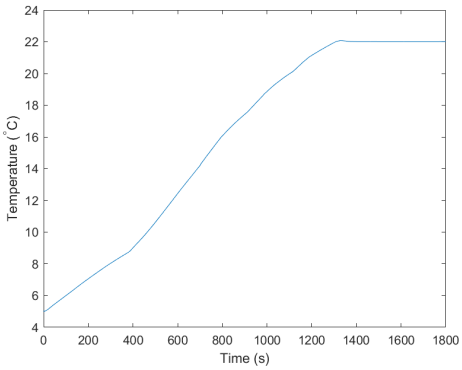

(c) Cabin temperature

Figure 5.20: Here the metrics corresponding to the different objective functions accounted for in the cost function, defined in Section 4.5, are presented. Figure 5.20a shows energy consumption which is represented by j_1, 5.20b shows DOD which is represented by j_2 and 5.20c shows cabin temperature which is represented by j_3.

5.9 Model demonstration

In this section the system's performance is evaluated using the baseline operational mode at 5°C and using the WLTP drive cycle. Here the vehicle's cumulative energy consumption, DOD and comfort are presented in correlation with j_1, j_2 and j_3 from the cost function defined in Section 4.5. This is the format which will be used at the end of each of the results chapters and used to discuss and quantify the progress made over the baseline. Figure 5.20 displays these results.

In addition to the graphical representation of the metrics, displayed in Figure 5.20, they have also been converted back into efficiency, range and comfort, which are the motivations for this research. These can be seen in Table 5.3. Here efficiency

Table 5.3: Here efficiency range and mean discomfort are presented using the WLTP drive cycle across a range of temperatures.

Ambient Temperature (°C)	Efficiency (Wh/km)	Range (km)	Discomfort (mean °C)
-15	369.2	139.8	31.9
-5	370.8	139.2	19.3
5	337.3	159.2	6.2
15	288.8	186.6	1.0

is calculated by dividing the energy consumption used to complete the WLTP by the length of the WLTP (23.25km). Range is calculated using Equation 5.11 and discomfort using Equation 5.12. The values presented in Table 5.3 can act as a baseline against which progress made through this research can be measured.

$$Range = L \times \frac{100}{DOD} \tag{5.11}$$

Here L is the drive cycle distance i.e. 23.25km for WLTP.

$$Dsicomfort = \frac{1}{t_{end}} \times \int_{t_0}^{t_e nd} (T_{target} - T_{Cabin}(t))dt \tag{5.12}$$

Where t_{end} is set to 1800 for the WLTP drive cycle and T_{target} is the cabin target temperature, set to 22°C.

The examples presented in Table 5.3 took an average time of 11 minutes and 25 seconds. Of the three drive cycles this was the longest, with the corresponding evaluations for the WarmUp and NEDC cycles taking an average time of 5 minutes and 10 seconds and 7 minutes and 26 seconds respectively. Hence the model has met the time requirements as the average drive cycle simulation time is less than the required 10 minutes.

5.10 Validation

Validation is an important part of any modelling process as it ensures that when a theoretical performance improvement is found there is justification for believing that it will translate to a real world benefit. The conceptual nature of the model used in this work means that there is not a physical system against which it can be directly validated. Instead the system will be broken down into sub-models, and where validation data exists, this can be used to validate the sub-model. For sub-models without validation data, the performance of the model can be judged against

known behaviours seen in literature. In these cases information from literature will be used to set representative bounds for the model and the model will be said to be valid if it falls within these bounds. This is also how the system can be judged on a higher level, by comparing against known ranges and range reductions. The comparison of the model to publicly available EV data is an established method for the validation of conceptual models [192, 193].

This method of validation is clearly limited in that the model cannot be definitively compared to a real system and proved beyond doubt to be fully representative, nor can an accuracy statistic be easily quoted since the model's output is compared to a distribution of results from different vehicles, rather than one well defined result. However, as Doucette explains, when a physical system is unavailable for validation (which is the case at the time of this work), comparison against a collection of external experimental data is the next best option for establishing confidence in the mode [193].

For this validation process the WLTP drive cycle will be used and an ambient temperature will be selected according to the validation task. For example, if the vehicle range is required, 23°C will be used with no heating, whereas if a range reduction is required a lower ambient temperature will be selected according to the available data for comparison. The validation will be structured in the same order as the sub-model sections of the this chapter and will conclude with the validation of the complete system from a high level perspective.

5.10.1 Heat Pump

The heat pump's key performance indicators are its heat output and its coefficient of performance. Since the heat output will be dependant on the size of the system, the fairest way to validate the performance of the heat pump is to use the COP for comparison. While an assortment of heat pump systems were discussed in Chapter 3, there were two systems that are particularly appropriate for comparison and validation. The baseline operational mode of this system collects heat from ambient and the electric motor, this was also the case for the systems presented by Ahn *et al.* [67] and Leighton [24]. The work by Leighton [24] did not provide details on COP or heat generation and so cannot be used for validation. However, in Ahn *et al.* the system was tested at −10°C, 0°C and 7°C using heat from ambient and 1kW of waste heat from the motor. Ahn reported a COP of 2.1, 2.8 and 3.2 at −10°C, 0°C and 7°C respectively. Hence for the heat pump model used in this research to be validated, its COP needs to fall within the range of 2.1 to 3.2 when operated between −10°C and 7°C.

Table 5.4: Heat pump validation metrics across full temperature range during WLTP.

	Ambient Temperature (°C)		
Metric	-5	5	15
Mean COP	2.02	2.02	2.21
Max COP	2.96	3.16	3.92

The COP values presented in Table 5.4 correspond to the system used for this research. Making direct comparisons between the results presented in Table 5.4 and the results presented by Ahn *et al.* is not simple since they have been recorded at different ambient temperatures. Additionally Ahn *et al.*'s results were found under steady state conditions while Table 5.4 was found during the WLTP drive cycle. Using a drive cycle (opposed to steady state) will increase the variability in performance of the heat pump; this coupled with controls based on cabin and battery temperature are likely to lead to a lower mean COP. This appears to be the case when comparing the mean COP in Table 5.4 to the results of Ahn *et al.* and can also be seen by the performance variability shown in Figure 5.21. The range found by Ahn *et al.* falls within the gap between mean and maximum in Table 5.4 which allows for the heat pump to be confirmed as representative of a system found in literature and is therefore validated.

5.10.2 Battery

For the purposes of this research the battery model should be validated in two key areas; its ability to capture the capacity reduction which has been seen throughout literature, and its temperature response. For the capacity test the model can be compared to the amalgamation of cell capacity data presented in Figure 1.1. For the thermal validation a dataset has been provided by Yashraj Tripathy with the maximum temperature of the cell during a discharge. This can be used for a direct validation of the model.

To assess the capacity of the cell as a function of temperature the model has been discharged at 0.1C, over the temperature range of $-15°C$ to $15°C$, which is the range set in Section 4.3. 0.1C was chosen as the discharge current in order to avoid any capacity increase due to internal self heating. As with other comparisons to literature the model validation will be deemed successful if the model produces a capacity which falls within the bounds defined by the amalgamation of data from literature.

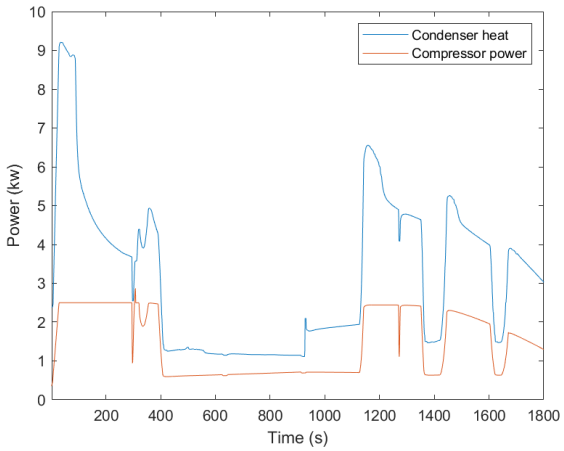

(a) Heat pump condenser and compressor power.

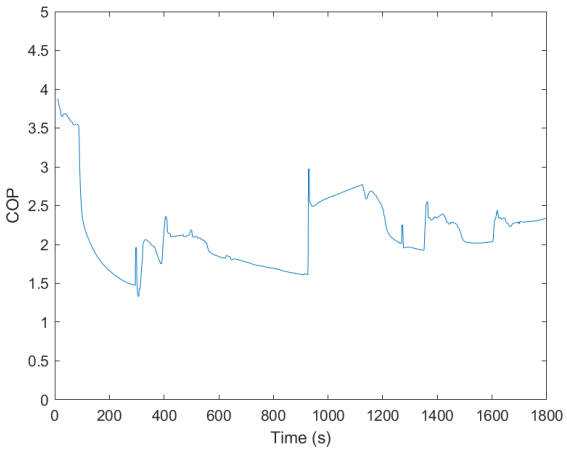

(b) Heat pump COP.

Figure 5.21: Heat pump performance for validation at 15°C during the WLTP cycle.

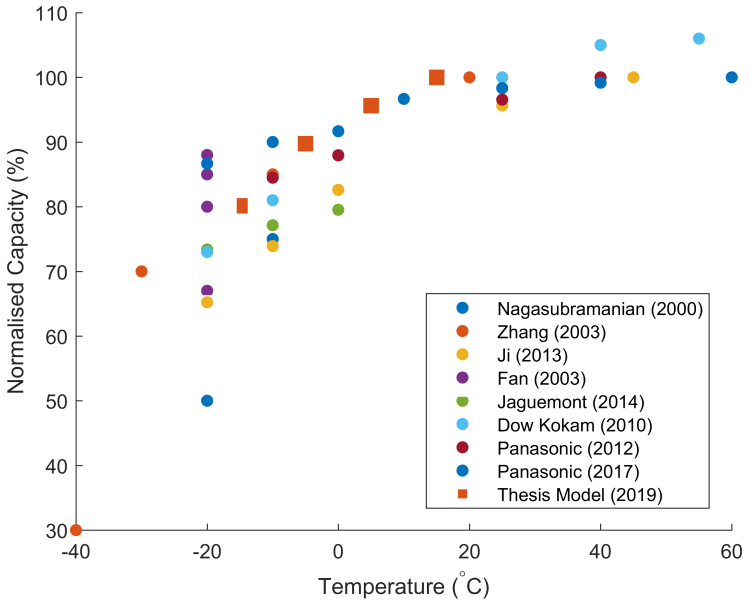

Figure 5.22: The model used in this thesis is compared to a selection of data reported in literature.

The results of this test have been combined with Figure 1.1, to produce Figure 5.22, in order to make an easy comparison to the behaviour seen in literature. Figure 5.22 shows that the model does indeed produce a capacity drop off with temperature which is reflective of the data seen in literature. This means that from an electrical aspect, the battery has met the requirements set.

In addition to the 0.1C discharge, further discharge tests have been performed to ensure that the battery model can accurately predict temperature. The battery temperature prediction is important to ensure that the battery SOC is calculated correctly according to Equation 5.5. The amalgamation of data seen in Figure 5.22 is separated into 10°C intervals, as this is the interval required to see a change in battery capacity. Hence this is the interval to which the battery thermal model should be accurate, that is to say that the battery thermal model should be accurate to within 5°C to be sufficient for the purposes of this research.

The battery model has been reduced to a single cell and compared to cell temperatures recorded by Yashraj Tripathy when performing low temperature discharge tests on Xalt 40Ah cells in temperature chambers. The tests carried out were at discharge rates of C/2, 1C and 2C, with ambient temperatures −20°C, −10°C, 0°C and 25°C. The results of this comparison are presented in Figure 5.23. When inspecting Figure 5.23b it can be seen that the absolute error is always less than

5°C and hence the model has sufficiently met the validation requirement.

5.10.3 Motor and Transmission

The key contribution of the motor and transmission to the validity of the model is their energy efficiency as this will define the amount of waste heat they can produce. As described in Sections 5.4 and 5.5 both of these component models receive efficiency values from look up tables which have been parameterised and validated by JLR and Claytex. For this reason there is no need to include another validation of the system. However, it should be added that the transmission used by JLR and Claytex for the population of this model was an 8 speed automatic, which is likely to have a lower efficiency than a single speed gearbox which are conventionally used in EV's. This is accounted for by limiting the amount of heat which is extracted from the transmission as explained in Section 5.5, so the performance of the heat pump should not be effected by the theoretical over estimate of waste heat.

5.10.4 Thermal storage

The key parameters of the thermal storage unit are the amount of heat stored and its ability to reject that heat into the HVAC coolant. The first of these is built into the model by design and so there is no need for it to be validated. However, the heat rejection to the coolant can be assessed. For this the system is compared against the data sheet provided by Sunamp and the experiment carried out by Taylor *et al.* [25, 26]. In Taylor *et al.* a specific power density of 30W/kg is quoted for the system they developed, whereas Sunamp quote a discharge power of $3,333$W/kg for their system. The system developed by Taylor *et al.* was a simple prototype, while the Sunamp example is more advanced in the development process, however this demonstrates the infancy of this technology making it hard to pick a value for which the thermal storage should be validated against. In addition to this, the working material of this model, Taylor *et al.*'s prototype and the Sunamp example are all different.

Figure 5.24 shows the discharge of the thermal storage model during the WLTP cycle at -15°C. Analysis of this discharge shows a mean discharge power of 6.8kW, thus a mean power density 234W/kg given the 29kg mass of the thermal storage unit used. These values fall comfortably with the limits set by literature. The variability shown in literature indicates that a thermal battery may be constructed with a wide variety of performance parameters; this is why the investigations preformed in Chapter 6 are necessary.

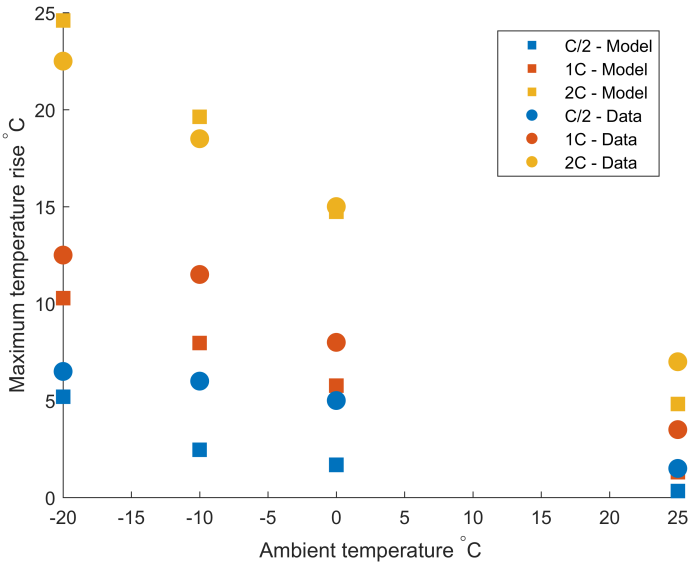

(a) The maximum temperature rise of the cell model under different discharge conditions.

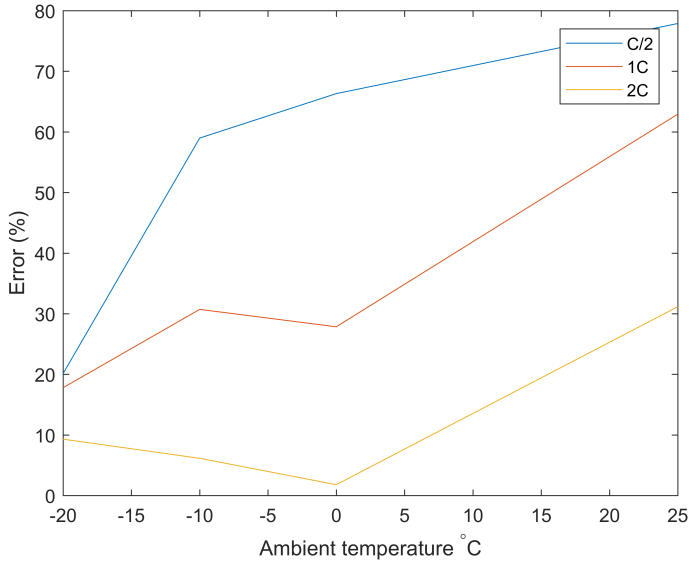

(b) Absolute difference between the model used and recorded cell temperature rise.

Figure 5.23: Here the battery thermal model is compared to cell temperature rises produced by Yashraj Tripathy.

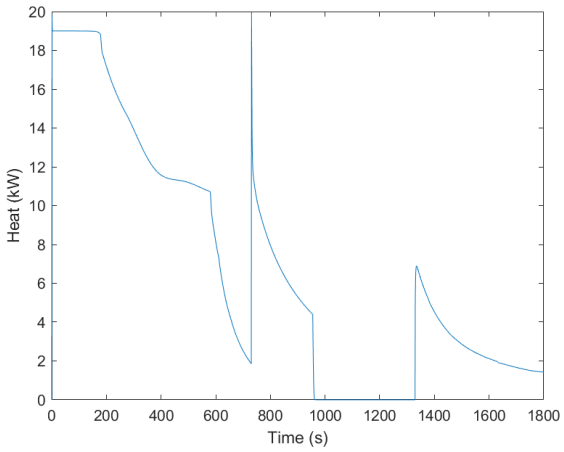

Figure 5.24: Thermal battery discharge power through WLTP drive cycle at $-15°C$.

5.10.5 Cabin

The cabin model is one of the higher priority components for validation as an accurate heating demand is required to assess and optimise the operation of the heat pump. Here the heating demand required in the model will be compared to those seen in literature to establish that the model is sufficiently accurate to produce reliable heating demands. Using this criteria the cabin should require between 4.5kW to 7.8kW at $-15°C$ as seen in Section 2.2 [19, 40, 96].

Two examples are provided which demonstrate that the cabin meets the objective set. Firstly the baseline mode is used with the addition of thermal storage, at $-15°C$ using the WarmUp scenario. Secondly the baseline with thermal storage, but without battery heating, is presented. These two examples can be seen in Figure 5.25. Here the addition of thermal storage is necessary to provide enough heat for the cabin to reach target temperature, this still takes over an hour to achieve, hence the longest drive cycle is used. Examples are presented with and without battery heating to demonstrate the impact that battery heating has on the systems ability to provide heat to the cabin.

In Figure 5.25b the heat received by the cabin is seen, during this test an average of 7.6kW of heat was delivered to the cabin. This is inline with the range seen in literature, 4.5kW to 7.8kW at $-15°C$ [19, 40, 96], and so it can be concluded that the cabin model has met the accuracy requirements for validation.

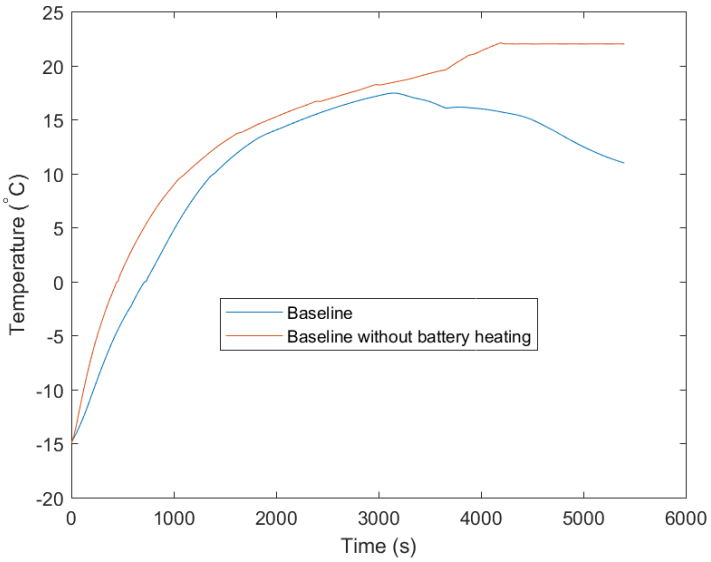

(a) Cabin temperature

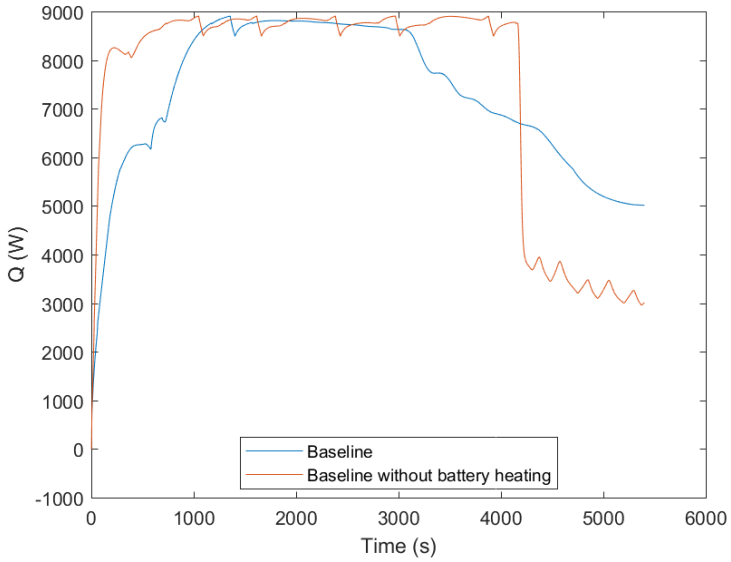

(b) Cabin heating

Figure 5.25: Cabin temperature and heating power using the baseline operational mode, with the addition of thermal storage, at −15°C on the WarmUp cycle. Average heating requirement corresponding to baseline without battery in Figure 5.25b was 7.4kW.

Table 5.5: Representative examples of the efficiency of real world vehicles collected from [3]

Vehicle	**Efficiency (Wh/km)**
Audi e-tron	244
Jaguar I-Pace	228
Byton M-Byte	241
Tesla Cybertruck	269
Mercedes EQC	222
Tesla Model X	216

5.10.6 Complete system validation

Here the complete model is validated against high level parameters available from literature. At this level the model is judged on energy efficiency which is key when assessing the performance of an electric vehicle and representative range reduction.

Firstly the vehicle model is validated at room temperature against known EV efficiencies. The range is not considered in this validation stage as it is intrinsically linked to the battery size. Adjusting the range according to the battery size of vehicles available in data would not be fair as this would adjust the vehicle weight and therefore invalidate the efficiencies quoted. Since the vehicle model is based upon the Jaguar I-Pace, it is sensible to use this and similar vehicles against which to assess the performance. Table 5.5 highlights a range of similar vehicles and their efficiency.

The model has also been simulated at 23°C using no HVAC. Doing so, the system used 243Wh/km which is within the boundaries set out in Table 5.5. The vehicle efficiency lies toward the higher end of this table, being exceeded only by the Audi e-tron and Tesla Cybertruck, and exceeding the Jaguar I-Pace efficiency. Since this is vehicle efficiency it is dominated by the battery, motor, transmission and kinematic characteristics (mass, frontal area, aerodynamic efficiency and rolling efficiency). It was highlighted in Section 5.10.3 that the transmission efficiency is likely to be lower than what would typically be expected for an EV, which explains the slightly high energy consumption. Regardless, the vehicle is operating in the defined window of acceptability and is therefore validated.

The final step of validation is to ensure that the vehicle captures a representative range reduction as the ambient temperature is lowered. Referring to literature, it has been seen that a range reduction in the region of 40% to 70% should be measured when moving from 15°C to −15°C [21, 22, 102]. This therefore defines the bounds which are used to validate the model.

Table 5.6: Here the efficiency, range and comfort are demonstrated with the heat pump switched off and the PTC capacity increased to 6.5kW, accounting for the reduction in compressor power consumption.

Ambient Temperature	Efficiency (Wh/km)	Range (km)	Discomfort (mean degC)
-15	450.9	104	21.7
-5	425.9	111	13.2
5	351.7	147	5.1
15	289.0	186	1.1

Table 5.3 shows a range loss of 25.4%, which is lower than required. However the vehicle demonstrated here is already more advanced than vehicles seen in literature, such as the original Nissan Leaf used by Meyer in [21]. To account for this a new operational mode is tested, where the heat pump is disengaged, the battery is not heated and the PTC capacity is increased to 6.5kW to account for the heat reduction caused by disengaging the heat pump. Using this new configuration the metrics shown in table 5.6 have been produced. Here it can be seen that moving from 15°C to −15°C reduces the range by 44%, which is inline with expectations.

The addition of Table 5.6 also allows for the comparison of the vehicle with and without the heat pump. BMW claimed that the addition of a heat pump into their i3 model led to a range increase of 10% to 30% depending on ambient temperature. When comparing the ranges found in Tables 5.3 and 5.6 it can be seen that the range improves by between 34.4% and 0.3% from the lowest to highest ambient temperatures. Although BMW claim a minimum of 10% improvement is available, this is unlikely since at approximately 22°C no HVAC energy will be used, hence there should not be a difference between heat pump and PTC models. The improvement can also be compared to the results shown by Chowdhury *et al.* [131], who showed a 16% reduction in energy consumption at −10°C, for a vehicle using a heat pump compared to PTC. Here if the results are interpolated between −15°C and −5°C then a 15.4% reduction in energy consumption is expected, which is in agreement with Chowdhury *et al.*'s report. Here the difference may be explained by the fact that the PTC system tested by Chowdhury *et al.* also heated the battery, which may have consumed extra energy hence resulting in a larger gain when the heat pump was used. Considering the comparisons to literature, the two versions of the model tested show a representative improvement when moving from PTC to heat pump technology.

These results show that at the highest level the vehicle is capable of replicating electric vehicle behaviour variations with temperature. The comparisons between Tables 5.3 and 5.6 also show that benefits gained through the inclusion of the heat pump have been adequately captured. The comparison to JLR's advertised figures confirms that the vehicle model is fit for purpose and that the requirements set have been accomplished.

5.11 Concluding points

- A model was required which could extract heat from the motor, transmission, thermal battery and cabin exhaust, while also heating the cabin and battery.
- The models and each of the sub-models for the major components have been described in Sections 5.1.0, 5.2 and 5.8.
- The model was then validated and its behaviour shown to be representative of electric vehicles in Section 5.10.

Chapter 6

Results 1, Optimum Thermal Battery Sizing

6.1 Introduction

In this chapter Research Objective 1, "What is the optimal sizing of a thermal battery for application in an electric vehicle with a heat pump", is addressed. As discussed in Section 4.1, when thermal storage is added to a vehicle there is extra heat for the cabin and battery, but this comes at a cost to compressor and water pump usage. This compromise is defined by the thermal energy stored by the thermal battery and its ability to deliver that heat to the system. This chapter explores the sizing of thermal storage in terms of battery mass, charge temperature and thermal power, as discussed in Section 4.1. The impact of the sizing on the performance of the vehicle will be described using the cost function defined in Section 4.5.

The sizing is split into two distinct cases; the first being where the thermal battery is added to the vehicle at no cost to the electric battery capacity. In the second case, the total energy storage onboard the vehicle is limited, and the addition of thermal storage comes at the reduction of electrical. Through the exploration of the first case, performed in Sections 6.4 to 6.4.11 an optimal specification of 29kg in mass, 131°C charge temperature and 19kW of thermal power is found and shown to be optimal for the problem set. In the final part of this chapter, while exploring the second case, it will be demonstrated that thermal storage is a viable alternative to electrical storage. It will be shown that when using a hybrid storage solution the optimal split of 9.5% thermal and 90.5% electrical should be used. Furthermore despite the reduction in electric battery size, it is shown that at and above -5°C

there is negligible impact on range.

The structure of the chapter is as follows;

- The optimisation problem is defined.
- A suitable search algorithm for the problem is identified from the choices presented in Section 4.2.1.
- An exploration of optimisations for different scenarios and objective function priorities is made.
- An investigation into thermal battery sizing in a scenario where the total energy storage capacity on board the vehicle is limited.
- The impact of the additional thermal battery on vehicle efficiency, range and comfort is presented.

6.2 Optimisation problem

It has been stated in Section 6.1 that the purpose of this chapter is an exploration of the specification of a thermal storage device in terms of mass, charge temperature and thermal power. This defines the optimisation control variables of the problem, which will be referred to as the thermal battery specification. The objective of this section is to produce a method for identifying a specification which minimises the cost function defined in Section 4.5. The first task is to identify limitations on the specification. Then the search space is evaluated at a rough resolution to understand how the cost function varies with the specification. This is used to identify a search algorithm which will be suited to the search space.

The charge temperature can be easily constrained using the knowledge presented in Sections 5.2 and 5.6. In Section 5.2 it was stated that the chiller circuit has an operating temperature of $-10°C$; since this will be used to extract the last energy from the thermal battery, before it is disconnected from the heat pump, this is the minimum allowed charge temperature. To set the upper limit of charge temperature the maximum temperature of $140°C$, set in Section 5.6, is used.

The limits on mass can now be defined according to the maximum required energy storage. This can be defined as the thermal energy required to replace 1 hour of PTC heater power consumption, which sufficiently covers the longest drive part of any drive cycle defined in Section 4.3. The combination of mass and charge temperature defines the energy stored by the thermal battery according to Equation 6.1.

$$E_{thermal} = M \times \int_{T_{min}}^{T_{max}} C_p(T)dT. \tag{6.1}$$

$E_{thermal}$ is the total thermal energy stored, M is the mass of the PCM, T_{min} and T_{max} are the minimum and maximum operating temperatures of the material, and $C_p(T)$ is the specific heat which is a function of temperature. In this research T_{min} will be set to $-10°$C, which is the minimum operating temperature of the chiller, and therefore the minimum temperature which the thermal battery can be cooled to.

Section 5.6 describes how the thermal battery is modelled and details the specific phase change material chosen for this research. Using this implementation of the thermal battery, the latent heat released through melting is delivered over a 1°C interval in the materials temperature. This interval will define the melting zone and will extend from the melting temperature to the melting temperature plus 1°C. The melting zone is described in Equation 6.2. This assumption was also made by Taylor *et al.* [25].

$$\begin{aligned} T_{melting} \leq T_{melting\ zone} \leq T_{melting} + 1, \\ T^{min}_{melting\ zone} = T_{melting}, \\ T^{max}_{melting\ zone} = T_{melting} + 1 \end{aligned}$$

Here $T_{melting}$ is the melting point of the material, $T_{melting\ zone}$ is the temperature window over which latent heat is released, $T^{min}_{melting\ zone}$ is the temperature at the bottom of the window and $T^{max}_{melting\ zone}$ is the temperature at the top of the window.

Due to the assumption made in this model the calculation to find thermal energy stored can be simplified to the following three cases;

If $T_{max} > T^{max}_{melting\ zone}$

$$E_{thermal} = M \times (C_p(T_{max} - T_{min} - 1) + C_l), \tag{6.2}$$

where C_l is the latent heat, and T_{max} is the maximum temperature of the material, this will be the same as the charge temperature which the material is heated to before a journey. T_{min} is the temperature of the material at the end of the journey (assuming it is not recharged mid journey which will be true for all of the work presented here).

If $T^{min}_{meltingzone} < T_{max} < T^{max}_{melting\ zone}$,

$$E_{thermal} = M \times (C_p(T_{melting} - T_{min}) + C_l(T_{max} - T_{melting})). \tag{6.3}$$

Or if $T_{max} < T_{melting}$

$$E_{thermal} = M \times C_p(T_{max} - T_{min}). \tag{6.4}$$

Using these approximations and the values given in Table 5.2, it can be seen that when the thermal battery is charged to its maximum temperature it is capable of storing $496,800$J/kg or 0.138kWh/kg. Hence a maximum mass of PCM of 30kg should be used, providing a total energy of 4.14kWh; which is equivalent to 1 hour and 8 minutes of PTC heating in this vehicle, using the 4kW PTC defined in Chapter 4, thus meeting the requirement set.

Finally the power limit value of 20kW was chosen to meet the combined thermal demand of the cabin and battery as defined in Chapter 4.

The optimisation problem is summarised in Equation 6.5 using the constraints defined here and the cost function defined in Section 4.5.

$$\begin{aligned} &find\ X\ which\ minimises\ J \\ Where\ X = [&mass,\ charge\ temperature,\ thermal\ power] \\ &subject\ to \\ 1kg \leq\ &mass \leq 30kg \\ -10°\mathrm{C} \leq\ &charge\ temperature \leq 140°\mathbf{C} \\ 1kW \leq\ &thermal\ power \leq 20kW \end{aligned} \tag{6.5}$$

It is important to consider the resolution to which the optimised parameters should be found. Should a thermal storage system be included on an electric vehicle, it is unlikely it will be designed to a higher resolution than 1kg. This is therefore the resolution to which the mass should be found at the end of this process. Likewise, it will be difficult to control the maximum temperature and heat delivery to a high resolution and therefore the search algorithm used should find the optimum values of these to the nearest 1°C and 1kW respectively.

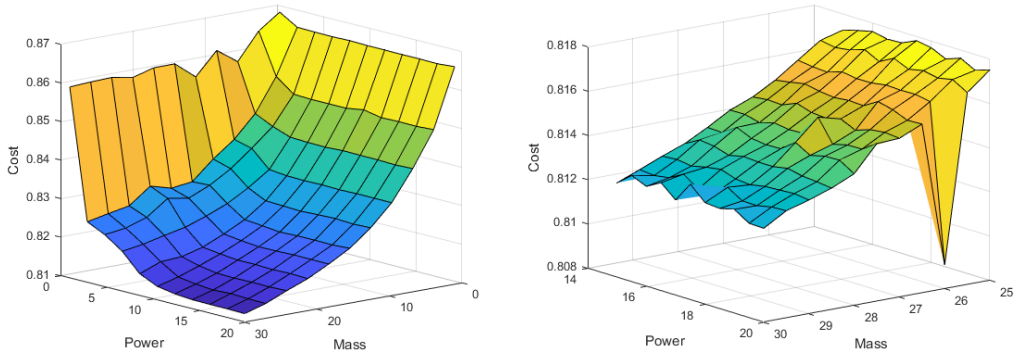

(a) Cost shown at full mass and power range. (b) Cost in region of global minima.

Figure 6.1: Surfaces showing the costs found in areas bound by the limits mass and power, seen in Figure 6.1a and a region bound by 25kg<mass< 30kg and 15kW<power< 20kW. Here it can be seen that the search space is shallow and rough in the region of the global minima.

6.3 Search algorithm selection.

The final step before performing the optimisation is selecting an appropriate search algorithm to return the optimal thermal battery specification. To do this some knowledge of the search space is required. Figure 6.1 shows two cost surfaces, Figure 6.1a covers the full range of allowed mass and power, while Figure 6.1b targets the area where the minimum is expected to be found. Both surfaces correspond to the WarmUp cycle at 5°C with the thermal battery starting at 140°C. Figure 6.1a shows that the global minima is likely to be found by maximising mass and power. When focussing in on this area, in Figure 6.1b, it can be seen that the minima found is likely to be in one of the local minima. Figure 6.1b also shows a strong local minimum; however, when inspecting the cost axis it can be seen that this minimum is approximately 1% lower in cost than the surrounding area. Since the model used is complex there is not a clear reason why this specification would produce a locally strong minima. That is to say that other minima like this are likely to exist between the points evaluated in Figure 6.1b. Additionally, away from the strong local minima it can be seen that the surface created is rough, with many small minima. The characteristics shown in Figure 6.1 lead to the requirement that the search algorithm chosen be resistant to local minima.

In Section 4.2.1 a series of search algorithms were discussed and their advantages and disadvantages reviewed. This was summarised in Table 4.1, which has been repeated here in Table 6.1. One of these search algorithm needs to be selected

according to the following criteria:

- Due to the simulation times presented in Section 5.9 it should be efficient.
- It should be robust to shallow and rough regions, and not likely to become stuck in local minima.

These criteria rule out grid search and random search methods, both of which are too inefficient to be considered further. The univarient method is automatically superseded by pattern search and so is also discounted. Due to the simplex method having a tendency to stagnate in shallow regions it will not be suitable for the search space shown in Figure 6.1. This leaves pattern search, Powell's method and genetic algorithms. Implementations of these algorithms were compared over a wide range of optimisation problems by Rios *et al.* [4] and were shown to perform similarly well. At this point it should be noted that any of these three algorithms would perform adequately and an objective comparison between their suitability to this specific problems becomes difficult. Time could be spent trialling all three to establish which is the most efficient for this task, however it is unlikely that this time could be recovered from the gained efficiency benefit. It is also worth considering that the objective of this research is to find the optimal design parameters to a resolution of 1kg, 1°C and 1kW and that changes in performance between different algorithm are likely to be smaller than the resolution of the output. Of the three, pattern search was selected as it had been used by the author in previous work and found to be easily implementable and reliable.

Table 6.1: The advantages and disadvantages of potential search algorithms are summarised. The information presented here has been collected from [4], [5] and [6]. For further details on these algorithms see Appendix A.

Method	**Advantages**	**Disadvantages**
Random Methods	- Resistant to local minima. - Can be used when other methods fail due to sharply varying functions or shallow areas.	- Inefficient at finding precise global minima. - Difficult to set search termination criteria.
Grid search	- Guaranteed to find global minima to the required resolution.	- Requires a prohibitively large number of function evaluations.
Univarient	- Simple implementation - More efficient than Random and Grid searches for some problems*.	- Converges slowly if precise locations of global minima are required. - *Steep valleys can prevent the search from converging.
Pattern Search	- Improved version of Univarient. - Achieves rapid convergence.	- Can be susceptible to local minima
Powell's Method	- Extension of pattern search. - Converges quickly when problem can be well approximated as a quadratic.	- Can be susceptible to local minima - Less effective away from the minimum
Simplex (Nelder-Mead)	- Most efficient method computationally.	- Tendency to stagnate in shallow regions.
Genetic Algorithms	- Highly effective at finding global minima - If population members can be evaluated in parallel it is highly efficient.	- If population members cannot be evaluated in parallel it can be very inefficient.

While pattern search is the most appropriate search algorithm it can also be susceptible to finding local minima. Commercially available implementations of pattern search use multiple randomised start points to overcome this [4]. This method will be applied here. The MATLAB implementation of pattern search is used and started from 5 random locations. The results pertaining to all random start points will be included in Sections 6.4 to 6.4.4. Robustness to local minima will be proved by comparing the cost resulting from each of the random starts, with abnormal costs and specifications indicating local minima were found.

6.4 Optimising the configuration of an additional thermal battery

In this section the specification is optimised for a system design case where the thermal storage can be freely added to the vehicle, without compromising the electrical energy storage. This also ignores any potential financial ramifications or challenges such as implementation. When considering the sizing for a thermal storage unit it is important to consider how useful it will be across a range of temperatures and drive cycles. In this section the optimisation procedure described in Sections 6.2 and 4.5 has been performed across the range of scenarios described in Sections 6.4.1, 6.4.2 and 6.4.6 where the titles of each section briefly describe the scenarios being addressed. As mentioned in Section 6.2, to avoid local minima the pattern search was reset from multiple randomised start points; in every following optimisation 5 random start points were considered.

6.4.1 WarmUp, Neutral Weighting, all temperatures

In this section the optimisation procedure described has been applied for a scenario where the vehicle completes the WarmUp cycle at all four ambient temperatures; $-15°C$, $-5°C$, $5°C$ and $15°C$. The WarmUp cycle is the longest cycle available out of the choices presented in Section 4.3. The 90 minutes of operational time makes it a good test case to identify the upper limit of useful thermal battery sizing; a shorter cycle may result in under-sizing of the thermal battery. Hence the resulting optimum solution found in this section will be used as the specification for the thermal battery in all subsequent chapters.

For this section the neutral weighting, described in Section 4.5, is used. The full results for each of the 5 randomised start points of the optimisation are presented in Tables 6.2 to 6.5, each corresponding to a different ambient temperature. Each of

Table 6.2: Optimised thermal battery specification for WarmUp cycle at −15°C using a neutral objective function weighting.

	Control Variable			
Pass	**Mass (kg)**	**Temperature (°C)**	**Thermal Power (kW)**	**Cost**
1	29	126.5	17.1	0.761
2	29.5	117.1	6.9	0.773
3	27.7	124.9	18.5	0.743
4	29.8	128.2	19.9	0.776
5	28	112.8	15.5	0.795
Mean	28.8	121.9	15.6	0.770
Std	0.9	6.6	5.1	0.019
Std as %	3.1	5.1	25.5	2.47

Table 6.3: Optimised thermal battery specification for WarmUp cycle at −5°C using a neutral objective function weighting.

	Control Variable			
Pass	**Mass (kg)**	**Temperature (°C)**	**Thermal Power (kW)**	**Cost**
1	28.7	121.9	19.4	0.743
2	29.8	93.8	18.6	0.747
3	29.5	118.3	16.5	0.747
4	29.1	119.5	18.3	0.745
5	29.7	99.2	19.2	0.745
Mean	29.4	110.5	18.4	0.745
Std	0.5	13	1.2	0.0015
Std as %	1.5	10	5.8	0.20

these tables contains information about the mean, standard deviation and standard deviation as a percentage of the variable range for the control variables. For the cost the standard deviation is given as a percentage of the mean cost. This is used to discuss confidence in the results and to confirm that the search algorithm used was robust to local minima as required. From these results the specification corresponding to the lowest associated cost is put into the final specification table, Table 6.6, where the optimal values at each temperature are averaged to give a final optimised value.

It should be noted from Tables 6.2 to 6.5 that the mean mass and power at each ambient temperature is similar with a low standard deviation and low spread in

Table 6.4: Optimised thermal battery specification for WarmUp cycle at 5°C using a neutral objective function weighting.

	Control Variable			
Pass	**Mass (kg)**	**Temperature (°C)**	**Thermal Power (kW)**	**Cost**
1	29.9	124.9	19.9	0.856
2	29.8	135.2	19.9	0.85
3	29.8	130.9	19.7	0.853
4	30	137.7	19.8	0.849
5	29.7	126.2	19.9	0.856
Mean	29.8	131	19.8	0.853
Std	0.1	5.5	0.1	0.0034
Std as %	0.4	4.3	0.4	0.39

Table 6.5: Optimised thermal battery specification for WarmUp cycle at 15°C using a neutral objective function weighting.

	Control Variable			
Pass	**Mass (kg)**	**Temperature (°C)**	**Thermal Power (kW)**	**Cost**
1	28.6	139.5	19.4	0.821
2	29.4	121.8	19.9	0.831
3	29.5	125.9	19.9	0.829
4	28.8	113.3	19.7	0.84
5	29.8	131.4	20	0.824
Mean	29.2	126.4	19.8	0.829
Std	0.5	9.9	0.2	0.0074
Std as	1.6	7.6	1.2	0.89

cost. The agreement seen here implies that the search algorithm chosen has indeed been robust to local minima. Should the search algorithm not have been robust to local minima, an increased distribution in cost would have been seen. Tables 6.2 to 6.5 also show that the uncertainty in the specification values (mass, charge temperature and thermal power) is higher than the standard deviation in cost. This implies that there is a region in the search space where the cost is no longer sensitive to the thermal battery specification; the cost function becomes flat (small gradient) but rough, creating local minima with similar cost. It is important to understand where this area begins, particularly with respect to mass, since this will define the package size. This is explored in Section 6.4.7.

The charge temperature has the largest variance of the control variables, with the exception of thermal power at $-15°C$. This is evidenced by the standard deviation and the standard deviation as a percentage of the maximum range of each variable, given in the statistics part of Tables 6.2 to 6.5. This implies that, above some value, the charge temperature has less impact on the cost function, a statement which is further explored in Section 6.4.7. It is likely that this happens soon above the materials melting point, which is where a significant proportion of the thermal energy is stored. The charge temperature does not necessarily influence the design of the thermal battery, but may be more important to the vehicles operation and management. Explicitly, the charge temperature will be defined during the charging of the vehicle, here the charger/vehicle may be able to control the charge temperature of the thermal battery according to the day's demand, regarding drive cycle and ambient temperature.

The mean of the specifications correlating to the lowest cost at each temperature was taken, as shown in Table 6.6. A final specification needs to be decided upon to be used in the following results chapters. Choosing a specification which represents the optimum for the neutral optimisation on the WarmUp cycle is the most sensible choice. Using the neutral optimisation ensures the specification does not favour either the battery or the cabin, while using the specification for the longest drive cycle ensures sufficient energy for the others. With these considerations a final specification of $29kg$, $131°C$ and $19kW$, which is the average of the optimum specification for each ambient temperature, shall be used as the specification for the thermal battery in the other results chapters. These values had a standard deviation of 0.94kg, 8.9°C and 0.57kW, which are small in comparison to the constrained range defined in Equation 6.5. This is used to demonstrate confidence that the control variables have been optimised.

It may be noticed from Table 6.6 that there are two apparent regions of cost.

Table 6.6: The specification corresponding to the lowest cost at each temperature are presented. The mean of these values is taken as the final value.

	Control Variable			
Ambient (°C)	**Mass (kg)**	**Temperature (°C)**	**Thermal Power (kW)**	**Cost**
-15	27.7	124.9	18.5	0.743
-5	28.7	121.9	19.4	0.743
5	30	137.7	19.8	0.849
15	28.6	139.5	19.4	0.821
Final Value	29	131	19	
Std	0.94	8.9	0.57	
Std as %	3.13	6.85	2.85	

The cost is normalised at each ambient temperature separately. In general this means at high ambient temperatures there will be less of an improvement in cost, since there is less ability to improve on thermal comfort and energy consumption. The appearance of two apparent regions does not have any significance.

In this section a neutral weighting was used to perform the optimisation, with the intention of providing a balance between vehicle performance and thermal comfort. This leads to the question of whether the optimal solution changes if the weighting between cost functions is set to favour either the cabin or the battery. This question is addressed in Sections 6.4.2 to 6.4.4.

6.4.2 WarmUp, Battery and Cabin Weighting, all temperatures

In this section the optimisation has been repeated using the alternative weightings proposed in Table 4.3. Tables 6.7 to 6.10 show the results of each optimisation for battery dominant weighting, while Tables 6.12 to 6.15 show results from a cabin dominant weighting.

6.4.3 Battery weighted

Here the same analysis is performed as in Section 6.4.1, with individual results from each temperature presented along with a summary of the results found in Table 6.11. From a battery perspective it can be seen from Table 6.11 that the optimised thermal battery has nearly the same configuration as the neutrally weighted optimisation. The only difference here is a 130°C charge temperature for battery weighting compared to a 131°C charge temperature for neutral weighting. However given the

Table 6.7: Optimised thermal battery specification for WarmUp cycle at −15°C using electric battery weighted objective function.

	Control Variable			
Pass	**Mass (kg)**	**Temperature (°C)**	**Thermal Power (kW)**	**Cost**
1	25.4	120.9	7.6	0.897
2	25.2	129.2	5.6	0.874
3	29.5	123.5	19.3	0.871
4	29.1	135.2	18.6	0.868
5	29.3	111.6	19.9	0.881
Mean	27.7	124.1	14.2	0.878
Standard Deviation	2.2	8.9	7	0.011
Std as %	7.2%	6.8%	35%	1.31

Table 6.8: Optimised thermal battery specification for WarmUp cycle at −5°C using electric battery weighted objective function.

	Control Variable			
Pass	**Mass (kg)**	**Temperature (°C)**	**Thermal Power (kW)**	**Cost**
1	27.6	122.9	19.8	0.81
2	28.8	111.2	16	0.81
3	24.7	83.8	19	0.811
4	29.1	104	18.2	0.809
5	29.6	96.2	19.4	0.809
Mean	28	103.6	18.5	0.810
Standard Deviation	1.9	14.8	1.5	0.0010
Std as %	6.5%	11.4%	7.4%	0.13

uncertainty in optimal charge temperature ranging from 6.8% to 11.4% as seen in Tables 6.7 and 6.8 respectively, this difference in temperature is likely to have a negligible impact.

This section shows that implementing a thermal storage device onto a vehicle, in addition to the main electric battery, should not have a detrimental impact on vehicle performance. This should be intuitively unsurprising since adding free energy to the vehicle should only result in enhanced performance.

Table 6.9: Optimised thermal battery specification for WarmUp cycle at 5°C using electric battery weighted objective function.

	Control Variable			
Pass	**Mass (kg)**	**Temperature (°C)**	**Thermal Power (kW)**	**Cost**
1	30	140	19.8	0.889
2	29.9	132.4	19.9	0.893
3	30	115.9	19.5	0.899
4	30	135.8	19.9	0.892
5	29.8	135.6	20	0.892
Mean	29.9	131.9	19.8	0.893
Standard Deviation	0.1	9.4	0.2	0.0037
Std as %	0.3%	7.2%	0.9%	0.42

Table 6.10: Optimised thermal battery specification for WarmUp cycle at 15°C using electric battery weighted objective function.

	Control Variable			
Pass	**Mass (kg)**	**Temperature (°C)**	**Thermal Power (kW)**	**Cost**
1	30	108.7	19.6	0.891
2	29.9	140	19.6	0.874
3	29.9	113	19.7	0.892
4	29.4	139.3	19.8	0.874
5	29.8	130.6	19.9	0.876
Mean	29.8	126.3	19.7	0.881
Standard Deviation	0.2	14.7	0.2	0.0091
Std as %	0.7%	11.3%	0.8%	1.02

Table 6.11: The specification corresponding to the lowest cost at each temperature are presented. The mean of these values is taken as the final value. These results correspond to an electric battery weighted objective function.

Ambient (°C)	**Mass (kg)**	**Temperature (°C)**	**Thermal Power (kW)**	**Cost**
−15°C	29.1	135.2	18.6	0.868
−5°C	29.1	104	18.2	0.809
5°C	30	140	19.8	0.889
15°C	29.4	139.3	19.8	0.874
Final Values	**29**	**130**	**19**	
Std	0.42	17.24	0.85	
Std as %	1.4	13.26	4.25	

6.4.4 Cabin weighted

In this section the results pertaining to the cabin weighted optimisation are presented in the same format as Sections 6.4.1 and 6.4.3. From the final summary of results, seen in Table 6.16, there is a slight change in the optimal configuration. Firstly, the optimised mass has reduced to $28kg$, which is surprising since it is expected that the cabin will benefit more than the electric battery from the addition of the extra thermal storage. Upon closer inspection of Table 6.16, at $-5°$C the optimised mass is 25.3kg, compared to at least 29.3kg at all other temperatures. Exploring this further and considering Table 6.13, it can be seen that pass 2 and pass 5 have the same cost to 3 decimal places, but pass 2 converged on a mass of $29.8kg$. It is likely that the cost seen at 25.3kg corresponds to the cost at a local minima, such as the ones seen in Figure 6.1. Since 5 randomised start points have been used it is possible to see this is a local minima, or even a joint global minima, hence demonstrating the intended robustness of the 5 random start point modification. Were 29.8kg to be used as the optimised mass, the mean across the 4 temperatures would increase to 30kg, which would be more in-line with expectations. This deviation from the expected reveals that in this mass range there is little further improvement in cost, and that secondary effects causing the local minima seen in Figure 6.1 are influencing the cost.

In Table 6.16 the thermal power is also low when compared with the other objective function weightings. The optimal thermal power value at $-15°$C can be identified as a particularly low outlier. When inspecting Table 6.12 it can be seen that 3 of the passes converged between 9kW and 10kW while the other 2 converged on 17.8kW and 19.8kW, with all costs between 0.658 and 0.668. It is unclear why these two regions have appeared, even after the further investigation performed in Section 6.4.7. It should therefore be concluded that the points corresponding to 9kW and 10kW have arisen due to local minima in those areas. So at lower ambient temperatures it appears that being able to deliver relatively high quantities of heat is less important. By contrast the passes at the other ambient temperatures had an average thermal power of 19kW, 19.9kW, and 19.5kW with standard deviations of 5.7%, 0.4% and 2% respectively.

6.4.5 Summary of WarmUp optimisation results

Table 6.17 summarises the findings from the results of the optimisations using the WarmUp cycle. This shows that the optimal sizing of the thermal battery falls just short of the upper limits set. It is possible that by reducing the termination tolerance

Table 6.12: Optimised thermal battery specification for WarmUp cycle at −15°C using cabin weighted objective function.

	Control Variable			
Pass	**Mass (kg)**	**Temperature (°C)**	**Thermal Power (kW)**	**Cost**
1	29.4	139.5	9.7	0.658
2	29.9	132.3	17.8	0.668
3	29.9	90.6	9.7	0.666
4	26.4	77.2	19.8	0.668
5	29.6	132.3	9.2	0.668
Mean	29	114.4	13.2	0.666
Std	1.5	28.4	5.1	0.004
Std as %	5	21.8	25.7	0.66

Table 6.13: Optimised thermal battery specification for WarmUp cycle at −5°C using cabin weighted objective function.

	Control Variable			
Pass	**Mass (kg)**	**Temperature (°C)**	**Thermal Power (kW)**	**Cost**
1	22.6	89.7	17.1	0.686
2	29.8	133	19.9	0.679
3	29.2	136.4	19.1	0.68
4	29.3	130.4	19.7	0.681
5	25.3	137.4	19.5	0.679
Mean	27.2	125.4	19	0.681
Std	3.2	20.2	1.1	0.003
Std as %	10.5	15.5	5.7	0.43

Table 6.14: Optimised thermal battery specification for WarmUp cycle at 5°C using cabin weighted objective function.

	Control Variable			
Pass	**Mass (kg)**	**Temperature (°C)**	**Thermal Power (kW)**	**Cost**
1	30	132.5	20	0.81
2	29.9	129.6	19.9	0.813
3	29.8	135.6	19.9	0.808
4	29.6	126.3	19.8	0.815
5	29.9	134.7	19.9	0.808
Mean	29.8	131.8	19.9	0.811
Std	0.2	3.8	0.1	0.003
Std as %	0.5	2.9	0.4	0.38

Table 6.15: Optimised thermal battery specification for WarmUp cycle at 15°C using cabin weighted objective function.

	Control Variable			
Pass	**Mass (kg)**	**Temperature (°C)**	**Thermal Power (kW)**	**Cost**
1	22.4	127.1	19.3	0.788
2	29.6	135.6	18.9	0.772
3	29.3	135.1	19.8	0.769
4	28.4	131.1	19.8	0.774
5	28.3	137.1	19.7	0.771
Mean	27.6	133.2	19.5	0.7750
Std	3	4	0.4	0.007
Std as %	9.9	3.1	2	0.96

Table 6.16: The specification corresponding to the lowest cost at each temperature are presented. The mean of these values is taken as the final value. These results correspond to a cabin weighted objective function.

	Control Variable			
Ambient (°C)	**Mass (kg)**	**Temperature (°C)**	**Thermal Power (kW)**	**Cost**
-15	29.4	139.5	9.7	0.658
-5	25.3	137.4	19.5	0.679
5	29.8	135.6	19.9	0.808
15	29.3	135.1	19.8	0.769
Final Value	28	137	17	
Std	2.14	1.99	5.02	
Std as %	7.13	1.53	25.1	

Table 6.17: Summary of final optimisations across WarmUp cycle with different weightings.

Weighting	**Mass (kg)**	**Temperature (°C)**	**Power (kW)**
Neutral	29	131	19
Battery	29	130	19
Cabin	28	137	17

of the search algorithm and/or by increasing the number of random passes used, the optimisation may converge on the upper limits of the problem. However, it was also implied through the data and analysis presented in this section that towards the upper limits of the allowed specification, improvements in the cost function are small and local minima are likely having an impact on the result. This is further investigated by looking at the sensitivity of the cost function to each control variable in Section 6.4.7.

Using the results from Section 6.4.1, the thermal battery configuration for the remaining chapters has been set to 29kg mass, 131°C charge temperature and 19kW of thermal power. As stated in Section 6.4.1, the WarmUp cycle is the longest cycle, both in duration and distance, and therefore has the highest thermal demand. The optimal specification for this cycle will therefore have sufficient thermal storage to meet the heating requirements of the other two cycles. However, given the short nature of the other drive cycles the point of diminishing returns may arrive sooner, leading to a different optimal specification. To ensure that the optimal specification of the thermal battery for the other two cycles is not drastically different, the optimisation process is repeated for altered scenarios in which NEDC and WLTP are the test cycles.

6.4.6 NEDC and WLTP, Neutral Weighting, extreme temperatures

After concluding the optimised thermal battery specification for the WarmUp cycle, the other drive cycles defined in Section 4.3 should also be considered. To address this the thermal battery is optimised in the same way for the NEDC and WLTP cycles, each at the two extreme temperatures i.e. −15°C and 15°C. The optimum solution is not expected to vary significantly for the intermediate temperatures, as demonstrated in Table 6.6. Here the optimal mass, charge temperature and power varied by 3.13%, 6.85% and 2.85% across all ambient temperatures. The thermal battery is optimised at these two temperatures using a neutral weighting.

The starting conditions for this investigation were altered in an attempt to reduce the number of iterations per search. An assumption is made that the optimised solution for NEDC and WLTP at the extreme temperatures will be similar to the solution found in Section 6.4.1, as evidenced by the agreement seen in Sections 6.4.3 and 6.4.4; therefore it would be sensible to initialise each search close to the results previously found. Hence the start value is defined by selecting a random number in the range defined by $X_i^{opt} \pm X_i^{max\ Std}$. Where X_i^{opt} is the optimum value of an optimisation component and $X_i^{max\ Std}$ is the maximum standard deviation of

that component, defined by the standard deviation of the component across the 5 random starts. Using this method the range of the random starting values is defined below.

- Mass, lower limit 26kg, upper limit 30kg.
- Temperature, lower limit 112°C, upper limit 140°C.
- Power, lower limit 12kW, upper limit 20kW.

The results of the individual optimisation passes at each ambient temperature for NEDC and WLTP are presented in Tables 6.18 to 6.21, with a summary of the findings shown in Table 6.22. Considering the final values for the thermal battery, optimised for the WLTP and NEDC cycles, presented in the final line of Table 6.22, it can be said that there is agreement between what is optimal for the NEDC and WLTP cycles and what is optimal for the WarmUp cycle. Comparing Tables 6.22 and 6.6, the mass has decreased by 3.5%, the charge temperature has increased by 6.1% and power has increased by 5%. Here mass and charge temperature have varied within the standard deviation given in Table 6.6, hence they show agreement. While power is outside of the standard deviation in power shown in Table 6.6, the change is dominated by rounding to the nearest integer, and it is still less than the standard deviation seen in charge temperature. These minor differences could be a result of the drive cycle being shorter, where thermal power and temperature might make a bigger difference at the start of the cycle. For example if the warm up phase (where the thermal battery is likely to make a big difference) is 5 minutes, then higher temperatures and thermal power, which improve warm up characteristics, will have a greater relative impact on a 20 minute cycle compared to a 90 minute cycle. Furthermore the slight decrease in mass might be explained by the reduced duration since less heating energy is needed, this is evidenced by the spread of optimal masses at the 15°C for both cycles, seen in Tables 6.19 and 6.21.

Given the minor differences in the optimal solution it can be concluded that a solution which is optimal for one drive cycle will transition well to other cycles. This applies given the drive cycle is no longer nor shorter than the ones tested here, i.e. the cycle is between 20 minutes and 90 minutes. Hence this method proposed, where the thermal battery is optimised for one drive cycle then checked against others, is a valid way to reduce simulation time while still having confidence in the final solution.

Table 6.18: Optimised thermal battery specification for NEDC cycle at −15°C using a neutral weighted objective function.

	Control Variable			
Pass	**Mass (kg)**	**Temperature (°C)**	**Thermal Power (kW)**	**Cost**
1	29.7	135.1	19.8	0.876
2	27.2	132.3	19.9	0.876
3	29.5	139.3	19.7	0.874
4	29.7	138.3	19.3	0.876
5	29.2	126.8	18.7	0.878
Mean	29.1	134.4	19.5	0.876
Std	1	5	0.5	0.0013
Std as %	3.5	3.9	2.4	0.15

Table 6.19: Optimised thermal battery specification for NEDC cycle at 15°C using a neutral weighted objective function.

	Control Variable			
Pass	**Mass (kg)**	**Temperature (°C)**	**Thermal Power (kW)**	**Cost**
1	25.7	136	19.6	0.854
2	28.2	134.4	19.7	0.854
3	24.6	139.7	20	0.853
4	29	129.7	19.9	0.854
5	27.7	135.2	19.7	0.853
Mean	27	135	19.8	0.854
Std	1.8	3.6	0.2	0.0003
Std as %	6.1	2.8	0.8	0.04

Table 6.20: Optimised thermal battery specification for WLTP cycle at −15°C using a neutral weighted objective function.

	Control Variable			
Pass	**Mass (kg)**	**Temperature (°C)**	**Thermal Power (kW)**	**Cost**
1	29.9	139.5	19	0.884
2	29.3	136.1	19.2	0.888
3	25.9	82.5	19.3	0.896
4	27.1	132.3	10	0.891
5	29.7	136	19.8	0.885
Mean	28.4	125.3	17.5	0.889
Std	1.8	24.1	4.2	0.0047
Std as %	5.9	18.5	20.8	0.53

Table 6.21: Optimised thermal battery specification for WLTP cycle at 15°C using a neutral weighted objective function.

	Control Variable			
Pass	**Mass (kg)**	**Temperature (°C)**	**Thermal Power (kW)**	**Cost**
1	25.3	131.6	19.9	0.838
2	24.9	134.7	19.8	0.837
3	28.5	137	19.9	0.836
4	29.8	135.6	20	0.837
5	26.4	134.1	18.5	0.839
Mean	27	134.6	19.6	0.837
Std	2.1	2	0.6	0.0011
Std as %	7.1	1.5	3.1	0.13

Table 6.22: The specifications corresponding to the lowest cost at each temperature are presented. The mean of these values is taken as the final value. These results correspond to a neutral weighted objective function for NEDC and WLTP at the extreme temperatures.

	Control Variable			
Ambient (°C)	**Mass (kg)**	**Temperature (°C)**	**Thermal Power (kW)**	**Cost**
NEDC -15	29.5	139.3	19.7	0.874
NEDC 15	24.6	139.7	20	0.853
WLTP -15	29.9	139.5	19	0.884
WLTP 15	28.5	137	19.9	0.836
Final Value	28	139	20	
Std	2.39	1.26	0.43	
Std as %	7.97	0.97	2.15	

6.4.7 Cost function sensitivity

One of the key findings from Sections 6.4.2 and 6.4.6 was the importance of understanding how the cost varied in the region where the global minimum is likely to be found. This has already been explored in Figure 6.1 using 121 points around the minima. However through the 5 separate optimisations through each scenario more than 1000 evaluations have been recorded, allowing a more thorough examination of the search space to be performed in this section. This allows for an approximation of a sensitivity analysis to be performed, where the complexity of the model used for this research prohibits the calculation of the Jacobian necessary for a formal sensitivity analysis.

In Section 6.4.4 two identical minimum costs were seen, one at 25.3kg and the other at 29.8kg, seen in Table 6.13, at an ambient temperature of $-5°$C. At $-15°$C in the same section the optimum power appeared to converge in two regions, one between 9kW and 10kW and the other between 17.8kW and 19.8kW, seen in Table 6.12. Additionally in Section 6.4.6, in Table 6.19 a 6.8% standard deviation in mass can be seen, correlating to a 0.03% standard deviation in cost. Similarly in Table 6.20 the charge temperature has standard deviation 18.5% and the power has a standard deviation of 20.8%, while the cost has a standard deviation of 0.47%. These observations imply there is a flat region of the search space, like the one seen in Figure 6.1a. This flat region is likely to be earlier for shorter drive cycles, where less heat is required. In response to this, further analysis needs to be made into the sensitivity of the cost function with respect to the three control variables.

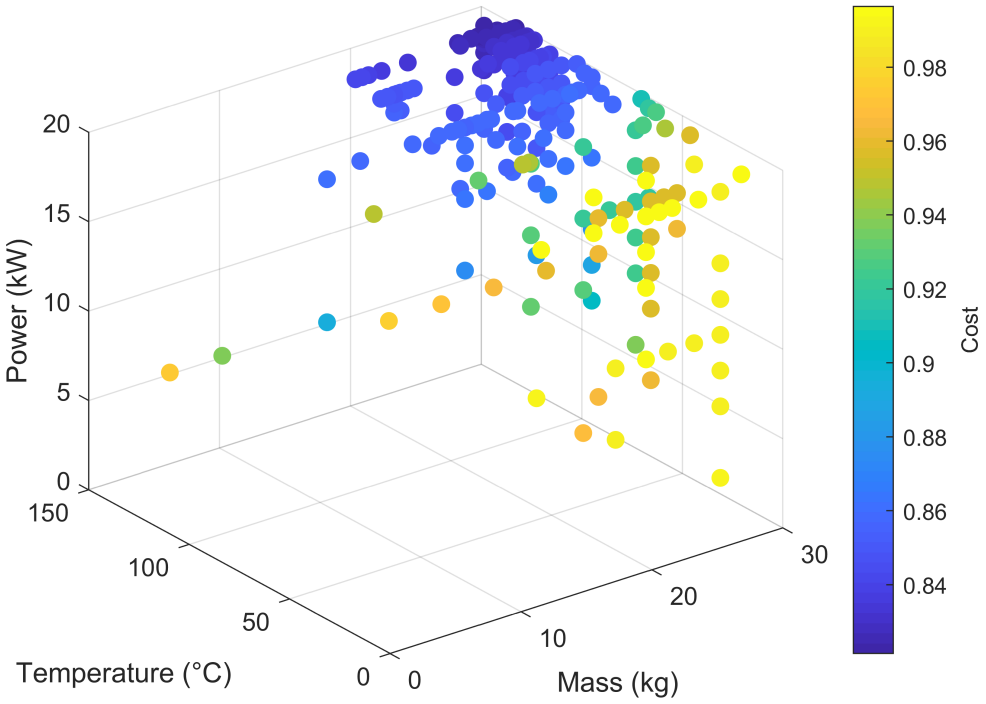

Figure 6.2: Search space and cost for the complete dataset of WarmUp, Neutral Weighting at 15°C.

During the optimisation process a log of the control vector X and the cost J was kept, which has been used to create Figure 6.2. Figure 6.2 shows the complete search space for WarmUp using the neutral weighting (Section 6.4.1). The region where the three control parameters reach their maximum allowed values is where the cost function is minimised. In this region there appears to be a non-insignificant space where the cost is unchanging. Thus it follows that for each parameter there is a point of diminishing returns, where further increases in size, temperature or power result in negligible reductions to cost. To investigate these regions further the image results shown in Figure 6.2 can be reduced to one-dimensional, effectively viewing each face of the three-dimensional search space. One example of this has been created for each of the mass, charge temperature and power axis, shown in Figures 6.3, 6.4 and 6.5 respectively. Here mass and power are shown at an ambient temperature of $-5°C$, while temperature is shown at an ambient temperature of $5°C$; these have been chosen as they best depict the points made in relation to each parameter. The full set of figures, for all temperatures, may be found in Appendix B. The red dots in Figures 6.3 to 6.5 show the optimal point found at the end of each search algorithm pass.

From an engineering design point of view, mass is arguably the most important control variable to optimise, as it will define the final size of the package. It is therefore imperative that the benefit provided to the system by additional mass is fully understood. It was identified in Section 6.4.2 that the cost function appeared not to be as sensitive to mass, specifically at $-5°C$ where masses of 25.3kg and 29.8kg produced the same cost. This was seen again in Section 6.4.6 during the optimisations at $15°C$, where the optimum mass ranged from 24.6kg to 29kg and 24.9kg to 29.8kg and the costs covered a range of 0.853 to 0.854 and 0.836 to 0.839 for NEDC and WLTP respectively, as seen in Tables 6.19 and 6.21. The addition of the thermal battery is in essence free energy; it would be intuitive to assume that the algorithm would maximise the available mass, but this was not the case. Instead the evidence suggests that there is little benefit in exceeding 25kg, this is further reinforced by Figure 6.3. Here it can be seen that the minimum achievable cost changes very little with mass between 25kg and 30kg. In this region the minimum cost varies by 0.8%, which is small compared to the 25% overall reduction in the complete search space. This may be taken into account if implementing in a real world vehicle as there would be value in minimising the mass and size of the component.

The results presented here help to explain some of the uncertainty seen in the final values presented in Sections 6.4.1, 6.4.2 and 6.4.6. Firstly it was noted

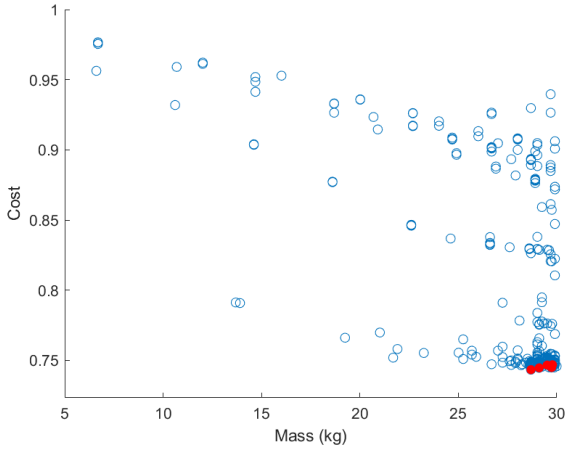

Figure 6.3: Sensitivity to mass at −5°C ambient. Blue dots show each point evaluated in the five passes, red points show the optimum point found at the end of each of the five passes.

that there was a large uncertainty in the optimal charge temperature, and it was postulated that above some temperature any further increase would produce diminishing returns. This is best exemplified in Figure 6.4 where it can be seen that above the PCM's melting point (75°C) there is little further improvement in cost. Here a discontinuity is seen around the PCM's melting point. This is expected as the material's latent heat is responsible for a large proportion of the stored energy. Beyond the melting point the cost continues to decrease as the charge temperature rises. It also appears that the rate of change increases (increased reduction in cost with temperature) after 120°C. It may be possible that continued reductions would be seen beyond 140°C, but this area was not explored as it would lead to the thermal breakdown of the material modelled.

The behaviour shown in Figure 6.4 poses an interesting problem for the charging algorithm which would be responsible for heating the thermal battery. Since there is little benefit in cost between 75°C and 100°C should the charger spend extra effort to charge the thermal battery to 100°C? Additionally, there is then a benefit if the charge is able to reach 140°C, and so if there is enough time should the charge go to this temperature? These are questions which would need to be investigated further if a thermal battery and heat pump were implemented in a real system.

Finally, Figure 6.5 shows a clear trend in cost reduction between 1kW and 20kW, with improvements appearing to stop at 20kW. This is likely a result of the system design, with the cabin and battery demanding 10kW of heat each, any extra

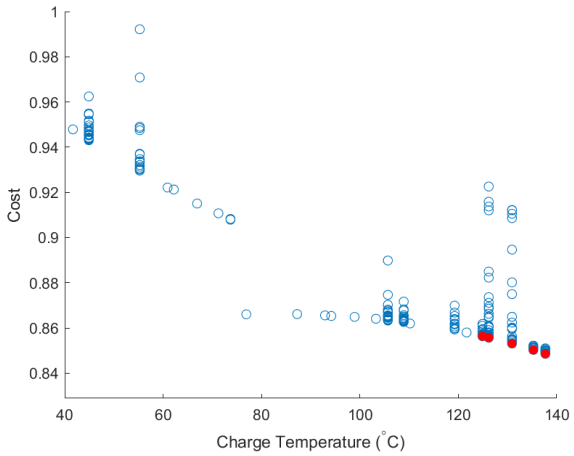

Figure 6.4: Sensitivity to charge temperature at 5°C ambient. Blue dots show each point evaluated in the five passes, red points show the optimum point found at the end of each of the five passes.

power beyond 20kW would be surplus, and therefore not lead to a cost improvement. Improvements in cost appear to slow down after 15kW, which indicates that there may not be any real world benefit in designing a system to produce more heat than this. It is likely this slow down begins at 15kW because of the heat supplied by the PTC heater and heat pump once they have warmed up. This would mean that between approximately 15kW and 20kW the increased heat is only beneficial during the warm up period of the heat pump and PTC, and is therefore small over the course of the entire cycle.

Through this looking at the sensitivity of the cost function, as in Figure 6.2 is has been possibly to identify a region of diminishing returns. Then when this was reduced to the three axis separately it has been possible to identify where the diminishing returns begin for each design parameter. In doing so it has been shown that increasing the mass beyond 25kg may not be worth doing in a real world example, the control of the charge temperature should also be considered carefully when going beyond 75°C, and the system may not see much benefit in producing more then 15kW of heat. Although the absolute minimum has been found in excess of these values, that was excluding any financial cost of implementation. If financial cost were considered in the cost function then it is likely the absolute minimum would be found closer to the values identified in this section.

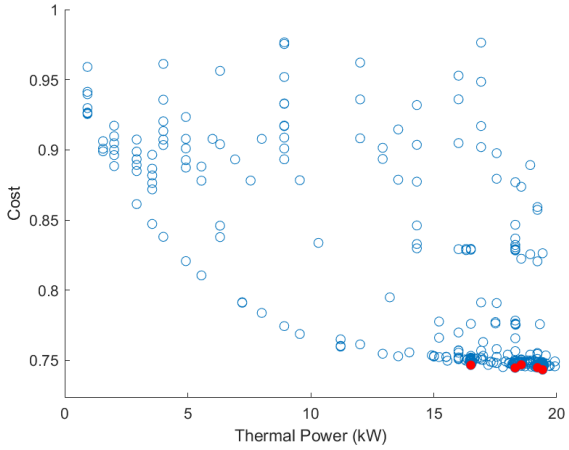

Figure 6.5: Sensitivity to power at −5°C ambient. Blue dots show each point evaluated in the five passes, red points show the optimum point found at the end of each of the five passes.

6.4.8 Statistics analysis of tables 6.2 to 6.21

In Tables 6.2 to 6.21 statistics were presented on the distribution of optimised design parameters for the thermal battery. In this section the meaning of these statistics is discussed in comparison with the data presented in Figures 6.3 to 6.5.

In general the distribution of results of each search indicates the importance of each component to the cost function, with narrow distributions indicating that the cost function is highly dependent on a component of the design and broad distributions indicating a weaker dependency on a component. Over all scenarios optimised (e.g. WarmUp, Neutral at all temperatures, etc.) the variation in mass between the five passes was between 0.3% and 10.5% with the majority being less than 5%. This is the smallest distribution of the three design components, an observation which is supported visually by the distribution of optimal points in Figure 6.3 compared to Figures 6.4 and 6.5. In Section 6.2 a 1kg resolution was set as a requirement for finding the mass of the thermal battery. In general the optimal mass has been found with a standard deviation of 1.5kg or less (equating to 5%). This spread is therefore higher than desired, and so if this were to go to production it should be sized at 27.5kg (29kg - 1.5kg known spread).

The temperature component of the design had a larger distribution within its passes compared to mass, with standard deviations ranging between 2.9% and 21.8%. When observing the distribution of optimal points shown in Figure 6.4 it appears that the spread in results may be dominated by the search algorithm finding

local minima, as there is a clear tendency towards higher temperatures to minimise the cost. This observation helps to justify the use of multiple starting points for the optimisation, without which a sub-optimal result may have been returned. Although the distribution of results is higher than with mass, the information provided by Figure 6.4 shows that the dependency of cost on temperature is not weak.

The combination of standard deviations from Tables 6.2 to 6.21 and the spread of optimal points in Figure 6.5 indicates that the cost function is weakly dependant on power. In Tables 6.2 to 6.21 the standard deviation ranges from 0.4% to 35.7%, with four instances being above 20%, indicating that power has the weakest influence on cost. This is supported by Figure 6.5 where it can be seen that the optimal points cover approximately 20% of the search space while having a very minimal change in cost. As discussed in section 6.4.7 this is somewhat expected since the system is built to supply a total of 20kW, of which 4kW can be supplied by the PTC heater, and more by the heat pump, and therefore anything above approximately 15kW of heat from the thermal battery is surplus to requirements.

Both the temperature and power distributions are higher than the desired resolution defined in Section 6.2. This is not necessarily a problem as both of these aspects of the thermal battery can be controlled in vehicle, and it is not as important if these are over rated. The temperature will be controlled in the charging phase of the vehicle's operation, and if the thermal battery is well insulated then overcharging is not an issue as unused energy can be saved for the next trip. Similarly, if the thermal battery is sized to produce 20kW of heat then it is able to supply the full heat load for the vehicle. However, it is not a problem if its full potential is not required, as long as it is capable of topping up the heat pump and PTC heaters output to meet the vehicle requirement, hence anything above 15kW is sufficient. This is not to say that finding the optimal value is unimportant as much has been learnt about thermal battery performance and sizing as a result of going through this process.

6.4.9 Optimised parameter validation

In this section the thermal battery depletion is used to validate the optimised thermal battery specification parameters. The depletion of the thermal battery can be used to indicate that the correct amount of energy storage has been added, and that the thermal power is appropriate. If these two factors are correct it is expected that the thermal battery will be almost fully depleted in the harshest testing conditions, i.e. it contains enough energy to be useful in any scenario. If the thermal battery has been undersized then its depletion will reach 100% in conditions which are less

Table 6.23: Optimised thermal battery depth of discharge over all drive cycles at all ambient temperatures. The depletion seen at −15°C during the WarmUp cycle indicates that the optimised thermal battery has been correctly sized.

Ambient Temperature (°C)	WarmUp	NED	WLTP
-15	97%	75%	77%
-5	71%	40%	40%
5	39%	39%	39%
15	28%	28%	28%

challenging then the harshest scenario. Similarly, if the battery is oversized, its depletion will be low in the most challenging conditions. Similar conclusions can be drawn about the thermal batteries heating capacity. If too much heat is extracted, then the thermal battery will be depleted before the end of the cycle, and if too little heat is extracted the thermal battery will be unable to deliver all its energy during the cycle and will be under utilised. If the heat and energy stored are balanced correctly it is expected that the thermal battery will be depleted in the region of 95% to 100% in the most challenging testing scenario.

The optimal specification for the thermal battery obtained in 6.4.1 was 29kg mass, 131°C charge temperature and 19kW thermal power. Here these values are used for all testing scenarios and the thermal battery depletion has been calculated and is presented in Table 6.23. Table 6.23 shows that at −15°C, during the warm up cycle, 97% of the thermal battery's operating range has been used. This indicates that the energy stored within the thermal battery (defined by the mass and charge temperature) and the thermal power are well balanced to meet the heating requirements during the most challenging scenario.

Further insight into the operation of the thermal battery can be gained through the closer examination of the data within Table 6.23. It may be noticed that there are distinct regions of depletion. The first region is at 39% and 40%, this corresponds to the temperature at which the latent heat is found. Since the latent heat accounts for 37% of the stored thermal energy it is likely that a range of scenarios will deplete into the melting window. Additionally, there is a second region at 28% depletion for all cycles at 15°C. Here the cabin warms up quickly and the thermal battery is not needed soon into the drive cycle. These two observations also indicate that charge depletion and thermal battery usage is independent of drive cycle dynamics, and predominately dependent on warm up time duration.

In Section 6.4.7 it was suggested that there may not be much benefit in

increasing the thermal storage mass beyond 25kg, since this was identified as the point of diminishing returns. The data presented in Section 6.4.7 covered the full range of temperatures, and so 25kg may represent the point of diminishing returns at high ambient temperatures, but more storage may still be beneficial at lower ambient temperatures.

Another method to validate the optimal parameters would be to use the optimal parameters as an initial guess for a new search in all the proposed scenarios. If the search algorithm fails to move away from the initial guess then it can be assumed to be optimal. This would ensure that the parameters chosen through the optimisation process are optimal for all scenarios. From the sensitivity analysis performed, and the discussion on distribution statistics made in Sections 6.4.7 and 6.4.8 it is known that the optimal point could be found in wide region of temperatures and powers, and therefore this strategy might not work, since the optimal location is always likely to change.

Through the inspection of thermal battery depletion it can be concluded that the thermal battery has been ideally sized. Any smaller and the thermal battery may have fully depleted before the end of the WarmUp cycle at $-15°C$, while any increase in size would be wasteful. In the next section the impact of this thermal battery sizing is evaluated against the individual cost metrics of the cost function.

6.4.10 Comparison of metrics.

The cost function used to assess optimality is comprised of three distinct components; vehicle energy consumption, comfort and depth of discharge. These have been chosen to address the concerns identified in Chapters 1 and 2. In this section the impact of an optimised thermal battery is demonstrated on these components individually. Firstly in Figures 6.6 and 6.7 the cumulative energy consumption through the drive cycle and cabin temperature are shown respectively for two vehicle configurations: no thermal battery and the optimised thermal battery.

The most notable aspect of the energy consumption, presented in Figure 6.6, is that at $-15°C$ ambient temperature using the optimised thermal battery consumes the most energy out of the three configurations presented. In Chapter 5 it was explained that when the thermal battery can no longer supply heat to the HTC it would switch to the chiller loop. This is the case at $-15°C$ and the consequence of this is that the heat pump has more work to do to extract the remaining heat from the thermal battery. The discharge process and the generation of additional compressor demand was shown and described in Section 5.6. Here it was seen that when the thermal battery switches to the chiller circuit the compressor demand is

Table 6.24: The cost of extracting the thermal battery's stored heat is presented. These values have been found by calculating the difference in compressor energy consumption when comparing the baseline operational mode and the baseline operational mode with the additional thermal battery.

	Extraction Cost (kWh)		
Ambient Temperature	WarmUp	NED	WLTP
-15	1.665	0.256	0.562
-5	0.205	0.290	0.401
5	-0.109	-0.002	-0.094
15	-0.077	0.048	-0.046

maximised.

Table 6.24 shows the additional energy required to extract the heat from the thermal battery through the heat pump. This is found by considering the compressor power consumption both with and without the addition of thermal storage to the system. Here it can be seen that the addition of thermal storage has increased compressor power consumption by 1.665kWh at $-15°C$ on the WarmUp cycle. This accounts completely for the additional 1.59kWh seen when comparing the optimised thermal battery to the baseline operational mode in Figure 6.6a. The additional energy seen in Figure 6.6a is not the same as the additional compressor consumption cost due to the increased regenerative braking energy recovery and improved battery efficiency. These two factors also explain why extra heat pump energy is used at $-5°C$, but Figure 6.6a shows an energy saving of 1.3kWh. At this temperature some of the saving is accounted for by reduction in PTC usage.

One of the advantages of the thermal battery is the ability to provide extra heat to the electric battery. This means the battery operates more efficiently, using less energy and potentially allows the battery to provide greater regenerative braking, resulting in a further energy benefit. Table 6.25 demonstrates the thermal battery's impact on the vehicle's ability to provide regenerative braking. The electric battery is able to reach its target temperature earlier in the drive cycle due to the added heat from the thermal battery. In NEDC and WLTP cycles, with numerous braking events, this allows for more energy to be recuperated. At $-15°C$ the thermal battery is able to generate an extra 61Wh (+21%) and 113Wh (+17%) in the NEDC and WLTP cycles respectively. The increase is more pronounced on the shorter drive cycle since the electric battery will be warming up for a greater proportion of the duration. There is no discernable difference in energy recuperated

Table 6.25: Energy recovered through regenerative braking using the baseline operational mode (Old) and the baseline operational mode with optimised thermal battery (New).

Ambient Temperature (°C)	WarmUp		NEDC		WLTP	
	Old	New	Old	New	Old	New
-15	140Wh	139Wh	283Wh	344Wh	651Wh	764Wh
-5	140Wh	139Wh	352Wh	361Wh	750Wh	801Wh
5	140Wh	139Wh	361Wh	372Wh	787Wh	822Wh
15	140Wh	140Wh	371Wh	373Wh	821Wh	819Wh

during the WarmUp cycle due to the single braking event 1 hour into the cycle, after the battery has warmed sufficiently regardless of the incorporation of a thermal battery.

It should also be noted that at $-15°C$, in Figure 6.7a, the cabin is not able to reach its target temperature. Part of the cause is because the battery is being heated, and therefore reducing the potential heat that the cabin may receive. This was seen when demonstrating the cabin model in Section 5.7. Chapter 8 investigates this area further, proposing a method for generating optimised battery heating trajectories to favour either the cabin or battery according to the cost function weighting.

From Figure 6.7 it can clearly be seen, especially at $-15°C$, that the optimised thermal battery has improved the comfort. The additional thermal battery has reduced the comfort cost metric by 53%, 50%, 33% and 59% at $-15°C$, $5°C$, $5°C$ and $15°C$ respectively. This saving is large compared to the changes in energy consumption seen in Figure 6.6, which were all less than 10%, with $-15°C$ having a 6.9% increase in energy consumption and other ambient temperatures seeing reductions of the same magnitude in energy consumption. This shows that including a thermal battery on a vehicle with a heat pump system can have a significant impact on comfort, while having only a minor detriment or improvement to energy consumption.

In Figures 6.8, 6.9 and 6.10 a comparison is made between the optimised thermal battery and the baseline. This is found by subtracting the baseline results pertaining to the optimised thermal battery specification, and hence positive values indicate a beneficial energy saving, DOD reduction or comfort improvement. The comparison is used to make further analysis into the difference in performance when using an optimised thermal battery specification.

Section 5.6 demonstrated that in the period between 720s and 2100s of the

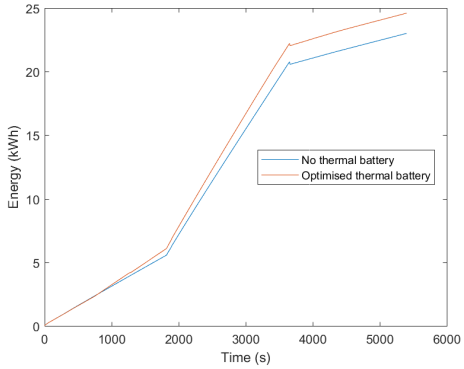

(a) Cumulative energy consumption at −15°C ambient.

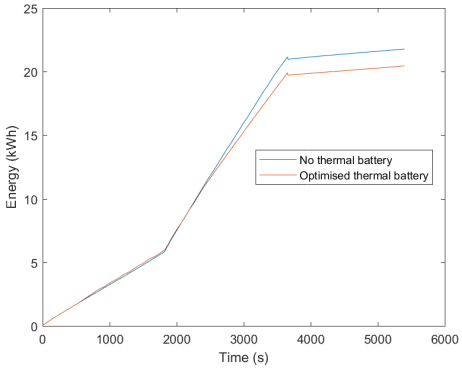

(b) Cumulative energy consumption at −5°C ambient.

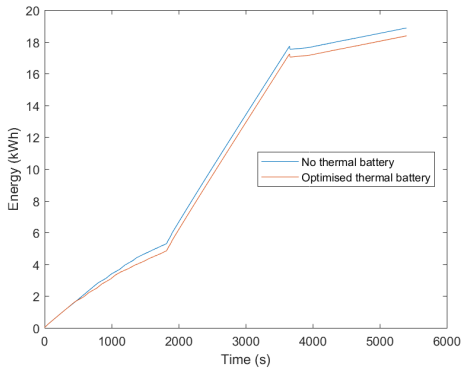

(c) Cumulative energy consumption at 5°C ambient.

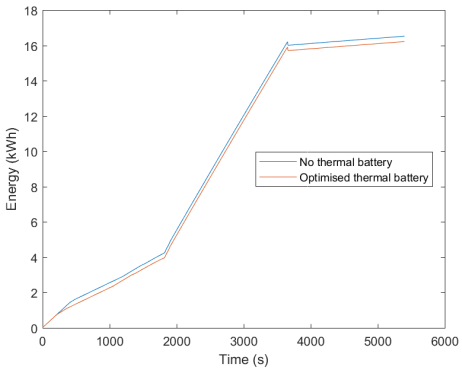

(d) Cumulative energy consumption at 15°C ambient.

Figure 6.6: Cumulative energy consumption is presented for the WarmUp cycle at the 4 ambient temperatures. Two configurations are demonstrated; no thermal battery and the optimised thermal battery with the final specifications (29kg, 131°C and 19kW).

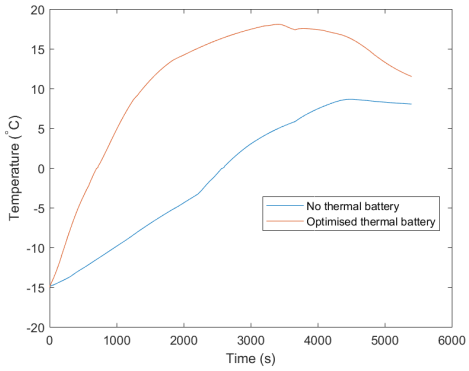

(a) Cabin temperature at −15°C ambient.

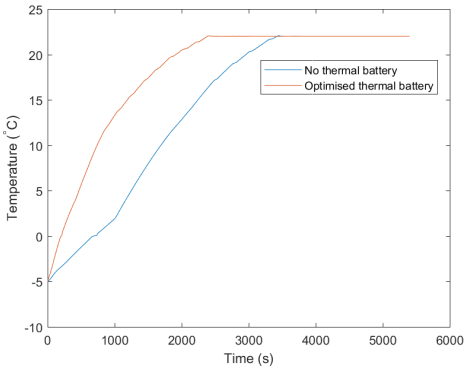

(b) Cabin temperature at −5°C ambient.

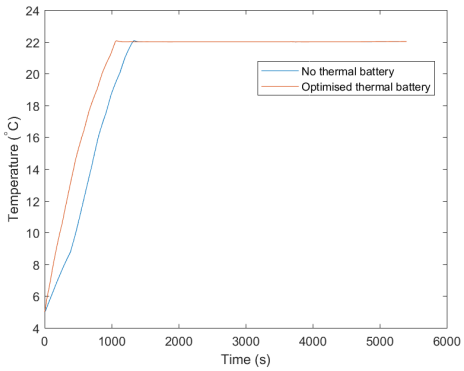

(c) Cabin temperature at 5°C ambient.

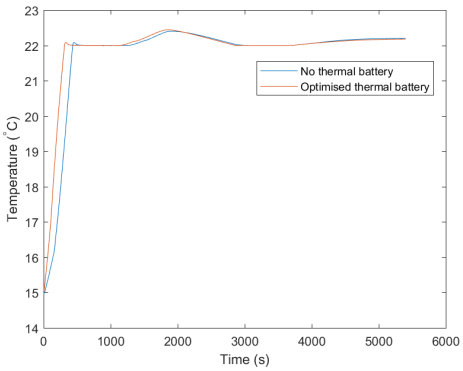

(d) Cabin temperature at 15°C ambient.

Figure 6.7: Cabin temperature is presented for the WarmUp cycle at the 4 ambient temperatures. Two configurations are demonstrated; no thermal battery and the optimised thermal battery with the final specifications (29kg, 131°C and 19kW).

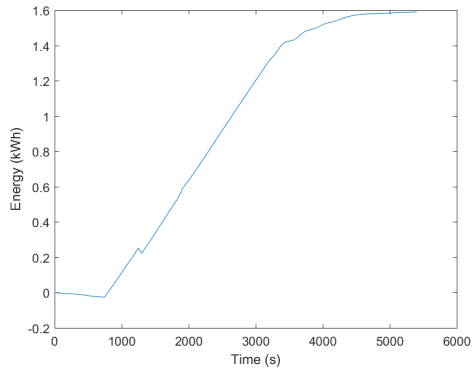

(a) Difference in cumulative energy at −15°C ambient.

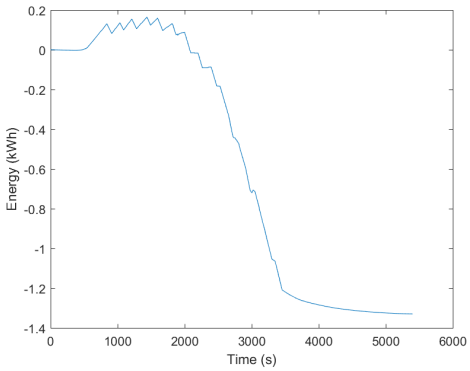

(b) Difference in cumulative energy at −5°C ambient.

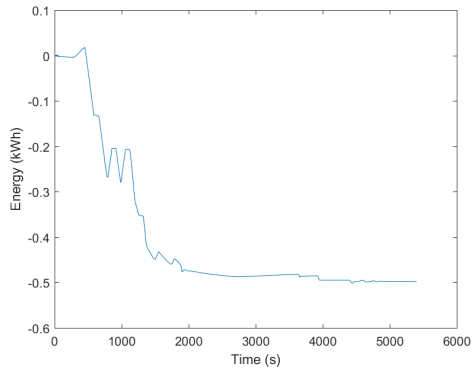

(c) Difference in cumulative energy at 5°C ambient.

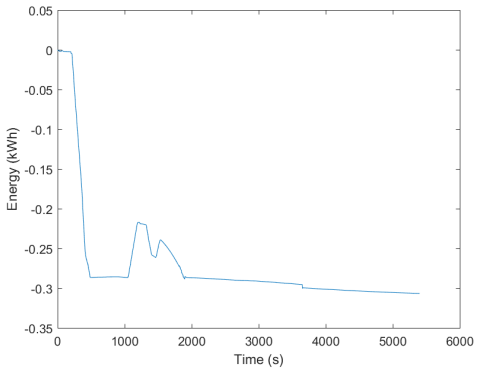

(d) Difference in cumulative energy at 15°C ambient.

Figure 6.8: The difference in cumulative energy is presented for the optimised thermal battery when compared to the baseline. Positive values show an energy saving compared to the baseline.

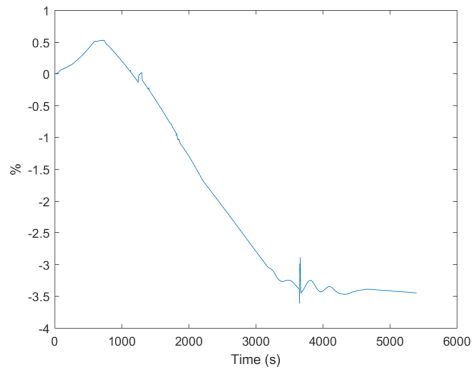

(a) Difference in DOD at −15°C ambient.

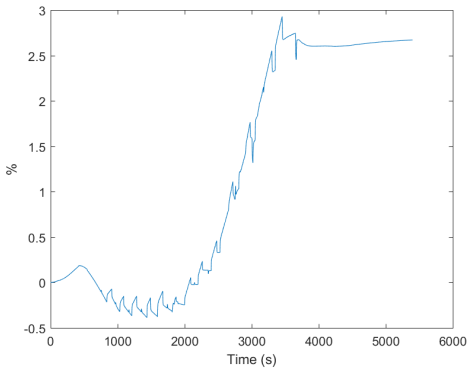

(b) Difference in DOD at −5°C ambient.

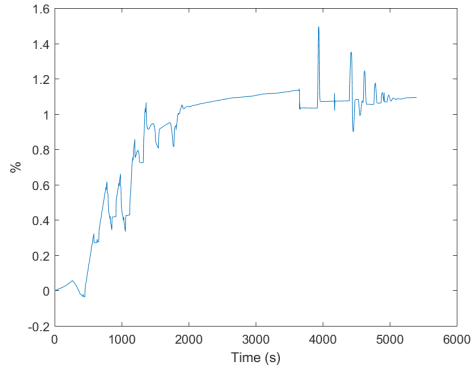

(c) Difference in DOD at −15°C ambient.

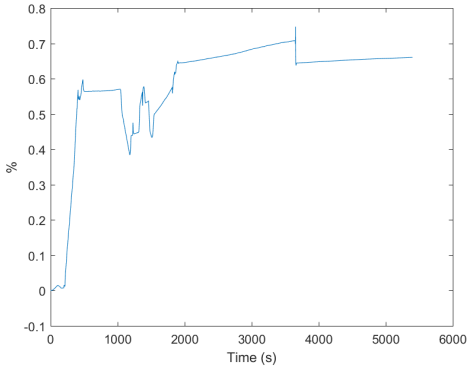

(d) Difference in DOD at −5°C ambient.

Figure 6.9: The difference in DOD is presented for the optimised thermal battery when compared to the baseline.

WarmUp cycle, at −15°C, the heat pump is working at full capacity to fully discharge the thermal battery. The effect of this can be seen in Figure 6.8a where there is an increase in power consumption compared to the no thermal battery scenario after 720s. It is apparent that this is happening at the other ambient temperatures as well. At ambient temperatures −5°C to 5°C, Figures 6.8b and 6.8c show there is a minima in energy difference, it is likely that this aligns with the time at which the HTC reaches temperature causing the PTC heater to shut off. In this case, the benefits in energy consumption would be dominated by the reduction in PTC usage. This may not be the case at −15°C as the failure to reach cabin temperature implies that the PTC heater would be active throughout. Otherwise it can be seen in Figure 6.8 that the improvement in energy consumption ranges between 1.33kWh at −5°C and 0.3kWh at 15°C, equating to 6.1% and 1.9% reductions in energy consumption.

Figure 6.9 shows the difference in DOD throughout the WarmUp cycle. Here similar conclusions can be drawn to those made for cumulative energy, savings are

obvious at −5°C and above, while −15°C uses additional energy. What is not clear from here is whether the additional heat to the battery improves the DOD. When the battery is cold, internal resistance increases, leading to lower terminal voltage (while the battery is under load) and therefore more current is required to produce the same power. Hence it is expected that the extra heat would provide a DOD improvement from the additional battery temperature. This benefit is seen at the start of the cycle, where the difference in battery temperature is highest, in the form of a small improvement in DOD. However, after a short amount of time the gradient becomes negative, causing the DOD to worsen compared to the baseline. This is evident in Figures 6.9a and 6.9b. At −15°C, in Figure 6.9a, the improvement begins to decline, and eventually worsen at 720s, which coincides with the thermal battery switching from the HTC to the chiller circuit, as described in Section 5.6. This leads to the conclusion that the additional heat does provide a benefit to DOD, but it is overcome by the increased load of extracting the thermal battery's heat at low temperatures, shown in Table 6.24. Referring back to Figure 6.8 it can be seen that at points in the drive cycle there is increased energy demand, likely due to the extra available energy from the thermal battery. This effect is best exemplified at −5°C in Figure 6.9b where the optimised thermal battery begins to improve DOD, but then switches to the chiller loop and starts consuming extra power through the compressor. After the cabin reaches target temperature at 2000s, as seen in Figure 6.7b, the DOD begins to improve in comparison to the baseline which will be spending energy after 2000s to continue heating the cabin.

Previously it has been noted that the thermal battery provides better cabin temperature response, particularly at the beginning of the cycle. This is clearly demonstrated in Figure 6.10 where in all scenarios the optimised thermal battery provides significant improvement in thermal comfort, returning an average reduction of 48.8% in j_3, the objective function relating to discomfort.

6.4.11 Conclusion to additional thermal storage

Section 6.4 presented the results for an optimised thermal battery, analysing how the metrics which comprise the cost function of the optimisation affect the complete problem, then understanding the benefit of the optimised thermal battery. One of the main findings from this section is that when additional storage is added to a vehicle, it is important to establish where the point of diminishing returns is. This was explored in detail in Section 6.4.7. Here it was seen that above the melting point of the PCM there was little more gain to be had by increasing the charge temperature, while at −15°C and −5°C the thermal power had very little impact

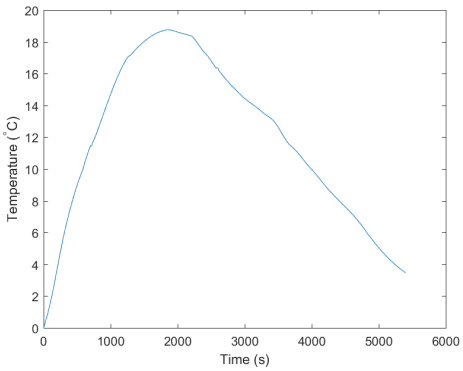

(a) Difference in cabin temperature at −15°C ambient.

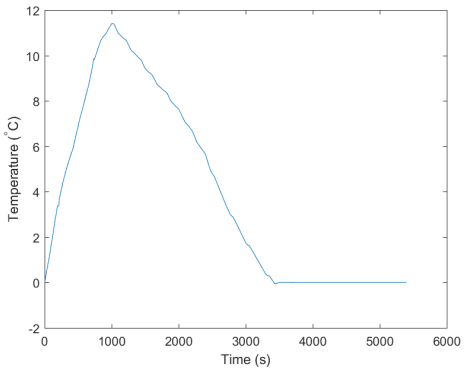

(b) Difference in cabin temperature at −5°C ambient.

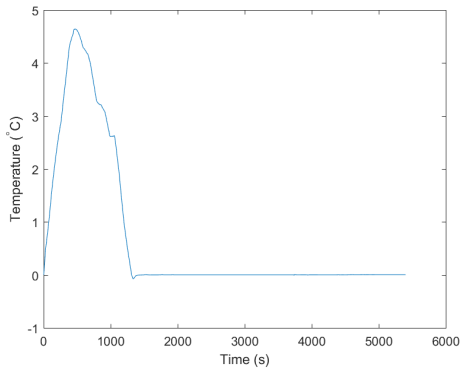

(c) Difference in cabin temperature at −15°C ambient.

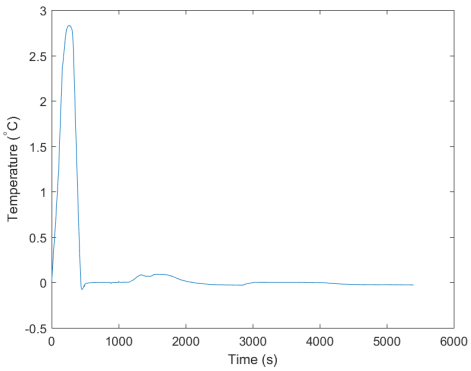

(d) Difference in cabin temperature at −5°C ambient.

Figure 6.10: The difference in cabin temperature is presented for the optimised thermal battery when compared to the baseline.

on the cost function. However, while these points are important to the operation of the vehicle, charge temperature will be predominantly controlled by the onboard charger, and at higher ambient temperatures the optimum power did converge on 20kW. From an engineering design perspective charge temperature would not make a significant difference to the battery design and it could be designed for 20kW heat delivery and then controlled to less than this at lower ambient temperatures for better performance.

The mass, on the other hand, would be the greatest cause of concern for a designer adding thermal storage to an electric vehicle because the electric battery would normally take priority. It was therefore crucial to understand how the mass of the thermal battery will improve vehicle performance. In Section 6.4.7 it was shown that despite the optimum mass being found at 29kg there is actually very little benefit in going above 25kg. At lower temperatures it was shown that increased mass leads to gains in thermal comfort but concordantly results in extra energy expenditure to fully extract the heat. Here manufacturers would need to carefully deicide where their priorities lay in order to correctly size their thermal battery. If there were an additional cost to increasing the size of the thermal battery during the optimisation, which would almost certainly be the case, the thermal battery might be less likely to exceed the point of diminishing returns, potentially resulting in a mass of 25kg, rather then 29kg. However, the fact that up to 97% of the energy stored in the thermal battery is used during the scenarios test, as seen in Table 6.23, shows that the thermal battery has been correctly sized to cope with the most demanding scenario.

Confidence in the search algorithm was tested using statistics on the cost results from each of the individual passes of the optimisations for different scenarios. It can be seen that the standard deviation in cost did not exceed 2.47% for any scenario. Hence, over the 5 randomised starts the search algorithm found the minimum cost to good agreement, showing that the algorithm chosen was sufficiently robust to local minima. The fact that in general the standard deviation in specification was higher shows that the minima of the problem is both broad and rough, leading to many solutions close to the global minima. It is likely this has arisen since the model used is large and complex, and not a simple function of the control variables, leading to an unpredictable search space where small changes in the specification can have larger secondary and tertiary effects on the cost function; having an impact on the local scale, but less so on the global scale.

In the next section a limit on total vehicle energy storage is imposed. This creates a compromise between thermal and electrical storage and explores the merits

of trading electrical battery capacity for thermal battery energy.

6.5 Optimising the configuration of a thermal battery with a fixed vehicle energy storage limit

In this section a limit is imposed on the total energy storage allowed on the vehicle. Since both lithium ion batteries and paraffin PCMs have similar energy densities this compromise could be one which manufacturers consider when deciding on the size of their on-board storage systems. While the electrical energy is more versatile and is required for driving the vehicle, it has been shown in literature that much of its energy can become devoted to thermal management, and it suffers at extreme temperatures. A thermal battery could replace some of the electrical energy devoted to climate control, while its storage capacity and performance are unaffected by changes in ambient temperature. This is not only applicable to the winter months, but as Jha showed in [137], it is also applicable in summer. However, this would require the thermal battery to be swapped for a cool battery with a very low melting point, for example ice/water.

To adjust for this new challenge, a 48kWh (the original size of the electric battery) limit is imposed on the vehicle. It was decided that a lower limit of electric battery capacity should be implemented to prevent the vehicle from fully depleting its electric battery during the cycle. This limit was chosen to be $23kWh$, which is the amount of energy consumed during the WarmUp cycle at $-15°$C, as found during the process of finding normalisation coefficients as described in Section 4.5.1. This was the highest energy consumption during normalisation, hence with this lower limit imposed, the vehicle will have the electric capacity to complete the drive cycles under consideration here at any temperature. This leaves 25kWh available for the thermal battery, which equates to 180kg of material (here it is assumed that the working material is the dominant mass of the storage system). During the test, as the mass of the thermal battery increases its energy capacity is calculated and the number of cells in the electric battery is reduced accordingly. Since the battery format is 108s3p, electric cells are removed to reduce the number of cells in series. This causes a lower operating voltage, resulting in the pack operating at a higher current to supply the same power, hence depleting charge quicker and increasing losses via ohmic heating. In a real vehicle this type of alteration would be impossible as the high voltage components of the drive train require a specific battery voltage to operate properly. However this limitation does not exist in the modelled vehicle, hence this is best way to adjust pack size as it is a smaller incremental change than

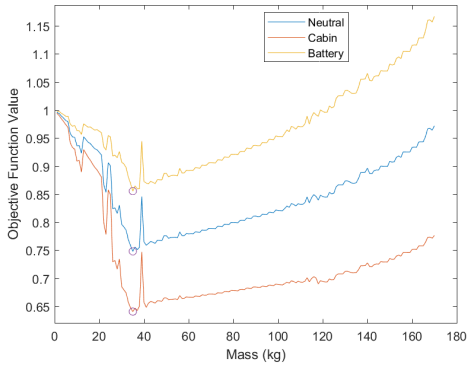

(a) Limited total energy at −15°C ambient.

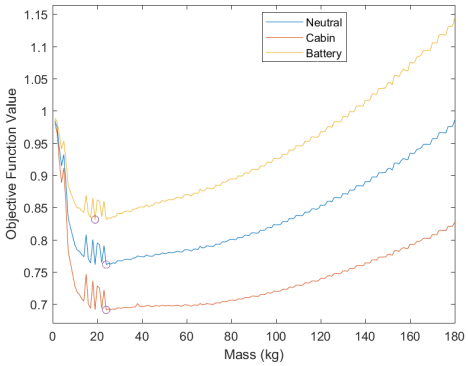

(b) Limited to energy at −5°C ambient.

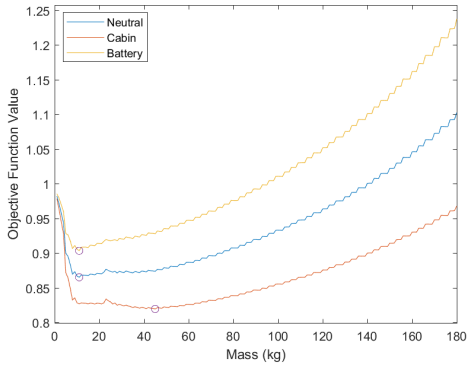

(c) Limited to energy at 5°C ambient.

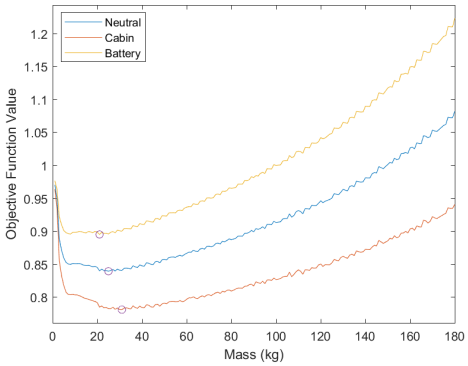

(d) Limited to energy at 15°C ambient.

Figure 6.11: The cost is shown as a function of mass on vehicle where the total energy capacity is limited to 48kWh for three optimisation weightings. Here circles indicate the location of the minimum cost.

reducing the number of strings in parallel. Reducing the pack size also reduces the thermal mass of the electric pack, resulting in shorter warm up times and longer operation in optimal conditions.

Since the optimal charge temperature and thermal power is known from section 6.4.1, this problem can be reduced to a single dimension: mass. A linear optimisation algorithm was trialled and produced a result within 16 iterations. However, the problem is small, with only 180 iterations (per ambient temperature) required to achieve a 1kg resolution and fully explore the search space. As such the exhaustive method was chosen to fully understand the problem. The results of the exploration can be seen in Figure 6.11.

The associated optimum values for the mass for each temperature and chosen weighting are given in Table 6.26. Referring to Table 6.26 and Figure 6.11 it can be seen that prioritising different objectives has an impact on the optimal sizing of

Table 6.26: The optimal mass at each ambient temperature and for each optimisation weighting is presented, corresponding to the minimum costs seen in Figure 6.11. Here it can be seen that prioritising comfort leads to the highest optimal masses, while prioritising the battery leads to the lowest optimal masses.

	Weighting		
	Neutral	**Cabin**	**Battery**
Ambient (°C)	**Optimal Mass (kg)**		
-15	35	35	35
-5	24	24	19
5	11	45	11
15	25	31	21

the thermal battery. The most extreme example of this can be seen at 5°C where prioritising the cabin leads to a 45kg optimally sized thermal battery, but prioritising neutrally or to the battery gives an 11kg optimally sized thermal battery. However, while at an ambient temperature of 5°C 45kg is the optimal size, it can be seen in Figure 6.11c that beyond approximately 10kg only small improvements in cost are seen. The same can be said of the result for 15°C, where the minimum is located in a wide region of low cost. This leads to uncertainty as to what value of mass should be chosen. In these cases of near steady cost it is likely the electrical battery would be prioritised over thermal storage as this maximises vehicle range and power. The two lower ambient temperatures, seen in Figures 6.11a and 6.11b, have much more certainty with regards to the minimum. This is significant as Table 6.6 showed that the thermal battery had a greater impact on cost at the two lower ambient temperatures, hence an optimum specification targeted towards the two lower ambient temperature is more likely to be selected.

To address the problem of uncertainty in optimal mass the average of the cost functions across the four temperatures has been taken. The result of this is presented in Figure 6.12, where it can be seen that there is a clear minimum in cost, which is located at 35kg for all priority weightings, leading to a greater level of confidence in the final value.

It can be noted from Figures 6.11 and 6.12 that the cost function follows a distinct shape regardless of the weighting. This indicates that one of the contributing objectives (either energy consumption, DOD or comfort) dominates the total cost at different parts of the exploration. To investigate this further the cost function has been broken down into is constituent parts; the result of this is presented in Figure 6.13.

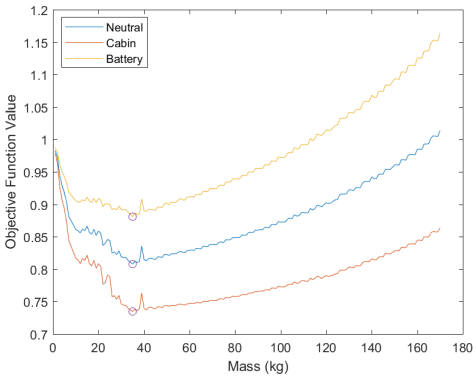

Figure 6.12: The average cost over four ambient temperatures is shown as a function of mass on vehicle where the total energy capacity is limited for three optimisation weightings. Here circles indicate the location of the minimum cost.

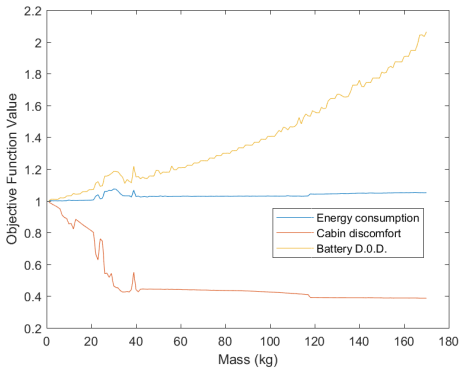

(a) Objective function components of limited total energy at $-15°$C ambient.

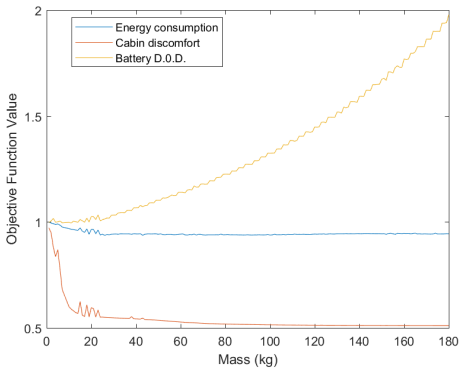

(b) Objective function components of limited total energy at $-5°$C ambient.

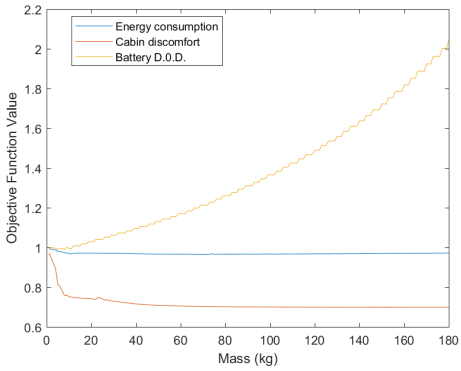

(c) Objective function components of limited total energy at 5°C ambient.

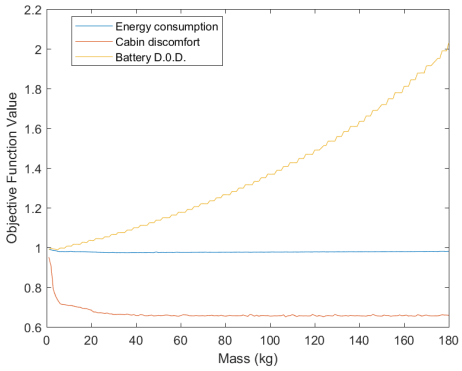

(d) Objective function components of limited total energy at 15°C ambient.

Figure 6.13: Here the cost is broken down into the individual normalised objective functions.

Figure 6.13 shows the un-weighted, normalised components of the cost function. At low masses the comfort component dominates the improvement in the cost, while battery DOD becomes dominant at high mass. By contrast the energy consumption changes very little through the range of mass, with higher ambient temperatures showing greater energy savings. This reflects the conclusion gained through Section 6.4.1, where it was postulated that gains in thermal comfort would coincide with increase in energy due to the cost of extraction. At higher temperatures the thermal battery is less likely to be fully depleted and energy benefits can be realised through termination of the PTC earlier in the cycle, due to the fast response and warm up times provided by the thermal battery. At $-15°C$ the heat pump cannot extract heat from ambient, so when the thermal battery depletes enough heat to swap to the chiller circuit the compressor needs to do more work. At some mass the thermal battery will have enough energy that it will not deplete enough to switch to the chiller circuit. This might explain the behaviour in the region of 30kg to 40kg. Additionally if the thermal battery has sufficient energy to not be depleted by the heat pump then that represents a limit in the additional comfort it can provide.

It can be noticed in Figure 6.13 that while the energy consumption appears smooth the DOD contains many discontinuities. This is caused by the integer decreases in pack size, removing three cells per increment (due to the three strings in parallel). Beyond this, the general shape could be described with a polynomial as it has a slight curve to it. This is important as it demonstrates the positive impact the thermal battery has had on the electric battery. If the thermal battery had no effect on DOD the result would be a linear step function as the size of the electric battery is reduced. The increased heat and smaller electric battery thermal mass have led to a warm, more efficient battery, helping to reduce DOD. Unfortunately the improvement is overshadowed by the reduced pack size throughout the range of thermal battery mass.

This point is further demonstrated in Figure 6.14 where the first twenty values of the optimisation have been plotted. Here it can be seen that increasing the mass of the thermal battery reduces DOD until the electric battery is forced to reduce in size to make room for the increasing thermal battery. This effect appears most dominant in the early part of $5°C$, shown in Figure 6.14c where a zigzag shape is formed due to the improvements before the next incremental decrease in electric battery size. By contrast, at $-15°C$ and $15°C$ in Figures 6.14a and 6.14d the improvement between increments is smaller, or even worsens, leading to much flatter steps.

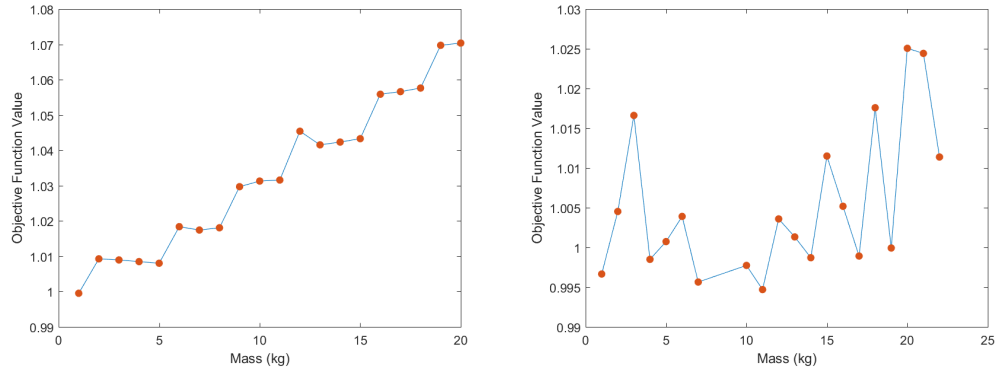

(a) −15°C ambient.

(b) −5°C ambient.

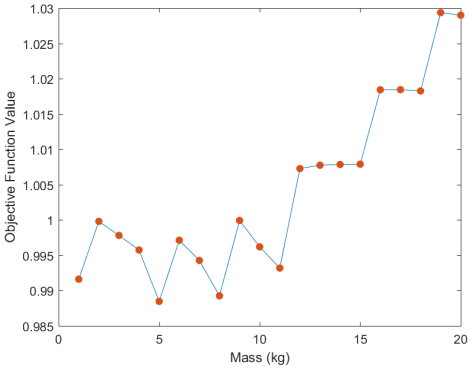

(c) 5°C ambient.

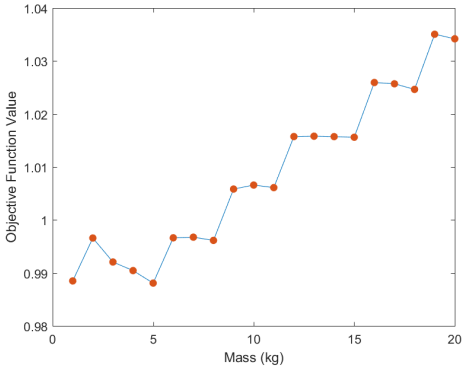

(d) 15°C ambient.

Figure 6.14: The depth of discharge component of the objective function is shown for the first 20 values of thermal battery mass.

Table 6.27: Presentation of metrics corresponding to the electrical storage (ES) versus hybrid electrical thermal storage (HETS) solutions presented in Section 6.5.

	Efficiency (Wh/km)			**Range (km)**			**Discomfort (mean °C)**		
Ambient Temperature	ES	HETS	Improvement (%)	ES	HETS	Improvement (%)	ES	HETS	Improvement (%)
-15	307	317	-3.26	157	141	-10.09	23	9.8	57.48
-5	291	272	6.4	172	170	-1.22	8.5	4.7	44.95
5	253	244	3.48	197	198	0.6	2.5	1.9	24.12
15	222	216	2.75	230	221	-3.92	0.4	0.3	29.4

6.5.1 Summary

In this section a hybrid storage system was created by reducing the electrical storage capacity in order to include the equivalent thermal storage capacity. It was shown in Figure 6.12 that by considering the average cost over all temperatures, a thermal storage mass of 35kg was optimal for all optimisation weightings. This corresponded to an energy split of 4.83kWh (9.5%) thermal and 43.17kWh (90.5%) electrical. Table 6.27 has been created, using the analysis described in Section 5.9, to show the impact the hybrid system has had on the metrics of concern to this thesis. Here the ES metrics correspond to the vehicle operated in the baseline operational mode, while the HETS metrics correspond to the baseline operational mode with the proposed hybrid storage system and utilising the thermal storage. It can be seen that, with the exception of $-15°$C, although the electrical capacity has been reduced by 9.5% the range reduction does not reflect this. The range has been reduced at three of the four ambient temperatures and increases slightly at 5°C. However the changes in range are small compared to the improvement in comfort. The benefit for sacrificing 10% of range at $-15°$C is a 57% reduction in discomfort. The addition of thermal storage has also reduced energy consumption at the three warmer temperatures, with a small increase seen at $-15°$C. In general this shows that creating a hybrid thermal/electrical storage system, by reducing electrical storage, has a small impact on range and efficiency, but will greatly improve the comfort of passengers.

6.6 Discussion

Through Chapter 1 it was revealed that the public perception of electric vehicles was that in winter a choice must be made between comfort and range. This was backed up in Chapter 2 by an understanding that an electric vehicle needs a warm battery to perform well, but it also takes up to 7.6kW of heat to warm the cabin.

Table 6.28: Vehicle efficiency, range and discomfort are presented for the WLTP drive cycle, with the addition of the thermal battery (WTB) and without (W/OTB). Also included is the percentage change for each metric. It can be seen that in general the thermal battery has a small benefit to the efficiency and range above $-15°C$, but has the greatest impact on discomfort at all temperatures.

	Efficiency (Wh/km)			**Range (km)**			**Discomfort (mean °C)**		
Ambient Temperature	W/OTB	WTB	Improvement (%)	W/OTB	WTB	Improvement (%)	W/OTB	WTB	Improvement (%)
-15	369.2	376.0	-1.8	139.8	136.3	-1.6	31.9	19.9	37.8
-5	370.8	368.5	1.6	139.2	139.6	1.2	19.3	11.6	40.1
5	337.3	315.8	7.6	159.2	169.9	7.9	6.2	4.2	33.0
15	288.8	276.8	4.1	186.6	194.6	4.3	1.0	0.6	43.3

In Chapter 3 one of the ways in which research has addressed this problem was the incorporation of a thermal battery to aid cabin heating. However no examples existed of this being done on a vehicle with a heat pump. Hence Research Objective 1, which stated "What is the optimal sizing of a thermal battery for application in an electric vehicle with a heat pump", has been addressed in this chapter. In doing so an optimal thermal battery specification of 29kg of mass, 131°C start temperature and 19kW of thermal power has been identified for the vehicle described in Chapter 5. Table 6.28 shows how the addition of this thermal battery has impacted the vehicle efficiency, range and discomfort, which define the motivation of this research. The values presented in Table 6.28 correspond to the WLTP cycle, where W/OTB is the baseline operational mode and WTB signifies the addition of thermal storage.

Table 6.28 shows that the thermal battery has made a positive impact on all metrics above $-15°C$. However with the additional cost of extraction, seen in Table 6.24, there is little to be gained in terms of range and efficiency at low temperatures. However, further energy and range improvements may be made by disengaging the PTC heater, relying on the thermal storage as an adequate replacement. The benefits to the system achieved by doing this are shown in Table 6.29. Here it can be seen that without the energy consumption through the PTC heater the vehicle is able to improve its range by 35% at $-15°C$, while the optimised thermal battery is still able to provide sufficient heat that the discomfort is reduced by 24.3%. The range increase percentage decreases at high ambient temperatures due to the baseline operational mode's reduced dependence on the PTC heater; however, every metric is improved at all temperatures tested. This shows that a thermal battery, combined with a heat pump, will enable the vehicle to travel further while still being more comfortable than a vehicle with a heat pump supported by a PTC heater.

The optimised specification was found using the pattern search search al-

Table 6.29: Vehicle efficiency, range and discomfort are presented for the WLTP drive cycle, with the addition of the thermal battery with no PTC (WTB No PTC) and the baseline without thermal storage (W/OTB). Also included is the percentage change for each metric. It can be seen that in general the thermal battery has a small benefit to the efficiency and range above $-15°C$, but has the greatest impact on discomfort at all temperatures.

	Efficiency (Wh/km)			**Range (km)**			**Discomfort (mean °C)**		
Ambient Temperature	W/OTB	WTB no PTC	Improvement (%)	W/OTB	WTB no PTC	Improvement (%)	W/OTB	WTB no PTC	Improvement (%)
-15	369.2	285.3	22.7	139.8	187.0	35.0	31.9	24.2	24.3
-5	370.8	296.0	20.9	139.2	179.7	30.3	19.3	13.6	29.8
5	337.3	295.9	13.4	159.2	180.9	14.8	6.2	5.0	19.4
15	288.8	271.2	6	186.6	199.3	6.8	1.0	0.6	38.2

gorithm, which was chosen for its efficiency over simpler methods and robustness compared to the simplex method. In Section 6.2 the search space covering the likely location of the global minima was shown to be wide, covering 5kg in mass and 5kW in power, and flat with a 1% variation in cost over this region. The area was also rough, having many local minima. To address these challenges the pattern search was restarted at 5 random locations during each optimisation. Section 6.4.1 showed that this technique had the intended results. Specifically Table 6.2 had a high standard deviation in cost (2.47% compared to less than 0.5% at other ambient temperatures), showing that if the pattern search was run only once it may have fallen into a local minima away from the global minimum. Since it was run 5 times the specification corresponding to the lower cost could be extracted and compared to other temperatures. Doing this led to a maximum standard deviation of 6.85% in specification across all ambient temperatures. This led to the final optimised specification of 29kg of mass, 131°C start temperature and 19kW of thermal power. This specification was tested on all scenarios defined in Section 4.3, in doing to it was seen that the thermal battery was 97% depleted on the longest cycle at the lowest ambient temperature. This indicates that the thermal battery was correctly sized, confirming the robustness of the optimisation method used.

Mass is the most crucial control variable to understand as it will determine the package size of the thermal battery, with larger pack sizes presenting greater engineering and integration challenges. It is therefore important that the benefit of increasing thermal storage mass is well understood. In Section 6.4.10 the optimum thermal battery was implemented and the metrics which contribute to the cost function were presented without any cost function weightings applied. Here it appeared as though there might be a point of diminishing returns after 25°C, however these results incorporated all ambient temperatures, and as Table 6.23 shows, the battery

is only 97% depleted at −15°C on the WarmUp cycles, with high temperatures using less of the stored energy. Hence 25kg does not indicate a point of diminishing returns but indicates the minimum mass that could be considered optimal on one of the scenarios tested, and is likely to correspond to a shorter drive cycle or higher ambient temperature, or both.

This uncertainty carried over into the optimisations of the thermal battery for WLTP and NEDC. Here it was not only the colder ambient temperatures which showed higher standard deviation in optimal mass values, but the high temperatures as well. By contrast the other control variables, charge temperature and thermal power, showed lower standard deviation throughout in comparison to the WarmUp cycle using a neutral weighting. The shorter cycles will be dominated by the warm up period, rather than the long sustained heating period in the WarmUp cycle. It is therefore unsurprising that temperature and power are maximised for these shorter cycles as this will have the greatest impact on the thermal response of the system.

In Section 6.4 it was postulated that due to the uncertainty in mass, the system had entered a space of diminishing returns. This led to the suggestion that if an additional cost were introduced, the optimum mass may reduce so that it does not enter an area of diminishing returns. In Section 6.5 this suggestion was tested by imposing a total energy limit on the vehicle and determining the ideal split between thermal and electrical storage. Surprisingly, in this section an optimum mass of 35kg was found by averaging the cost over the ambient temperature range. This is equivalent to 4.6kWh of thermal storage, leaving an electric battery pack size of 43.4kWh, which is a 9.5% reduction compared to the baseline specification. Upon further analysis of the individual objective functions, it was seen that comfort and DOD dominated the cost at different points in the mass range. At lower masses improvement in cost is dominated by the reduction in discomfort; however, this plateaus at approximately 40kg at −15°C and 20kg elsewhere, with little or no improvement found beyond this point. The DOD on the other hand shows a very minor improvement in the first 10kg for ambient temperatures of 5°C and above, but then rapidly diminishes as the pack size shrinks. The combination of these creates another plateau where small improvements in comfort are traded for the inconvenience of a reduced pack size.

The findings of this chapter will help to guide the decision making process of including a thermal battery on an electric vehicle. Given the results presented in Section 6.5, further research should be conducted in the area of thermal storage as a valid alternative to maximising electrical storage.

6.7 Concluding points

- Research Objective 1 has been addressed through the optimisation and deep analysis of thermal battery sizing.
- The addition of the thermal battery has little impact on range if the PTC heater is still operated, although the comfort increases by an average of 48.8%.
- Ceasing operation of the PTC heater allowed for a range increase of up to 35% at $-15°C$ whilst maintaining a 24.3% increase in comfort.
- In the case where the thermal storage can only be included at the expensive of electrical storage, the optimal split in energy is 9.5% thermal and 90.5% electrical. At $-5°C$ and above this has a minor impact on range, but improves comfort by between 24.12% and 44.95%.

Chapter 7

Results 2, Operational Mode Identification and Comparison

7.1 Introduction

In this chapter Research Objective 2, "What opportunity is there in controlling range and comfort through the systematic comparison and selection of a specific combination of heat sources and sinks", is addressed. Chapter 3 showed the variety of potential heat pump configurations which arise due to the choice of thermal sources and sinks (the battery and the cabin) on an electric vehicle. In Chapter 3 an ensemble of heat pump configuration options, investigated by various authors, was summarised in Table 3.3. Then in Table 3.4 the thermal sources and sinks were categorised as optional or fixed. The optional thermal sources and sink were used to create an exhaustive list of operational modes, presented in Table 4.2 and repeated in Table 7.1.

Table 7.1: List of heat sources, their operational mode options, and an example of how each operational mode is constructed. Here all components act as sources to the heat pump, except for the battery which is a heat sink.

	Heat Source				
Operational Mode	**Motor and Inverter**	**Thermal Battery**	**Electric Battery**	**Transmission**	**Cabin Exhausted**
1	0	0	0	0	0
2	0	0	0	0	1
3	0	0	0	1	0
4	0	0	0	1	1
5	0	0	1	0	0
6	0	0	1	0	1
7	0	0	1	1	0
8	0	0	1	1	1
9	0	1	0	0	0
10	0	1	0	0	1
11	0	1	0	1	0
12	0	1	0	1	1
13	0	1	1	0	0
14	0	1	1	0	1
15	0	1	1	1	0
16	0	1	1	1	1
17	1	0	0	0	0
18	1	0	0	0	1
19	1	0	0	1	0
20	1	0	0	1	1
21	1	0	1	0	0
22	1	0	1	0	1
23	1	0	1	1	0
24	1	0	1	1	1
25	1	1	0	0	0
26	1	1	0	0	1
27	1	1	0	1	0
28	1	1	0	1	1
29	1	1	1	0	0
30	1	1	1	0	1
31	1	1	1	1	0
32	1	1	1	1	1

In this chapter the list of operational modes defined in Table 7.1 are exhaustively tested on the 12 scenarios (3 drive cycles at 4 temperatures) defined in Section 4.3. Here the objective is to identify optimal operational modes, for each scenario and each objective function weighting according to the cost function defined in Section 4.5. Since it is unlikely that one set of thermal sources will be optimal for the entirety of a drive cycle, an additional objective is to identify at which points in the drive cycle a component should be connected to the heat pump. This will require the operational modes to be compared at incremental time steps within the drive cycles, revealing more information about under what conditions, within a scenario, an operational mode is optimal.

The remainder of this chapter will be structured as follows. Firstly, method details specific to this chapter are covered in Section 7.2. Then, the identification of a time step length, over which operational modes will be compared within drive cycles is found in Section 7.3.1. Next, an exploration into the percentage of time steps during which particular operational modes and components are optimal is performed in Section 7.3.2. Afterwards, in Section 7.3.3, each scenario (drive cycle at a temperature) is broken down into individual time steps, where the optimal modes and constituent components are identified and compared. This will be used to identify when during a scenario the use of each component becomes favourable. Penultimately, in Section 7.4 the impact of optimal operational modes for each scenario is shown for cumulative energy consumption, DOD and comfort. Finally, in Section 7.5 a comparison is made of the efficiency, range and comfort using the baseline operational mode and using the optimal operational mode for the scenario and objective function weighting. Here it will be demonstrated that through the identification of optimal operational modes an electric vehicle configuration can be set which prioritises comfort or range, or a mixture of the two. This demonstration will show that the chapter has responded to the Research Objective in a manor which suits the motivations of the thesis.

7.2 Chapter specific method

In this chapter the vehicle maintains the 48kWh battery pack sizing as specified in Chapter 5. Secondly, in this chapter the objective function defined in Chapter 4 is used to identify the optimal operational mode. Here there is no necessity for an operational mode to meet the cabin's target temperature. This is not necessary since comfort is accounted for in j_3, defined in Section 4.5.1. The justification for this metric is based on the hypothetical example given in Figure 7.1, where

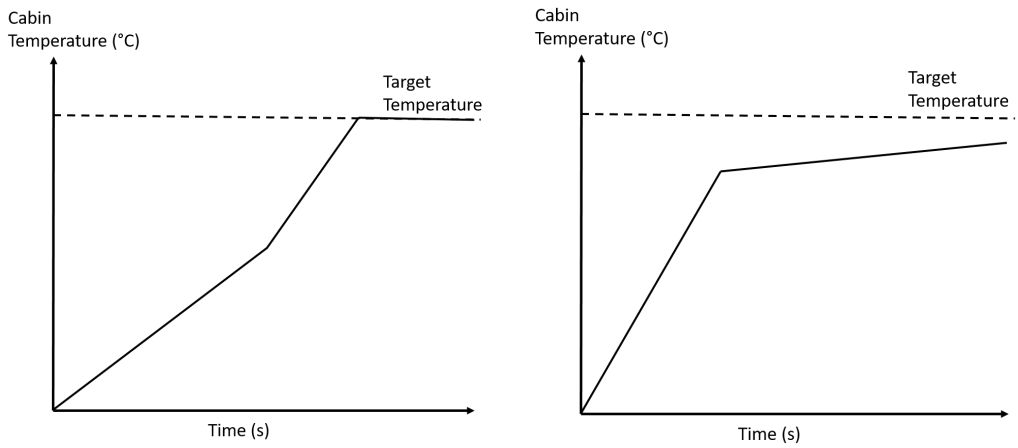

(a) Low thermal comfort, relating to a larger j_3 value.

(b) High thermal comfort, relating to a smaller j_3 value.

Figure 7.1: Examples used to depict j_3 which describes the area between actual and target cabin temperatures.

the profile shown in Figure 7.1b is preferable to the profile shown in Figure 7.1a, despite the first profile not reaching target temperature. Here these two examples might represent two operational modes; since Figure 7.1b performs well early in the cycle it should be identified as the optimal operational mode. However it fails to reach target temperature, and so at some point it may be preferable to switch to an operational mode where the cabin target temperature is met. This is important since an optimised operational mode trajectory may choose to use the mode pertaining to Figure 7.1b at the start of the cycle, then the mode pertaining to 7.1a at the end of the cycle.

Beyond comparing the performance of each operational mode over each scenario as a whole, it was stated in Section 7.1 that the optimal operational mode during each time step of the drive cycle should also be identified. This will provide insight into how switching between operational modes will lead to further energy savings or thermal comfort improvements. In accordance with this, the results of each scenario will be broken down into time steps of length 5s, 10s, 30s, 60s, 120s, 300s or 600s. These lengths have been chosen to cover a range of characteristic time scales identified in drive cycles. The NEDC cycle uses a selection of accelerating events ranging between $4s$ and $41s$ in duration, hence 5s captures the transient events. 600s relates to longer cruises, such as the 1800s fixed speed cruises of the WarmUp cycle. 600s has been chosen as the longest option since this is half the length of the NEDC cycle, hence this is the longest time step which allows all cy-

cles to be divided into more than one integer sections. The cost function is then compared at each time step, and used to identify the optimal operational mode. A time step will then be chosen through the analysis of the distribution of optimal operational modes using each of the time step lengths stated. The chosen time step length will then be used for the remainder of analysis in this chapter.

Once the operational modes have been compared at different time steps during the drive cycles it is possible to identify when each component should be used during the drive cycle for optimal operation. Identifying the optimal operational mode at each time step for a scenario will create an optimal mode trajectory. This can then be implemented on the scenario in an effort to switch between operational modes to find further improvement. However, since the vehicles history is not taken into account during these comparisons, a control trajectory based on these results does not represent an optimised control trajectory. This is explained with the following theoretical example.

When a time step, T_n is taken along with the operational modes compared in Section 7.3.3, the performance of that mode is dependent on the state of the vehicle at the end of T_{n-1} which is dependent on which operational mode the vehicle was operated in during T_1 to T_{n-1}. Since the vehicle is operated in thirty two operational modes independently it would be wrong to assume that switching from mode 1 to mode 2 will lead to a lower cost, even if mode 2 has a lower cost than mode 1 during that time step, because the vehicle will be in a different and incomparable state. This notion is summarised by Equations 7.1 to 7.8, which describe a hypothetical scenario where J, the cost function from Section 4.5, is an explicit function of X and U.

$$J_i^{[n]} = F(X_i^{[n]}, U^{[n]}) \tag{7.1}$$

where $J_i^{[n]}$ is the cost at time step i using operational mode n and X is some vector describing the state of the vehicle. By subjecting the vector to a control, $U^{[n]}$ which is dependent on the operational mode, the next sequential vehicle state can be found, denoted with its control history, $[1, 1]$.

$$X_{i+1}^{[1,1]} = F'(X_i^{[1]}, U^{[1]}) \tag{7.2}$$

here F' denotes a new function which generates the next vehicle state. Similarly operating the vehicle in a different operational mode, mode 2, creates a new vehicle state.

$$X_{i+1}^{[2,2]} = F'(X_i^{[2]}, U^{[2]}). \tag{7.3}$$

For illustrative purposes, let us assume that for these two sequential steps, the first operational mode has a lower associated cost than the second operational mode for the first step, and then the opposite is true for the next time step, i.e.

$$J_i^{[1]} < J_i^{[2]} \tag{7.4}$$

and

$$J_{i+1}^{[1,1]} > J_{i+1}^{[2,2]}. \tag{7.5}$$

Consequently it is then decided that $U^{[2]}$ should be applied to $X_i^{[1]}$ in an attempt to lower the total cost.

$$X_{i+1}^{[1,2]} = F'(X_i^{[1]}, U^{[2]}) \tag{7.6}$$

However, since

$$X_{i+1}^{[1,2]} \neq X_{i+1}^{[1,1]} \text{ nor } X_{i+1}^{[1,2]} \neq X_{i+1}^{[2,2]}, \tag{7.7}$$

so,

$$J_i^{[1]} + J_{i+1}^{[1,2]} \neq J_i^{[1]} + J_{i+1}^{[2,2]}. \tag{7.8}$$

Hence it would be invalid to assume that constructing a path from the optimal modes identified would be equivalent to producing an optimised control trajectory for the operational modes. The theoretical problem above can be exemplified by the hypothetical scenario presented in Figure 7.2. In this example the vehicle is cruising slowly between t_0 to t_1, and cruising quickly between t_1 and t_2. In mode 2 the battery is heated and so the energy consumption during the first time step increases compared to mode 1 in which the battery is not heated ($J_1^{[1]} < J_1^{[2]}$). However, in time step 2, mode 2 now benefits from a warmer and more efficient battery and therefore $J_2^{[2]} < J_2^{[1]}$, but $J_1^{[1]} + J_2^{[1]} < J_1^{[2]} + J_2^{[2]}$. Since $J_2^{[2]} < J_2^{[1]}$ it might be natural to assume that operating the vehicle in mode 1 then mode 2 for the first and second time steps respectively would lead to an energy reduction. However, in this hypothetical example, it can be seen that starting the fast second time step with a cold battery and heating the battery during this time step has increased the overall cost, thus $J^{[1,2]}$ is greater than either $J^{[1,1]}$ or $J^{[2,2]}$.

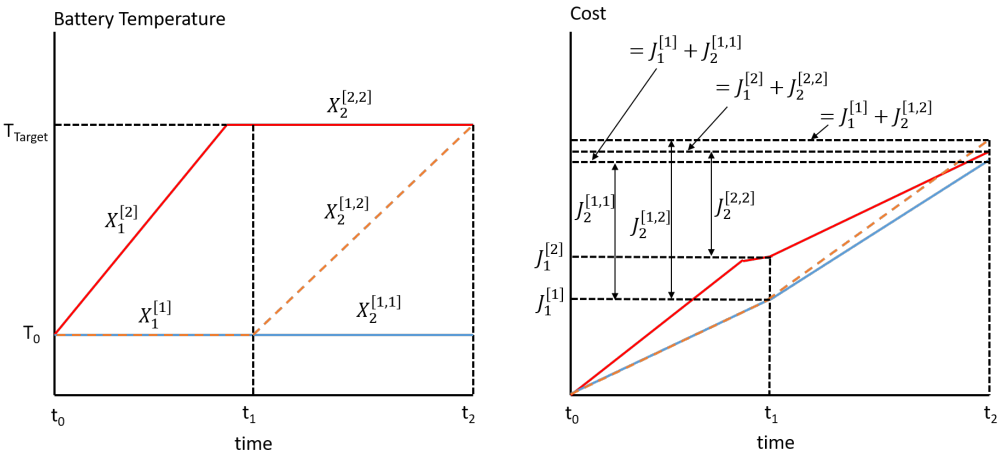

Figure 7.2: A hypothetical scenario is presented where the vehicle is operated in mode 1 exclusively, mode 2 exclusively and then switches from mode 1 to mode 2 at time t_1.

While it is not possible to use the information available to predict what the cost would be if a constructed optimal trajectory were used, it is possible that the cost could be lower than using just one operational mode throughout. So, alongside identifying the optimal operational mode during each drive cycle and comparing that to the baseline operational mode, Section 7.4 will also present the result following the mode trajectory found by identifying the optimal operational mode during each time step of the drive cycle. It should also be noted that in the context of this chapter the defined baseline is equivalent to operational mode 20.

7.3 Results

The thirty two operational modes defined in Section 4.2.2 have been simulated on all 12 scenarios (3 drive cycles at 4 temperatures) defined in Section 4.3. The analysis of these evaluations are presented in this section with the intention of answering the question: in a heat pump system with multiple potential heat sources and sinks, which sources and sinks should be used for the optimal operation of the vehicle? To comprehensively answer this question the operational modes defined should be compared throughout the drive cycle, revealing under what conditions a component's interaction with the heat pump is preferable. To make this comparison, a suitable time step length needs to be found, over which the operational modes can be compared during the drive cycle. In Section 7.3.1 several time step lengths have been evaluated, and the optimal operational modes during every time step of all 12

scenarios have been identified.

7.3.1 Different time step lengths

In this section a series of histograms are presented, showing the frequency during which each mode was optimal, according to the cost function defined in Section 4.5, using the neutral objective function weighting over all drive cycles and ambient temperatures. This section is used to identify which time step should be used to compare operational modes. Figure 7.3 and 7.4 shows 6 histograms, each corresponding to a choice of time step length; 5s, 30s, 60s, 120s, 300s, or 600s.

Figures 7.3a, 7.3b, 7.3c and 7.4a each show that all defined operational modes are optimal at least once during the spectrum of scenarios tested. In order to reduce computational effort when comparing operational modes, as few time steps should be used as possible, hence a long time step is wanted. However, doing so reduces the resolution of the results and limits the understanding which can be gained. Given this trade off, the ideal choice of time step length is the longest time step in which all operational modes appear at least once. Figures 7.3 and 7.4 shows that a time step length of 120s meets this requirement and so will be used as the time step for the remainder of this chapter.

The histograms presented in Figures 7.3 and 7.4 also reveal that some operational modes are dominant. To identify if there are any trends in the dominant operational modes, the top five modes from Figures 7.3 and 7.4 have been identified and broken down into their constituent components.

Table 7.2 shows the top five operational modes, which account for 38.5% of all data in Figure 7.4a. Here it can be seen that the thermal battery and cabin appear to be the most useful sources of heat, appearing in four of the top five optimal operational modes. Similarly the transmission and motor appear to be useful sources of heat appearing in three of the top five. Electric battery heating is less prevalent, only appearing twice. This is not unexpected since even using the neutral weighting the objective function is skewed towards the cabin, due to the potential of improvement in cabin comfort compared to the battery related objectives.

Tables 7.3 and 7.4 show the top five operational modes for the cabin and battery weighted objective functions, here 40.6% and 38.1% of all time steps are represented respectively. The most notable difference in Tables 7.2, 7.3 and 7.4 is the modes which become optimal more often when the objective function is weighted in favour of the battery. In Table 7.3 it can be seen that three out of the top five modes make use of battery heating, this is expected as battery heating will lead

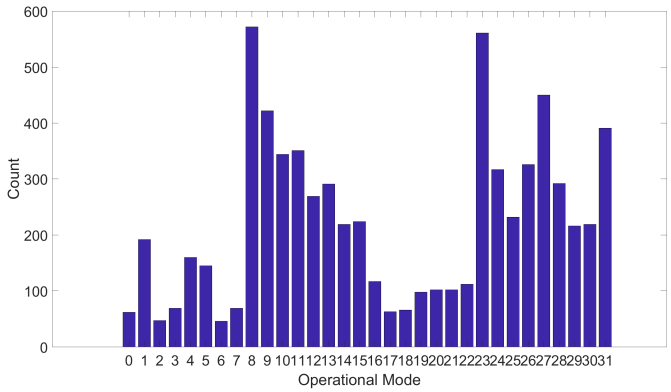

(a) Optimal mode histogram with 5 second time step

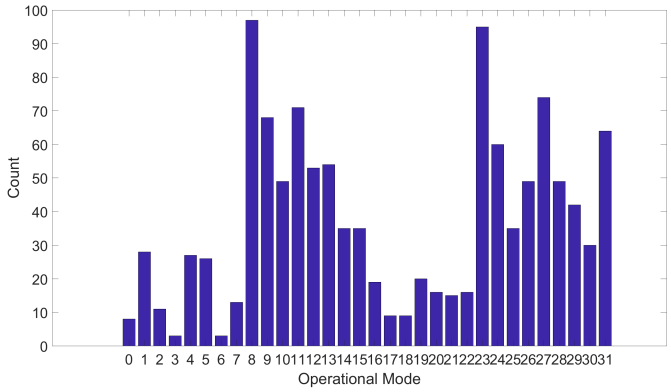

(b) Optimal mode histogram with 30 second time step

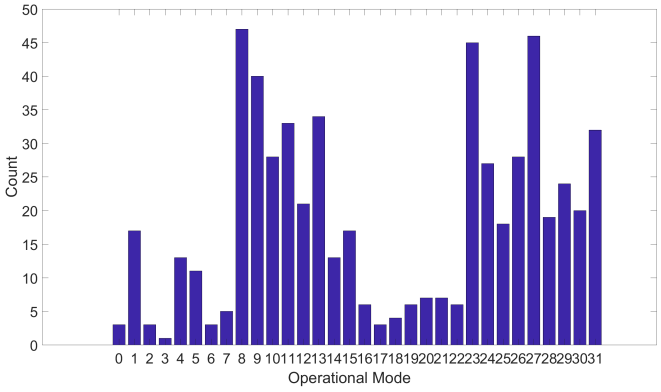

(c) Optimal mode histogram with 60 second time step

Figure 7.3: Histograms showing the most common operational modes to be the optimal considering a neutral weighting for time step lengths 5s, 60s and 120s.

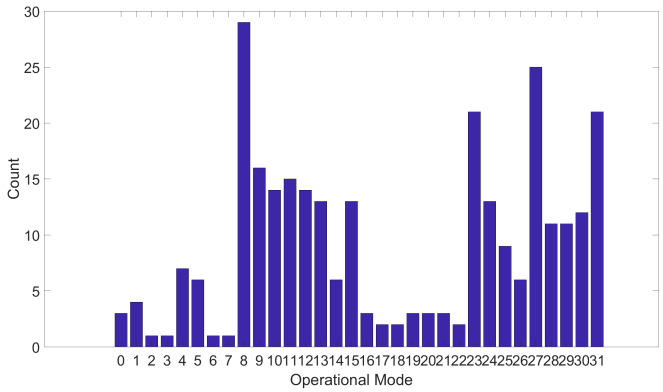

(a) Optimal mode histogram with 120 second time step

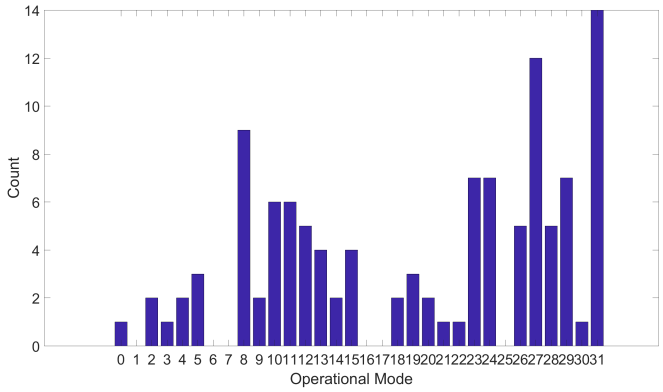

(b) Optimal mode histogram with 300 second time step

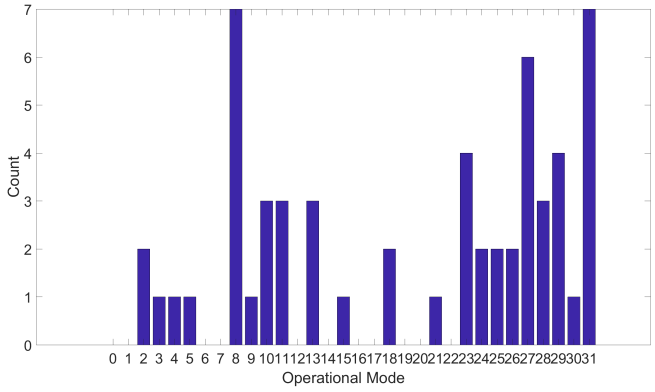

(c) Optimal mode histogram with 600 second time step

Figure 7.4: Histograms showing the most common operational modes to be the optimal considering a neutral weighting for time step lengths 120s, 300s and 600s.

Table 7.2: Top five most commonly optimal operational modes using a 120s time step and neutral weighting

Rank	Mode	Occurrences	Motor	Thermal Battery	Electric Battery	Transmission	Cabin Exhaust
1	8	29	0	1	0	0	0
2	27	25	1	1	0	1	1
3	23	21	1	0	1	1	1
4	31	21	1	1	1	1	1
5	9	16	0	1	0	0	1

to a more efficient battery, hence benefiting j_1 and j_2 of the objective function, as defined in Section 4.5.1. By contrast, in Tables 7.2 and 7.4 the objective function is not weighted in favour of the battery and the top five modes only contain two modes which makes use of battery heating. More heat remains available for the cabin by not heating the battery, and so the neutrally and cabin weighted objective functions are less likely to utilise battery heating. Aside from the difference in battery heating, the top five modes across the three weightings share similarities in their use of components; in all weightings the motor appears three times, the thermal battery four times and the transmission three times. Additionally, Tables 7.2 and 7.4 share the same modes, in the same order, which is further evidence that the neutral objective function already favours cabin heating.

Another point of interest is the positioning of the modes which make use of the thermal battery in Table 7.3. While still having four modes which use the thermal battery, the mode which does not use the thermal battery (mode 23) has moved from third most common to fourth, meaning the top three modes now all use the thermal battery. This indicates the extra thermal load required for battery heating. Battery heating is conducted in addition to cabin heating, with the cabin and the battery each requesting 10kW of heat. However, as demonstrated in Section 5.7, the heat pump is not capable of supplying 20kW of heat, and so when the battery is connected to the heat pump the heat provided to the cabin reduces, causing the reduction in comfort. Hence when the battery is prioritised there is an increase in the usage of the thermal battery, in response to the increased total heating demand.

The representation of the motor in Tables 7.2, 7.3 and 7.4 is surprising since the motor's efficiency is not dependent on temperature, meaning extracting its heat does not compromise vehicle efficiency, whereas the extraction of heat from the transmission does. Sections 7.3.2 and 7.4 reveal more detail into the relationship between the heat pump and the motor.

The correct time step length has been chosen, and so further analysis can

Table 7.3: Top five most commonly optimal operational modes using a 120s time step and battery weighting

Rank	Mode	Occurrences	Motor	Thermal Battery	Electric Battery	Transmission	Cabin Exhaust
1	12	31	0	1	1	0	0
2	8	23	0	1	0	0	0
3	31	23	1	1	1	1	1
4	23	21	1	0	1	1	1
5	27	20	1	1	0	1	1

Table 7.4: Top five most commonly optimal operational modes using a 120s time step and cabin weighting

Rank	Mode	Occurrences	Motor	Thermal Battery	Electric Battery	Transmission	Cabin Exhaust
1	8	29	0	1	0	0	0
2	27	24	1	1	0	1	1
3	23	21	1	0	1	1	1
4	31	21	1	1	1	1	1
5	9	16	0	1	0	0	1

be performed on the prevalence of each component within the optimal operational modes throughout the range of scenarios tested. To get a true representation of the usefulness of individual components a comparison needs to be made for all modes, rather than just those represented in the top five optimal operational modes. This is completed in Section 7.3.2 where bar graphs are presented to show component appearances in all time steps. Furthermore, the data is broken down into temperatures and drive cycles. At this point trends start to become apparent in when individual components become useful.

7.3.2 Mode histograms

In this section a selection of bar charts are presented which display the prevalence with which each component was found in the optimal operational modes identified in each time step of the scenarios described. This percentage is calculated by breaking down all of the optimal operational modes found in a set of scenarios into their constituent components, then counting how many times each component appears in the optimal operational modes. For example, if mode 16 is optimal for every time step during WarmUp at $-15°C$, then the motor will have a prevalence of 100% as mode 16 exclusively uses the motor and was optimal in 100% of time steps tested. In this example all other components would have a prevalence of 0% as they are

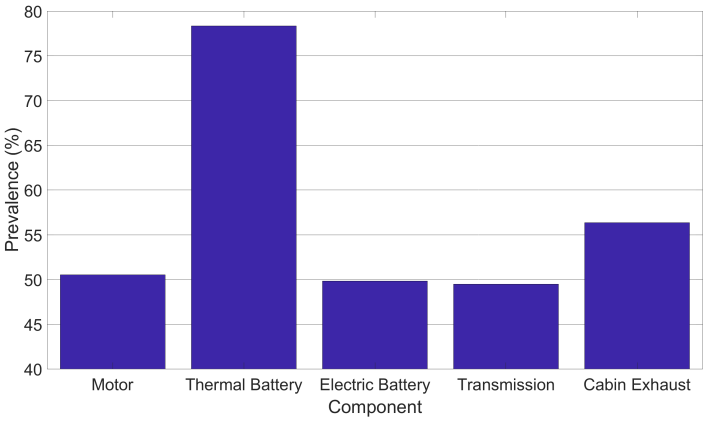

(a) Neutral weighting.

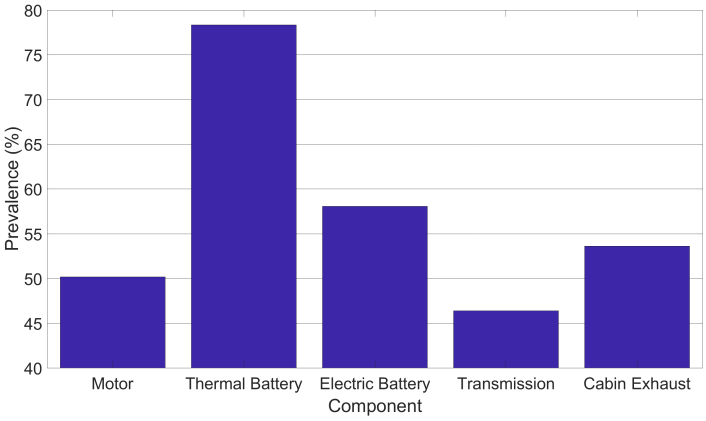

(b) Battery weighting.

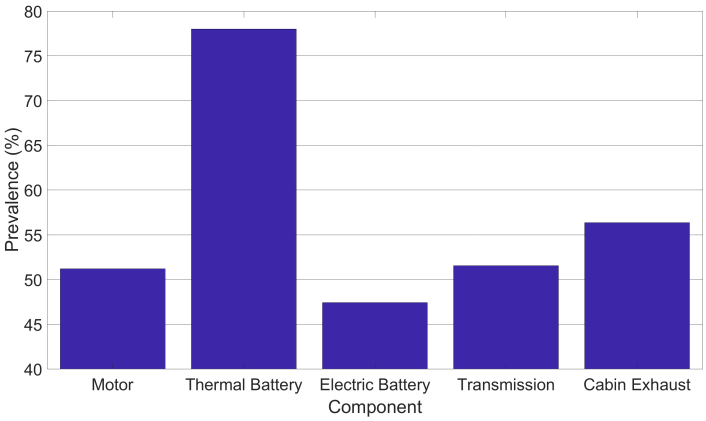

(c) Cabin weighting.

Figure 7.5: The occurrence of each component being included in the optimal operational modes is presented as a percentage of time steps. Here all time steps from each temperature and drive cycle have been included.

not represented in the single optimal operational mode. Conversely, if mode 16 is optimal for the first half of time steps, and mode 24 is optimal for the second half, then the motor would have a prevalence of 100%, the thermal battery would have a prevalence of 50% and all other components would be unrepresented and have a prevalence of 0%. The resulting percentage acts as a proxy for the effective usefulness of each component as a thermal contributor to the heat pump system. This metric will be referred to as a component's prevalence as it describes the percentage of times that a component was prevalent in the optimal operational modes found for a scenario.

Firstly, all of the optimal operational modes across all twelve scenarios have been included for three weightings and are presented in Figure 7.5. Figure 7.5 further confirms the findings from Tables 7.2, 7.3 and 7.4 discussed in Section 7.3.1, i.e. the use of battery heating is dependent on how much weight is given to battery oriented objectives of the objective function. This is seen in Figures 7.5b and 7.5c where the battery prevalence varies from 58.1% to 47.4% respectively. This point is demonstrated further in Figure 7.6. Figure 7.6 shows the prevalence of the battery in optimal operational modes across all scenarios, as the weighting of the cost function with regards to the battery objectives is varied from 2% to 98% ($0.01 \leq j_1 \leq 0.49$, $0.01 \leq j_2 \leq 0.49$, $0.98 \geq j_3 \geq 0.02$). These results point to a crucial link between objective function priority and prevalence of battery heating, indicating that controlling battery heating is the best way to control cabin comfort and battery performance. This is confirmed when comparing the variation in battery heating prevalence to other component prevalence over the same range, seen in Figure 7.7. Hence in Chapter 8 a set of optimal battery heating trajectories are created according to the different cost function priorities.

The thermal battery is the most useful component identified in Figure 7.5, with a prevalence of 78.4%, 78.4% and 78.0% over the three weightings. The thermal battery initially provides a free and powerful source of heat for the system. However, as discussed in Chapter 6, during longer drive cycles the cost of extracting all of the heat available can outweigh the benefit of the heat, this was seen in Section 5.6 and Table 6.24. This would explain why the thermal battery is not always useful when the drive cycle is broken down into time steps. During the later time steps of the WarmUp cycle there is cost associated with extracting heat from the thermal battery, with less benefit available from the heat; hence in these time steps the thermal battery becomes less useful. This is shown explicitly in Section 7.3.3.

The scenarios tested have been separated into different temperatures and then into different drive cycles, providing more information about under what con-

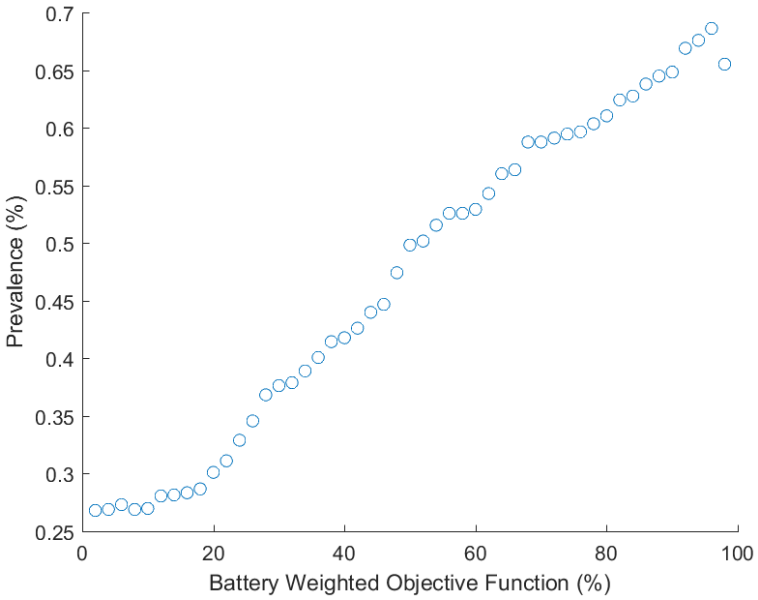

Figure 7.6: The prevalence of battery heating in the optimal operational modes is plotted as a function of cost function weighting towards the battery (100% means only the energy consumption and DOD contribute towards the cost function). Here it can be seen that the prevalence of the battery is approximately linearly dependent on cost function weighting, with high battery priority resulting in high battery heating prevalence.

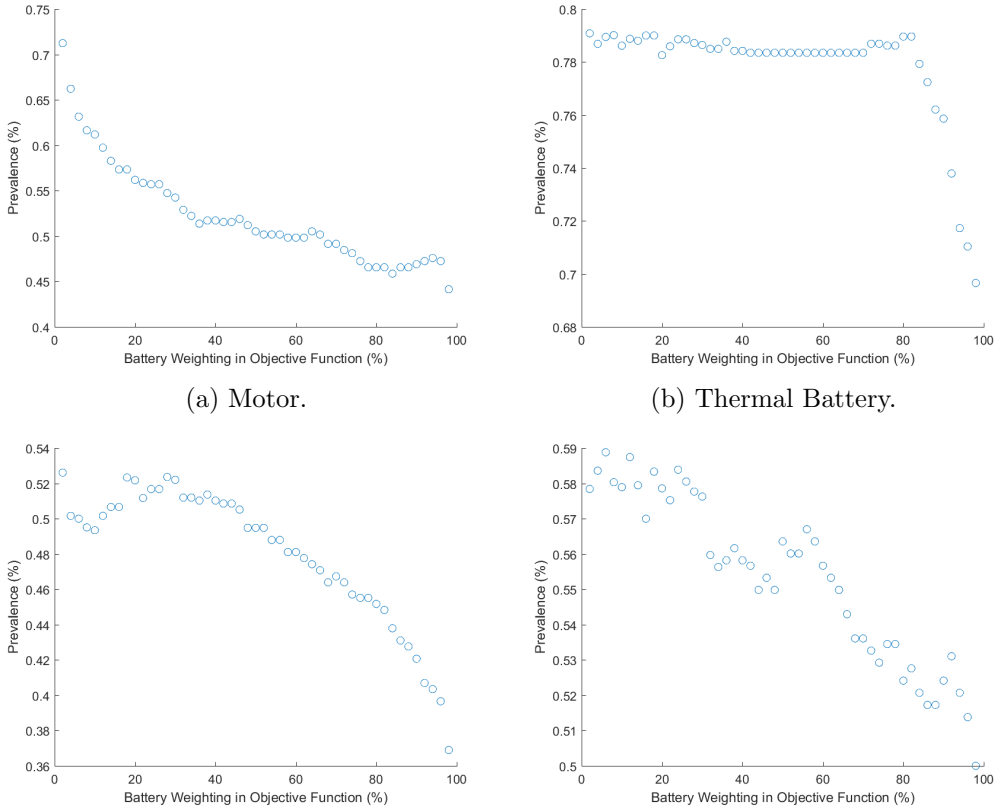

(a) Motor.

(b) Thermal Battery.

(c) Transmission.

(d) Cabin Exhaust.

Figure 7.7: The prevalence of each component (except the battery) is plotted as a function of cost function weighting towards the battery (100% means only the energy consumption and DOD contribute towards the cost function).

ditions the use of individual components is more favourable. Figure 7.8 shows the prevalence of each component over all drive cycles for different ambient temperatures. From Figure 7.8 it is clear that the prevalence of each component is dependent on ambient temperature. The motor becomes more useful at higher temperatures, while the thermal battery generally becomes less useful. While it is not obvious why the motor shows this trend, further investigations lead to an explanation of the motor's behaviour in Section 7.3.3. The behaviour of the thermal battery, on the other hand, is somewhat explainable; as the ambient temperature increases the cabin requires less heating, hence the thermal battery becomes less useful. The electric battery shows a more complex relationship with temperature compared to the motor and thermal battery. One hypothesis which fits this relationship is that heating the battery is very beneficial at the lowest temperatures, but as the temperature increases slightly heating the battery becomes less effective. In this case, at medium temperatures, saving the heat for cabin heating has more of an impact on the objective function. Then at the highest temperature tested, when the cabin requires less heat, heating the electric battery can be done at little cost to comfort and hence becomes more useful. This hypothesis is evaluated through investigation of when during each drive cycle, at each temperature, components become prevalent in the optimal operation modes, performed in Section 7.3.3.

The transmission demonstrates a similar behaviour to the electric battery, where the prevalence of extracting heat is greater at the extreme ambient temperatures. This is likely to be a compromise between the necessity of the heat being extracted versus the added inefficiency of operating the transmission at a lower temperature. At the lowest ambient temperature the need to extract the heat from transmission to heat the cabin, and potentially the battery, outweighs the extra energy consumed. If the objective function were purely oriented towards the battery it is likely that extracting heat from the transmission would become less preferable. At the highest temperature, while the need for heat is diminished it can be extracted more cheaply from the transmission without compromising the efficiency as much as at lower ambient temperatures.

Finally, cabin exhaust recovery becomes more useful at higher temperatures. It is likely that this is due to the increased temperature difference between the cabin exhaust and the target temperature of the chiller circuit ($-10°C$). This increased difference allows more heat to be extracted, making the cost of extraction more useful. Then at the lowest ambient temperature the necessity for heat outweighs the cost of extraction. Here the cost of extraction refers exclusively to the increased compressor consumption caused by adding more heat into the evaporator through

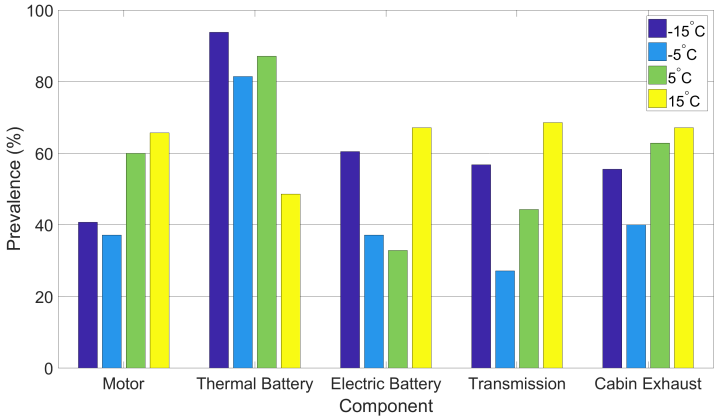

(a) Neutral weighting.

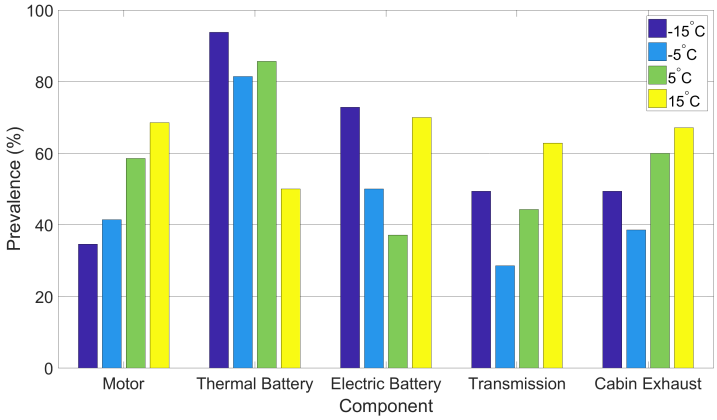

(b) Battery weighting.

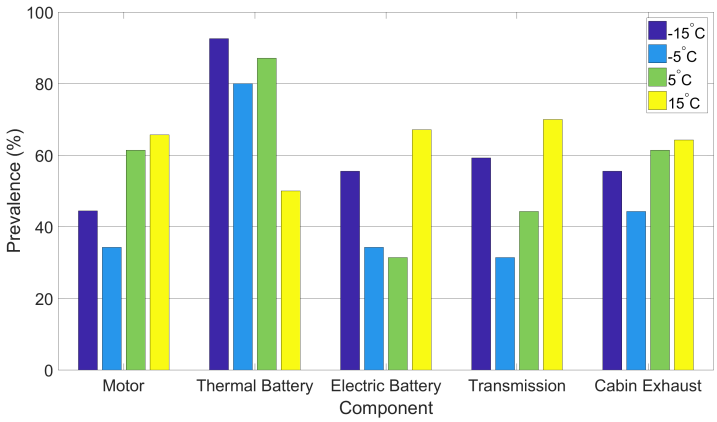

(c) Cabin weighting.

Figure 7.8: The prevalence of each component being included in the optimal operational modes is presented as a percentage of the total number of time steps. Here all time steps from all drive cycles have been included and the bars are split according to ambient temperature.

the chiller, therefore causing the compressor to work more.

When considering the differences between Figures 7.8a, 7.8b and 7.8c, there is not an apparent dependency of objective function weighting on the relationship between ambient temperature and component prevalence. This observation is with the exception of the battery. The battery shows significant variations in prevalence, compared to other components, when the objective function weighting is varied. The change between the different weightings causes an increase in battery heating prevalence from 55.6% in Figure 7.8c at $-15°C$, to 72.8% in Figure 7.8b at the same ambient temperature. In contradiction to the battery, the other components varied by a maximum of 9.9% prevalence at $-15°C$, as seen when comparing motor and transmission prevalence in Figures 7.8c and 7.8b.

The relationship between component use and ambient temperature has been initially explored, but this area needs further work. It is clear that the vehicle should be operated in different operational modes dependent on ambient temperature; however, the optimum operational mode will also depend on the drive cycle. To explore this the optimal operational modes have been analysed over separate drive cycles and the corresponding graphs are presented in Figure 7.9. It is expected that the average speed, duration and number/intensity of acceleration events will make some operational modes more beneficial than others to the vehicles operation.

Figure 7.9 shows how the prevalence of the components is dependent on the chosen drive cycle. Here the data has been split by drive cycle and arranged in descending order of duration, this appears to have the most impact on prevalence, as seen by considering the profiles of the bar charts made by the electric battery, transmission and cabin exhaust in Figure 7.9. This order also reflects the average speed of the WarmUp (50km/h), WLTP (46km/h) and NEDC (33km/h) cycles. Due to the long periods of steady state cruising in the WarmUp cycle, this order does not reflect the average tractive power consumption ordering, which is; WLTP (12.5kW), WarmUp (9.8kW) then NEDC (7.5kW). Here the average tractive power consumption excludes regenerative braking which is highly dependant on battery temperature. With an increase in braking and accelerating events comes an increase in power throughput through the motor, producing more waste heat. It would be expected that the motor would be more useful with higher vehicle dynamics, but this is not seen. It may appear then that use of the motor is more preferable under steady state conditions. Alternatively, it is possible that the choice of a 120s time step does not encapsulate the dynamics significantly enough to capture the periods where the motors use may be more beneficial, i.e. immediately after accelerating and braking events.

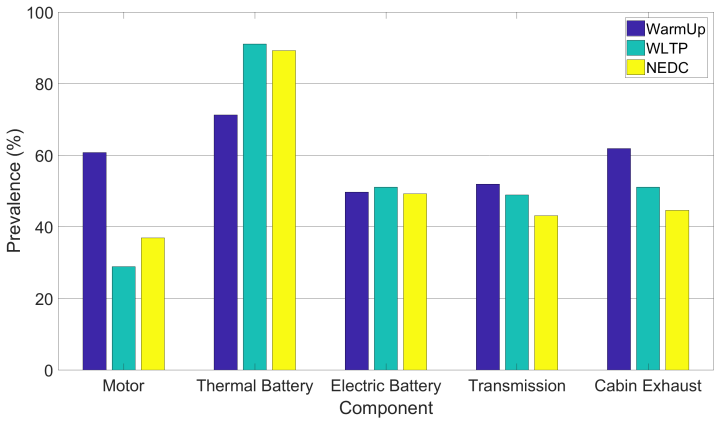

(a) Neutral weighting.

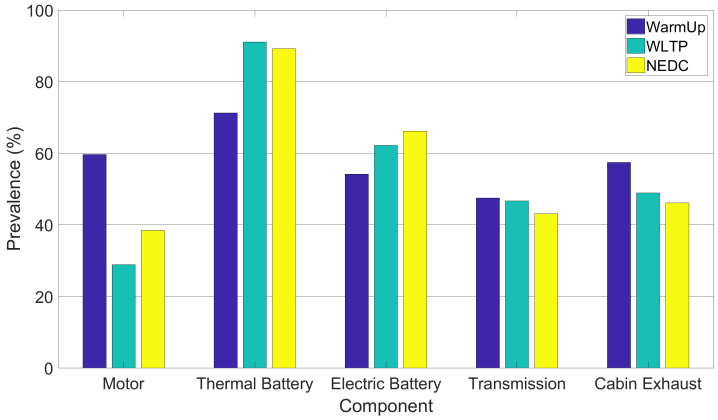

(b) Battery weighting.

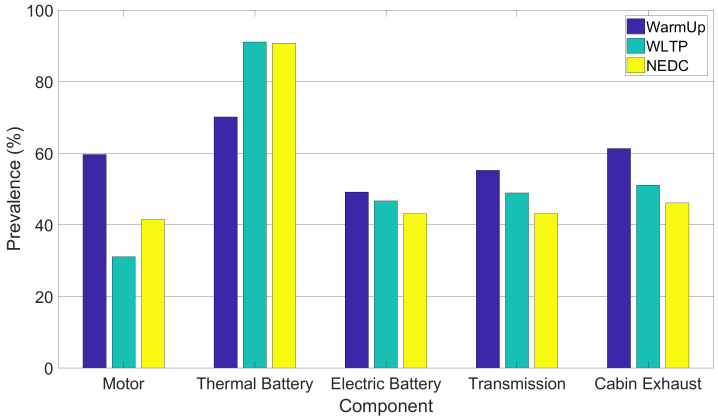

(c) Cabin weighting.

Figure 7.9: The prevalence of each component being included in the optimal operational modes is presented as a percentage of the total number of time steps. Here all time steps from each ambient temperature have been included and the bars are split according to drive cycle.

The length of the drive cycle correlates with the prevalence of the electric battery, transmission and cabin exhaust. Intuitively this should be expected; during a longer drive cycle the cabin spends proportionally more time at target temperature and so battery heating can be conducted with no adverse effects on cabin comfort. This would explain the decreasing prevalence of the battery heating with decreasing drive cycle duration when the cabin is prioritised in Figure 7.9c. Conversely, when the battery is prioritised the reverse is true, heating the battery is more useful on the shorter drive cycles. During the shorter drive cycles there is less time for the battery to self heat; thus, when the battery is prioritised in the cost function, heating the battery for proportionally more of the cycle is more beneficial than saving the heat for the cabin.

The transmission prevalence also correlates with drive cycle duration. With the increased duration the transmission spends more time at a higher temperature, operating more efficiently. This allows for some heat to be extracted at low cost to the vehicle efficiency, rather than extracting heat from a warming transmission as would happen in a shorter cycle. Moreover, the WarmUp cycle has a 30 minute rest period in the last third of the cycle, during this time heat can be extracted from the transmission with zero compromise to vehicle efficiency.

The thermal battery is least useful during the longest cycle. As has been shown in Section 5.6 and discussed in Chapter 6, during longer cycles the thermal battery needs to be fully depleted through the chiller circuit which increases compressor power consumption. If the cabin has reached target temperature and the thermal battery still has significant energy left, as might be the case at the higher ambient temperatures, then the thermal battery will not be benefiting the cabin heating but will be costing energy. Section 7.3.3 will show when this situation comes into effect, and hence when during the drive cycle the thermal battery should be disconnected. The period during which the cabin is at target temperature will obviously be extended in longer drive cycles, hence resulting in a proportionally less useful thermal battery. This does not however mean that the thermal battery is not useful at all during the longer cycles since it will have a positive impact during the warm up portion of the cycle.

This section has begun the investigation into how the individual components could be used with the heat pump in order to maximise the vehicle's performance according to the objective function defined. The dominant realisations for each component considered are summarised in the following list:

- Operational modes which included the motor as a thermal source were found to be optimal in approximately 50% of all time steps tested. Its prevalence is

also dependent on ambient temperature and drive cycle duration. Regarding the latter it was proposed that this was caused by the necessity of time for the motor to warm up to become useful, a point which will be further confirmed in Section 7.3.3.

- The thermal battery was the most useful of all components. It was however less useful at higher ambient temperatures and longer drive cycles. This reflected conclusions drawn in Chapter 6 and will be re-addressed in Section 7.3.3.

- Electric battery heating showed an unusual relationship with regards to how its use was dependent on ambient temperature. This relationship was explained by the compromise between the benefit of battery heating on efficiency and the necessity to save heat for cabin heating. It was suggested that at the lowest ambient temperatures the benefit of heating the battery outweighs the cost of cabin discomfort but, as the temperature rises, less impact on battery efficiency can be seen and so the heat is best saved for cabin heating. This is true until the ambient temperature is sufficiently hot that battery heating can resume at little cost to comfort. Furthermore, in Section 7.3.2 the prevalence of the electric battery was highly dependent on how the objective function is weighted. Given the unusual relationship between ambient temperature and whether the electric battery should be heated, in conjunction with the fact that heating has the greatest impact on cost, its heating should be considered more closely going forward. This is an important consideration and will be examined in detail in Chapter 8.

- The transmission showed a similar dependency on ambient temperatures to electric battery heating. A similar conclusion can be made, that the use of transmission heat is necessary at the lowest temperature to improve cabin comfort. Then as the ambient temperature increases the heat is not needed as much and the transmission can be left to warm up, resulting in a more efficient drivetrain, therefore saving energy. Again this is true until the highest ambient temperature where the transmission reaches optimal temperature more quickly and heat can be extracted cheaply with respect to vehicle efficiency.

- The cabin exhaust is the second most useful heat source, as seen in Figure 7.5. However it was also seen to demonstrate similar trends to the motor in Section 7.3.2. It will be shown in Section 7.3.3 that the cabin exhaust, like the motor, becomes more useful as the drive cycle progresses, this is likely due to the cabin warming up and therefore increasing the amount of heat expelled.

The next step is to inspect the time steps individually, with the intention of identifying trends in when components become useful during the drive cycles.

7.3.3 Operational mode comparison at each time step during the scenarios tested

Figures 7.10 to 7.12 show the optimal operational modes found during each 120s time step of the three drive cycles at all four ambient temperatures using a neutral objective function weighting. These modes have been found when comparing the full simulation of the thirty two operational modes defined in Section 4.2.2 and so their optimality is dependant on the vehicles operational history before that time step. The optimal operational mode for each time step is represented by a blue dot. From Figures 7.10 to 7.12 some trends and patterns can be qualitatively discussed regarding the general behaviour of the optimal operational mode through the drive cycle.

The first notable result is the apparent correlation of the optimum operational mode with speed. While the operational mode number is not continuous, but describes a set of discrete vehicle operational modes, in general a higher operational mode indicates more components are interacting with the heat pump. Moreover, since the motor represents 16 in the binary system used, and is the highest digit, modes 16 and above must include use of the motor. Since the higher modes (over 16) appear optimal at higher vehicle speeds, it can be concluded that the motor becomes a more useful thermal contributor at higher vehicle speeds. This is a good check that the results are intuitive, since higher vehicle speeds result in more power throughput through the motor, consequently providing more heat for the heat pump to use.

In some of the scenarios one time step may have two optimal operational modes, an example of this can be seen in Figure 7.11a. Here the optimal mode numbers are separated by two, which when considering the definition of the operational modes and the list of modes presented in Table 7.1 indicates that the same cost is achieved regardless of the state of the transmission with respect to the heat pump. As explained in Section 5.8, each component must surpass a 0.5°C temperature threshold between itself and the chiller circuit, which ensures that heat will flow from the component to the chiller circuit and not vice versa. Since these modes are separated by two it is likely that the transmission has not surpassed the required threshold and is therefore not connected to the heat pump despite the request from the operational mode, hence both modes are technically the same until the transmission warms up sufficiently to pass the 0.5°C temperature threshold.

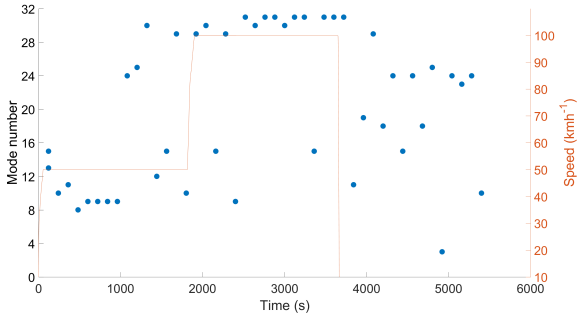

(a) Optimal operational mode identified at $-15°C$

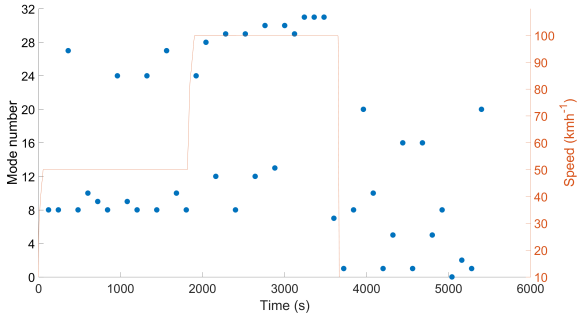

(b) Optimal operational mode identified at $-5°C$

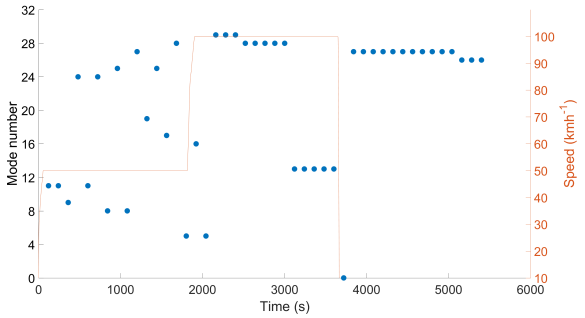

(c) Optimal operational mode identified at $5°C$

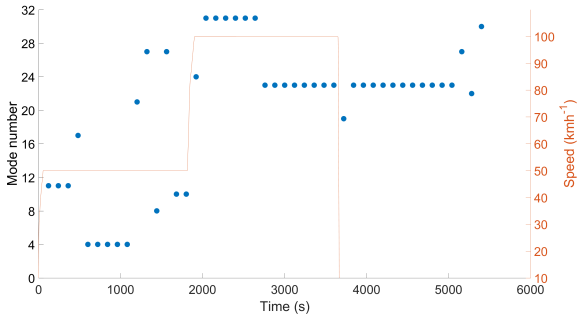

(d) Optimal operational mode identified at $15°C$

Figure 7.10: Optimal operational mode identified for WarmUp drive cycle using a neutral weighting.

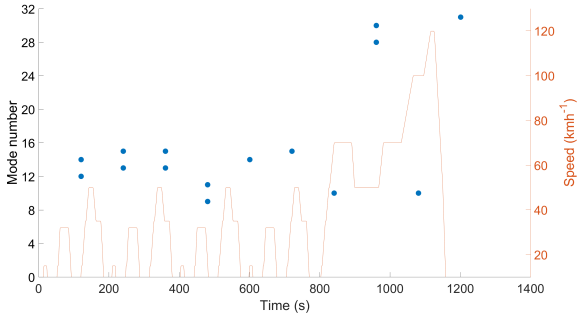

(a) Optimal operational mode identified at $-15°$C

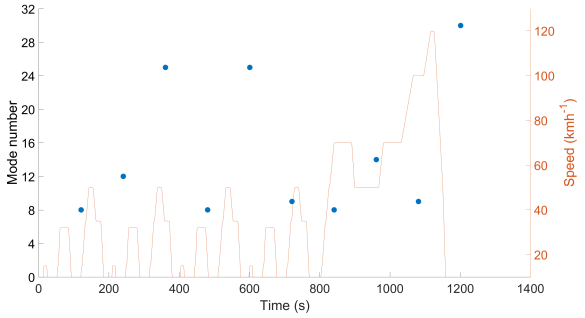

(b) Optimal operational mode identified at $-5°$C

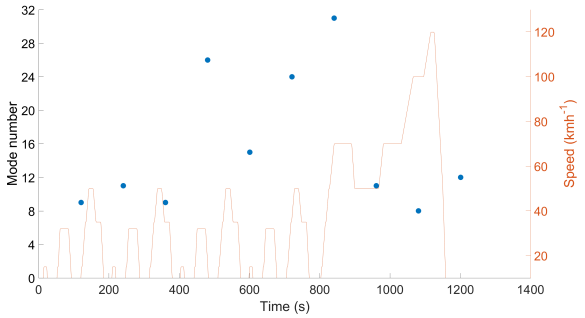

(c) Optimal operational mode identified at $5°$C

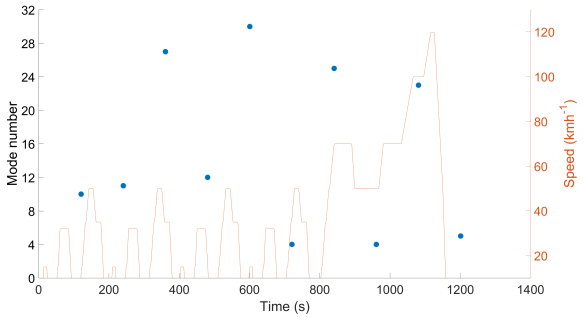

(d) Optimal operational mode identified at $15°$C

Figure 7.11: Optimal operational mode identified for NEDC drive cycle using a neutral weighting.

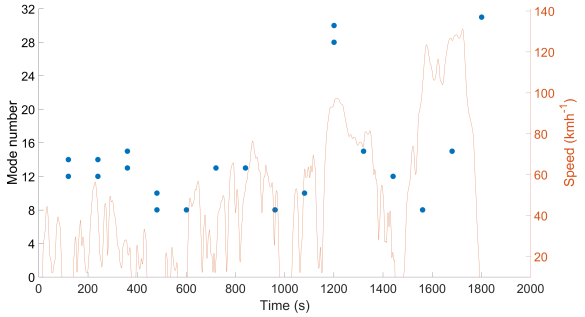

(a) Optimal operational mode identified at −15°C

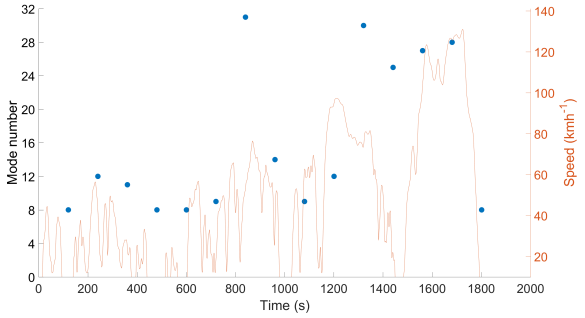

(b) Optimal operational mode identified at −5°C

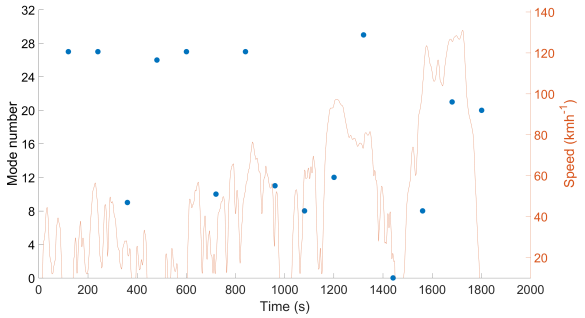

(c) Optimal operational mode identified at 5°C

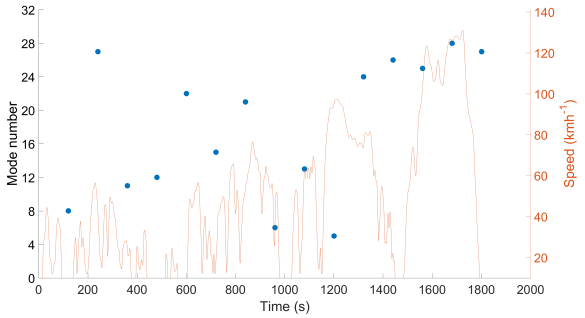

(d) Optimal operational mode identified at 15°C

Figure 7.12: Optimal operational mode identified for WLTP drive cycle using a neutral weighting.

Another notable feature of Figures 7.10, 7.11 and 7.12 is the variety of operational modes used. It can be seen in Figures 7.10c and 7.10d that during the steady state sections of the cycle some modes remain continuously optimal for consecutive time steps.

Figures 7.10, 7.11 and 7.12 revealed that the optimal operational mode changes as the drive cycle progresses. However, further analysis can reveal more about when during a drive cycle individual components become useful. In Figures 7.13 to 7.15 the optimal operational modes found in Figures 7.10 to 7.12 have been deconstructed into their constituent components. From Figure 7.13 it can be seen that some of the hypotheses proposed thus far have been confirmed. Firstly, after noticing that the thermal battery was not always useful it was suggested that the extraction cost at the end of longer cycles out weighed the cabin comfort benefit. This is predominantly seen by a reduction in thermal battery prevalence at the end of the drive cycle as ambient temperature increases, this can be seen in Figures 7.13a, 7.13c and 7.13d. It is also seen at the high ambient temperatures during the other drive cycles, in Figures 7.14d, 7.15c and 7.15d. However, due to the reduced length of these cycles the thermal battery will be needed continuously at lower ambient temperatures. This also shows why the thermal battery is less useful at higher ambient temperatures. There is less cabin heating requirement and therefore its heat becomes less useful after the cabin has reached target temperature.

Considering Figures 7.13 to 7.15 it can be concluded that the motor becomes more useful at the end of the drive cycle. At $-15°C$, in Figures 7.13a, 7.14a and 7.15a the first occurrence of the motor being prevalent in the optimal operational mode is around 1000s. Since all the drive cycles are different in the first 1000s this implies that the inclusion of the motor as a useful heat source is more dependent on time than vehicle speed. At higher ambient temperatures the motor appears in the optimal mode earlier in the drive cycle. When the ambient is $5°C$ the chiller takes approximately 200s to reach its operating temperature of $-10°C$, hence in this short period a large temperature difference has been created between the motor (which starts at $5°C$ with ambient) and the chiller, allowing more heat to flow between the two. When ambient temperature is lower and the motor starts with a lower temperature, more time is needed for the temperature difference between the two to be such that the heat flow is useful.

Figure 7.13 shows another expected behaviour with regards to the battery. The majority of optimal operational modes which make use of battery heating are optimal during the high speed segment of the drive cycle. Here the most current is being drawn from the battery, so minimising ohmic losses by reducing internal

resistance through heating will lead to a reduction in DOD. It has also been shown that battery heating at the start of the drive cycle is only optimal at the lowest ambient temperature, where the impact on battery performance is highest. This is seen in Figures 7.13a, 7.14a and 7.15a.

Battery heating is not necessarily optimal when it appears in the optimal operational mode later in the drive cycle at higher ambient temperatures, for instance in Figures 7.13d, 7.14c, 7.14d, 7.15c and 7.15d. Heating the battery takes a short time (dependent on ambient temperature) compared to the length of the drive cycle, so at higher ambient temperatures modes which utilise battery heating will see the battery reaching target temperature soon after the start of the cycle. Therefore modes which utilise battery heating at the end of the cycle are benefiting from an already warm battery, rather than benefiting from heating the battery at the end of the cycle. However it has been shown that at higher ambient temperatures, heating the battery is not optimal at the start of the cycle. This implies there is some trade off in battery heating, further showing the requirement for an optimised battery heating trajectory which will be demonstrated in Chapter 8.

Figure 7.13 shows that the transmission is particularly prevalent in the optimal modes during the stationary segment at the end of the drive cycle. The transmission has a temperature dependent efficiency, hence there is no vehicle efficiency loss when the heat is extracted from the transmission if the vehicle is stationary. Otherwise no clear pattern can be gained regarding when the transmission is most useful during a drive cycle through Figures 7.14 and 7.15. The transmission will be generating the most waste heat during high speed and high acceleration events, it is expected that the transmission will appear in optimal modes later within the cycle, such as in Figure 7.14b, where the transmission appears exclusively in the high speed section of the drive cycle. However this is rare and the transmission is more likely to be seen in optimal modes spread out through the cycle. It should also be noted that while the transmission's prevalence in optimal modes is dependent on the objective function weighting, its variation between fully battery weighted and fully cabin weighted is 17% compared to a 43% variation in electric battery heating prevalence, seen in Figures 7.7c and 7.6 respectively. This indicates that the transmission is less important to the cost function than the battery.

Finally, the cabin exhaust also shows no discernable pattern in when it should be used during a drive cycle. An intuitive assumption about the cabin exhaust would be that it may be more useful once the cabin has warmed, but there is no evidence to support this in Figures 7.13 to 7.15, with Figures such as 7.13a showing the opposite. It has been seen in Figure 7.5 that the cabin was found to be optimal in

more then half of all times steps, hence it should be used as a thermal source since it is beneficial overall. But the timing of using cabin exhaust during a drive cycle does not seem to be important.

In this section it was seen that there was not a single operational mode which was optimal during every time step of the drive cycle. It was also seen that the WarmUp cycle with fewer transient events appeared to have less variation in optimal operational modes; this can be seen explicitly at 15°C in Figure 7.10d, however other temperatures were less conclusive. Finally the optimal operational modes found in Figure 7.10 were broken down into their constituent components and analysed further in Figure 7.13. This indicated when each component should be connected to the heat pump during a drive cycle for optimal vehicle performance. The following suggested rules have been extracted qualitatively considering the information presented in Figures 7.13 to 7.15:

- The motor becomes more useful later in the drive cycle; this likely reflects its warm up time and that it will waste more heat during the high speed section of the cycle. This was reflected by the motor first appearing in the optimal mode at 1000s at -15°C, regardless of drive cycle.

- The thermal battery is better used at the beginning of the cycle, especially at lower ambient temperatures. The thermal battery can deliver a quick thermal response and so using its heat at the start of the cycle, while other components warm up, makes intuitive sense.

- The battery is best heated at the start of, or before, the faster part of the drive cycle, where its efficiency will have the greatest impact on the objective function. It should not be heated at the start of the cycle unless ambient is particularly cold. It is likely that the best time to heat the battery would be during a period between the cabin reaching target temperature and the vehicle reaching a high speed section of the drive cycle, should these not overlap. If the drive cycle is sufficiently slow, or short, battery heating may not be required at all. Electric battery heating opens multiple avenues of possibilities in controlling the compromise between comfort and range. These ideas will be explored more in Chapter 8.

- The transmission and cabin exhaust did not show a clear pattern in Figures 7.13 to 7.15 and so it cannot be concluded when during a drive cycle they should be included as heat sources to the heat pump. With regards to these components, further exploration may be required into how much heat should

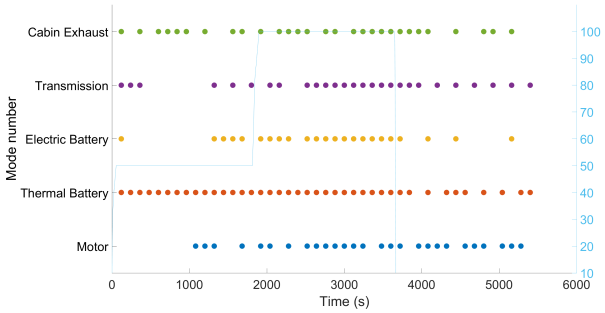

(a) Optimal operational mode identified at $-15°C$

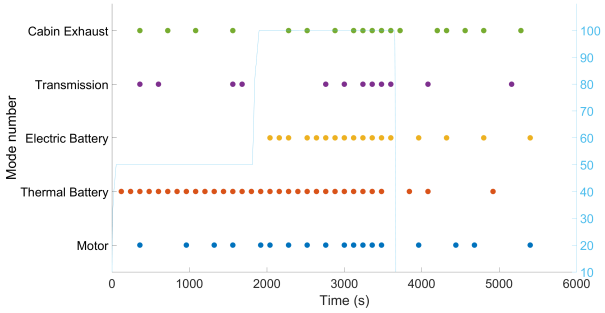

(b) Optimal operational mode identified at $-5°C$

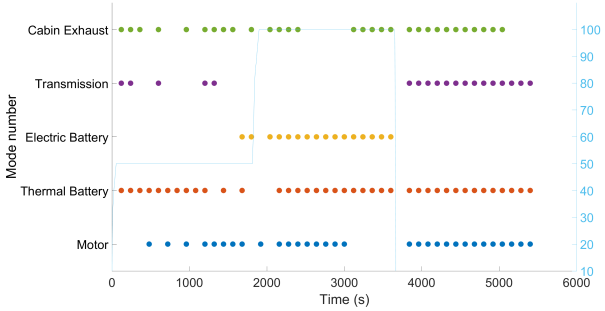

(c) Optimal operational mode identified at $5°C$

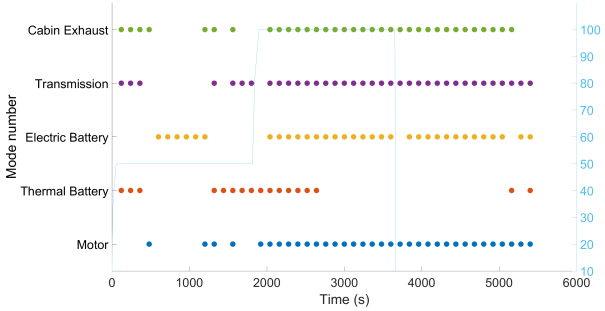

(d) Optimal operational mode identified at $15°C$

Figure 7.13: Optimal operational mode identified for WarmUp drive cycle using a neutral weighting.

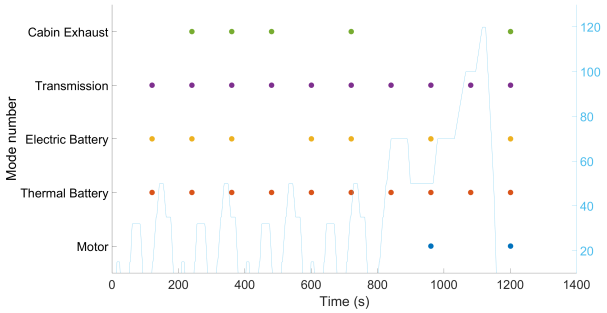

(a) Optimal operational mode identified at $-15°C$

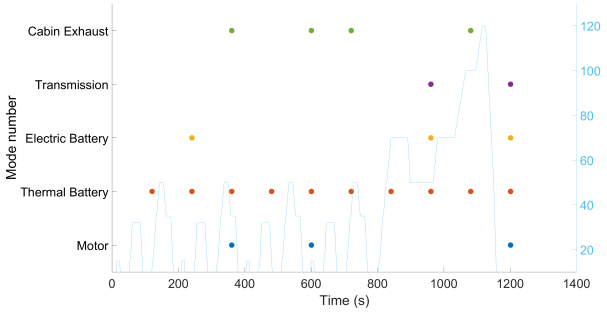

(b) Optimal operational mode identified at $-5°C$

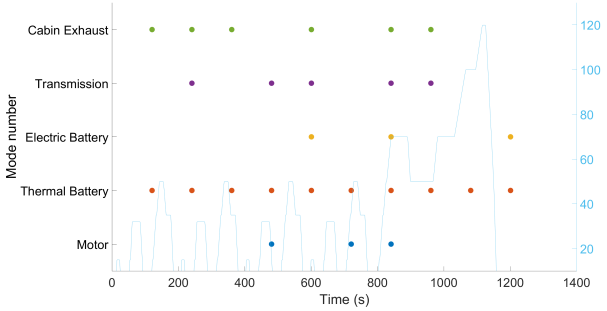

(c) Optimal operational mode identified at $5°C$

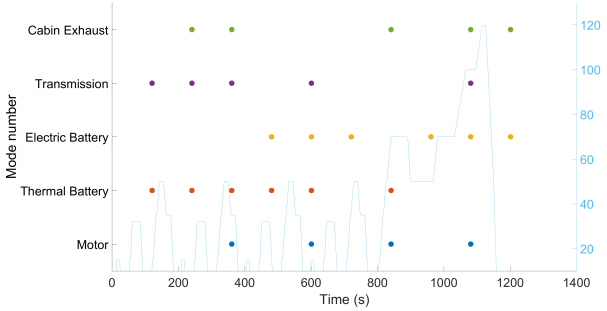

(d) Optimal operational mode identified at $15°C$

Figure 7.14: Optimal operational mode identified for NEDC drive cycle using a neutral weighting.

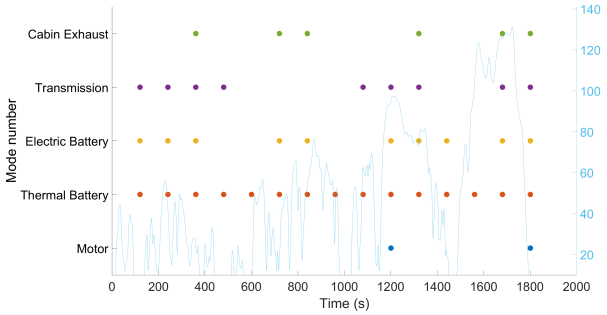

(a) Optimal operational mode identified at −15°C

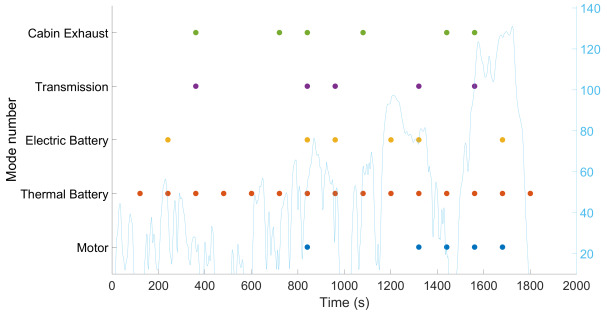

(b) Optimal operational mode identified at −5°C

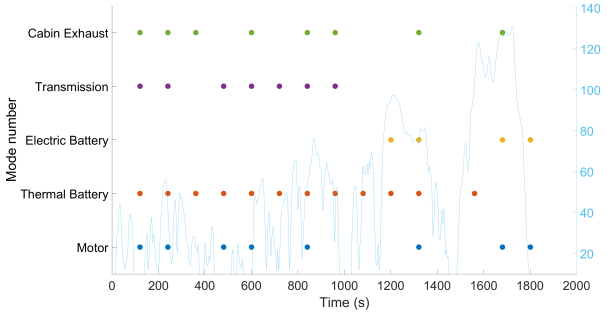

(c) Optimal operational mode identified at 5°C

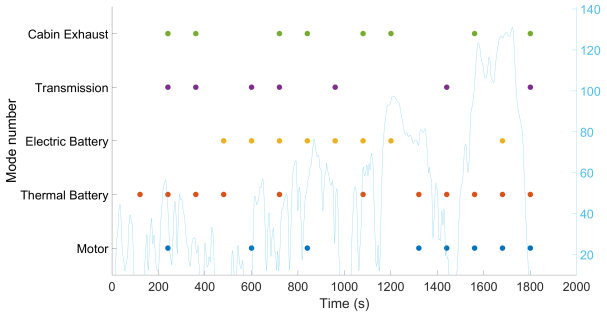

(d) Optimal operational mode identified at 15°C

Figure 7.15: Optimal operational mode identified for WLTP drive cycle using a neutral weighting.

be extracted, this may reveal more about how they can be used more optimally with the heat pump. These investigations are not performed in this research as the results indicate that battery heating has the most influence on the cost function. As a rule for operation then, the cabin exhaust should be included as a heat source. However, since it has been shown in Figure 7.5 that the transmission is the least useful heat source, and in Figures 7.10 to 7.12 that in some time steps the transmission will not be contributing heat, it can be concluded that the transmission does not make a useful heat source.

Section 7.3 has focused on identifying the optimal operational modes through different scenarios using the objective function defined in Section 4.6. While this implicitly contains information on the energy consumption, DOD and cabin comfort, these have not yet been explicitly addressed. In the final part of this chapter an investigation is made into how the findings so far can benefit the individual components of the objective function. This is completed in Section 7.4.

7.4 Single optimal mode improvement

In this section the found optimal operational modes are compared against the baseline operational mode in their ability to improve the individual components of the cost function. Since the optimal operational mode has been seen to change through the drive cycle, it would be intuitive to use this information to create a control trajectory which can change the operational mode, minimising the cost function. This trajectory would be used to create a switching schedule (referring to dynamic connecting and disconnecting of the component to/from the heat pump at each time step during a drive cycle) for each component given the found optimal operational mode for that time step. Hence this approach will be referred to as the switching schedule found from the trajectory of optimal modes (SSTOM). Optimal operational mode trajectory are found by following the mode trajectory seen in Figures 7.10 to 7.12. Hence individual component trajectories within the optimal trajectory are defined by Figures 7.13 to 7.15. This is used to create the SSTOM for each component.

The cost corresponding to the use of single optimal modes for each scenario and weighting are presented in Tables 7.5, 7.6 and 7.7. Tables 7.8 to 7.11 show quantitatively how the identification of optimal modes according to different objective function priorities has affected the individual components of the cost function [1]. The identified operational modes are compared to the baseline operational mode

[1]The cost metrics in Tables 7.8 to 7.11 are normalised but unweighted to make results of each

Table 7.5: Optimal operational mode through the entire scenario using a neutral weighting

Scenario		Mode	Motor	Thermal Battery	Electric Battery	Transmission	Cabin Exhaust
WarmUp	−15°C	27	1	1	0	1	1
	−5°C	25	1	1	0	0	1
	5°C	27	1	1	0	1	1
	15°C	27	1	1	0	1	1
NEDC	−15°C	13	0	1	1	0	1
	−5°C	8	0	1	0	0	0
	5°C	25	1	1	0	0	1
	15°C	26	1	1	0	1	0
WLTP	−15°C	28	1	1	1	0	0
	−5°C	8	0	1	0	0	0
	5°C	27	1	1	0	1	1
	15°C	27	1	1	0	1	1
Mean Comp Use			75%	100%	16.7%	50%	66.7%

Table 7.6: Optimal operational mode through the entire scenario using a battery weighting

Scenario		Mode	Motor	Thermal Battery	Electric Battery	Transmission	Cabin Exhaust
WarmUp	−15°C	31	1	1	1	1	1
	−5°C	25	1	1	0	0	1
	5°C	27	1	1	0	1	1
	15°C	27	1	1	0	1	1
NEDC	−15°C	13	0	1	1	0	1
	−5°C	12	0	1	1	0	0
	5°C	25	1	1	0	0	1
	15°C	26	1	1	0	1	0
WLTP	−15°C	13	0	1	1	0	1
	-−5°C	12	0	1	1	0	0
	5°C	27	1	1	0	1	1
	15°C	24	1	1	0	0	0
Mean Comp Use			66.7%	100%	41.7%	41.7%	66.7%

Table 7.7: Optimal operational mode through the entire scenario using a cabin weighting

Scenario		**Mode**	**Motor**	**Thermal Battery**	**Electric Battery**	**Transmission**	**Cabin Exhaust**
WarmUp	−15°C	27	1	1	0	1	1
	−5°C	25	1	1	0	0	1
	5°C	27	1	1	0	1	1
	15°C	27	1	1	0	1	1
NEDC	−15°C	15	0	1	1	1	1
	−5°C	8	0	1	0	0	0
	5°C	25	1	1	0	0	1
	15°C	26	1	1	0	1	0
WLTP	−15°C	31	1	1	1	1	1
	−5°C	8	0	1	0	0	0
	5°C	27	1	1	0	1	1
	15°C	27	1	1	0	1	1
Mean Comp Use			75%	100%	16.7%	66.7%	75%

Table 7.8: Objective function components and total cost presented for different optimal operational modes and the SSTOM for WLTP at −15°C ambient temperature.

Weighting		Baseline Mode 20	Neutral Mode 28	Battery Mode 13	Cabin Mode 31	SSTOM
Energy	j1	1	1.021	1.009	1.038	1.002
DOD	j2	1	1.024	1.014	1.018	1.012
Comfort	j3	1	0.622	0.635	0.62	0.644
Cost	J	3	2.667	2.658	2.676	2.658

which was defined in Section 4.4 as using heat from the motor and ambient, while also heating the electric battery. In the context of this chapter the defined baseline is equivalent to operational mode 20. The SSTOM is also included. The SSTOM refers to the switching schedule constructed according to the results using the neutral weighting and is included to investigate if any benefit can be gained through dynamically switching between modes through the drive cycle, hence the equivalent battery and cabin weighted SSTOMs are not included. It is only therefore fair to compare the performance of the SSTOM against the results corresponding to the neutral weighting.

One of the first things that can be noticed from Tables 7.8 to 7.11 is that the

weighting comparable. This also means the total cost does not sum to 1 or less as described in Section 4.5.

Table 7.9: Objective function components and total cost presented for different optimal operational modes and the SSTOM for WLTP at −5°C ambient temperature.

Weighting		Baseline Mode 20	Neutral Mode 8	Battery Mode 12	Cabin Mode 8	SSTOM
Energy	j1	1	1.046	0.975	1.046	1.031
DOD	j2	1	1.094	0.981	1.094	1.034
Comfort	j3	1	0.502	0.616	0.502	0.614
Cost	J	3	2.642	2.573	2.642	2.68

values for j_3 are between 40% and 60% lower than those for j_1 and j_2. This indicates that the cabin may have a disproportionate influence on the objective function and that there is more potential to improve comfort than energy consumption or DOD. This may impact the selection of optimum operational mode. For instance, at −15°C, mode 13 was selected to minimise the objective function when the battery weighting is applied, but it can be seen in Table 7.8 that the battery costs increase, compared to the baseline, while using this mode. However, mode 13 is still selected as optimal instead of mode 20 because the improvements in comfort outweigh the extra energy and DOD costs. j_1 and j_2 still improve using mode 13 compared to modes 28 and 31, which were optimal for neutral and cabin respectively, at the expense of some comfort.

The SSTOM is able to produce a lower cost than the neutrally weighted optimal operational mode at −15°C. It achieves this by improving on battery performance compared to mode 28 while only sacrificing comfort very slightly. At all other ambient temperatures the SSTOM does not perform as well as using the neutral operational mode. In Table 7.9 the SSTOM reduces battery related costs by 1.4% and 5.5% for j_1 and j_2 respectively, but with a 22% increase in discomfort. This is likely to be a consequence of early battery heating seen in Figure 7.15b which will improve battery performance but impact cabin comfort. In Table 7.10 the SSTOM performs worse than the neutral mode in every objective function metric. This is interesting because Figure 7.15c shows the SSTOM is mostly operating in mode 27 (motor, thermal battery, transmission and cabin exhaust) in time steps before 1000s, with more diversity in operational mode occurring after 1000s. This proves the point demonstrated by Equations 7.1 to 7.8; the optimal modes identified at time steps during the cycle are optimal because of the vehicle state created by their operation in the previous time steps, under a different vehicle state these modes may not be optimal. For example, in Figure 7.15c battery heating modes are optimal during the high speed time steps (1200s onwards), this does not mean the

Table 7.10: Objective function components and total cost presented for different optimal operational modes and the SSTOM for WLTP at 5°C ambient temperature.

Weighting		Baseline Mode 20	Neutral Mode 27	Battery Mode 27	Cabin Mode 27	SSTOM
Energy	j1	1	0.921	0.921	0.921	0.997
DOD	j2	1	0.966	0.966	0.966	1.012
Comfort	j3	1	0.558	0.558	0.558	0.646
Cost	J	3	2.445	2.445	2.445	2.655

Table 7.11: Objective function components and total cost presented for different optimal operational modes and the SSTOM for WLTP at 15°C ambient temperature.

Weighting		Baseline Mode 20	Neutral Mode 27	Battery Mode 24	Cabin Mode 27	SSTOM
Energy	j1	1	0.967	0.963	0.967	0.986
DOD	j2	1	0.972	0.969	0.972	0.975
Comfort	j3	1	0.43	0.434	0.43	0.425
Cost	J	3	2.369	2.366	2.369	2.386

battery should be heated here, as it would have warmed up early in the cycle using this mode, but rather that the vehicle operates optimally if the battery is already warm by these time steps. This makes sense since a warmer battery is more efficient and so will be beneficial at higher speeds. It will be shown when reviewing Figures 7.16 to 7.19 that while this effect of vehicle history will extend to other components, switching on battery heating part way through a drive cycle has the greatest impact on the cost metrics. Table 7.11 shows that at 15°C the SSTOM performs very similarly to the neutrally optimised mode, costing slightly more on battery objectives but improving comfort slightly.

When comparing the individual modes in Tables 7.8 to 7.11 the objective function weighting has performed as expected. The best example of this is at −15°C in Table 7.8, where the cabin weighted mode produces the best comfort but worst battery costs. The battery weighted mode is the least comfortable but also has the least battery associated costs and the neutrally weighted mode fits in between the two. This observation excludes the baseline, which has the best battery performance but is the least comfortable of the modes tested. This is again caused by the cabin's disproportionate influence on the objective function.

Figures 7.16 to 7.19 further investigate how the cost improvements presented in Tables 7.8 to 7.11 are made. In these Figures, data pertaining to the three different weightings as well as the SSTOM is presented, where the operational mode

used will be given in the legend. As shown in Tables 7.5 to 7.7, some of the objective function weightings return the same optimal operational modes. These duplications will appear as missing trajectories in Figures 7.16 to 7.19, but are in fact hidden underneath the duplicate.

Figure 7.16 shows the difference in cumulative energy (j_1) through the drive cycle between the optimal operational modes (including the SSTOM) and the baseline. Here the optimal operational mode consumption is subtracted from the baseline consumption, hence positive values indicate an energy saving. At $-15°C$ in Figure 7.16a all options improve on energy consumption until a turning point between 800s and 1000s. When comparing to Figure 5.17 in Chapter 5 this is likely caused by the thermal battery switching from the HTC to the chiller circuit, which will cause the compressor to increase power consumption. At this point it may seem sensible to switch off the thermal battery and continue with energy savings, however this could have unintended side effects. One might be that it would impact cabin comfort as the heat pump would not be able to output as much heat. Another noticeable feature of Figure 7.16a is the divergence of neutral and cabin, and battery and optimal. This is explained by the break down of the optimal operational modes as seen in Tables 7.5 to 7.7. The main difference between these two groups is the incorporation of the motor, with the cabin optimised mode using the transmission as well. While using the motor as a heat source does not affect vehicle efficiency, it does cost extra energy to extract the heat, causing the groups to diverge. Similarly, using the transmission in the case of the cabin optimised operational mode causes extra energy cost from extracting. However it also costs extra energy due to a reduction in component efficiency; compounding the cost and causing the cabin optimised operational mode to use the most energy.

The lowest ambient temperature was the only example of the SSTOM strategy beating the neutrally optimised single operational mode. This is not expected since Equations 7.1 to 7.8 highlight that there is no basis to assume the trajectory created through this method can improve on a single operational mode. Figures 7.15a, 7.16a and 7.17a show that the SSTOM saves cost predominantly through the timing of electric battery heating. The heating at the start of the cycle improves battery efficiency, causing a similar energy saving to mode 13, which was optimal for the battery. Between 360s and 720s the battery heating is paused, allowing the cabin temperature to recover compared to mode 28, which was optimal for the neutrally weighted objective. Hence the SSTOM has reduced battery heating compared to mode 13, allowing for better cabin heating, but increased battery heating compared to mode 28, giving better energy efficiency. The benefit from the efficiency

outweighs the reduction in comfort, as seen in Table 7.8, hence leading to an overall improved performance.

The importance of battery heating has been demonstrated throughout this chapter, for example Figures 7.6 and 7.16b may best exemplify this. At $-5°C$ mode 8 (thermal battery) is optimal for a neutrally or cabin weighted objective function and mode 12 (thermal battery and electric battery heating) is optimal for a battery weighted objective function. The only difference between modes 8 and 12 is that the latter heats the battery while the former does not. The effect of this is demonstrated in Figure 7.16b where mode 12 saves 0.2kWh compared to the baseline, but mode 8 uses an extra 0.4kWh compared to the baseline; i.e. there is approximately a 0.6kWh saving from using battery heating. The consequence of this energy saving is a reduction in comfort.

Figure 7.17 shows the cabin temperature profile using the baseline mode, the identified optimal modes and the SSTOM. In Figure 7.17b it can be seen that heating the battery reduces the cabin temperature throughout the drive cycle. The SSTOM shows the potential for this trade off to be managed. Figure 7.15b shows the SSTOM provides heat to the battery during the second time step of the cycle, then disconnects from the battery and harvests heat from both the cabin exhaust and transmission in the next time step. In Figures 7.16b and 7.17b this choice appears to provide the necessary electric battery efficiency benefits, while not compromising cabin comfort as much as keeping the battery heating on for the duration of the cycle. Using the SSTOM the battery is also heated at 720s, which can be seen in the reduction in cabin temperature in Figure 7.17b. It is likely this decision has been made because if the battery were warm at this point then the vehicle would start saving more energy; however, since it is not, and heating must be administered, the result is a reduction in cabin comfort. This is an example of the hypothetical scenario described in Equations 7.1 to 7.8.

The effect of switching between heating and not heating the battery can also be seen clearly in Figure 7.16c. In Figure 7.15c battery heating begins at $1200s$, at which point the cumulative energy begins to diverge significantly from that of mode 27, as seen in Figure 7.16c, increasing compared to the optimised modes and nearly matching the final energy consumption of the baseline. In addition to the increased energy consumption, the cabin temperature, shown in Figure 7.17c, drops below its target temperature and then recovers. The combination of these two consequences of battery heating indicates that it occurred too late. Firstly there was not enough duration left in the drive cycle to make use of the benefits of a more efficient battery. Secondly, the extra load on the HVAC system, caused by the

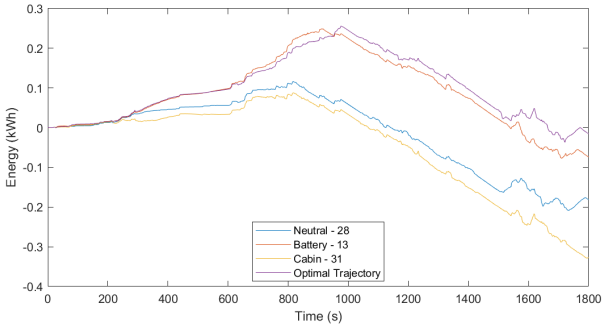

(a) Cumulative energy at $-15°C$

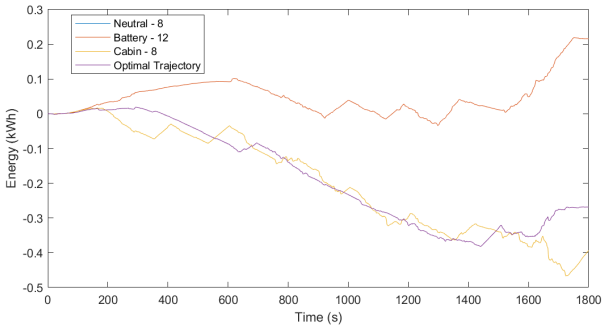

(b) Cumulative energy at $-5°C$

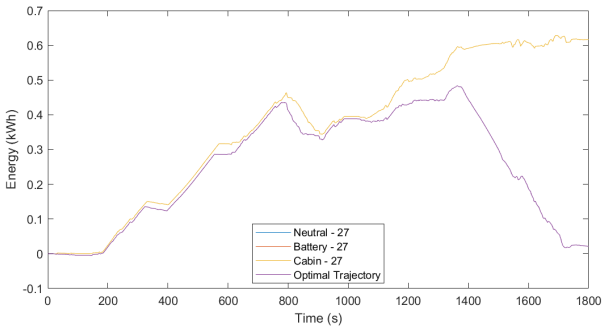

(c) Cumulative energy at $5°C$

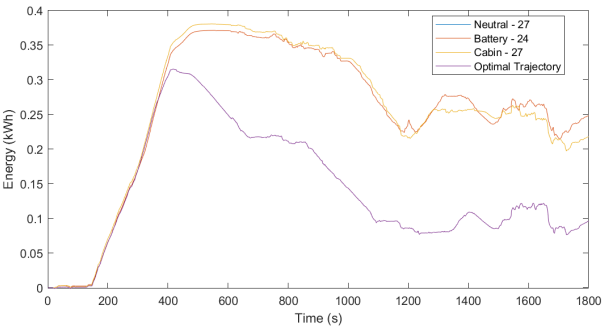

(d) Cumulative energy at $15°C$

Figure 7.16: Cumulative energy consumption using found optimal operational modes and SSTOM for the WLTP drive cycle.

additional battery heating demand, results in the cabin temperature reduction seen in Figure 7.17c at 1200s. Consequently more heat needs to be produced to cope with both heating loads, requiring extra energy for the compressor. It is likely that the dip in cabin temperature is not helped by the amount of battery heating used. If different levels of battery heating were available then a controller may be able to manage the reduction in cabin comfort by reducing the requested heat to the battery. It is also noteworthy that the SSTOM turned on battery heating after the cabin reached its target temperature and during the high speed section of the drive cycle. This could be a key insight into when an optimised battery heating trajectory may choose to heat the battery. This is supported by the timing of battery heating seen at 15°C ambient temperature, in Figure 7.15d.

At 15°C Figures 7.15d and 7.17d show that the SSTOM waits for the cabin to get to target temperature before beginning battery heating, it then ceases battery heating before the high speed section of the drive cycle. This time the cabin temperature is not affected, as shown by Figure 7.17d. There are many reasons why this may be the case. Some possible explanations are; it happens early within the cycle so the thermal battery will be able to cope with the additional load, the battery only requires a small amount of heat to reach target temperature or the cabin does not require much heat to stay at target temperature. These are not mutually exclusive and all could be true. The decision to heat the battery has changed the cumulative energy consumption, regardless of not impacting the cabin comfort. The point at which the switch happens can be clearly seen in Figure 7.16d as the SSTOM energy consumption diverges from the optimal mode's consumptions. This indicates that heating the battery at this point was not beneficial to the system, but having a heated battery at this point would have been. This is again a result of the optimal mode at this time step being optimal as a consequence of its operation in the previous time steps creating a favourable vehicle state. At this ambient temperature the battery will be operating efficiently compared to lower ambient temperatures. The fact that the cumulative energy is not able to recover from energy consumed in heating the battery may indicate that the battery should not be heated at all at this higher ambient temperature.

Figure 7.18 shows the improvement in DOD that the optimal modes and SSTOM have made in comparison to the baseline. As with Figure 7.16, positive values show an improvement compared to the baseline. The results for DOD improvement corroborate what has already been demonstrated in the analysis of Figure 7.16, with some worthwhile additional insight available. Figures 7.18b and 7.18d demonstrate the necessary separation of energy consumption and DOD. In Figure

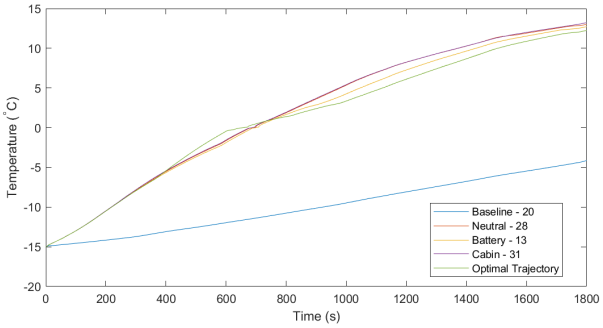

(a) Cabin temperature at −15°C

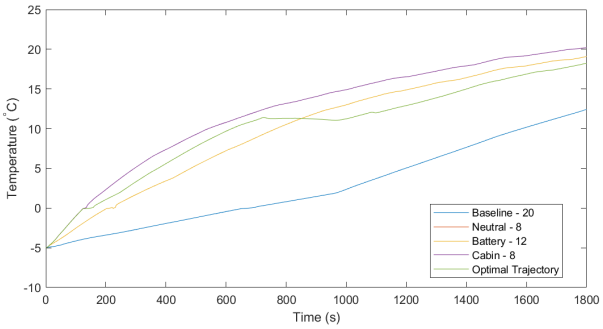

(b) Cabin temperature at −5°C

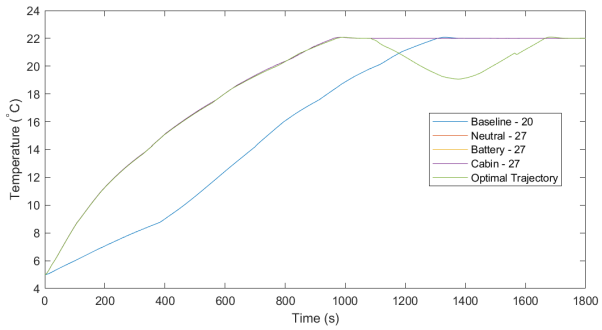

(c) Cabin temperature at 5°C

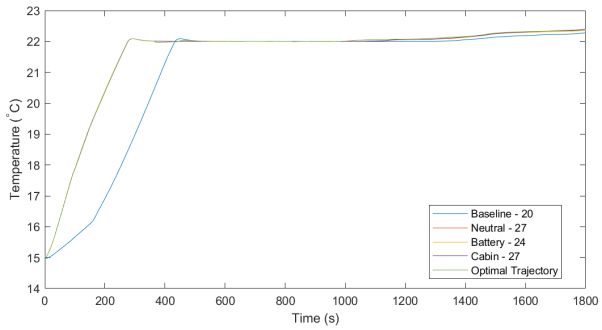

(d) Cabin temperature at 15°C

Figure 7.17: Cabin temperature using found optimal operational modes and SSTOM for the WLTP drive cycle.

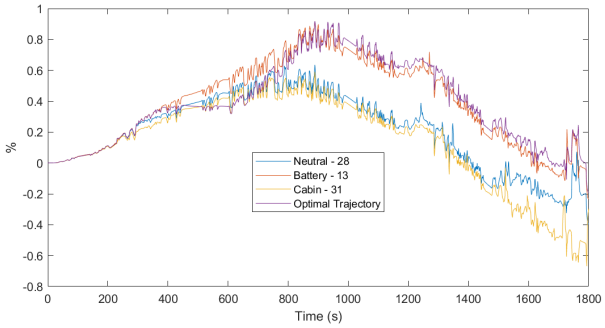

(a) Different in DOD at −15°C

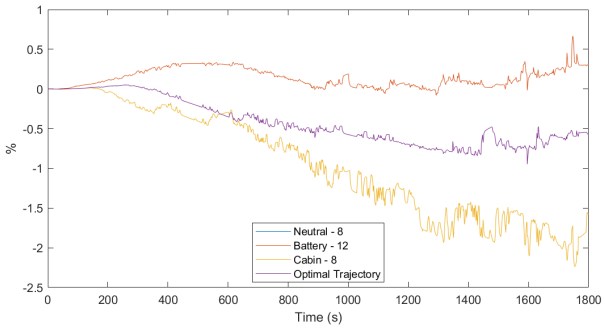

(b) Different in DOD at −5°C

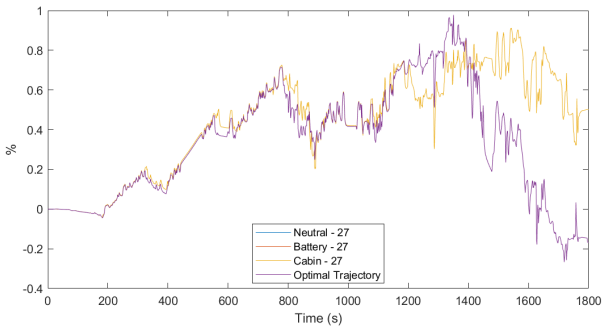

(c) Different in DOD at 5°C

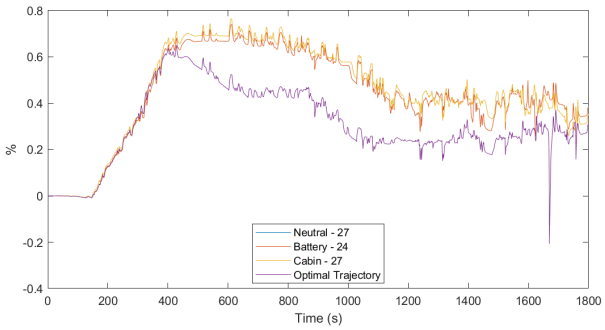

(d) Different in DOD at 15°C

Figure 7.18: Difference between DOD for found optimal operational modes and SSTOM compared to the baseline operational mode, for the WLTP drive cycle.

7.16b mode 8, which was optimal for the cabin and neutrally weighted objective function, uses a similar amount of energy to the SSTOM. However, because the SSTOM is also utilising battery heating, which reduces the battery's internal resistance and therefore reduces the amount of current needed to produce the same power, it does not use as much DOD as mode 8. Concordantly, at 15°C Figure 7.16d implied that there was not a good reason to heat the battery, since the energy consumption did not improve. However, by comparing Figures 7.16d and 7.18d it can be seen that the battery heating costs comparatively less DOD than energy. This is reinforced in Table 7.11, where SSTOM has $j_1 = 0.986$ and $j_2 = 0.975$ compared to mode 28 with $j_1 = 0.967$ and $j_2 = 0.972$. This difference in j_1 and j_2 across SSTOM and mode 27 has arisen since the battery with a higher operating temperature will be using less current and therefore starting to save DOD.

Figure 7.19 shows the battery temperature through the WLTP cycle using different operational modes and the SSTOM. Here it can be seen that when the battery is heated its temperature increases rapidly. Given that battery heating has been seen to have a large impact on the energy consumption and comfort, the amount of heat delivered to the battery may be unnecessarily high. Certainly this indicates that further work should include multiple levels of battery heating in order to gain more control of the trade off between comfort and energy consumption.

This section has focused on the improvements which can be made by selecting the optimal operational mode according to the weighting applied to the cost function. Table 7.8 showed that the optimal modes selected had the desired effect on the components of the cost function, with the cabin optimised mode being the most comfortable, with an associated cost of $j_3 = 0.62$ compared to $j_3 = 0.622$, $j_3 = 0.635$ and $j_3 = 0.644$ for the neutrally optimised mode, battery optimised mode and SSTOM respective. At 15°C the most energy efficient mode was mode 13, which was optimal when using a battery weighted objective function. It had a cost of $j_1 = 1.009$ and $j_2 = 1.014$, which improved compared to other optimal modes but was worse than the baseline. Although it had a worse energy consumption and DOD than the baseline, it was still chosen as optimal because it incorporated some cabin weighting. This provided a 36% improvement compared to the baseline, hence dominating the cost improvements. Additionally an SSTOM was created using the results of the optimal operational mode identification at each time step of the drive cycle, as seen in Figure 7.15. Due to the flaw, highlighted in Equations 7.1 to 7.8, in assuming this trajectory would be optimal, it was only able to improve the total cost at −15°C. The use of SSTOM provided insight into how switching between operational modes could be useful. This insight was extracted through the analysis

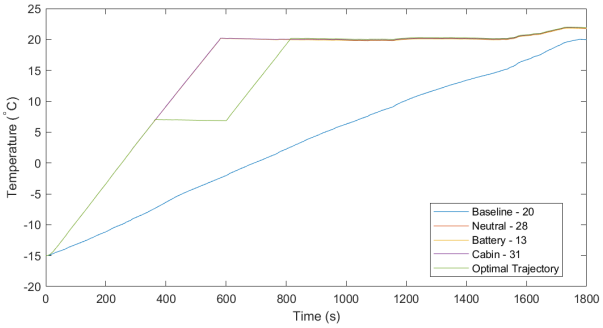

(a) Battery temperature at −15°C

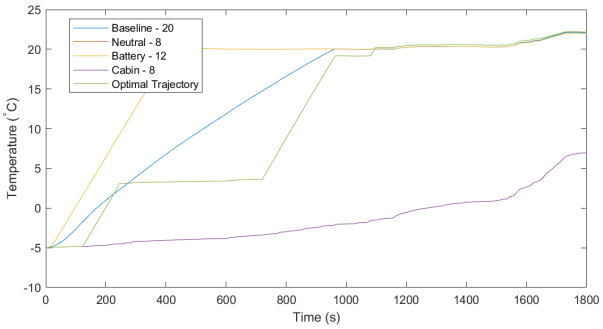

(b) Battery temperature at −5°C

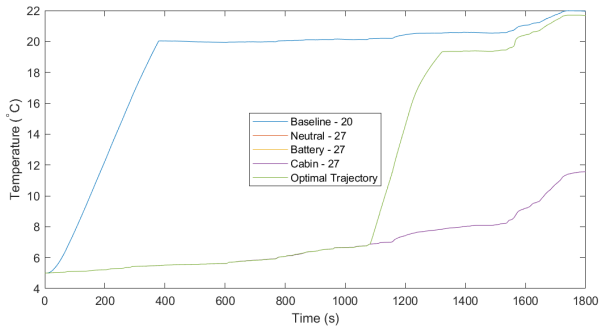

(c) Battery temperature at 5°C

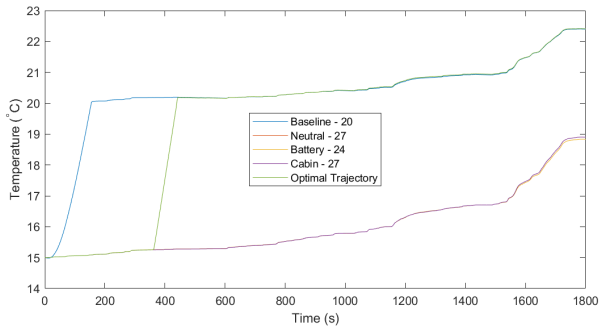

(d) Battery temperature at 15°C

Figure 7.19: Battery temperature using found optimal operational modes and SSTOM for WLTP drive cycle.

Table 7.12: Vehicle metrics at −15°C

Weighting (mode)	Efficiency (Wh/km)	Range (km)	Comfort (mean degC)
Baseline (20)	369.2	139.7	31.9
Neutral (28)	377.1	136.5	19.8
Battery (13)	372.4	137.8	20.3
Cabin (31)	383.3	137.3	19.8
SSTOM (n/a)	369.9	138.1	20.6

of Figures 7.16 to 7.19, where the consequences of changing operational mode could be seen and suggestions for improvements made. For instance, Figures 7.15a, 7.16a and 7.17a showed that an energy saving could be made without sacrificing too much cabin comfort by improving the timing of battery heating. Additionally, comparing Figures 7.15c and 7.15d with Figures 7.17c and 7.17d indicated that the best time to heat the battery is likely to be after the cabin reaches target temperature, in scenarios where the the cabin reaches target temperature. The same conclusion may not be drawn from −15°C and −5°C since the cabin did not reach target temperature. Through this analysis it can be confirmed that the battery heating has the biggest impact on the objective function factors. This conclusion is drawn from differences found between modes which use battery heating and modes which do not, and by observing the impact that battery heating has on the cumulative energy, DOD and cabin temperature when it is turned on mid cycle using the SSTOM.

7.5 Discussion

In Section 7.4 it was shown from a cost perspective in Tables 7.8 to 7.11 that selecting the operational mode which is optimised for the scenario and cost function priority had the desired effect on the cost metrics. Tables 7.12 to 7.15 show how these cost metric improvements translate to efficiency, range and comfort improvements.

The metrics presented in Tables 7.13 to 7.15 show when the battery is prioritised the range is maximised. At −15°C the battery optimised mode is not able to improve range compared to the baseline. When the battery is prioritised in the cost function, energy and range make up two thirds of the cost, while comfort accounts for the rest. Since comfort is still taken into account a large gain opportunity in comfort can mean that the battery objectives do not get fully optimised. This is designed so that prioritising the battery does not completely jeopardise comfort. Hence at −15°C, while the baseline gives a better range it is 50% more uncomfort-

Table 7.13: Vehicle metrics at −5°C

Weighting (mode)	Efficiency (Wh/km)	Range (km)	Comfort (mean °C)
Baseline (20)	370.8	139.2	19.3
Neutral (8)	387.7	127.2	9.7
Battery (12)	361.5	141.8	11.9
Cabin (8)	387.7	127.2	9.7
SSTOM (n/a)	382.4	134.5	11.9

Table 7.14: Vehicle metrics at 5°C

Weighting (mode)	Efficiency (Wh/km)	Range (km)	Comfort (mean degC)
Baseline (20)	337.3	159.2	6.2
Neutral (27)	310.7	164.9	3.5
Battery (27)	310.7	164.9	3.5
Cabin (27)	310.7	164.9	3.5
SSTOM (n/a)	336.3	157.4	4.0

Table 7.15: Vehicle metrics at 15°C

Weighting (mode)	Efficiency (Wh/km)	Range (km)	Comfort (mean degC)
Baseline (20)	288.8	186.6	1.0
Neutral (27)	279.4	192.0	0.4
Battery (24)	278.1	192.6	0.4
Cabin (27)	279.4	192.0	0.4
SSTOM (n/a)	284.6	191.4	0.4

able than mode 13, which was optimal for battery priority. Cabin and neutral both give the joint best comfort, while being able to improve range over the baseline at 5°C and above. Finally, when the neutral weighting is prioritised a compromise is achieved between range and comfort. Tables 7.13 to 7.15 show that the same operational mode is optimal for both the cabin and neutral weightings, while in Table 7.12 two different optimal modes are identified, but both have the same comfort performance. In Table 7.12 it is seen that mode 28 (neutral) is more energy efficient while mode 31 (cabin) gets better range. It is possible that the use of more extreme cost function weightings would result in different optimal operational modes when prioritising the battery or cabin. However, the method used has been seen to improve upon the baseline case in the metrics that the objective function priority is concerned with.

The results presented in Section 7.3 serve three important purposes:

1. They show that the method chosen to identify and compare operational modes has been successful.

2. They have revealed important relationships between thermally active components and the optimal operation of the heat pump.

3. They guide the direction of further research.

In justification of the first point, expected outcomes have been realised. For instance, the thermal battery provides an effectively free source of energy (post charging) and has been seen to be useful in nearly all scenarios, as seen in Figure 7.5. Another example would be the fact that the transmission and cabin exhaust became more useful as the cycle duration increased, as seen in Figure 7.8. This should be expected as a longer cycle gives these components more opportunity to warm up, making them more useful. These demonstrations of expected behaviours give trust to the method used, so that when a more unusual or subtle relationship is discovered it can be believed and investigated to be understood further.

With regards to the second important purpose of the result, battery heating showed an important relationship with the heat pump in relation to controlling the cost function. There are three areas which indicate that the battery heating is of high importance. Firstly when comparing component prevalence, as in Figures 7.5, 7.8 and 7.9, the battery showed the most variance in prevalence when the objective function was changed. This was highlighted further in the second indicative result; Figure 7.6 showed that the battery was the most sensitive component to objective function weighting. While the motor varied 28% in Figure 7.7a, the battery varied

by 33%. This indicates that battery heating is highly valued when battery metrics are prioritised and not valued when the cabin is prioritised. This relationship seems obvious, however it can be complicated when considering the timing of battery heating. Heating at the start of the cycle may unnecessarily impeach cabin heating and harm comfort, but waiting too late in the cycle may negate the usefulness of heating the battery in the first place. This trade off in timing could be visually appreciated in Figure 7.13, where battery heating was particularly useful during the high speed section of the WarmUp cycle. The vehicle was operated in each of the thirty two operational modes for the duration of the cycle separately, meaning the modes which used battery heating and that were optimal during the high speed section already had a warm battery, since it would have been heated from the beginning of the cycle. It can therefore be concluded that the optimal time to heat the battery would be before any high speed section of the drive cycle, but not so early that it harms the cabin warm up. For the WLTP this means that at 5°C battery heating should be performed after 900s and before 1500s, while at 15°C the window would be defined between 300s and 1500s according to Figures 7.17c and 7.17d respectively. Here 1500s represents the beginning of the extra high speed section of the WLTP cycle. These windows cannot be defined at −15°C and −5°C since the cabin target temperature is not met. Optimising the battery heating presents an interesting and worthwhile challenge in the pursuit of understanding how the thermal energy onboard an electric vehicle can be used to optimise the operation of the vehicle, and is addressed in Chapter 8.

In Sections 7.3.1 and 7.4 a vulnerability in this methodology was eluded to: a true comparison and identification of which operational mode is optimal during a drive cycle cannot be made since the optimality of the mode is dependent on the consequences of its use in all previous time steps, which is not accounted for in the comparison. As discussed in 7.4 there is no justification to assume that following the trajectory created by the identified optimal operational modes would be the same as following a dynamically optimised trajectory. This is not however to say that the comparison has no value. Studying the operational modes used, their constituent component compositions, and how component usage varies according to different ambient temperatures and cycles revealed important information about how thermal energy around the vehicle may be used beneficially.

The cabin exhaust was found to be a component of little concern in changing the cost function. While it was shown to be predominantly useful in Figure 7.5, its prevalence varied the least in Figure 7.7. Additionally in Sections 7.3.2 and 7.3.3 there was no clear pattern identified in why the cabin exhaust was useful under

different scenarios, or at different points in the drive cycle. However, since the cabin exhaust was prevalent in 66.6% to 75% of optimal operational modes, as seen in Table 7.5 to 7.7, it should be considered as a permanent thermal source to the heat pump.

The prevalence of the motor as a heat source presented added subtleties and complications. In Figure 7.8 it was seen that the motor generally becomes more useful at higher temperatures, as does the transmission and cabin exhaust. This is with the exception of the lowest ambient temperature, where the need for thermal energy to satisfy cabin comfort outweighed the incentive to conserve energy through compressor usage. However, the behaviour seen in Figure 7.9, where the motor was most useful during the WarmUp cycle, then NEDC and then WLTP, was less predictable. This does not conform to the order of the drive cycles in terms of tractive effort, nor duration. A sensible conclusion to draw from this might be that the motor is better suited, as a heat source, to steady state operation. This is partially supported by the results seen in Figure 7.13, where the motor showed particular prevalence during the high speed cruising section of the warm up cycle.

The prevalence of the motor was also highly dependent on how the objective function was weighted; rising to approximately 72% when the cabin is fully prioritised, and falling to approximately 44% when the battery was fully prioritised, as seen in Figure 7.7. This shows that the heat extracted from the motor is good for cabin heating, but the extraction cost is bad for vehicle performance. It is likely that the size of this difference is influenced by the amount of heat available for extraction; for comparison, the cabin exhaust reached 59% and fell to 50% when the cabin and battery were fully prioritised respectively. Neither of these components can directly effect the efficiency of the vehicle through having heat extracted, but the fact that more heat can be extracted from the motor means that it is both more useful as a heat source when high heat is desired, and more energetically costly. This is due to increased compressor consumption when less heat is desired. The cabin exhaust having less heat available is both less useful and less costly compared to the motor. Given the increased range in prevalence shown in Figure 7.6 and the behaviour seen and discussed in Figure 7.9, controlling the thermal exchange between the heat pump and the motor may be one of the better ways to control the objective function, i.e. operating the vehicle to maximise comfort or battery performance.

7.6 Concluding Points

- Thirty two operational modes have been identified from four heat sources and one heat sink, their impact on the cost function evaluated, and the results comprehensively compared, thereby addressing Research Objective 2.
- In comprehensively comparing all heat modes, the knowledge gap identified in Chapter 3 has been closed for the purpose of this project.
- It was shown that the motor, thermal battery and cabin exhaust should be used as permanent heat sources as they are predominantly beneficial.
- When extracting heat from the transmission, the reduction in its efficiency generally out weighs its usefulness as a heat source, and hence it is predominantly not useful.
- Dynamically switching modes with the SSTOM approach has the potential of further benefiting the cost function, however a mode switching mechanism should be devised using a more robust manor. This will first be applied to the component whose connection to the heat pump has the biggest impact on the cost function.
- The priority of the cost function has the greatest impact on the prevalence of battery heating in the identified optimal operational mode. The timing of battery heating also has a significant impact on both comfort and battery performance. Therefore creating a optimal heating trajectory for the battery is the best way to control the balance of range and comfort.

Chapter 8

Results 3, Dynamic Optimisation of Battery Heating

8.1 Introduction

In this chapter the Research Objective "What control can be gained over the balance of comfort and range through the dynamic control of battery heating during a drive cycle?" is addressed. It was seen in Chapter 7 that at $-15°C$, switching between operational modes can enable a reduction in the cost. In Chapter 7 the method for producing a component switching schedule was known to be unreliable due to the dependency of optimal operational modes on the history of that mode's operation. Hence a systematic methodology for creating a switching schedule which minimises the cost function is needed. Chapter 7 also identified that heating the electric battery had the biggest impact on the control of the cost function. This motivates the need for the optimised switching schedule to target the battery's interaction with the heat pump. The binary control of the battery's heating was seen to impact the cabin's temperature when heating was dynamically switched on. Introducing new heating levels for the battery allows more control of the impact on cabin temperature when the battery is heated. In summary, a set of optimised battery heating trajectories, utilising multiple battery heating levels, is needed to minimise the cost function according to the desired priority (range, comfort or a balanced strategy). The heating trajectory will create a warm up path for the cabin temperature and battery temperature, which both implicitly define the objective function cost, that minimises the objective function cost. The development of this provides the vehicle with an ability to tune cabin comfort based on the range required for the duty cycle by strategically heating the battery.

8.2 Chapter specific methodology

This chapter will use the WLTP cycle at two ambient temperatures; $-7°$C and $14°$C. The former is the recommended low temperature for testing while the latter is an official testing temperature [194].

8.2.1 T definition of the problem

For this chapter the baseline vehicle operational mode is changed. Instead of operational mode 20, as defined in Section 4.2.2, the results will be compared to modes 25 and 29. These modes are comprised of the motor, thermal battery and cabin exhaust, with the difference being that mode 29 utilises battery heating whereas mode 25 does not. These sources are chosen as they were seen to be used in the majority of optimal operational modes for the 12 scenarios shown in Tables 7.5 to 7.7. The optimal battery heating trajectory will then explore the potential of operating between modes 25 and 29, creating a balance of the two which can be tuned for comfort or range. With this understanding, it is therefore expected that the optimal trajectory which prioritises comfort will align more closely with mode 25 and may not utilise any battery heating, while prioritising the battery may produce a control strategy better aligned with mode 29.

This optimisation requirement can be described by Equation 8.1

$$\begin{aligned} &find\, U(i)\ which\ minimises\ J(U, X_s) \\ &for\ i = 1\ to\ N_{ts} \\ &where\ U(i)\ is\ the\ battery\ heating\ during\ the\ i^{th}\ time\ step \\ &and\ N_{ts} = \frac{drive\ cycle\ duration}{length\ of\ time\ step} \\ &and\ X_s\ are\ s\ state\ variables \\ &subject\ to \\ &U(k) = 0\text{kW}\ or\ 3.33\text{kW}\ or\ 6.66\text{kW}\ or\ 10\text{kW} \end{aligned} \tag{8.1}$$

Here the electric battery heating has been split into four levels; none (0kW), low (3.33kW), medium (6.66kW) and high or full (10kW). This was required to control the impact which battery heating has on the cabin. For simplification, a uniform discretisation with full heating and no heating is chosen, with 3.33kW being close to the 4kW PTC consumption. Hence 6.66kW is chosen as the final heating power, providing a sensible and uniform discretisation of the control. Increasing the precision of the control vector would enable the cost to be reduced further. Chapter

7 identified that the likely windows where battery heating may be optimal, at 5°C and 15°C, were 900s to 1500s and 300s to 1500s respectively. The extra high speed section of the WLTP drive cycle is defined between 1500s and 1800s. Since the problem appears to be breakable into 300s segments it is appropriate to use this length as the time step length to discretise the problem.

8.2.2 State variables and static parameters

For Equation 8.1 the state variables have been identified as the cabin and battery temperatures, as the cost to be minimised is an implicit function of these. The state variables define the range of initial starting conditions that are permitted at the start of each time step when producing the cost matrix in dynamic programming (DP). The choice of battery heating level will have the most impact on battery and cabin temperatures, and it is this path over the cycle which defines the cost; hence these are the state variables for the problem. Chapter 4 explains the "curse of dimensionality", which describes how a DP problem's computational requirements grow exponentially with each additional state variable. So while variables such as DOD and coolant temperatures could be considered as state variables, the assumption has been made that the variation in these variables caused by the different battery heating options has negligible impact on the cost. Although DOD is coupled to the cost function it is assumed that the starting condition of SOC will not vary sufficiently that look up tables reliant on SOC are effected by the variation caused by different heating strategies. DOD is therefore considered as a static parameter where a reference SOC trajectory will be used to initialise SOC at the start of each time step. Other vehicle variables also require static parameters so that the vehicle reinitialises correctly, as if it had not been cold started in the middle of a drive cycle. The variables used as static parameters are:

- Vehicle speed
- Thermal battery temperature
- Motor temperature
- High temperature and chiller circuit temperatures
- Refrigerant temperatures

Using a reference profile for each of these parameters ensures that when the vehicle reinitialises at different time steps in DP, the vehicle operates as if it were

continuing a drive cycle and not performing a cold start. This ensures that the cost matrix accurately represents the cost of control decisions at each point, since if a cold start were performed it would have an adverse effect on battery temperature, cabin temperature, and the vehicles ability to deliver heat. Mode 25 is used to generate the reference profile for the static parameters.

8.2.3 Implementation

An implementation method needs to be selected which can create and solve the required cost matrix, producing the optimised heating trajectories. This should be a well documented open source solution which has been proven within the industry. Within the examples presented in Chapter 4, Shojaei *et al.* [73] used an open source MATLAB implementation of DP developed by Sundström [195]. Shojaei *et al.* used Sundström's DP algorithm to investigate the optimal timing of battery cooling during a 24 hour duty cycle in a hot climate on a PHEV. Here battery ageing, comfort and energy consumption were used as costs, making the problem and implementation similar to that of this research, hence the DP implementation used would be well suited to this research. Sundström designed the open source implementation to address the power split problem in hybrid vehicles, as described in Section 4.2.3. It has been validated in literature to efficiently solve problems of this nature [196–198], and its implementation is well documented in Sundström's PhD thesis [195,199]. In these respects the open source tool created by Sundström meets the needs of this research and will be used to generate the optimal heating trajectories.

This algorithm creates a cost matrix in X and U for each time step. The cost matrix informs the algorithm of what the cost of starting at each initial condition (defined in X) and using every control option (U) will be, it also predicts the final state of X having applied control U. The algorithm finds the cheapest path in X and the corresponding U required to execute this path. This process is reliant on being able to accurately predict what the end state of the vehicle will be given X and U at each time step. If this is not accurate a path could be created in X which is not possible, which could lead to an increase in cost. It is therefore important that the static variables, listed in Section 8.2.2 correctly reinitialise the vehicle so that the final state of X at the end of each time step is an accurate prediction of X if that control strategy were implemented from the beginning of the cycle. Correctly identifying the static variables for a large model becomes an iterative process, where after each execution of the DP algorithm it is possible to identify another vehicle variable which needs to be included or adjusted. The repetition of this process improves the outcome of the DP algorithm by increasing the accuracy

of state predictions made in the cost matrix. However, since some of the static variables, such as coolant temperature and SOC, will vary depending on the control strategy it is not possible to ensure the cost matrix is fully accurate unless every static parameter is included as a state variable; however this is not advisable due to the "curse of dimensionality". Hence with a large, complex model such as the one used here, a balance must be found between the number of state and static variables.

Once the cost matrix is found the algorithm then solves the matrix backwards, identifying which control value should be used depending on the state of the vehicle. The problem is then run forward with the control strategy being decided by the control matrix which resulted from the backwards solution. The result of this determines the optimal control strategy.

8.3 Results

Using the DP implementation described in Section 8.2, the optimal trajectories shown in Figures 8.1 and 8.2 were produced. At 14°C one trajectory was found to be optimal for the three optimisation priorities, hence only one control profile is shown in Figure 8.2 . In Figure 8.1, the three trajectories optimise battery heating when the priority is set to neutral (Figure 8.1a), battery (Figure 8.1b) and cabin (Figure 8.1c). In Figure 8.1c it is seen that when the cabin is prioritised the optimal trajectory is set not to heat the cabin. This result is expected as stated in Section 8.2, as no battery heating leaves the most heat available for the cabin. Figure 8.1b shows that the battery is fully heated in the first time step, then partially heated with the low heating level in the next time step, before being full heated again in the third step. It is likely this approach is optimal, as it allows the cabin temperature increase in the second time step; this will help to minimise the cost function, as cabin comfort still accounts for one third of the cost when the battery is prioritised. The neutral weighting is intended to produce a balanced strategy, balancing range and comfort.

In Chapter 7 it was suggested, through the analysis of Figures 7.15c and 7.15d, that when a scenario is able to reach cabin target temperature before the high speed section of the drive cycle the optimum time to heat the battery would be in the window created between reaching cabin target temperature and the beginning of the drive cycle. This is certainly the case in Figure 8.2 where cabin target temperature is reached before 400s and battery heating begins at 900s. Here the battery does not require much assistance to get to target temperature, so although the control

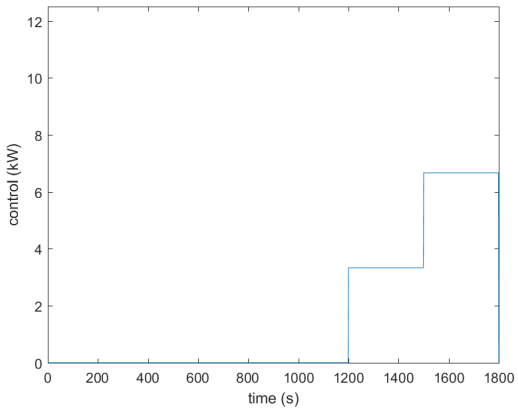

(a) Control trajectory for a neutral objective function priority.

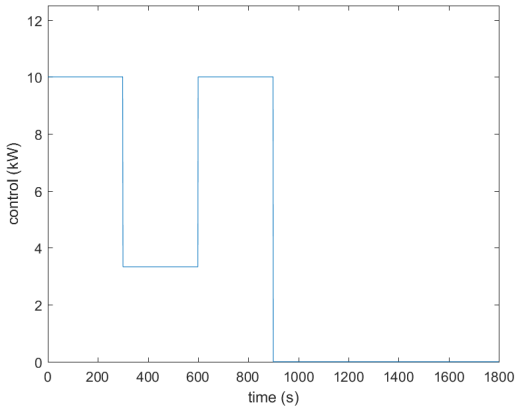

(b) Control trajectory for a battery objective function priority.

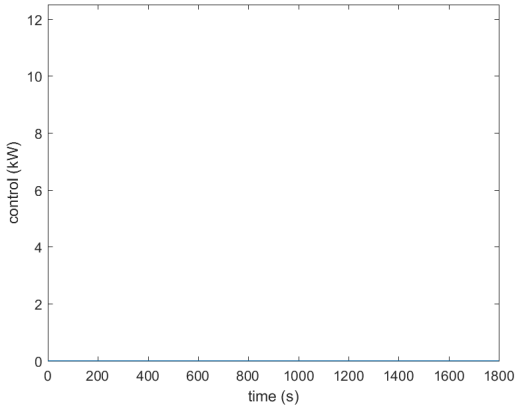

(c) Control trajectory for a cabin objective function priority.

Figure 8.1: The optimal control trajectories for the three objective function priorities at $-7°$C are shown.

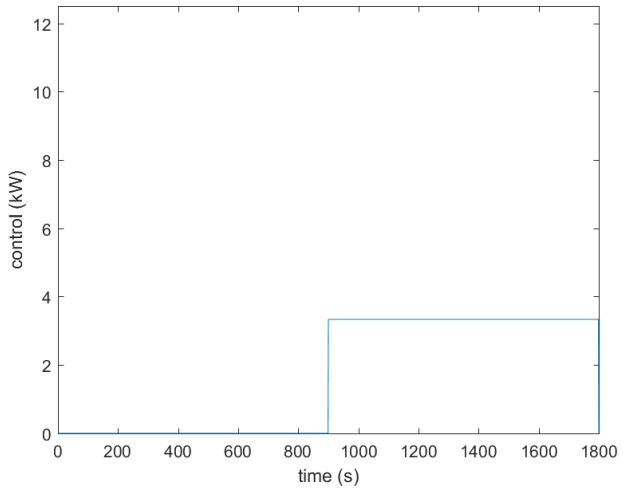

Figure 8.2: The optimal control trajectory for the three objective function priorities at 14°C is shown.

is set to heat the battery for 900s the vehicle's controllers will isolate the battery as soon as it reaches target temperature as explained in Section 5.8. The isolation of the battery and the effect of battery heating on cabin temperatures can be seen in Figures 8.3 and 8.6. Here the optimised trajectory (neutral, battery or cabin in the legend) is compared to "No battery heating" and "Full battery heating" which correspond to operational modes 25 and 29 respectively.

In Figure 8.3 it is seen that the battery follows the heating profiles set in Figure 8.1. The battery temperature profiles shown follow the expected behaviour according to the cost function. Figure 8.3a has a conservative profile in comparison to full heating and battery optimised heating, saving heat for the cabin then heating the battery at the end of the cycle, starting before the highest speed section. However, Figure 8.5a shows that when the neutral battery heating profile engages in medium heating at the end of the cycle, there is an impact on cabin temperature and the final temperature falls below both of the simple heating profiles. This is done to improve battery performance at the end of the cycle, but if the cycle is nearly finished this decision may not be needed. Before implementation of a strategy like this, there may be the decision to prevent battery heating if it is known that the cycle is about to finish, unless the cycle is unable to finish without the heating.

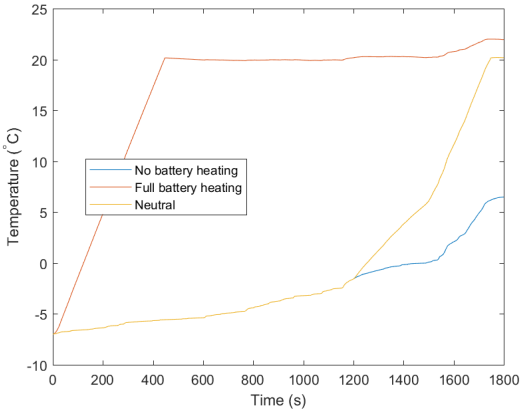

(a) Battery temperature using neutrally optimised trajectory.

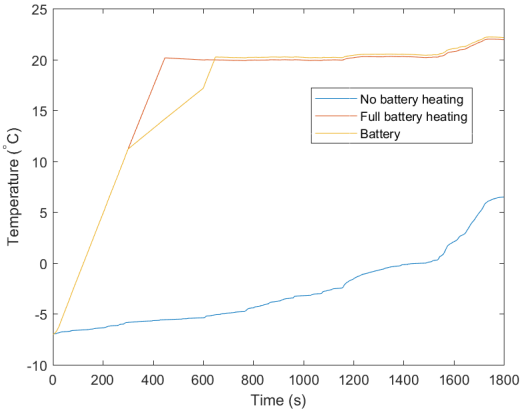

(b) Battery temperature using battery optimised trajectory.

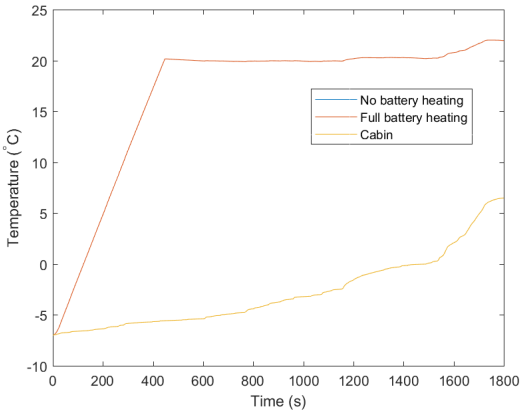

(c) Battery temperature using cabin optimised trajectory.

Figure 8.3: Battery temperature using the optimised control trajectories, seen in Figure 8.1, at $-7°$C.

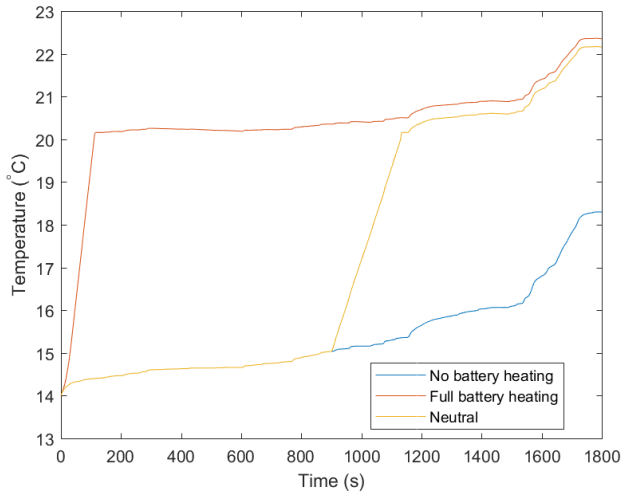

Figure 8.4: Battery temperature using the optimised control trajectory, seen in Figure 8.2, at 14°C.

Table 8.1: Here the metrics are shown corresponding the optimised battery heating profiles shown in Figure 8.1.

Weighting (mode)	Efficiency (Wh/km)	Range (km)	Comfort (mean °C)
No Battery Heating (25)	405.8	116.9	10.9
Full Battery Heating (29)	373.8	140.4	13.1
Neutral	405.5	124.6	12.2
Battery	377.4	136.4	13.2
Cabin	405.8	116.9	10.9

8.4 Discussion

In this chapter the Research Objective "What control can be gained over the balance of comfort and range through the dynamic control of battery heating during a drive cycle" has been addressed. DP was selected to produce a series of optimal battery heating trajectories which minimise the cost function according to the different priorities. These optimal trajectories and the consequences of their implementation on the battery and cabin temperatures were demonstrated in Section 8.3.

The implementation of the optimised battery heating profiles corresponds to the metric changes seen in Tables 8.1 and 8.2 for ambient temperatures of −7°C and 14°C respectively. Here it can be seen that the neutral and cabin optimised profiles have had the desired effect. Table 8.1 shows that a window in range and

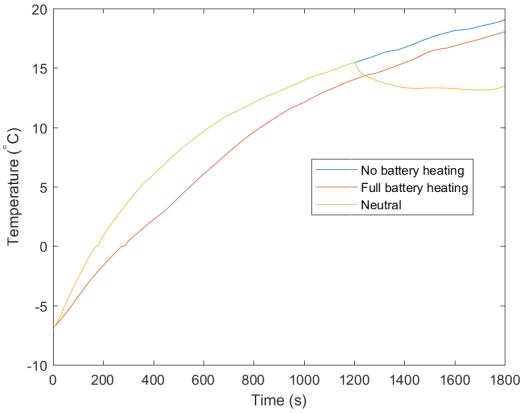

(a) Cabin temperature using neutrally optimised trajectory.

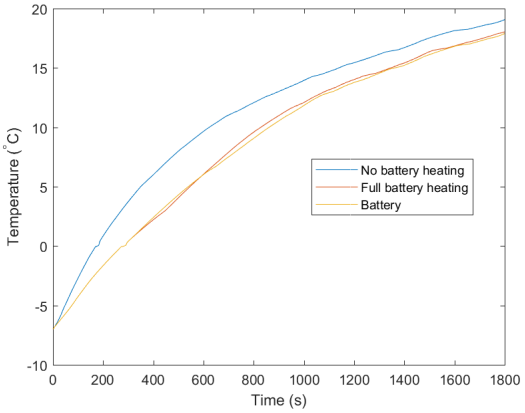

(b) Cabin temperature using battery optimised trajectory.

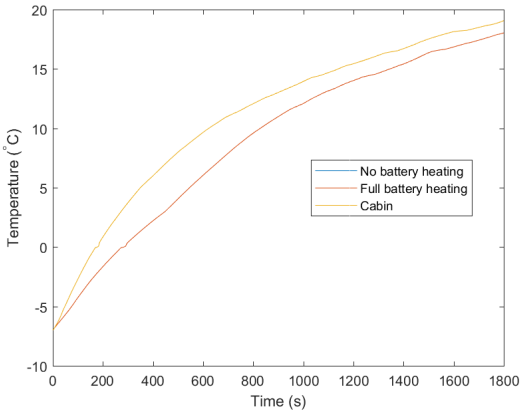

(c) Cabin temperature using cabin optimised trajectory.

Figure 8.5: Cabin temperature using the optimised control trajectory, seen in Figure 8.1, at $-7°C$.

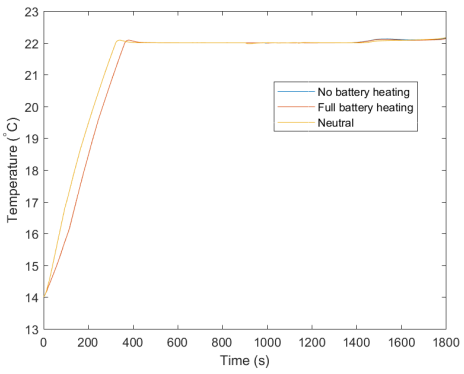

Figure 8.6: Cabin temperature using the optimised control trajectory, seen in Figure 8.2, at 14°C.

Table 8.2: Here the metrics are shown corresponding the optimised battery heating profile shown in Figure 8.2.

Weighting (mode)	Efficiency (Wh/km)	Range (km)	Comfort (mean °C)
No Battery Heating (25)	281.2	189.29	0.64
Full Battery Heating (29)	280.0	191.91	0.8
Optimum	284.2	189.31	0.64

comfort is created by implementing the simple control strategies. This window spans 116.9km to 140.4km and 10.9°C to 13.1°C in range and discomfort respectively. The intention of optimising the heating trajectory of the battery was to prove that the vehicle could operate inside this window. The neutrally optimised profile has created a balance between range and comfort, improving range by 7% compared to the no heating strategy, while improving comfort by 9% in comparison to the full heating strategy. The cabin-prioritised optimal trajectory has reproduced the no heating control strategy, which is to be expected as not heating the battery maximises heat availability for the cabin.

Although the neutrally optimised electric battery heating profile causes a reduction in cabin temperature at the end of the cycle, it is able to improve comfort compared to full battery heating and improve range compared to no battery heating. Not heating the battery at the start of the cycle also allows for maximum thermal perception and brings the cabin away from the minimum temperature quickly. In this respect an import point of consideration should be whether the cabin metric used fully captures thermal comfort. In response to this, a new cost objective is created to investigate the impact on thermal perception. j_3 has been adapted to show the squared difference between the cabin temperature and target temperature, thus creating j_3', which is shown explicitly in Equation 8.2. This is not implemented into the DP algorithm, but is used to demonstrate and investigate how thermal sensation may be perceived.

$$j_3' = \int_{t_0}^{t_{end}} = (22 - T_{cabin})^2 dt \tag{8.2}$$

This new cost metric penalises the discomfort cost more when the cabin temperature is further from target temperature, meaning it will have more impact at the start of the cycle when the cabin is coldest. This will therefore incentivise thermal sensation and thermal response of the system more than the ability to reach cabin target temperature. Implementing this change the new discomfort metric for no heating, full heating and the neutrally optimised trajectory would be 165°C^2, 222°C^2 and 182°C^2 respectively. Hence in terms of thermal response the neutral trajectory has performed 18% better than full battery heating and is 10% less responsive than the no battery heating strategy. In this respect the neutral heating trajectory offers a good balance of providing thermal comfort and sensation. Research into thermal perception in the area of vehicle comfort is highly active [113, 115, 200, 201] and research from Zhange *et al.* [114] indicates that although the cabin temperature drops at the end of the cycle, since the drop in temperature is still within 9.3°C

of the cabin's target temperature, this would not be an issue for 80% of passengers if they were provided with heated seats. However further investigation would need to be made into the energetic consequences of activating the heated seats in this period.

When the optimal control strategy is found according to a cabin priority there is also a $1/3$ battery weighting in the cost function, but Figure 8.1c shows that no battery heating is used when prioritising the cabin. This indicates that any battery heating during the cycle would be too detrimental to cabin temperature to be worth the improved battery performance. If the space between the neutrally optimised heating profile and the no heating profile is to be explored then the cost function weighting needs to be adjusted. Instead of a $2/3$ cabin and $1/3$ battery weighting, perhaps a $3/5$ cabin and $2/5$ battery weighting could be used. This incentivises battery heating more and may result in the smaller sub-window between no heating and the neutrally optimised profile being explored. A similar approach could be taken in the other direction, between neutrally optimised and full heating. These adjustments would allow for further control of the balance between range and comfort within the window created.

Table 8.1 shows that the trajectory which prioritises battery performance improves the range and energy consumption in comparison to the neutral trajectory and the cabin optimised trajectory, but does not improve these metrics compared to full battery heating. In Figure 8.1b it can be seen that the optimal trajectory starts with full heating, then reduces to low heating, before increasing to full heating again. It is clear that the intention of this profile is to exchange some battery performance in the early part of the cycle in exchange for improved comfort. However, it can be seen in Figure 8.5c that the reduction in battery heating in the second time step has a small effect on cabin temperature, then when full heating resumes the cabin temperature drops slightly below the full heating trajectory's cabin temperature. This results in a 0.7% reduction in cabin comfort. Although it is clear what the intention of the optimal trajectory was, the cost matrix has not been able to predict the consequence of this trajectory accurately enough to improve the cost. The cost matrix accuracy can be refined by iteratively improving the reinitialisation of the vehicle by identifying which static parameters should be included. With multiple components interacting with the cabin and defining the cabin temperature this is a likely place where improvements in reinitialisation would create a more accurate cost matrix.

The cost can also be improved by increasing the discretisation of the control. It can be seen in Figure 8.5c that when the battery heating begins the cabin tem-

perature reduces, even when using the lowest battery heating level available. This can be improve in two ways. Firstly, more battery heating levels can be introduced. To produce the control strategy at $-7°$C took three days, so doubling the number of control options extends that to one week. Hence it is important to set the discretisation of the problem according to how much time can be spent producing the cost matrix. Secondly, the time step duration can be discretised further. If the model has no initialisation time and the time required to obtain a result is only proportional to the length of the time step simulated then there is no penalty. In this case the total time required would be defined by;

$$t_{CostMatrix} = N_{ts} \times N_{X_1} \times N_{X_2} \times N_U \times t_{sim}(\propto length\ of\ time\ step). \tag{8.3}$$

Here $t_{CostMatrix}$ is the time to compute the cost matrix, N_{ts} is the number of time steps, N_{X_i} is the number of points to be evaluated in each of the state variables, N_U is the number of control options and t_{sim} is the time required per simulation; which here is directly proportional to the length of the time step simulated. Hence, if the time step length is halved and the number of time steps is doubled, then the time to acquire the cost matrix is the same. However if the initialisation time is a significant proportion of the simulation time and does not reduce with simulation duration, then the time to produce the cost matrix grows. This is the case for the research here and so a reduction in the time step length increases the acquisition time of the cost matrix. The reward for improving time discretisation is a control strategy which can be more precise. For example in Figure 8.2 it may have been preferable to initialise cabin heating 100s earlier or later, but the algorithm is unable to do this because of the current time discretisation of the cost matrix.

Table 8.2 shows that between the full heating strategy and no heating strategy a window in vehicle range of 2.62km is created. The window is small since at 14°C there are only small potential battery gains and small potential HVAC savings to be made. However the optimisation method used has been successful in exploring the space between the two simple strategies. Even in the small window created the new optimised battery heating profile has extended the range while not compromising comfort. This technique has led to an increase in energy consumption compared to the baseline. However, if minimum energy consumption was required for a particular energy efficiency rating or standard then the cost function weighting could be redefined to put more of a priority on energy consumption over DOD and comfort. In the real world a window of this size would be overshadowed by the day

to day variability of driving, such as traffic, driver's mood, precipitation, visibility etc. In this respect, while an optimised battery heating strategy may not have an impact at higher ambient temperatures, its ability to balance range and comfort has still been proven. This ability will be more useful at lower ambient temperatures as demonstrated by the exploitation of the 23.5km window created at $-7°C$.

The method presented here has been used to control the interaction of the electric battery with the heat pump, this was decided as electric battery heating appeared to have the most impact on the cost function in Chapter 7. Had Chapter 7 shown that a different component had more impact on the cost function, the method could be redeployed to control the new components interaction with the heat pump. For example if the cabin were also considered as an optional heat sink, its interaction with the heat pump would have a significant impact on the cost function. In this research, cabin heating has been prioritised, with compromises and improvements coming from other optional interactions with the heat pump. Using the methodology proposed here to create cabin heating trajectories would be another way to control the compromise between comfort and range. This methodology is also applicable at high ambient temperatures where battery cooling is needed to control ageing, however this comes at the expense of extra energy and cabin discomfort. Therefore, it would be desirable to produce optimal cooling trajectories which could balance these factors.

The objective of this chapter was to produce a set of optimal heating trajectories which could be used to tune the thermal management of the battery according to the desired priority of the user, either comfort or range. Tables 8.1 and 8.2 have demonstrated that this is possible. The best example of this is the neutrally optimised heating trajectory in Table 8.1; here it was seen that a balance between range and comfort could be found at $-7°C$.

8.5 Concluding points

- Dynamic programming has been used to create dynamically optimised battery heating trajectories which can balance range and comfort, thereby addressing Research Objective 3.
- At $-7°C$ the neutrally optimised trajectory improved range by 7% compared to not heating the battery, and improved comfort by 9% compared to fully heating the battery at the start of the cycle.

Chapter 9

Conclusion

9.1 How the research question has been answered

The Research Question addressed in this thesis was "In an electric vehicle with a heat pump, how can the combination of potential sources and sinks be systematically compared; hence identifying important components to be controlled to minimise energy consumption, maximise range and maximise comfort?". This has been answered through the creation of a notional optimisation framework which is constructed through the three results chapters. This framework is summarised in Figure 9.1.

The process framework shown in Figure 9.1 could be used by a researcher or designer to develop an optimally thermally managed vehicle. This will produce an optimal split between thermal and electrical storage, which was solved in Chapter 6. Chapter 7 then provides a method for comparing the usefulness of each component and provides a way to identify optimal operational modes for different situations. Finally, Chapter 8 demonstrates how optimal heating trajectories can be found. Paramount to answering the Research Question, by the end of Chapter 8, if the procedure has been followed correctly, the user will have developed a control strategy which can actively balance the trade off between comfort and range.

9.1.1 Achievements of applying the notional optimisation framework

In general the research conducted in this thesis has been benchmarked against a hypothetical vehicle with a 48kWh battery and heat pump capable of using ambient and the electric motors as heat sources, while delivering heat to the battery. Quantitative evaluations of improvements have been made using the WLTP drive

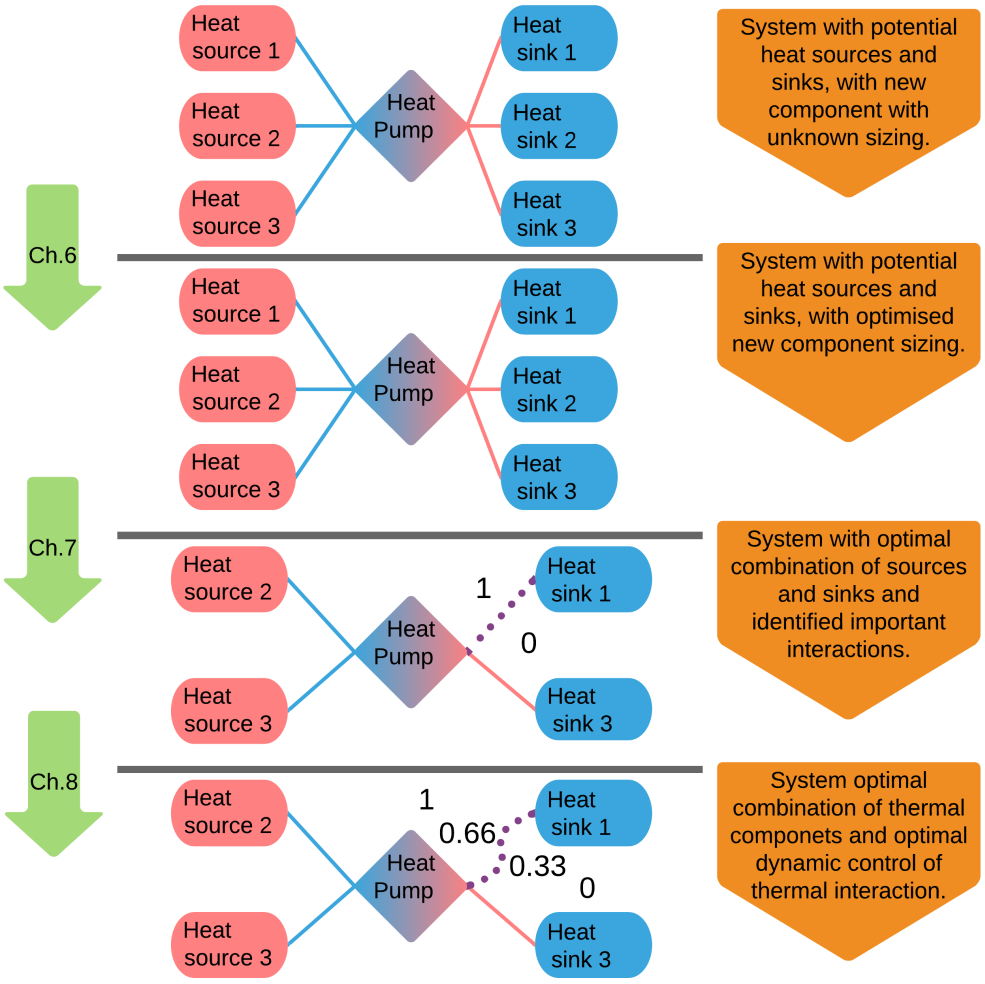

Figure 9.1: Graphical representation of the process created by the methodology and model within this thesis applied to a hypothetical system.

cycle at −15°C to 15°C in 10°C increments. There are two exceptions to this, firstly in Section 6.5 the vehicle was only tested on the WarmUp cycle, for which its energy storage split was optimised. Then in Chapter 8 an alternative baseline was used, based on the results of Chapter 7. In Chapter 8 alternative testing temperatures were also used in recognition of official WLTP testing temperatures. While these sections will be reviewed independently, it is possible to make a broader comparison of the results shown across the rest of Chapters 6 and 7. Figure 9.2 shows the variation in efficiency, range and comfort at key points during Chapters 6 and 7.

Figure 9.2 demonstrates the range in performance that can be achieved by an electric vehicle given different operational modes. This is demonstrated most by the difference in range between respectively operating the vehicle with an optimised thermal battery, while disabling PTC heaters, and operating the vehicle using only PTC heaters. Considering the 'No heat pump' and 'Chapter 6 - No PTC' results, shown in Figure 9.2b, the range is seen to increase by 80%; this has been achieved through reducing the vehicle's dependence on PTC heaters and improving the battery performance. This new low temperature range of 187km represents an 18% range loss compared to the maximum range of 227km found in Chapter 5. Given the expected range reduction is between 40% and 70% in this temperature range, a reduction in deficit to 18% demonstrates progress. However, disabling the PTC heaters did lead to less comfort compared to the implementation of the PTC heaters with the optimally sized thermal battery, which can be seen in Figure 9.2c. At −15°C, −5°C and 5°C, 'Chapter 6 - No PTC' produces the second least comfortable experience. It should be noted that this increase in performance was seen with the addition of 29kg of active material, which would equate to a package size of about 30l. The Jaguar I-Pace has cargo capacity of approximately 1200l, hence the installation of this package would not significantly affect the vehicle. Furthermore it was demonstrated in Chapter 6 that the electric battery could be reduced in size by approximately 10% and replaced with thermal storage, improving comfort and not significantly affecting range at −5°C and above.

Chapter 7 used the optimally sized thermal battery and explored its incorporation into the heat pump system in combination with three other thermal sources and the optional ability to heat the battery. In doing so, operational modes were found which minimised the cost functions according to different priorities. Additionally, it was seen that one mode could sometimes satisfy the optimality conditions for more than one priority; for example, Tables 7.5 to 7.7 showed that at 5°C mode 27, which uses all sources and does not heat the battery, was optimal for all objective function priorities. Since it is not realistic to implement a heat pump system

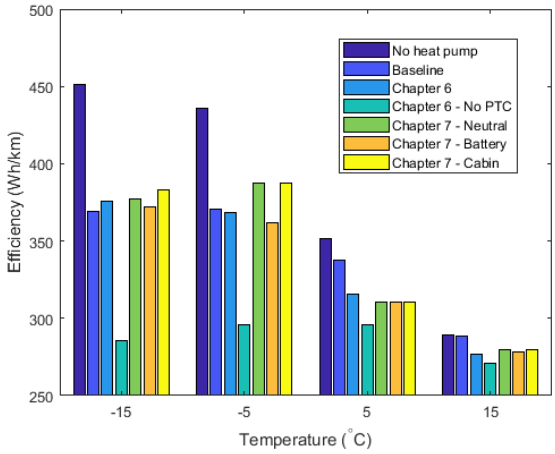

(a) Vehicle Efficiency

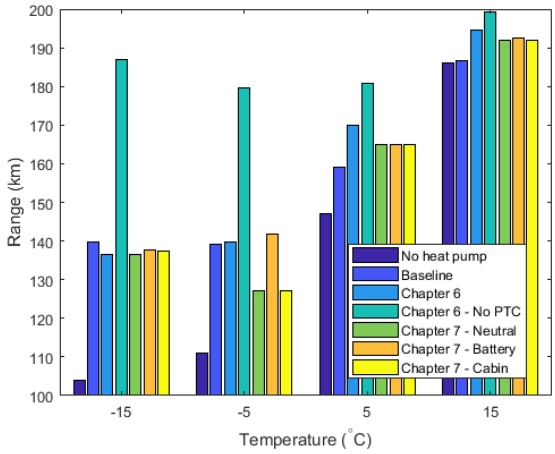

(b) Vehicle Range

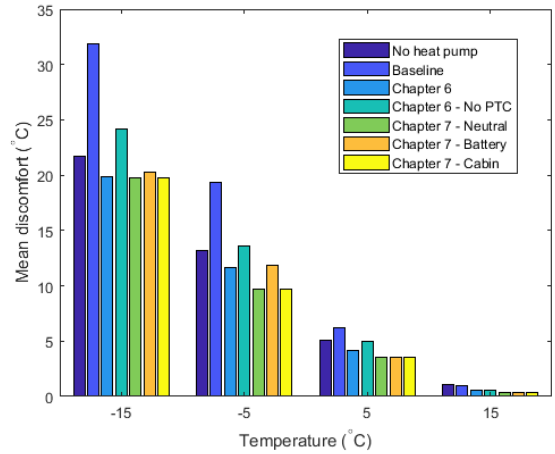

(c) Vehicle Discomfort

Figure 9.2: Improvements and variations in vehicle efficiency, range and comfort achieved across Chapters 6 and 7.

capable of operating in 32 unique heat pump modes according to the environmental and duty cycle demands, it is far more likely that a small number of well performing modes would be selected to cover all conditions. In Chapter 7 it was also seen that when operating on the WLTP drive cycle and prioritising battery performance, battery heating was only used at $-15°C$ and $-5°C$, indicating that it is not worth heating the battery unless it is at $-5°C$ or below. The same was true for the NEDC drive cycle, although on the WarmUp cycle it was only worth heating the battery at $-15°C$. It is likely that above these temperatures the extra cost of heating the battery, in terms of comfort lost and compressor or PTC usage, outweighs any potential range gains from higher battery temperatures.

This generalisation of battery heating applies for the binary heating options, i.e. full battery heating or no battery heating, administered at the start of the cycle. However, Chapter 8 showed that if a dynamic optimisation of battery heating is performed then battery heating can be useful at 14°C. Here it was shown that even when the window of operation was small in comparison to the total range, constituting 1%, the optimisation technique was able to slightly improve range, while not compromising comfort, by waiting until 900s and heating the battery with a low heating setting. At $-7°C$ the operational window between the binary heating strategies was extended to between 116.9km and 140.4km, while the discomfort window extended from 10.9°C to 13.1°C. In this scenario a neutrally optimised heating strategy increased the range by 7% compared to the no heating strategy and increased comfort by 9% in comparison to the full heating strategy.

In general the results have shown that a vehicle with many options of collecting and distributing heat can have a wide range of operational performance at low temperatures. However, by following the notional optimisation framework leading to correctly sized components, the identification of optimal operational modes, and an optimised thermal exchange between components which have the most impact on the cost, the balance of range and comfort can be controlled.

9.2 Research methodology and the model review

Throughout this thesis traditional and proven methodologies have been coupled with a novel model to satisfy the research objectives.

In Chapter 6 a combination of the pattern search algorithm and exhaustive approach were implemented to explore the sizing of a thermal storage system for application in an EV. For the sizing optimisation several search algorithms were considered, including genetic algorithms, Powell's method and the simplex method,

among other more simple methods. It was seen at the start of Chapter 6 that in the region of the global minimum the search space was flat, with small variations in cost being seen over relatively large variations in parameter value. This made the task of finding the global minimum difficult for the search algorithm. The results from the pattern search method suggested that above 25kg (mass), 80°C (charge temperature) and 15kW (thermal power), any further improvements in cost were very small. Now that this result is known it is also possible to know that other search algorithms would likely return the same result, and some would do so in far fewer iterations. If the objective was to find the point of diminishing returns for this problem it may have been more sensible to use a different search algorithm.

For the 1D optimisation performed in Section 6.5 the optimal mass could have been found more quickly, and to greater precision, by using a 1D search algorithm, such as accelerated step. The exhaustive approach was used for two reasons; high precision in mass was not desired and it was deemed important to search the entire space to learn the consequences of trading a high proportion of the electric battery for thermal storage. In this regard, the exhaustive method was the correct approach.

For Chapter 7 it was important that all operational modes be identified and compared. There was therefore no other option than the exhaustive approach. In this chapter consecutive modes had no mathematical relationship and were completely unique and discrete in nature; therefore a traditional search algorithm could not be used to identify the optimal operational mode, and exhaustive simulation was the only option.

In Chapter 8 dynamic programming was identified as the best option for producing an optimised control trajectory. While this is true, due to the curse of dimensionality, dynamic programming can take a long time to generate the cost matrix required for finding optimal solutions. In this time it would be possible to execute hundreds, or even thousands of iterations of test trajectories. By generating and testing enough random battery heating trajectories, it is possible that one, or several could be found with similar performance to the dynamic programming result in the same time period. This should be considered when deciding whether to use dynamic programming. In order to save time in finding optimal profiles, a bank of random profiles could be generated and tested (the number of which could be calculated based on the time it takes to perform a dynamic optimisation) then from this bank of results, it would be possibly to find out how many random profiles need to be tested before results close to DP are achieved. If this number of results takes significantly less time to execute, then randomly generating and trialling optimal trajectories might be a more efficient process.

Confidence in the results and improvements presented can be gained through the validation and description of the model used for this research. Confidence in the model should also be taken from the fact that a paper documenting the model and modelling process was published at a modelling conference [1]. The high level validation of the model against commercially available vehicles, and improvements demonstrated through the addition of a heat pump, show that the improvements found using the model are representative of improvements from real world examples. At 23°C, using the WLTP drive cycle, the model had a range of 227km which was 9% less than a Jaguar I-Pace at the same temperature on the same cycle; this shows an acceptable level of agreement considering the variation in range caused by day to day driving. The model had an efficiency of 243Wh/km which is in good agreement with the range of vehicle efficiencies found for similar electric vehicles (216Wh/km-269Wh/km). The model was demonstrated to have a range reduction of 54% when configured to use the PTC heater only, this was within the 40% to 70% window identified in Chapter 2, indicating its baseline operation is comparable to existing EVs. It was then demonstrated that when the heat pump was active the range improvement varied between 3% and 32% depending on ambient temperature, which was in agreement with the 10% to 30% improvement range identified in Chapter 3 which can be expected when adding a heat pump to a vehicle. In a specific scenario the model used in this thesis produced an efficiency improvement of 15.4% when switching from using the PTC heaters to using the heat pump at −10°C, this showed excellent agreement to a comparable example in literature which reported a 16% improvement in efficiency [131]. Since the improvement in range due to a technology change is verified against literature, any improvements from further technology changes can be treated with confidence.

9.3 How the research objectives were addressed

The first research objective, "What is the optimal sizing of a thermal battery for application in an electric vehicle with a heat pump?" was addressed in Chapter 6. Through the use of pattern search, which is an established optimisation search, the optimal mass, charge temperature and thermal power of the thermal storage device were found to be 29kg, 131°C and 19kW respectively. The use of the optimised thermal storage device improved range between 22.7% and 6% through the temperature range of −15°C to 15°C, compared to operating the vehicle with just the heat pump, as shown in Table 6.29. Hence the optimal sizing of the thermal battery was identified. The process for identifying the optimal sizing of the thermal battery

was also supported in a publication at the Vehicle Power and Propulsion Conference (VPPC) [28].

The second research objective, "What opportunity is there in controlling range and comfort through the systematic comparison and selection of a specific combination of heat sources and sinks?" was addressed in Chapter 7. A process was established for identifying all possible operational modes on an electric vehicle using binary control of the heat sources and sinks. All modes were then compared and the best modes for range, comfort or a balance of both were identified using the cost function and its weightings. Tables 7.12 to 7.15 then showed which mode should be using according to the priority given, and the benefit that could be achieved by using these modes. The process and work presented in Chapter 7 is supported by the publication [27].

The third research objective, "What control can be gained over the balance of comfort and range through the dynamic control of battery heating during a drive cycle?" was addressed in Chapter 8. Dynamic programming was used to produce optimised control trajectories for heating the battery. In doing so it was shown that by correctly timing the heat delivered to the battery it was possible to improve range by 7% compared to not heating the battery, while simultaneously improving comfort by 9% compared to fully heating the battery at the start of the cycle. Hence comfort and range were balanced in comparison to two simple control strategies. It was therefore demonstrated that DP offers the opportunity of controlling range and comfort within a given operational window.

9.4 Contributions to knowledge

The contribution to knowledge provided by this thesis can be summarised by the proposed notional optimisation framework shown in Figure 9.1. Previously the component sizing, configuration and dynamic control process for a complex heat pump with multiple heat sources and sinks had not been established. The thesis provides a process for optimally designing and controlling such a system, with each step in the process using novel approaches which constitute contributions to knowledge.

Before this thesis, research had been conducted into the combination of thermal storage with a heat pump in the automotive setting. Steiner *et al.* [70] and Meyer *et al.* [71] use the electric battery and electric motor respectively to store heat for the heat pump. This work extends upon that by adding a dedicated thermal storage device to the heat pump system. This is supported by the publication [28]. It should also be stated, that Kaygusuz *et al.* [68] implemented thermal storage with

a heat pump, but in a domestic dwelling, and hence the benefit in the automotive setting was unknown. LaClair *et al.* [69] added a dedicated thermal storage device to a vehicle in replacement of the PTC heater, but did not combine the device with a heat pump. In LaClair *et al.*'s work, the sizing of the thermal storage device was calculated based on a direct replacement of the heat which would be provided by the PTC heater. This work provides a more comprehensive sizing methodology which can also be used to evaluate the point of diminishing returns. Hence the contribution of Chapter 6 is the new application of a dedicated thermal storage device in combination with a heat pump, along with a novel approach to its sizing and the analysis of its sizing.

Previously multiple operational modes have been identified for a heat pump with different potential heat sources, the list of combinations was summarised in Table 3.3. However, Leighton [24], Kim *et al.* [72] and Lee *et al.* [66] tested their heat pumps in a single mode, making comparisons to PTC heaters only. Ahn *et al.* [67], Steiner *et al.* [70] and Meyer *et al.* [71] demonstrated their heat pumps in competing operational modes, but were all limited to one variation in the sources of their system. Ahn *et al.*'s [67] was the most comprehensive, comparing a heat pump in three modes; ambient only, waste heat only and waste heat plus ambient. This exhaustive approach has been extended to all suggested heat pump thermal source options, along with the option to heat the battery. Hence this extends upon the work of many, by comparing thirty two operational modes on a single system. This contribution was supported by [27]. Furthermore, developing a model with the capability of being reconfigured to support the thirty two operational modes identified shows a novelty in itself as confirmed by [1].

Dynamic programming is an established technique in optimising the split of electrical and ICE power in hybrid vehicles, with examples of its use including Perez *et al.* [154], Wang *et al.* [155] and Sundstrom̈ *et al.* [195]. Dynamic programming had also been applied to battery cooling in high temperature climates by Shojaei *et al.* [73]. This works extends upon the work of Shojaei *et al.* [73] by applying DP to the low temperature domain.

9.5 Reflections

In this section some changes to the methodology are contemplated with the benefit of hindsight. Although the methodology and results presented in this thesis are believed to be sound the suggestions posed here could have increased the impact of results, or improved the efficiency of certain methods used. It is therefore important

that should others be interested in revisiting these areas they consider the points highlighted here.

The focus of this work was on the balance of range and comfort as these were the two factors of most concern to EV users in low temperature climates. However, in an attempt to include the HVAC energy consumption, the total power consumption of the vehicle was also included in the cost function. Upon reflection this seems unnecessary as it convolutes the cost function and increases the complexity of understanding the results. Using only range and comfort as the key performance indicators may have simplified the results and parts of the method without losing impact on improving the user experience.

The results of each chapter of this thesis would be heavily influenced by the type of EV being tested. With a small battery size requiring more thermal management, and a larger battery size involving less. If time constraints had permitted it would have been beneficial to duplicate some results for the case of a vehicle with half and/or double the battery sizing.

In Chapter 6 the pattern search algorithm was identified as one of the best search algorithms for the task of optimising the thermal battery design parameters. It was also highlighted that other algorithms may have performed equally well. It is therefore suggested that instead of using the pattern search algorithm from the outset, a trial run of optimisation algorithms could have been made. This would have allowed for the best option to be found for this specific problem. However, when performing this test one must consider whether the time spent running the test could be saved through the use of the most efficient algorithm. Unless many tens of different scenarios are to be optimised it may be the case that the researcher is better off picking a search algorithm and sticking to it, rather than spending extra time in testing.

Due to the complexity of DP, and the time taken to find results, there might have been an opportunity to get results more quickly, and explore a wider range of control trajectories by adopting a "brute force" approach and evaluating a large number of random control trajectories. This would have had the additional benefit of providing much more data to work with, and allow for data analysis similar to that performed in Chapters 6 and 7.

Chapter 10

Further work

Although this thesis demonstrated progress in maximising the thermal potential of electric vehicles there is still much work to be done in the area. In Section 10.1, focus is given to how this work can be used if the physical challenge changes and battery technology changes such that different operating conditions are preferred. The work within this thesis could also be adapted to address challenges of high temperature operation, this is discussed in Section 10.2. Finally the direction one should take if they wish to extend the work of this thesis is discussed in Section 10.3.

10.1 Technology change challenge

In Chapter 2 the notion of different battery chemistries changing the engineering challenge was discussed. In Section 2.1.1 solid-state electrolytes such as $LiBH_4$ were identified as an emerging technology which may replace conventional liquid electrolytes. $LiBH_4$ has an operating temperature of 120°C, and so the challenge in operating the vehicle changes significantly. In this case it seems unlikely that heating the battery from an ambient temperature would be possible at the start of the cycle as the battery would take too long to warm and use too much internal energy. A likely solution would be to keep the battery at a high operating temperature during the charging phase. This means that the challenge in Chapter 6 changes as the thermal storage would not be required to heat the electric battery, hence a much smaller thermal battery would be likely to result from the optimisation process.

In Chapter 7 the battery was an optional heat sink in the thermal management modes. If the battery technology changes such that the electrical storage device no longer needs thermal management then it may be removed as an option for the thermal management system, i.e. Chapter 7 would only consider the four heat

sources and resulting sixteen operational modes. However, if the new technology still needs thermal management then the method used in Chapter 7 is unchanged.

In its current form Chapter 8 would become obsolete if a new battery technology was agnostic to temperature. However, in this case the methodology could be adjusted slightly, and instead of optimising the heat delivered to the battery, the task would become the optimal heat delivery to the cabin. In this case the cabin thermal comfort would be considered more directly, considering more carefully what is an acceptable level of cabin heating and how to maximise range.

The changes described in this section demonstrate that the notional framework proposed is robust to changes in technology. Even if a battery technology is developed where its operation is completely independent of its temperature, the cabin will still need to be heated in an efficient manner to maximise range.

10.2 High ambient temperature challenge

In a similar way to how the thesis is robust to technology changes, the notional framework can also be adapted for high ambient temperature challenges. For example, in Chapter 6 heat is stored in the thermal battery to quickly heat the coolant at the beginning of the cycle. In a hot climate the high temperature phase change material can be replaced with a low temperature equivalent, for instance water. When the vehicle is plugged-in the water would be frozen by running the refrigeration system, then when the vehicle starts its journey there is a large cold heat sink to buffer the air conditioning system. The sizing of this unit would need to be optimised with the same objectives as used in Chapter 6 and so the same method could be used.

The method shown in Chapter 7 can also be adapted to be useful in high temperature challenges. In a high temperature climate it is necessary to cool the battery to prevent excessive ageing, and so the method would need to be adapted so that the battery is used as a sink, rather than a source. It is likely that the motor and transmission would no longer be considered in this method as their waste heat is no longer useful. Finally, the cabin exhaust could be used as a heat sink as the cabin air would be colder than the ambient air, providing an additional source of cooling. The effect of this change is that the number of component interactions with the heat pump falls to three (low temperature thermal battery, electric battery cooling and cabin exhaust heat sink), equating to eight operational modes to be evaluated and compared.

Finally in Chapter 8 the challenge is changed from sharing the heating capacity between the cabin and battery to sharing the cooling capacity between the

cabin and battery. This can be achieved using the same methodology, but swapping the heating demand to the battery to a cooling demand. Alternatively, like with a change in cell technology, the focus could be on creating optimised cooling trajectories for the cabin.

10.3 Subsequent research steps.

One of the limitations of the method proposed is the computational effort required to generate the data necessary to produce optimised battery heating trajectories. If this were to be implemented and used on a real vehicle, a much higher fidelity model, validated against a real vehicle, would be needed. This research was theoretical, validated against general electric vehicle behaviour described in Chapters 1 to 3 and demonstrated in Chapter 5. If a higher fidelity model were used, it is likely the computational time per simulation would be much longer, hence taking much longer to reproduce the results shown here. If much greater computational resources were available this may not be a problem. However, as Chapter 4 explains, DP produces optimal trajectories specific to the initial conditions given. The implementation of DP results is achieved through pattern recognition in the optimal profiles and implementation of a rule based controller. For example, Zhang *et al.* used DP to minimise energy consumption on an electric bus by optimally shifting gears and controlling the torque split between front and rear motors [202]. Once a set of optimal trajectories were produced the authors used the results to inform rule based controllers, creating speed thresholds for gear shifts etc. Any controller which is made to imitate the results of DP is not optimal.

The ideal solution would be to produce dynamically optimised trajectories for the predicable future as the vehicle operates, i.e. if the satellite navigation was in use, or the route is commonly and predictably driven, such as commuting. This is clearly limited by the time required to produce optimised trajectories. One method to reduce this time would be the use of a self learning neural network (NN). This is a mathematical model of linear equations which represents the system. Due to its simple nature, thousands of model evaluations can be made per second which significantly reduces the time required for dynamic optimisation. The self learning nature of the NN means that coefficients and weightings are updated and improved using live data from the vehicle, keeping the model accurate over the vehicle's lifetime. The NN could then be paired with a control technique known as model predictive control (MPC). MPC has previously been considered for use as a controller. It is similar to a PID controller but is capable of producing multiple

control outputs based on multiple state variables. Here the MPC is attempting to produce control trajectories which minimise the difference between a state variable value after the control and a target state variable value, for example moving a robot arm. MPCs have been repurposed to minimise an objective function. For example, Esen *et al.* [203] uses MPC to control heater core power, PTC power and engine power in a hybrid vehicle to minimise fuel consumption. Here a simple mathematical model was used, which would be substituted for an NN in a more complex system.

Developing an NN and combining it with MPC would be a challenging piece of research, but would bridge the gap between the method implemented in this thesis and an implementable controller on a vehicle. It is suggested that anyone interested in pursuing this course of action would start be replicating the achievements of Chapter 8 using an NN-MPC based technique, then expand the NN and MPC to perform the same task but for all thermally active components simultaneously. This would represent the pinnacle of thermal management possibilities.

One of the next steps in using this work should be considering implementation; although the NN-MPC approach describes a likely best implementation approach, this would not immediately be applied to a vehicle. Instead the thermal management strategies should be bench tested using a physical test rig. One way to make this achievable is to build a rig similar to the one presented by Leighton *et al.* [24] but with the capability to recreate the system shown in Figure 5.1 from Section 5.1. Once this rig is built the vehicle could be computationally modelled and linked to the physical rig in a hardware in loop set up, as demonstrated by Chowdhury *et al.* [131]. This next step brings the research demonstrated in this thesis closer to an implementable reality.

Appendix A

Direct Search Methods

In this appendix procedural background information is given on the search algorithms introduced in Chapter 4 and used in Chapter 6.

One of the simplest methods available is called grid search. In this method the entire parameter space is divided into the desired optimisation resolution and the objective function is evaluated at every point. The point with the lowest objective function value is then chosen as the optimal solution. The benefits of this method are the simplicity and the resilience to finding local minima. The shortcomings are the number of iterations required to complete a search at the desired resolution. For example, if the resolution required is corresponds to 1% of the control variable constrained range, and the control vector is comprised of three variables, then 10^6 iterations are needed. By comparison, more sophisticated techniques, with forthcoming descriptions, take in the region of 10^2 iterations to converge.

Random searches are also simple optimisation algorithms. There are two types of random search algorithm; random jump and random walk. Random jump operates in a similar way to grid search in that a finite number of trial points are generated and and trialled; the difference is that rather than systematically generating the evaluation points, random jump uses a random number generator to produce a set of trial points. This can produce similar results to grid search in fewer evaluations, making it more efficient, but it is less able to find precise locations of minima. Random walk uses a randomised starting location, then takes a defined step in a random search direction. If the new location has a lower cost the algorithm moves and the search is repeated. If the cost has not improved after the step then the algorithm stays at the original point and tries a new direction. This is more efficient than random jump, but can take lots of iterations to converge precisely on the minimum. Random walk can be improved by using a one dimensional optimisation

method to set the step length when a preferable direction has been found. This is usually the accelerated step search. The accelerated step search finds the cost at $X_0 + s$, where X_0 is the starting point and s is the defined step length, then if the cost is preferably it will try $X_0 + 2s$, then $4s$, then $8s$, until the new cost is no longer preferable. When it has found the highest multiple of s, say 8 for example, the search restarts at the point defined by $X_0 + 8s$, i.e. the next point will be $X_0 + 8s + s$. This is repeated until the cost at the found point is less than the cost at the found point + the smallest step, i.e. $J(X_n) < J(X_n \pm s)$. This is a common and efficient way to preform direct searches in 1 dimension [5].

The univarient method is a more systematic approach to searching cost functions. This method performs one dimensional optimisations, such as accelerated step search, in each of the problem's control vector directions. Once it has searched all directions and found a new point with a lower cost, the search is repeated. This is continued until the minimum is found. This method is generally faster than random and grid approaches, but can oscillate around the minimum, inhibiting or sometimes preventing convergence. Steep valleys are also likely to prevent convergence [5].

Pattern search is an improved variant of the univarient method. From an initial guess, X_0, the pattern search algorithm performs a 1-dimensional optimisation in each of the n available search directions, where n is the number of control variables. At the start of the algorithm the n search directions are defined along each of the control variables. This is the same as the univarient method, however, once each has been explored the first direction is replaced with the direction defined by subtracting X_0 from the location reached after the first n searches. This new, more favourable direction better guides the search, improving the time to convergence and general robustness to steep valleys and oscillations. Every time n searches have been competed another direction is replaced with the pattern direction. This progressively builds a better set of search directions based on the previous pattern [4,5].

Powell's method further improves upon the pattern search method. Powell's method uses conjugate directions [1]. This method works well if the problem can be approximated well as a quadratic near the minimum. The details of this method, and the calculation of conjugate directions can be found in [5].

Genetic, or evolutionary, algorithms are intended to resemble the natural selection process found in biology. A population of test points are associated to each other through identity genes. The population adapts and mutates in a probabilistic fashion, with each subsequent generation retaining the fittest (lowest cost)

[1] S_i are conjugate directions if $S_i^T A S_j = 0$ for $i = 1, 2, ..., n$ and $j = 1, 2, ..., n$ and A is a symmetric matrix describing a quadratic function in n dimensions.

members of the population thereby converging on the global minima. It is recommended that the population starts with 50-100 members to prevent failure due to bias by the lowest cost individuals, which can lead to a high number of iterations if many generations are need before the finishing criteria is met [4]. One of the key advantages of genetic engineering is that the each generation can be evaluated in parallel, opposed to other methods where information about the current point is required to make the next guess, leading to a serial type search. If the problem can be evaluated on a computer system with many physical cores (or a graphics card), then this can speed up the search process as the entire generation can be evaluated simultaneously. However, computer system has limited cores for running simulations then this is no more efficient than other search algorithms [6].

Finally Nelder-Mead simplex algorithm is a much faster but more complicated method [4]. In this method an n dimensional shape known as the simplex, with $n + 1$ vertices is created, where n is the number of control variables. The objective function is evaluated at each vertex then the one with the highest objective function value is identified. A better location for that vertex is found by moving along the line defined by the vertex's original location and the centre of the simplex. The procedure is then repeated by identifying the new worst vertex and shifting it to a better position; the result of which is an expanding, contracting, rotating and transforming simplex which locates and contracts about the optimum control variables. This method is much quicker than grid search, requiring far fewer iterations to complete. Its drawback however, is that the simplex can stagnate and become trapped in an endless cycle, making this method unreliable [5].

Appendix B

Complete set of thermal battery optimisation figures

In this appendix the full set of cost function sensitivity Figures are presented corresponding to the Figures shown in Section 6.4.7. These figures are generated using a log of all the points which the pattern search algorithm passed through when optimising the design parameters of the thermal battery in Chapter 6.

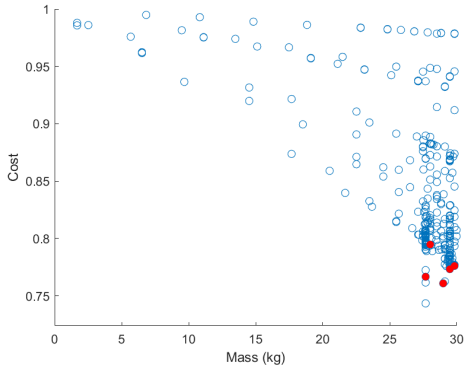

(a) Sensitivity to mass at −15°C ambient.

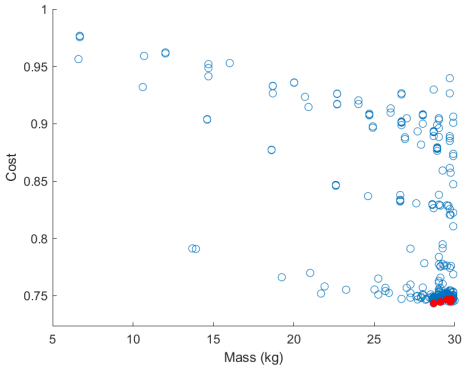

(b) Sensitivity to mass at −5°C ambient.

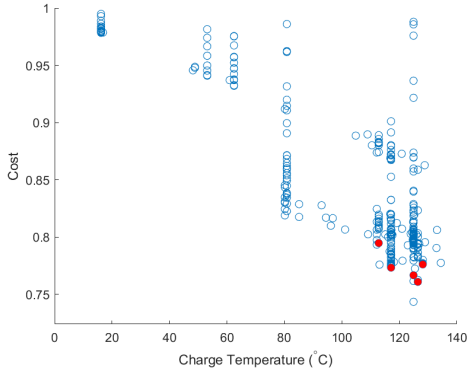

(c) Sensitivity to charge temperature at −15°C ambient.

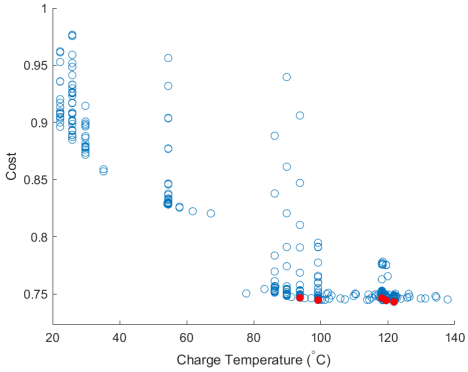

(d) Sensitivity to charge temperature at −5°C ambient.

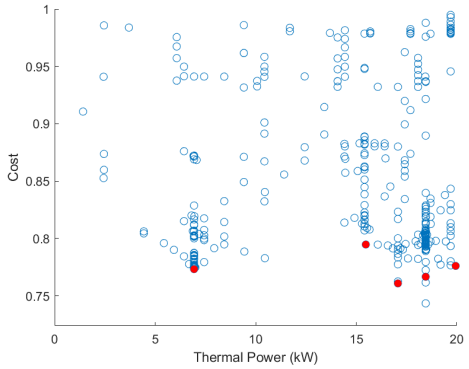

(e) Sensitivity to power at −15°C ambient.

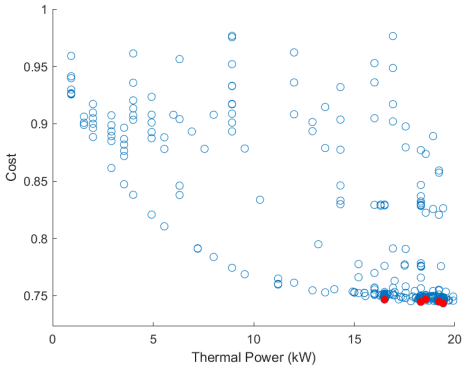

(f) Sensitivity to power at −5°C ambient.

Figure B.1: Sensitivity analysis from optimisation history, −15°C and −5°C ambient temperatures. Blue dots show each point evaluated in the five passes, red points show the optimum point found at the end of each of the five passes.

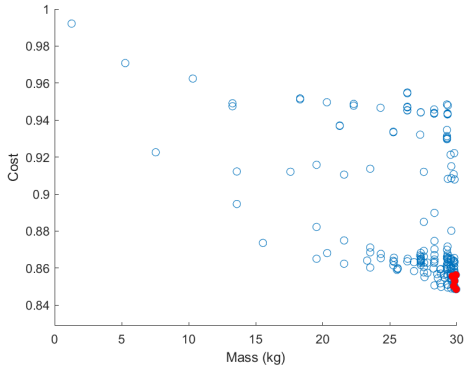

(a) Sensitivity to mass at 5°C ambient.

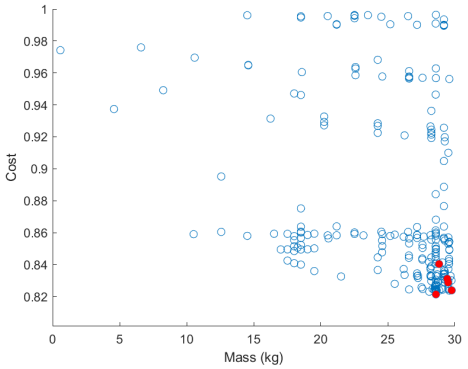

(b) Sensitivity to mass at 15°C ambient.

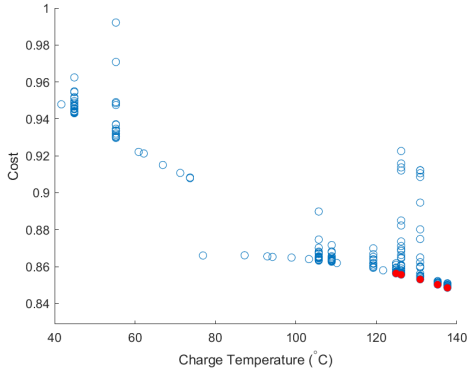

(c) Sensitivity to charge temperature at 5°C ambient.

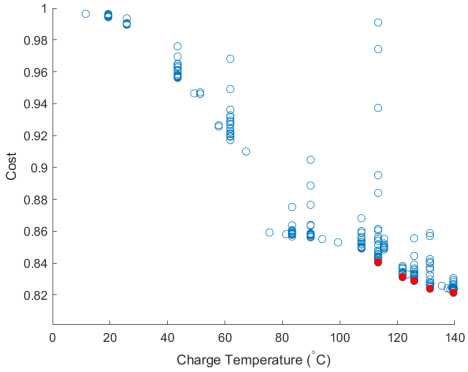

(d) Sensitivity to charger temperature at 15°C ambient.

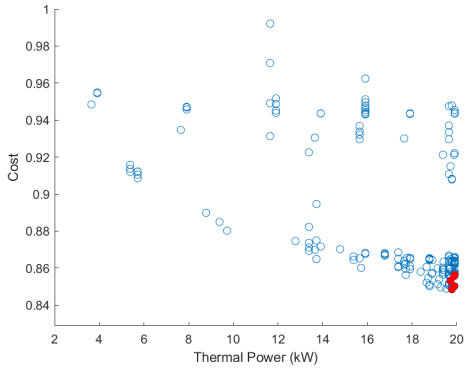

(e) Sensitivity to power at 5°C ambient.

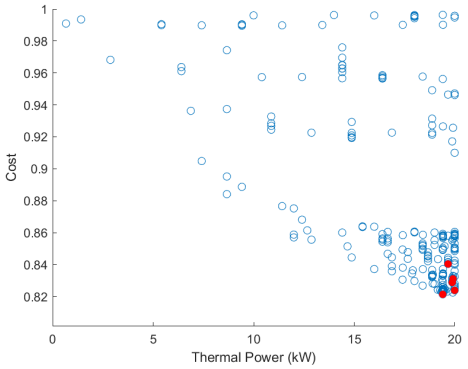

(f) Sensitivity to power at 15°C ambient.

Figure B.2: Sensitivity analysis from optimisation history, 5°C and 15°C ambient temperatures. Blue dots show each point evaluated in the five passes, red points show the optimum point found at the end of each of the five passes.

Bibliography

[1] J. Jeffs, A. McGordon, A. Picarelli, S. Robinson, and W. D. Widanage, "System level heat pump model for investigations into thermal management of electric vehicles at low temperatures." in *Proceedings of the 13th International Modelica Conference, Regensburg, Germany, March 4–6, 2019*, no. 157. Linköping University Electronic Press, 2019.

[2] http://www.engineeringtoolbox.com/, accessed 05/10/2016.

[3] "Tesla model s p100d," https://ev-database.uk/car/1075/Tesla-Model-S-P100D, 2017, accessed 05/12/2018.

[4] L. M. Rios and N. V. Sahinidis, "Derivative-free optimization: a review of algorithms and comparison of software implementations," *Journal of Global Optimization*, vol. 56, no. 3, pp. 1247–1293, 2013.

[5] S. S. Rao, *Engineering optimization: theory and practice*. John Wiley & Sons, 2009.

[6] M. Kumar, M. Husain, N. Upreti, and D. Gupta, "Genetic algorithm: Review and application," *Available at SSRN 3529843*, 2010.

[7] G. Nagasubramanian, "Electrical characteristics of 18650 li-ion cells at low temperatures," *Journal of applied electrochemistry*, vol. 31, no. 1, pp. 99–104, 2001.

[8] S. Zhang, K. Xu, and T. Jow, "The low temperature performance of li-ion batteries," *Journal of Power Sources*, vol. 115, no. 1, pp. 137–140, 2003.

[9] Y. Ji, Y. Zhang, and C.-Y. Wang, "Li-ion cell operation at low temperatures," *Journal of The Electrochemical Society*, vol. 160, no. 4, pp. A636–A649, 2013.

[10] J. Jaguemont, L. Boulon, Y. Dubé, and D. Poudrier, "Low temperature discharge cycle tests for a lithium ion cell," in *2014 IEEE Vehicle Power and Propulsion Conference (VPPC)*. IEEE, 2014, pp. 1–6.

[11] *Superior Lithium Polymer Cell: Technical Data Sheet*, Dow Kokam, 9 2010.

[12] *Lithium Ion NCR18650*, Panosonic, 2012.

[13] *Lithium Ion NCR18650BF*, https://www.batteryspace.com/prod-specs/NCR18650B.pdf, Panosonic, 2017, accessed: 06/05/2020.

[14] R. Korthauer, *Lithium-ion batteries: basics and applications*. Springer, 2018.

[15] H. Budde-Meiwes, J. Drillkens, B. Lunz, J. Muennix, S. Rothgang, J. Kowal, and D. U. Sauer, "A review of current automotive battery technology and future prospects," *Proceedings of the Institution of Mechanical Engineers, Part D: Journal of Automobile Engineering*, vol. 227, no. 5, pp. 761–776, 2013.

[16] M. Broussely, "Battery requirements for hevs, phevs, and evs: an overview," *Electric and Hybrid Vehicles: Power Sources, Models, Sustainability, Infrastructure and the Market*, pp. 305–347, 2010.

[17] Y. Zhang, C.-Y. Wang, and X. Tang, "Cycling degradation of an automotive lifepo 4 lithium-ion battery," *Journal of Power Sources*, vol. 196, no. 3, pp. 1513–1520, 2011.

[18] S. Tippmann, D. Walper, L. Balboa, B. Spier, and W. G. Bessler, "Low-temperature charging of lithium-ion cells part i: Electrochemical modeling and experimental investigation of degradation behavior," *Journal of Power Sources*, vol. 252, pp. 305–316, 2014.

[19] A. Enthaler, T. Weustenfeld, F. Gauterin, and J. Köhler, "Thermal management consumption and its effect on remaining range estimation of electric vehicles," in *2014 International Conference on Connected Vehicles and Expo (ICCVE)*. IEEE, 2014, pp. 170–177.

[20] "Cbe thermal comfort tool," https://comfort.cbe.berkeley.edu/, accessed 16/05/2020.

[21] N. Meyer, I. Whittal, M. Christenson, and A. Loiselle-Lapointe, "The impact of the driving cycle and climate on electrical consumption and range of fully electric passengers vehicles," in *Proceedings of EVS*, vol. 26, 2012.

[22] J. R. M. D. Reyes, R. V. Parsons, and R. Hoemsen, "Winter happens: The effect of ambient temperature on the travel range of electric vehicles," *IEEE Transactions on Vehicular Technology*, vol. 65, no. 6, pp. 4016–4022, 2016.

[23] A. Biaou and M. Bernier, "Achieving total domestic hot water production with renewable energy," *Building and Environment*, vol. 43, no. 4, pp. 651–660, 2008.

[24] D. Leighton, "Combined fluid loop thermal management for electric drive vehicle range improvement," *SAE International Journal of Passenger Cars-Mechanical Systems*, vol. 8, no. 2015-01-1709, 2015.

[25] R. A. Taylor, C.-Y. Chung, K. Morrison, and E. R. Hawkes, "Analysis and testing of a portable thermal battery," *Journal of Thermal Science and Engineering Applications*, vol. 6, no. 3, p. 031004, 2014.

[26] https://www.sunamp.com/wp-content/uploads/2017/09/Fast-Engine-Warm-Up-EV-air-heating-dehumidification-leaflets.pdf.

[27] J. Jeffs, A. McGordon, A. Picarelli, S. Robinson, Y. Tripathy, and W. Widanage, "Complex heat pump operational mode identification and comparison for use in electric vehicles," *Energies*, vol. 11, no. 8, p. 2000, 2018.

[28] J. Jeffs, A. McGordon, W. D. Widanage, S. Robinson, and A. Picarelli, "Use of a thermal battery with a heat pump for low temperature electric vehicle operation," in *2017 IEEE Vehicle Power and Propulsion Conference (VPPC)*, Dec 2017, pp. 1–5.

[29] M. A. Roscher, W. Leidholdt, and J. Trepte, "High efficiency energy management in bev applications," *International Journal of Electrical Power & Energy Systems*, vol. 37, no. 1, pp. 126–130, 2012.

[30] C. Brand, "The health costs of air pollution from cars and vans," 2018.

[31] "Hybrid electric vehicle (hev) and electric vehicle (ev) terminology," http://standards.sae.org/j1715_201410/, 2014, accessed 05/10/2016.

[32] "Stats of the week: Us & calif. ev sales vs hybrids 2011-2017," http://evadoption.com/stats-of-the-week-us-calif-ev-sales-vs-hybrids-2011-2017/, 2018, accessed 28/11/2018.

[33] E. Tate, M. O. Harpster, and P. J. Savagian, *The electrification of the automobile: from conventional hybrid, to plug-in hybrids, to extended-range electric vehicles*. SAE, 2008, vol. 1.

[34] https://www.mitsubishi-motors.com/, accessed 16/05/2020.

[35] S. Saxena, C. Le Floch, J. MacDonald, and S. Moura, "Quantifying ev battery end-of-life through analysis of travel needs with vehicle powertrain models," *Journal of Power Sources*, vol. 282, pp. 265–276, 2015.

[36] "Zapmap," https://www.zap-map.com/, 2020, accessed 10/01/2020.

[37] "Polar," https://polar-network.com/live-map/, 2020, accessed 10/01/2020.

[38] P. Revereault, C. Rouaud, and A. MarchI, "Fuel economy and cabin heating improvements thanks to thermal management solutions installed in a diesel hybrid electric vehicle," SAE Technical Paper, Tech. Rep., 2010.

[39] M. Shams-Zahraei, A. Z. Kouzani, S. Kutter, and B. Bäker, "Integrated thermal and energy management of plug-in hybrid electric vehicles," *Journal of power sources*, vol. 216, pp. 237–248, 2012.

[40] S. Shahidinejad, E. Bibeau, and S. Filizadeh, "Design and simulation of a thermal management system for plug-in electric vehicles in cold climates," SAE Technical Paper, Tech. Rep., 2012.

[41] R. B. Farrington, R. Anderson, D. M. Blake, S. D. Burch, M. R. Cuddy, M. A. Keyser, and J. P. Rugh, "Challenges and potential solutions for reducing climate control loads in conventional and hybrid electric vehicles," *National Renewable Energy Laboratory, Golden, CO, USA, Download from: www. ott. doe. gov/coolcar/pubs. html*, 1999.

[42] S. S. Williamson, "Electric drive train efficiency analysis based on varied energy storage system usage for plug-in hybrid electric vehicle applications," in *Power Electronics Specialists Conference, 2007. PESC 2007. IEEE.* IEEE, 2007, pp. 1515–1520.

[43] Z. Qi, "Advances on air conditioning and heat pump system in electric vehicles–a review," *Renewable and Sustainable Energy Reviews*, vol. 38, pp. 754–764, 2014.

[44] Y. H. Shin, S. K. Ahn, and S. C. Kim, "Performance characteristics of ptc elements for an electric vehicle heating system," *Energies*, vol. 9, no. 10, p. 813, 2016.

[45] T. Waldmann, M. Wilka, M. Kasper, M. Fleischhammer, and M. Wohlfahrt-Mehrens, "Temperature dependent ageing mechanisms in lithium-ion batteries–a post-mortem study," *Journal of Power Sources*, vol. 262, pp. 129–135, 2014.

[46] V. Zinth, C. v. Lüders, M. Hofmann, J. Hattendorff, I. Buchberger, S. Erhard, J. Rebelo-Kornmeier, A. Jossen, and R. Gilles, "Lithium plating in lithium-ion batteries at sub-ambient temperatures investigated by in situ neutron diffraction," *Journal of Power Sources*, vol. 271, pp. 152–159, 2014. [Online]. Available: http://www.sciencedirect.com/science/article/pii/S0378775314012233

[47] M. Petzl, M. Kasper, and M. A. Danzer, "Lithium plating in a commercial lithium-ion battery–a low-temperature aging study," *Journal of Power Sources*, vol. 275, pp. 799–807, 2015.

[48] D. Kundu, E. Talaie, V. Duffort, and L. F. Nazar, "The emerging chemistry of sodium ion batteries for electrochemical energy storage," *Angewandte Chemie International Edition*, vol. 54, no. 11, pp. 3431–3448, 2015.

[49] U. of Concerned Scientists, "Do electric vehicles work in cold temperatures?" https://www.ucsusa.org/clean-vehicles/electric-vehicles/cold-weather-electric-cars-batteries#.XAAHWWj7SUk, 2018, accessed 03/12/2018.

[50] F. Lambert, "Electric car range is affected by extreme cold, but at least the cars can start," https://electrek.co/2018/01/02/electric-car-range-affected-extreme-cold-they-start/, 2018, accessed 03/12/2018.

[51] J. Kelly, "An inconvenient truth: How much does cold weather reduce an electric car's range?" https://leasing.com/car-leasing-news/electric-vehicle-range-in-winter/, 2018, accessed 03/12/2018.

[52] "Electric car vs. winter," http://www.mrmoneymustache.com/2017/10/06/electric-car-vs-winter/, 2017, accessed 03/12/2018.

[53] J. Voelcker, "Five electric cars tested in cold norwegian winter: how did they do?" https://www.carreports.com/news/1115893_five-electric-cars-tested-in-cold-norwegian-winter-how-did-they-do, 2018, accessed 03/12/2018.

[54] ——, "Driving electric cars in winter: tips from experienced owner," https://www.greencarreports.com/news/1109449_driving-electric-cars-in-winter-tips-from-experienced-owner, 2018, accessed 03/12/2018.

[55] D. Booth, "Motor mouth: The inconvenient truth about evs in cold weather," https://driving.ca/tesla/auto-news/news/314908, 2018, accessed 03/12/2018.

[56] B. Howard, "Why do electric cars suck in cold weather?" http://www.mister-auto.co.uk/en/heater/nissens-73002_g467_a12373002.html, 2013, accessed 03/12/2018.

[57] "Rapidgate," https://www.electrive.com/2018/04/08/leaf-drivers-complain-of-rapidgate/, 2020, accessed 10/01/2020.

[58] T. a. Stuart and a. Hande, "Hev battery heating using ac currents," *Journal of Power Sources*, vol. 129, no. 2, pp. 368–378, 2004.

[59] H. S. Song, J. B. Jeong, B. H. Lee, D. H. Shin, B. H. Kim, T. H. Kim, and H. Heo, "Experimental study on the effects of pre-heating a battery in a low-temperature environment," *2012 IEEE Vehicle Power and Propulsion Conference, VPPC 2012*, pp. 1198–1201, 2012.

[60] J. Jaguemont, L. Boulon, Y. Dubé, and F. Martel, "Thermal management of a hybrid electric vehicle in cold weather," *IEEE Transactions on Energy Conversion*, vol. 31, no. 3, pp. 1110–1120, 2016.

[61] Y. Ji and C. Y. Wang, "Heating strategies for li-ion batteries operated from subzero temperatures," *Electrochimica Acta*, vol. 107, pp. 664–674, 2013. [Online]. Available: http://dx.doi.org/10.1016/j.electacta.2013.03.147

[62] A. Pesaran, A. Vlahinos, and T. Stuart, "Cooling and preheating of batteries in hybrid electric vehicles," in *6th ASME-JSME Thermal Engineering Joint Conference*. Citeseer, 2003.

[63] R. A. Barnitt, A. D. Brooker, L. Ramroth, J. Rugh, and K. A. Smith, "Analysis of off-board powered thermal preconditioning in electric drive vehicles," *National Renewable Energy Laboratory, Golden, CO*, 2010. [Online]. Available: https://www.osti.gov/biblio/1001443

[64] K. Chua, S. Chou, and W. Yang, "Advances in heat pump systems: A review," *Applied Energy*, vol. 87, no. 12, pp. 3611–3624, 2010. [Online]. Available: http://www.sciencedirect.com/science/article/pii/S030626191000228X

[65] A. Hepbasli and Y. Kalinci, "A review of heat pump water heating systems," *Renewable and Sustainable Energy Reviews*, vol. 13, no. 6, pp. 1211–1229, 2009.

[66] D.-Y. Lee, C.-W. Cho, J.-P. Won, Y. C. Park, and M.-Y. Lee, "Performance characteristics of mobile heat pump for a large passenger electric vehicle," *Applied Thermal Engineering*, vol. 50, no. 1, pp. 660–669, 2013.

[67] J. H. Ahn, H. Kang, H. S. Lee, H. W. Jung, C. Baek, and Y. Kim, "Heating performance characteristics of a dual source heat pump using air and waste heat in electric vehicles," *Applied Energy*, vol. 119, pp. 1–9, 2014.

[68] K. Kaygusuz, "Performance of solar-assisted heat-pump systems," *Applied Energy*, vol. 51, no. 2, pp. 93–109, 1995.

[69] T. J. LaClair, Z. Gao, O. Abdelaziz, M. Wang, E. Wolfe, and T. Craig, "Thermal storage system for electric vehicle cabin heating-component and system analysis," SAE Technical Paper, Tech. Rep., 2016.

[70] A. Steiner and A. Mladek, "Reducing the energy consumption for comfort and thermal conditioning in evs," in *Ecological Vehicles and Renewable Energies (EVER), 2017 Twelfth International Conference on.* IEEE, 2017, pp. 1–4.

[71] J. J. Meyer, J. Lustbader, N. Agathocleous, A. Vespa, J. Rugh, and G. Titov, "Range extension opportunities while heating a battery electric vehicle," SAE Technical Paper, Tech. Rep., 2018. [Online]. Available: https://www.sae.org/publications/technical-papers/content/2018-01-0066/

[72] K. Kim, S. Kim, and M. Kim, "Experimental studies on the heating performance of the ptc heater and heat pump combined system in fuel cells and electric vehicles," *International Journal of Automotive Technology*, vol. 13, no. 6, pp. 971–977, 2012.

[73] S. Shojaei, A. McGordon, S. Robinson, and J. Marco, "Improving the performance attributes of plug-in hybrid electric vehicles in hot climates through key-off battery cooling," *Energies*, vol. 10, no. 12, p. 2058, 2017.

[74] S. K. Mohammadian, Y.-L. He, and Y. Zhang, "Internal cooling of a lithium-ion battery using electrolyte as coolant through microchannels embedded inside the electrodes," *Journal of Power Sources*, vol. 293, pp. 458–466, 2015.

[75] H.-M. Cho, W.-S. Choi, J.-Y. Go, S. E. Bae, and H.-C. Shin, "A study on time dependant low temperature power performance of a lithium-ion battery," *Journal of Power Sources*, vol. 198, pp. 273–280, 2012.

[76] F. Zheng, J. Jiang, B. Sun, W. Zhang, and M. Pecht, "Temperature dependent power capability estimation of lithium-ion batteries for hybrid electric vehicles," *Energy*, vol. 113, pp. 64–75, 2016.

[77] O. Erdinc, B. Vural, and M. Uzunoglu, "A dynamic lithium-ion battery model considering the effects of temperature and capacity fading," in *Clean Electrical Power, 2009 International Conference on.* IEEE, 2009, pp. 383–386.

[78] A. R. Chaudhari and R. H. Thring, "Energy economy analysis of the g-wiz: a two-year case study based on two vehicles," *Proceedings of the Institution of Mechanical Engineers, Part D: Journal of Automobile Engineering*, vol. 225, no. 11, pp. 1505–1517, 2011.

[79] J. Hsu, C. Ayers, C. Coomer *et al.*, *Report on Toyota/Prius motor design and manufacturing assessment.* United States. Department of Energy, 2004.

[80] A. Khaligh and Z. Li, "Battery, ultracapacitor, fuel cell, and hybrid energy storage systems for electric, hybrid electric, fuel cell, and plug-in hybrid electric vehicles: State of the art," *IEEE transactions on Vehicular Technology*, vol. 59, no. 6, pp. 2806–2814, 2010.

[81] X. Li, Y. Qiao, S. Guo, K. Jiang, M. Ishida, and H. Zhou, "A new type of li-rich rock-salt oxide li2ni1/3ru2/3o3 with reversible anionic redox chemistry," *Advanced Materials*, vol. 31, no. 11, p. 1807825, 2019.

[82] J. Fan, "On the discharge capability and its limiting factors of commercial 18650 li-ion cell at low temperatures," *Journal of Power Sources*, vol. 117, no. 1, pp. 170–178, 2003.

[83] G. Hunt and C. Motloch, "Freedom car battery test manual for power-assist hybrid electric vehicles," *INEEL, Idaho Falls*, 2003.

[84] *High Power Lithium Ion APR18650: data sheet*, A123, 2009.

[85] J. Remmlinger, S. Tippmann, M. Buchholz, and K. Dietmayer, "Low-temperature charging of lithium-ion cells part ii: Model reduction and application," *Journal of Power Sources*, vol. 254, pp. 268–276, 2014.

[86] J. Jaguemont, L. Boulon, P. Venet, Y. Dubé, and A. Sari, "Low temperature aging tests for lithium-ion batteries," *24th IEEE International Symposium on Industrial Electronics*, pp. 1–6, 2015.

[87] C.-K. Huang, J. Sakamoto, J. Wolfenstine, and S. Surampudi, "The limits of low-temperature performance of li-ion cells," *Journal of the Electrochemical Society*, vol. 147, no. 8, pp. 2893–2896, 2000.

[88] S. Zhang, K. Xu, and T. Jow, "Low temperature performance of graphite electrode in li-ion cells," *Electrochimica acta*, vol. 48, no. 3, pp. 241–246, 2002.

[89] A. N. Jansen, D. W. Dees, D. P. Abraham, K. Amine, and G. L. Henriksen, "Low-temperature study of lithium-ion cells using a liysn micro-reference electrode," *Journal of Power Sources*, vol. 174, no. 2, pp. 373–379, 2007.

[90] D. Abraham, J. Heaton, S.-H. Kang, D. Dees, and A. Jansen, "Investigating the low-temperature impedance increase of lithium-ion cells," *Journal of The Electrochemical Society*, vol. 155, no. 1, pp. A41–A47, 2008.

[91] A. Tourani, P. White, and P. Ivey, "Analysis of electric and thermal behaviour of lithium-ion cells in realistic driving cycles," *Journal of Power Sources*, vol. 268, pp. 301–314, 2014.

[92] C. Hendricks, N. Williard, S. Mathew, and M. Pecht, "A failure modes, mechanisms, and effects analysis (fmmea) of lithium-ion batteries," *Journal of Power Sources*, vol. 297, pp. 113–120, 2015.

[93] Q. Kellner, E. Hosseinzadeh, G. Chouchelamane, W. D. Widanage, and J. Marco, "Battery cycle life test development for high-performance electric vehicle applications," *Journal of Energy Storage*, vol. 15, pp. 228–244, 2018.

[94] D. Worwood, E. Hosseinzadeh, Q. Kellner, J. Marco, D. Greenwood, R. McGlen, W. Widanage, A. Barai, and P. Jennings, "Thermal analysis of a lithium-ion pouch cell under aggressive automotive duty cycles with minimal cooling," in *Proceedings of Hybrid and Electric Vehicles Conference*.

[95] The European Commission, *Commission Regulation (EU) No 672/2010*. The European Commission, 2010. [Online]. Available: http://eur-lex.europa.eu/legal-content/EN/TXT/?uri=CELEX%3A32010R0672

[96] J. Lindgren and P. D. Lund, "Effect of extreme temperatures on battery charging and performance of electric vehicles," *Journal of Power Sources*, vol. 328, pp. 37–45, 2016.

[97] J. Pavlovic, A. Marotta, and B. Ciuffo, "Co2 emissions and energy demands of vehicles tested under the nedc and the new wltp type approval test procedures," *Applied energy*, vol. 177, pp. 661–670, 2016.

[98] Y. Zheng, B. Mark, and H. Youmans, "A simple method to calculate vehicle heat load," SAE Technical Paper, Tech. Rep., 2011.

[99] "Jaguar i-pace," https://ev-database.uk/car/1097/Jaguar-I-Pace, 2018, accessed 06/12/2018.

[100] A. ASHRAE, "Standard 55-2004," *Thermal environmental conditions for human occupancy*, p. 56, 2004.

[101] http://www.fleetcarma.com/electric-car-range-in-bitter-cold/, accessed: 15/09/2016.

[102] http://newsroom.aaa.com/2014/03/, accessed: 15/09/2016.

[103] https://www.technologyreview.com/s/522496/electric-vehicles-out-in-the-cold/, accessed: 15/09/2016.

[104] A. Vlahinos and A. A. Pesaran, "Energy efficient battery heating in cold climates," SAE Technical Paper, Tech. Rep., 2002.

[105] J. Zhang, H. Ge, Z. Li, and Z. Ding, "Internal heating of lithium-ion batteries using alternating current based on the heat generation model in frequency domain," *Journal of Power Sources*, vol. 273, pp. 1030–1037, 2015. [Online]. Available: http://dx.doi.org/10.1016/j.jpowsour.2014.09.181

[106] H. Baba, K. Kawasaki, and H. Kawachi, "Battery heating system for electric vehicles." SAE International, 2015. [Online]. Available: https://doi.org/10.4271/2015-01-0248

[107] A. Jarrett and I. Y. Kim, "Design optimization of electric vehicle battery cooling plates for thermal performance," *Journal of Power Sources*, vol. 196, no. 23, pp. 10 359–10 368, 2011.

[108] X. Zhang, X. Kong, G. Li, and J. Li, "Thermodynamic assessment of active cooling/heating methods for lithium-ion batteries of electric vehicles in extreme conditions," *Energy*, vol. 64, pp. 1092–1101, 2014.

[109] D. Worwood, Q. Kellner, M. Wojtala, W. Widanage, R. McGlen, D. Greenwood, and J. Marco, "A new approach to the internal thermal management of cylindrical battery cells for automotive applications," *Journal of Power Sources*, vol. 346, pp. 151–166, 2017.

[110] G. Bower, "Tesla or gm: Who has the best battery thermal management?" https://insideevs.com/tesla-or-gm-who-has-the-best-battery-thermal-management-bower/, 2018, accessed 13/12/2018.

[111] R. D. Chalgren, "Thermal comfort and engine warm-up optimization of a low-flow advanced thermal management system," SAE Technical Paper, Tech. Rep., 2004.

[112] C. Sprouse and C. Depcik, "Review of organic rankine cycles for internal combustion engine exhaust waste heat recovery," *Applied thermal engineering*, vol. 51, no. 1, pp. 711–722, 2013.

[113] H. Zhang, "Human thermal sensation and comfort in transient and non-uniform thermal environments," *Center for the Built Environment*, 2003.

[114] Y. F. Zhang, D. P. Wyon, L. Fang, and A. K. Melikov, "The influence of heated or cooled seats on the acceptable ambient temperature range." *Ergonomics*, vol. 50, no. 4, pp. 586–600, 2007.

[115] K.-H. Chen, J. Bozeman, M. Wang, D. Ghosh, E. Wolfe, and S. Chowdhury, "Energy efficiency impact of localized cooling/heating for electric vehicle," SAE Technical Paper, Tech. Rep., 2015.

[116] Z. Qi, "Advances on air conditioning and heat pump system in electric vehicles - a review," *Renewable and Sustainable Energy Reviews*, vol. 38, pp. 754–764, 2014. [Online]. Available: http://dx.doi.org/10.1016/j.rser.2014.07.038

[117] D. Y. Lee, C. W. Cho, J. P. Won, Y. C. Park, and M. Y. Lee, "Performance characteristics of mobile heat pump for a large passenger electric vehicle," *Applied Thermal Engineering*, vol. 50, no. 1, pp. 660–669, 2013. [Online]. Available: http://dx.doi.org/10.1016/j.applthermaleng.2012.07.001

[118] "Marta," 2020, accessed 07/02/2020.

[119] A. N. Ajah, A. C. Patil, P. M. Herder, and J. Grievink, "Integrated conceptual design of a robust and reliable waste-heat district heating system," *Applied thermal engineering*, vol. 27, no. 7, pp. 1158–1164, 2007.

[120] H. HANMMER, "Carbon dioxide (r744) as supplementary heating device," in *SAE Phoenix Forum 2000*, 2000.

[121] D. Antonijevic and R. Heckt, "Heat pump supplemental heating system for motor vehicles," *Proceedings of the Institution of Mechanical Engineers, Part D: Journal of Automobile Engineering*, vol. 218, no. 10, pp. 1111–1115, 2004.

[122] T. Murata, T. Nakagawa, H. Nishino, and K. Matsuura, "Efficiency improvement in exhaust heat recirculation system," SAE Technical Paper, Tech. Rep., 2016.

[123] D. Takahashi, K. Nakata, Y. Yoshihara, Y. Ohta, and H. Nishiura, "Combustion development to achieve engine thermal efficiency of 40% for hybrid vehicles," SAE Technical Paper, Tech. Rep., 2015.

[124] M. Hosoz, M. Direk, K. S. Yigit, M. Canakci, A. Turkcan, E. Alptekin, and A. Sanli, "Performance evaluation of an r134a automotive heat pump system for various heat sources in comparison with baseline heating system," *Applied Thermal Engineering*, vol. 78, pp. 419–427, 2015.

[125] http://sam-koblenski.blogspot.co.uk/2013/08/a-year-and-half-with-nissan-leaf-part-3.html, accessed: 22/03/2018.

[126] https://www.greencarreports.com/news/1081982_electric-cars-in-winter-six-steps-to-maximize-driving-range, accessed: 22/03/2018.

[127] M. De Gennaro, E. Paffumi, G. Martini, U. Manfredi, H. Scholz, H. Lacher, H. Kuehnelt, and D. Simic, "Experimental investigation of the energy efficiency of an electric vehicle in different driving conditions," SAE Technical Paper, Tech. Rep., 2014.

[128] H. Helms, M. Pehnt, U. Lambrecht, and A. Liebich, "Electric vehicle and plug-in hybrid energy efficiency and life cycle emissions," in *18th International Symposium Transport and Air Pollution, Session*, vol. 3, 2010, p. 113.

[129] T. Hofman and C. Dai, "Energy efficiency analysis and comparison of transmission technologies for an electric vehicle," in *Vehicle Power and Propulsion Conference (VPPC), 2010 IEEE*. IEEE, 2010, pp. 1–6.

[130] G. Suck and C. Spengler, "Solutions for the thermal management of electrically driven vehicles," *ATZ worldwide*, vol. 116, no. 7-8, pp. 4–9, 2014.

[131] S. Chowdhury, L. Leitzel, M. Zima, M. Santacesaria, G. Titov, J. Lustbader, J. Rugh, J. Winkler, A. Khawaja, and M. Govindarajalu, "Total thermal man-

agement of battery electric vehicles (bevs)," MAHLE, Lockport, NY, Tech. Rep., 2018.

[132] A. Sharma, V. Tyagi, C. Chen, and D. Buddhi, "Review on thermal energy storage with phase change materials and applications," *Renewable and Sustainable energy reviews*, vol. 13, no. 2, pp. 318–345, 2009.

[133] R. Sabbah, R. Kizilel, J. Selman, and S. Al-Hallaj, "Active (air-cooled) vs. passive (phase change material) thermal management of high power lithium-ion packs: Limitation of temperature rise and uniformity of temperature distribution," *Journal of Power Sources*, vol. 182, no. 2, pp. 630–638, 2008.

[134] N. Ukrainczyk, S. Kurajica, and J. Šipušić, "Thermophysical comparison of five commercial paraffin waxes as latent heat storage materials," *Chemical and biochemical engineering quarterly*, vol. 24, no. 2, pp. 129–137, 2010.

[135] H. De Wit, C. De Kruif, and J. Van Miltenburg, "Thermodynamic properties of molecular organic crystals containing nitrogen, oxygen, and sulfur ii. molar heat capacities of eight compounds by adiabatic calorimetry," *The Journal of Chemical Thermodynamics*, vol. 15, no. 9, pp. 891–902, 1983.

[136] R. Schaake, J. Van Miltenburg, and C. De Kruif, "Thermodynamic properties of the normal alkanoic acids ii. molar heat capacities of seven even-numbered normal alkanoic acids," *The Journal of Chemical Thermodynamics*, vol. 14, no. 8, pp. 771–778, 1982.

[137] K. K. Jha and R. Badathala, "Low temperature thermal energy storage (tes) system for improving automotive hvac effectiveness," SAE Technical Paper, Tech. Rep., 2015.

[138] https://www.sunamp.com/automotive/.

[139] S. Shojaei, S. Robinson, A. McGordon, and J. Marco, "Passengers vs. battery: calculation of cooling requirements in a phev," SAE Technical Paper, Tech. Rep., 2016.

[140] J. Neubauer and E. Wood, "Thru-life impacts of driver aggression, climate, cabin thermal management, and battery thermal management on battery electric vehicle utility," *Journal of Power Sources*, vol. 259, pp. 262–275, 2014.

[141] N. Kim, J. Jeong, A. Rousseau, and H. Lohse-Busch, "Control analysis and thermal model development for plug-in hybrid electric vehicles," *SAE International Journal of Alternative Powertrains*, vol. 4, no. 2, pp. 260–268, 2015.

[142] J. Park, Y. L. Murphey, and M. A. Masrur, "Intelligent energy management and optimization in a hybridized all-terrain vehicle with simple on–off control of the internal combustion engine," *IEEE Transactions on Vehicular Technology*, vol. 65, no. 6, pp. 4584–4596, 2016.

[143] A. Picarelli, V. Avila, and S. Robinson, "Thermal management strategies for integrated hybrid vehicle subsystems," 2016, accessed 16/05/2020. [Online]. Available: https://digital-library.theiet.org/content/conferences/10.1049/cp.2016.0975

[144] S. Bellocchi, G. L. Guizzi, M. Manno, M. Salvatori, and A. Zaccagnini, "Reversible heat pump hvac system with regenerative heat exchanger for electric vehicles: Analysis of its impact on driving range," *Applied Thermal Engineering*, vol. 129, pp. 290–305, 2018.

[145] H. Hammond-Scott and M. Dempsey, "Vehicle systems modelling and analysis (vesyma) platform-industrial paper," in *Proceedings of the 2nd Japanese Modelica Conference Tokyo, Japan, May 17-18, 2018*, no. 148. Linköping University Electronic Press, 2019, pp. 61–65.

[146] R. B. Parambu, M. Dempsey, and A. Picarelli, "Modelling & analysis of a fuel cell hybrid electric vehicle using real-world & standard driving conditions," in *Proceedings of the 2nd Japanese Modelica Conference Tokyo, Japan, May 17-18, 2018*, no. 148. Linköping University Electronic Press, 2019, pp. 99–108.

[147] R. Kossel, W. Tegethoff, M. Bodmann, and N. Lemke, "Simulation of complex systems using modelica and tool coupling," in *5th Modelica Conference*, vol. 2, 2006, pp. 485–490.

[148] A. V. Rao, "A survey of numerical methods for optimal control," *Advances in the Astronautical Sciences*, vol. 135, no. 1, pp. 497–528, 2009.

[149] J. A. Cook, J. Sun, J. H. Buckland, I. V. Kolmanovsky, H. Peng, and J. W. Grizzle, "Automotive powertrain control—a survey," *Asian Journal of Control*, vol. 8, no. 3, pp. 237–260, 2006.

[150] V. H. Johnson, K. B. Wipke, and D. J. Rausen, "Hev control strategy for real-time optimization of fuel economy and emissions," SAE Technical Paper, Tech. Rep., 2000.

[151] D. Sinoquet, G. Rousseau, and Y. Milhau, "Design optimization and optimal control for hybrid vehicles," *Optimization and Engineering*, vol. 12, no. 1-2, pp. 199–213, 2011.

[152] B. Skugor, V. Ranogajec, and J. Deur, "On smoothing hev/erev supervisory control action using an extended ecms approach," in *2013 World Electric Vehicle Symposium and Exhibition (EVS27)*. IEEE, 2013, pp. 1–10.

[153] T. Hofman, M. Steinbuch, R. Van Druten, and A. Serrarens, "Rule-based energy management strategies for hybrid vehicles," *International Journal of Electric and Hybrid Vehicles*, vol. 1, no. 1, pp. 71–94, 2007.

[154] L. V. Pérez, G. R. Bossio, D. Moitre, and G. O. García, "Optimization of power management in an hybrid electric vehicle using dynamic programming," *Mathematics and Computers in Simulation*, vol. 73, no. 1-4, pp. 244–254, 2006.

[155] R. Wang and S. M. Lukic, "Dynamic programming technique in hybrid electric vehicle optimization," in *2012 IEEE International Electric Vehicle Conference*. IEEE, 2012, pp. 1–8.

[156] N. Kim, S. Cha, and H. Peng, "Optimal control of hybrid electric vehicles based on pontryagin's minimum principle," *IEEE Transactions on control systems technology*, vol. 19, no. 5, pp. 1279–1287, 2010.

[157] A. Sciarretta and L. Guzzella, "Control of hybrid electric vehicles," *IEEE Control Systems Magazine*, vol. 27, no. 2, pp. 60–70, 2007.

[158] J. Pavlovic, B. Ciuffo, G. Fontaras, V. Valverde, and A. Marotta, "How much difference in type-approval co2 emissions from passenger cars in europe can be expected from changing to the new test procedure (nedc vs. wltp)?" *Transportation Research Part A: Policy and Practice*, vol. 111, pp. 136–147, 2018.

[159] M. Safari and C. Delacourt, "Aging of a commercial graphite/lifepo4 cell," *Journal of The Electrochemical Society*, vol. 158, no. 10, pp. A1123–A1135, 2011.

[160] "Average january temperatures for cities in europe," https://www.currentresults.com/Weather/Europe/Cities/temperature-january.php#c, 2019, accessed 24/01/2019.

[161] "Introduction to electric vehicle battery systems."

[162] "Porche's 800v electric sports car taycan makes world debut."

[163] https://www.nissan.co.uk/, accessed: 26/03/2019.

[164] https://www.renault.co.uk/, accessed:26/03/2019.

[165] https://www.jaguar.co.uk/index.html, accessed:27/03/2019.

[166] S. Shojaei, S. Robinson, C. Chatham, A. McGordon, and J. Marco, "Modelling the electric air conditioning system in a commercially available vehicle for energy management optimisation," SAE Technical Paper, Tech. Rep., 2015.

[167] S. Quoilin, A. Desideri, J. Wronski, I. Bell, and V. Lemort, "Thermocycle: A modelica library for the simulation of thermodynamic systems," in *Proceedings of the 10th International Modelica Conference 2014*, 2014.

[168] "Heat exchanger, interior heating," https://www.extremetech.com/extreme/173256-why-do-electric-cars-suck-in-cold-weather, 2018, accessed 24/04/2018.

[169] K. J. Chua, S. K. Chou, and W. Yang, "Advances in heat pump systems: A review," *Applied energy*, vol. 87, no. 12, pp. 3611–3624, 2010.

[170] W. Wang, Z. Ma, Y. Jiang, Y. Yang, S. Xu, and Z. Yang, "Field test investigation of a double-stage coupled heat pumps heating system for cold regions," *International Journal of Refrigeration*, vol. 28, no. 5, pp. 672–679, 2005.

[171] O. University, "R134a p-h diagram," https://www.ohio.edu/mechanical/thermo/property_tables/R134a/ph_r134a.html, 2008, accessed 30/07/2019.

[172] S. Nejad, D. Gladwin, and D. Stone, "A systematic review of lumped-parameter equivalent circuit models for real-time estimation of lithium-ion battery states," *Journal of Power Sources*, vol. 316, pp. 183–196, 2016.

[173] T. Zhu, H. Min, Y. Yu, Z. Zhao, T. Xu, Y. Chen, X. Li, and C. Zhang, "An optimized energy management strategy for preheating vehicle-mounted li-ion batteries at subzero temperatures," *Energies*, vol. 10, no. 2, p. 243, 2017.

[174] L. Lu, X. Han, J. Li, J. Hua, and M. Ouyang, "A review on the key issues for lithium-ion battery management in electric vehicles," *Journal of power sources*, vol. 226, pp. 272–288, 2013.

[175] F. Yan, J. Wang, and K. Huang, "Hybrid electric vehicle model predictive control torque-split strategy incorporating engine transient characteristics," *IEEE transactions on vehicular technology*, vol. 61, no. 6, pp. 2458–2467, 2012.

[176] H. He, R. Xiong, H. Guo, and S. Li, "Comparison study on the battery models used for the energy management of batteries in electric vehicles," *Energy Conversion and Management*, vol. 64, pp. 113–121, 2012.

[177] J. Jaguemont, L. Boulon, and Y. Dubé, "Characterization and modeling of a hybrid-electric-vehicle lithium-ion battery pack at low temperatures," *IEEE Transactions on Vehicular Technology*, vol. 65, no. 1, pp. 1–14, 2016.

[178] T. R. Grandjean, A. McGordon, and P. A. Jennings, "Structural identifiability of equivalent circuit models for li-ion batteries," *Energies*, vol. 10, no. 1, p. 90, 2017.

[179] Y. Xing, W. He, M. Pecht, and K. L. Tsui, "State of charge estimation of lithium-ion batteries using the open-circuit voltage at various ambient temperatures," *Applied Energy*, vol. 113, pp. 106–115, 2014.

[180] Y. Tripathy, A. McGordon, and C. Low, "A new consideration for validating battery performance at low ambient temperatures," *Energies*, vol. 11, no. 9, p. 2439, 2018.

[181] S. Al Hallaj, H. Maleki, J.-S. Hong, and J. R. Selman, "Thermal modeling and design considerations of lithium-ion batteries," *Journal of power sources*, vol. 83, no. 1-2, pp. 1–8, 1999.

[182] E. Musk, "Tesla adds titanium underbody shield and aluminum deflector plates to model s," https://www.tesla.com/blog/tesla-adds-titanium-underbody-shield-and-aluminum-deflector-plates-model-s?redirect=no, 2014, accessed 31/07/2019.

[183] T. L. Bergman, F. P. Incropera, D. P. DeWitt, and A. S. Lavine, *Fundamentals of heat and mass transfer*. John Wiley & Sons, 2011.

[184] Y. Tripathy, A. McGordon, J. Marco, and M. Gama-Valdez, "State-of-charge estimation algorithms and their implications on cells in parallel," in *2014 IEEE International Electric Vehicle Conference (IEVC)*. IEEE, 2014, pp. 1–6.

[185] A. Barai, K. Uddin, W. Widanalage, A. McGordon, and P. Jennings, "The effect of average cycling current on total energy of lithium-ion batteries for electric vehicles," *Journal of Power Sources*, vol. 303, pp. 81–85, 2016.

[186] S. T. Lundmark, A. Bergqvist, and S. D. Chakarova-Kaeck, "Coupled 3-d thermal and electromagnetic modelling of a liquid-cooled ipm traction motor,"

in *2017 IEEE Vehicle Power and Propulsion Conference (VPPC)*, Dec 2017, pp. 1–6.

[187] A. Boglietti, A. Cavagnino, D. Staton, M. Shanel, M. Mueller, and C. Mejuto, "Evolution and modern approaches for thermal analysis of electrical machines," *IEEE Transactions on industrial electronics*, vol. 56, no. 3, pp. 871–882, 2009.

[188] P. Mellor, D. Roberts, and D. Turner, "Lumped parameter thermal model for electrical machines of tefc design," in *IEE Proceedings B (Electric Power Applications)*, vol. 138, no. 5. IET, 1991, pp. 205–218.

[189] H. Long, A. Lord, D. Gethin, and B. Roylance, "Operating temperatures of oil-lubricated medium-speed gears: numerical models and experimental results," *Proceedings of the Institution of Mechanical Engineers, Part G: Journal of Aerospace Engineering*, vol. 217, no. 2, pp. 87–106, 2003.

[190] G. Song, S. Ma, G. Tang, Z. Yin, and X. Wang, "Preparation and characterization of flame retardant form-stable phase change materials composed by epdm, paraffin and nano magnesium hydroxide," *Energy*, vol. 35, no. 5, pp. 2179–2183, 2010.

[191] A. Pesaran, S. Santhanagopalan, and G. Kim, "Addressing the impact of temperature extremes on large format li-ion batteries for vehicle applications (presentation)," National Renewable Energy Lab.(NREL), Golden, CO (United States), Tech. Rep., 2013.

[192] C. Fiori, K. Ahn, and H. A. Rakha, "Power-based electric vehicle energy consumption model: Model development and validation," *Applied Energy*, vol. 168, pp. 257–268, 2016.

[193] R. T. Doucette and M. D. McCulloch, "Modeling the prospects of plug-in hybrid electric vehicles to reduce co2 emissions," *Applied Energy*, vol. 88, no. 7, pp. 2315–2323, 2011.

[194] R. Suarez-Bertoa and C. Astorga, "Impact of cold temperature on euro 6 passenger car emissions," *Environmental pollution*, vol. 234, pp. 318–329, 2018.

[195] O. Sundstrom and L. Guzzella, "A generic dynamic programming matlab function," in *2009 IEEE control applications,(CCA) & intelligent control,(ISIC)*. IEEE, 2009, pp. 1625–1630.

[196] C. Cubito, L. Rolando, A. Ferraris, M. Carello, and F. Millo, "Design of the control strategy for a range extended hybrid vehicle by means of dynamic programming optimization," in *2017 IEEE Intelligent Vehicles Symposium (IV)*. IEEE, 2017, pp. 1234–1241.

[197] P. Elbert, S. Ebbesen, and L. Guzzella, "Implementation of dynamic programming for n-dimensional optimal control problems with final state constraints," *IEEE Transactions on Control Systems Technology*, vol. 21, no. 3, pp. 924–931, 2012.

[198] O. Sundström, D. Ambühl, and L. Guzzella, "On implementation of dynamic programming for optimal control problems with final state constraints," *Oil & Gas Science and Technology–Revue de l'Institut Français du Pétrole*, vol. 65, no. 1, pp. 91–102, 2010.

[199] O. Sundström, "Optimal control and design of hybrid-electric vehicles," Ph.D. dissertation, ETH Zurich, 2009.

[200] H. Oi, K. Tabata, Y. Naka, A. Takeda, and Y. Tochihara, "Effects of heated seats in vehicles on thermal comfort during the initial warm-up period," *Applied Ergonomics*, vol. 43, no. 2, pp. 360–367, 2012.

[201] S. A. Ziolek, J. Pryor, T. Schwenn, and A. Steinman, "Heated seat simulation study for thermal seat comfort improvement," *SAE International Journal of Passenger Cars-Mechanical Systems*, vol. 8, no. 2015-01-1391, pp. 594–599, 2015.

[202] S. Zhang, C. Zhang, G. Han, and Q. Wang, "Optimal control strategy design based on dynamic programming for a dual-motor coupling-propulsion system," *The Scientific World Journal*, vol. 2014, 2014.

[203] H. Esen, T. Tashiro, D. Bernardini, and A. Bemporad, "Cabin heat thermal management in hybrid vehicles using model predictive control," in *22nd Mediterranean Conference on Control and Automation*. IEEE, 2014, pp. 49–54.